CHARACTERISING DELAMINATION IN COMPOSITE MATERIALS

A COMBINED GENETIC ALGORITHM - FINITE ELEMENT APPROACH

by

ALEJANDRO MARANON

A Doctoral Thesis Submitted in Partial Fulfilment of the Requirements for the Award of Doctor of Philosophy of Loughborough University.

Structural Integrity Research Group
Wolfson School of Mechanical and Manufacturing Engineering
Loughborough University
United Kingdom

December, 2004

THESIS
CONTAINS CD
ROM

Dedicated to

MY MOTHER

for her love and her longer hours of work

that allowed me to finish my studies.

- I hope you recover your health soon! -

MY SISTER

for her immense enthusiasm and love toward me

- I hope this work would inspire you! -

MY DEAREST FRIEND HILDA VELANDIA

for her friendship, love, and encouragement

- Fil, there is hope! -

MY SMALL "'BROTHER"' FELIPE

for his love, tenderness and charm

- Pipe, keep going! -

MY BELOVED DIANA

for being the love of my life

- Baby, You'll have my love for ever! -

MY GRAND MOTHER "'NONOS"'

who died one year ago

for her endless love and her lessons

about rightness, gentleness, honor, honesty.

- I will never forget you! -

CHARACTERISING DELAMINATION IN COMPOSITE MATERIALS

A COMBINED GENETIC ALGORITHM - FINITE ELEMENT APPROACH

ALEJANDRO MARANON

Submitted for the degree of Doctor of Philosophy
December, 2004

ABSTRACT

A novel delamination identification technique based on a low-population genetic algorithm for the quantitative characterisation of a single delamination in composite laminated panels is developed, and validated experimentally. The damage identification method is formulated as an inverse problem through which system parameters are identified. The input of the inverse problem, the central geometric moments (CGM), is calculated from the surface out-of-plane displacements measurements of a delaminated panel obtained from Digital Speckle Pattern Interferometry (DSPI). The output parameters, the planar location, size and depth of the flaw, are the solution to the inverse problem to characterise an idealised elliptical flaw. The inverse problem is then reduced to an optimisation problem where the objective function is defined as the L_2 norm of the difference between the CGM obtained from a finite element (FE) model with a trial delamination and the moments computed from the DSPI measurements. The optimum crack parameters are found by minimising the objective function through the use of a low-population real-coded genetic algorithm (LARGA). DSPI measurements of ten delaminated T700/LTM-45EL carbon/epoxy laminate panels with embedded delaminations are used to validate the methodology presented in this thesis.

KEYWORDS: DELAMINATION; IDENTIFICATION; CHARACTERISATION; GEOMETRIC MOMENTS; GENETIC ALGORITHMS; LARGA; DIGITAL PATTERN SPECKLE INTERFEROMETRY; DSPI.

Acknowledgments

I owe my deepest gratitude to my supervisor Dr Andrew Nurse, for his direction, enthusiasm and optimistic attitude towards research and life in general that have inspired me during these years. He has given me an exceptional opportunity to carry out the present work. It has been a privilege to work with you.

I also wish to thank my director of research, Professor Jon Huntley, for sharing his vision and comments. His interest in my work has been of great importance.

I specially want to thank Dr Pablo Ruiz, and Dr Luis Rivera for all the help in the preparation and testing of the composite laminate samples; you were irreplaceable in this work.

I wish to thank my friends and co-workers in the office; Rebecca Phelps, Tim Barnett, Alastair McCourt, Andras Bulkai, David Panni, Paul Sherrat.

I would like to thank specially to my friend Muzaffer Aziz, for his immense friendship, collaboration, and the endless hours of conversation about quantum mechanics, general relativity, and most importantly, women.

Finally, my warmest thanks belong to my beloved Diana. Thank you for everything.

This work was supported financially by the Engineering and Physical Sciences Research Council (EPSRC), BAe Sowerby Research Centre and Rolls-Royce plc . All these are gratefully acknowledged.

Contents

Acknowledgments v
List of Figures xiii
List of Tables xix

1. PROBLEM STATEMENT AND RESEARCH OBJECTIVES 1
   1.1 Background 1
   1.2 Problem Statement 2
   1.3 Objectives and Research Questions 4
   1.4 Methodology and Experimental Setup 5
      1.4.1 Research question 1 5
      1.4.2 Research question 2 5
      1.4.3 Research question 3 6
      1.4.4 Research question 4 6
   1.5 Scope of the Research 7
   1.6 Relevance of the Research 7
   1.7 A Road Map to This Thesis 7
   1.8 Dissemination and Exploitation 8

2. LITERATURE REVIEW 11
   2.1 Introduction 11
   2.2 Delamination: A Mode of Damage 12
      2.2.1 The genesis 12
      2.2.2 The experimental age 13
      2.2.3 The renaissance 15
      2.2.3.1 Delamination as hybrid element interface 16
      2.2.3.2 Delamination as a de-equivalenced crack 17
      2.2.3.3 Delamination as degraded inter-laminar layer 17
      2.2.3.4 Delamination as a sub-structure 18
   2.3 Digital Speckle Pattern Interferometry (DSPI) 20
      2.3.1 Introduction 20
      2.3.2 DSPI and damage detection 20
   2.4 Two-Dimensional Moments 24

2.4.1 Geometric moments 24
2.4.2 Zernike moments - an orthogonal family 27
2.5 Damage Characterisation in Engineering Structures 28
2.5.1 Inverse problems and system Identification 29
2.5.2 The approach of modal analysis 31
2.5.3 The approach of the static displacements 33
2.5.4 The approach of neural networks 35
2.5.4.1 Neural networks and damage characterisation 36
2.5.5 The approach of genetic algorithms 40
2.5.5.1 Genetic algorithms and damage characterisation 42
2.6 State of the Art - David Panni's Research 44
2.6.1 The finite element model 44
2.6.2 The genetic algorithm 46
2.6.3 The results 46
2.7 Summary and Conclusions 46
2.7.1 Research Question 1 47
3. A FINITE ELEMENT MODEL FOR EMBEDDED DELAMINATION 53
3.1 Introduction 53
3.2 Problem Statement 54
3.3 Objectives and Research Questions 55
3.4 Methodology and Experimental Setup 56
3.4.1 Subquestion A 56
3.4.1.1 The mathematical model 57
3.4.1.2 Numerical implementation 61
3.4.2 Subquestion B 61
3.4.2.1 Basic assumptions 62
3.4.2.2 Mapped meshing 62
3.4.2.3 Free meshing 65
3.4.3 Subquestion C 66
3.4.4 Subquestion D 67
3.5 Results and discussion 68
3.5.1 Parametric representation of delamination 68
3.5.1.01 Second model 68
3.5.2 FE mesh for representation of delamination 72
3.5.2.1 Mapped mesh and delamination 72
3.5.2.2 Free mesh and delamination 75
3.5.2.21 First example 75
3.5.2.22 Second example 76
3.5.3 Delamination model 78
3.5.3.1 The de-equivalenced crack model 78
3.5.3.2 The sub-structure model 79
3.5.3.3 Closing discussion 80
3.5.4 Boundary conditions 81
3.5.4.1 The mathematical model 81

3.6 Conclusion 85
3.6.1 Parametric representation of delamination - Subquestion A 86
3.6.2 Type of FE mesh to represent delamination - Subquestion B 86
3.6.3 Delamination model - Subquestion C 87
3.6.4 Boundary conditions - Subquestion D 87

4. THEORETICAL BACKGROUND ON INVERSE PROBLEMS, OPTIMISATION AND GENETIC ALGORITHMS 89
4.1 Introduction 89
4.2 Problem Statement 90
4.3 Objectives and Research Questions 91
4.4 Methodology and Experimental Setup 92
4.4.1 Subquestion A 92
4.4.2 Subquestion B 92
4.4.3 Subquestion C 94
4.5 Results and discussion 94
4.5.1 Output-error formulation of the inverse problem 94
4.5.2 Cost-effective reformulation of the inverse problem 96
4.5.2.1 Two dimensional geometric moments 96
4.5.2.2 Two dimensional central geometric moments 97
4.5.2.3 Numerical computation of geometric moments 97
4.5.2.4 Numerical computation of central moments 99
4.5.2.5 Similarity measure 99
4.5.2.6 Reformulation of the inverse problem 100
4.5.3 Delamination characterisation and genetic algorithms 102
4.5.3.1 Genetic Structures 103
4.5.3.2 Genetic Operators - Operators affecting genes 110
4.5.3.3 Genetic Operators - Operators affecting chromosomes 112
4.5.3.4 Genetic Operators - Operators Affecting Populations 115
4.5.3.5 Convergence and stopping criteria 118
4.6 Conclusion 118
4.6.1 Formulation of the inverse problem - Subquestion A 118
4.6.2 Reformulation of the inverse problem - Subquestion B 119
4.6.3 Solution of the inverse problem - Subquestion C 120

5. DELAMINATION IDENTIFICATION BY GENETIC ALGORITHMS 121
5.1 Introduction 121
5.2 Problem Statement 122
5.3 Objectives and Research Questions 123
5.4 A Methodology for Identification of Delamination - Sub question A 123
5.4.1 Laplacian-based edge detection - Step 1 124

5.4.2 Determination of initial parameters of delamination - Step 2 125
5.4.3 Central geometric moments from DSPI measurements - Step 3 125
5.4.4 FE representation of a delaminated laminate - Step 4 126
5.4.5 Central geometric moments from FE response - Step 5 127
5.4.6 Delamination identification through a genetic algorithm - Step 6 127
5.5 Experimental Validation - Sub question B 128
5.5.1 Experimental Samples 128
5.5.1.1 Manufacturing of composite laminates 129
5.5.1.2 DSPI experimental setup 130
5.5.2 Laplacian-based edge detection - Step 1 131
5.5.3 Determination of initial parameters of delamination - Step 2 132
5.5.4 Central geometric moments from DSPI measurements - Step 3 133
5.5.5 FE representation of a delaminated laminate - Step 4 133
5.5.6 Central geometric moments from FE response - Step 5 135
5.5.7 A low-population adaptive-range genetic algorithm (LARGA) - Step 6 135
5.5.7.1 LARGA Evaluation - Materials and methods 137
5.5.7.2 LARGA Evaluation - Theoretical feasibility study 139
5.5.7.3 LARGA Evaluation - Experimental validation study 139
5.6 Results 139
5.6.1 LARGA Evaluation - Theoretical feasibility study 139
5.6.2 LARGA Evaluation - Experimental validation study 141
5.6.3 Identification Methodology: Sample 1 - 10C12D 141
5.6.4 Identification Methodology: Sample 2 - 10C23D 143
5.6.5 Identification Methodology: Sample 3 - 20C12D 144
5.6.6 Identification Methodology: Sample 4 - 20C23D 145
5.6.7 Identification Methodology: Sample 5 - 40C12D 146
5.6.8 Identification Methodology: Sample 6 - 40C23D 147
5.6.9 Identification Methodology: Sample 7 - E2012D90 148
5.6.10 Identification Methodology: Sample 8 - E2023D0 149
5.6.11 Identification Methodology: Sample 9 - E4012D90 150
5.6.12 Identification Methodology: Sample 10 - E4023D0 151
5.7 Discussion and Conclusion 152
5.7.1 Formulation of the identification methodology - Sub question A 163
5.7.2 Experimental validation of the methodology - Sub question B 166
6. CONCLUSION AND FUTURE WORK 169
6.1 Conclusions about research questions 169
6.1.1 Research Question 1 169
6.1.2 Research Question 2 173

6.1.2.1 Parametric representation of delamination - Sub question A 173
6.1.2.2 Type of FE mesh to represent delamination - Subjection B 174
6.1.2.3 Delamination model - Sub question C 174
6.1.2.4 Boundary conditions - Sub question D 175
6.1.3 Research Question 3 175
6.1.3.1 Formulation of the inverse problem - Sub question A 175
6.1.3.2 Reformulation of the inverse problem - Sub question B 176
6.1.3.3 Solution of the inverse problem - Sub question C 177
6.1.4 Research Question 4 177
6.1.4.1 Formulation of the identification methodology - Sub question A 177
6.1.4.2 Experimental validation of the methodology - Sub question B 178
6.2 Main Contributions of this Thesis 180
6.3 Future Work 182
6.3.1 The use of new materials and loading conditions 182
6.3.2 The use of other optimisation paradigms 182
6.3.2.1 Ants Colony 182
6.3.2.2 Memetic Algorithms 183
6.3.2.3 Particle Swarm 183
6.3.2.4 Neural Networks 183
6.3.2.5 Case-based reasoning 183

References 185

List of Figures

1.1 Definition of the research problem studied in this thesis. 3

2.1 Definition of sub-laminates in the context of this thesis. 16

2.2 Delamination as hybrid element interface. 17

2.3 Delamination as a de-equivalenced crack. 18

2.4 Delamination as degraded inter-laminar layer. 19

2.5 Delamination as a sub-structure. 19

2.6 Typical Digital Speckle Pattern Interferometry (DSPI) system. 22

2.7 Wrapped phase map of a carbon fibre panel with delamination obtained by out-of-plane DSPI. 22

2.8 Equivalent out-of-place displacements field obtained from the wrapped phase map showed in figure 2.7. 23

2.9a Unwrapped phase map of a carbon fibre panel with delamination obtained by out-of-plane DSPI. Measurements were obtained from a delaminated panel placed in a vacuum chamber. 25

2.9b Equivalent two-dimensional density distribution function $f(x, y)$ (out-of-plane displacements). It is possible to appreciate the bulging phenomenon that occurs on the panel's surface as a consequence of the pressure differential between the surface of the specimen and the internal delamination interface. 25

2.10 Three layer neural network. 36

2.11 A basic genetic algorithm. 41

2.12a Pixelated representation of an elliptical delamination in a 16 x 16 bitmap grid. 45

2.12b Pixelated representation of a circular delamination in a 16 x 16 bitmap grid. 45

2.12c Section through reduced thick FE shell model used by Panni to simulate a delamination in carbon-fibre panels. This model can be classified as a sub-structure delamination modelling. 45

2.12d Top view of the FE model proposed by Panni. It is possible to appreciate the pixelated representation of the delamination. 45

3.0a Laminate in a vacuum chamber when the chamber is not in operation. 55

3.0b Laminate in the same chamber when a vacuum pressure $P_{chamber}$ is applied. Note the bulging effect. 55

3.1 Typical out-plane-displacements field obtained from a carbon fibre panel with a circular delamination. 55

3.2 Geometrical parameters needed to define delamination. 56

3.3 Edge detection algorithm. 58

3.4 Geometrical parameters of an ellipse in polar coordinates. 59

3.5 Two dimensional model of a mapped mesh of a model containing an elliptical delamination. 63

3.6 Edge detection and delamination parameters for an embedded circular delamination with radius 15 *mm*, located at $(37.5, 37.5)$ *mm*. 69

3.7 Edge detection and delamination parameters for an embedded elliptical delamination with radius 15 *mm*, located at $(37.5, 37.5)$ *mm* and θ 90 degrees. 70

3.8 Edge detection and delamination parameters for an embedded elliptical delamination 40*x*20 *mm*, located at (37.5, 37.5) *mm* and θ 45 degrees. 71

3.9 Penny shaped delamination with a radius of 16.5 *mm* in a finite element mesh composed of 100 elements. 73

3.10 Elliptical shaped delamination with a length of 40 *mm*, width of 20 *mm* and angle of ration of 45^o. The centre of the delamination was placed at $(37.5, 37, 5)$ *mm*. 73

3.11 Elliptical shaped delamination with a length of 40 *mm*, width of 20 *mm* and angle of ration of 45^o. The centre of the delamination was placed at $(20, 30)$ *mm*. 74

3.12 Process followed to generate a free mesh representing a penny shaped delamination with a radius of 10 *mm* located at $(65, 40)$ *mm*. 76

3.13 Process to be followed to generate an elliptical shaped delamination with a length of 40 *mm*, width of 30 *mm*, angle of orientation of 45^o, and planar location $(65, 65)$ *mm*. 77

3.14 Delamination representation in a FE model by de-equivalencing the mid-side nodes. (a) Single de-equivalenced node crack. (b) Longer de-equivalenced crack. 79

3.15 Process in the generation of a de-equivalenced crack. (a) FE mesh, with the parameters of the delamination to be included: length $2a$ and depth represented by the solid line. (b) de-equivalenced mesh. 79

3.16 Definition of sub-laminates in the context of this thesis. 80

3.17 Free body diagram of the delaminated region. (a) at the beginning of the experiment, and (b) at the end of the DSPI test. 83

3.18 Forces on a differential portion of the delamination at its final position. 84

4.1 Calculation of geometric moments in a FE mesh. 100

4.2 A basic genetic algorithm. The four stages in every genetic algorithm are: generation of a new population, selection, crossover, and mutation 103

4.3 Geometrical parameters needed to define delamination. 106

5.1 Methodology of identification of delamination from DSPI measurements. 128

5.2 Optical set-up of the high-speed out-of-plane speckle interferometer. 131

5.3 Adaptive-range Genetic Algorithm (ARGA) flowchart. 136

5.4 (a) Comparison of convergence histories of five model replications for simulated out-of plane displacements. Noise 0%, population = 5. Figure not at scale. (b) Comparison of convergence time of five model replications for simulated out-of plane displacements. Noise 0%, population = 5, 10, 15 and 20. 140

5.5 (a) Comparison of predicted delamination area for simulated out-of plane displacements. Noise 0%, population = 5, 10, 15 and 20. (b) Comparison of average solution time for simulated out-of plane displacements. Noise 0%, population = 5, 10, 15 and 20. 140

5.6 (a) Probability density plot of solution time for real DSPI measurements. (b) Comparison of predicted delamination area of twenty model replications for real DSPI measurements. Population = 5. 141

5.7 Comparison of predicted delamination depth of twenty model replications for real DSPI measurements. Real delamination depth is 0.25 mm. Population = 5. 142

5.8 Results of damage characterisation for a sample one (10C12D). 153

5.9 Results of damage characterisation for a sample two (10C23D). 154

5.10 Results of damage characterisation for a sample three (20C12D). 155

5.11 Results of damage characterisation for a sample four (20C23D). 156

5.12 Results of damage characterisation for a sample five (40C12D). 157

5.13 Results of damage characterisation for a sample six (40C23D). 158

5.14 Results of damage characterisation for a sample seven (E2012D90). 159

5.15 Results of damage characterisation for a sample eight (E2023D0). 160

5.16 Results of damage characterisation for a sample nine (E4012D90). 161

5.17 Results of damage characterisation for a sample ten (E4023D0). 162

List of Tables

5.1 Experimental composite laminates used for validation. 130

5.2 Laplacian based edge detection for all experimental samples. 152

5.3 Initial estimation of size and position of delamination from bulge's edge. 163

5.4 Delamination Identification Methodology: convergence history for all experimental samples. 164

5.5 Delamination Identification Methodology: prediction of size and position of delamination for all experimental samples. 165

5.6 Delamination Identification Methodology: prediction of depth of delamination and pressure of air trapped inside of the crack. 166

Chapter 1

PROBLEM STATEMENT AND RESEARCH OBJECTIVES

1.1 Background

Damage and general material degradation reduce the life-time of composite laminates. Among types of damage, delamination is one of the most important because it can significantly reduce the compressive strength and stiffness of the laminate, primarily because the delaminated region loses flexural stiffness. For this reason the *detection* and posterior *characterisation* of the extent of delamination is important during the manufacturing process and the in-service operation of composite laminates.

Detection of delamination has been performed and demonstrated by several authors using a wide range of experimental non-destructive techniques (NDT). Nowadays NDT of composites range from tapping to advanced neutron tracking techniques. At the leading edge are optical interferometric techniques (OIP) that are able to deliver two or three dimensional defect maps, at lower cost, and without physical contact with the sample being tested. The main drivers in the development of OIP for industrial application have been the need to (a) provide the measurement results as rapidly as possible, and (b) in a form which allows non-specialists to visualise readily the damage state of the sample under test.

One of the latest developments in the optical field is Digital Speckle Pattern Interferometry (DSPI), a full field strain measurement technique that can be used to extract out-of-plane displacement field from samples that are excited with a mechanical load as either temperature gradient, or negative pressure

in a vacuum chamber. Typically, DSPI provides a set of experimental data in the form of an array containing upwards $3x10^5$ individual measurements. Although DPSI has been successfully used to *detect* sub-surface delamination in composite panels, little success has been achieved in post-processing the measurements contained in the resultant array, to *characterise* the flaw in terms of geometry, location and depth.

1.2 Problem Statement

When a delaminated composite laminate containing an embedded crack[1] is placed in a vacuum chamber, the external surface of the laminate tends to bulge. Bulging is the result of a pressure differential between the reference vacuum pressure inside of the chamber and the pressure of the air trapped in the delamination. The latter may be either the pressure at which the laminate was manufactured or the atmospheric pressure[2]. Using the DSPI technique, it is possible to detect the bulging effect aforementioned. The result of such technique is an array of measurements of out-of-plane displacements that fully describes the curvature map of the laminate surface that is closer to the detector. The left-hand side of Figure 1.1 shows graphically the description of the problem.

Based on the description given in the previous paragraph, the following statement condenses the research problem that is investigated in this thesis:

> *Given a set of measurements of out-of-plane surface displacements, contained in an array of size upwards 512 by 512 elements obtained through the DSPI technique, determine quantitatively the geometry, planar location and depth of the delaminated portion of a composite laminate, as a means of damage characterisation.*

Damage characterisation under the conditions described above is a so-called inverse problem because known loads and measured displacement fields are being used to infer information about the spatial distribution of the material constitutive behaviour.

---

[1] From here in, the terms delamination and embedded delamination are used indifferently.

[2] It has been suggested [1] that in most cases the delamination surface is expected to be at atmospheric pressure, due to porosity in composite laminates that allows air to slowly ingress inside of the delamination

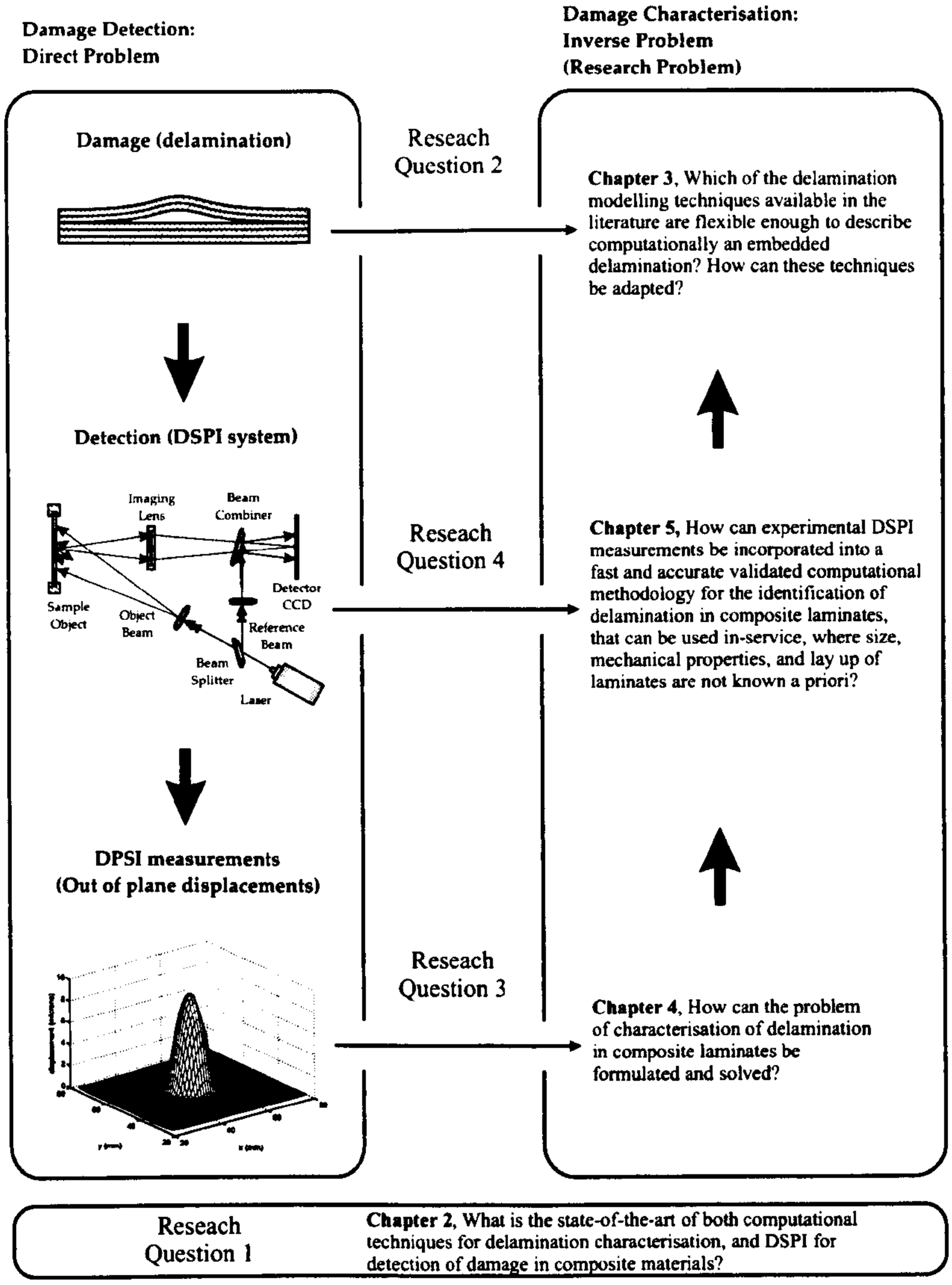

Figure 1.1. Definition of the research problem studied in this thesis.

The left-hand side of the image shows the so called *direct problem.* In this direct problem, given a delaminated panel, then is necessary to *detect* o ascertain the presence of the damage. This kind of problem is usually solved through an experimental technique like DSPI. In this thesis the problem to be solved is classified as an *inverse problem.* Then, given the experimental results from the detecting technique is necessary to find the causes that generated such results.

The following two sections presents the objectives, specific research questions and method of the work carried out in this thesis.

1.3 Objectives and Research Questions

Clearly, there is a need for an inverse technique that can be used to map DSPI measurements into precise topology of delamination in composite laminates. The main objectives in this thesis can be stated as:

1 Develop an *inverse computational technique* to determine quantitatively the geometry, planar location and depth of a single embedded delamination within a composite laminate from a set of experimental measurements obtained from the DSPI technique.

2 This technique must be *flexible* and allow the easy integration of both changing materials and laminate lay up, situation that is common in-service.

3 This technique must be *efficient* at the time of manipulate experimental measurements from DSPI.

4 This technique should provide the characterisation results as *fast* as possible.

These four objectives can be met if the following research questions are answered:

1 What is the state-of-the-art of both computational techniques for delamination characterisation, and DSPI for detection of damage in composite materials? This can be split into the following sub-questions:

- What computational techniques exist to model delamination in composite materials? What are the limitations of these approaches?
- What are the latest developments of DSPI to *detect* damage?
- What numerical tools are available to represent in a compact manner the experimental information from optical interferometry techniques? What are the shortcomings of these tools?
- What numerical techniques are available to *characterize* damage in engineering structures?
- What is latest research on delamination characterisation involving optical interferometric techniques?

2 Which of the delamination modelling techniques available in the literature are accurate and efficient enough to describe computationally an embedded delamination? How can these techniques be adapted?

3 How can the problem of characterisation of delamination in composite laminates be formulated and solved?

4 How can experimental DSPI measurements be incorporated into a fast and accurate validated computational methodology for the identification of delamination in composite laminates, that can be used in-service, where size, mechanical properties, and lay up of laminates are not known a priori?

1.4 Methodology and Experimental Setup

1.4.1 Research question 1

Damage characterisation is inherently cross-disciplinary since it combines four broad disciplines stress-analysis, non-destructive testing, inverse problems and materials science. The first research question is answered through an extensive literature on delamination modelling, Digital Speckle Pattern Interferometry for damage detection, two dimensional moments, and damage characterisation.

1.4.2 Research question 2

The basic approach to the characterisation of a single delamination is the parameterization of the expected flaw. It is proposed that an embedded single delamination can be approximated as an elliptical-shaped crack with six parameters: the coordinate of the centre in the plane of the laminate, the major and minor axes of the ellipse, the depth below of the measured surface and the orientation of the major axis with respect a frame of reference. Also, it is proposed that from a computationally point of view, a delamination can be introduced in a finite element (FE) mesh using the sub-structure technique. The strength of the FE approach lies in the fact that it combines the experimental DSPI data into a model that can be easily ported into an inverse technique for damage characterisation.

1.4.3 Research question 3

DSPI has the property to reveal damage as irregularities in a fringe pattern. This pattern is then post-processed as displacements gradients or out-of-plane displacements measurements that are typically contained in an array of 512 by 512 pixels, this is nearly $3x10^5$ individual measurements. DSPI measurements can be used in computerised damage diagnostic techniques. However, the main prerequisite for this is to decrease the amount of data contained in the resulting array. The problem to be considered here is how to reduce the size of the output array maintaining, at the same time, the physical significance of such results. It is proposed that the theory of two-dimensional geometric moments can applied to satisfy the above purpose.

1.4.4 Research question 4

It is proposed that genetic algorithms is a viable alternative for quantitative characterization of a single delamination in composite laminated panels. The damage identification procedure is formulated as an input-output inverse problem through which system parameters are identified. The input of the inverse problem, the two dimensional geometric moments (GM) set, is calculated from the experimental surface displacements of a delaminated panel in a vacuum chamber. The output parameters, the planar location, geometry and depth of the flaw, are the solution to the inverse problem to characterize the idealized debonding crack. The inverse problem is solved as an optimization procedure. The objective function of the optimization algorithm is defined as the normalized squared difference of the GM obtained from both the convolution of the experimental DSPI measurements, and from a FE model with a trial debonding. The optimum crack parameters are found by minimizing the objective function through the use of a novel implementation of real-coded genetic algorithms (LARGA). The performance of the characterisation technique is evaluated using a set of carbon-fibre epoxy composite samples with systematically-varying and well-characterized defect geometries [3].

---

[3]The author of this thesis acknowledge the collaboration of Dr Pablo Ruiz at Loughborough University for providing the DSPI experimental results that were used in this work.

1.5 Scope of the Research

This thesis concentrates on characterisation of delamination in composite laminates from experimental DSPI measurements. The mechanical properties of the composite laminate used in the DSPI experiment are assumed to be known and accurate. Although DSPI is an emerging technology, issues like precision, accuracy, and error analysis of the technique are not well understood, then the description and research related to these topics are beyond the scope of this thesis. Readers can refer to Rastogui [2] for the latest developments on DSPI.

1.6 Relevance of the Research

Immediate beneficiaries of this research are companies that manufacture a wide range of composite components which must meet stringent performance criteria. Then, quality control of the manufacturing process is seen as one of the main initial applications of the technique described in this thesis.

1.7 A Road Map to This Thesis

Chapter 2, "Literature Review," presents the other research publications that are relevant to the work reported in this thesis. This chapter addresses Research question 1.

Chapter 3, "A finite element model for embedded delamination,". discusses the principles of finite element modelling of embedded delaminations, focusing on speed and accuracy of the solution. This chapter addresses Research Question 2.

Chapter 4, "A Theoretical Background on Inverse Problems, Optimisation and Genetic algorithms," presents a revision on identification of cracks, inverse problems and their solution through genetic algorithms. This chapter addresses Research Question 3.

Chapter 5, "Delamination identification through genetic algorithms," addresses Research Question 4. This chapter bring together the lessons learned in chapters 2 to 4 to develop a GA technique that provide quantitative measurements of delamination in composite laminates.

Chapter 6, "Conclusion and Future Work," seals this thesis. It takes a broad look at the research findings of this thesis, and compares them to the results of other approaches for characterisation of delamination. Finally, it discusses possible future extensions, including case based reasoning, neural networks, and other optimisation paradigms.

1.8 Dissemination and Exploitation

Selected portions of the work carried out during the research project have been published in international referred conferences and journals, as listed below.

- Maranon, A., A. D. Nurse, J. M. Huntley, and P. D. Ruiz. (2004). *A low-population genetic algorithm to characterize sub-surface delamination.* Applied Soft Computing. *Submitted for review.*

- Maranon, A., A. D. Nurse, J. M. Huntley, and P. D. Ruiz. (2004). *A low population genetic algorithm applied to characterization of sub-surface delamination.* In International Conference on Computational Intelligence for Modelling, Control and Automation (CIMCA'2004). July 12-14 2004. Gold Coast, Australia.

- Maranon, A., A. D. Nurse, and J. M. Huntley. (2003). *Characterisation of a single delamination using geometric moments and genetic algorithms.* Optical Engineering **42**(5): 1328–1336.

- Huntley, J. M., C. R. Coggrave, A. Maranon, A. D. Nurse, and P. D. Ruiz. *Detection and sizing of delamination cracks in composite panels using speckle interferometry and genetic algorithms.* In Optical Measurement Systems for Industrial Inspection III (EOM01) - SPIE's Optical Metrology., June 23-26, 2003. Munich, Germany.

- Maranon, A., A.D. Nurse, and J. M. Huntley. *Quantitative determination of defect geometries in composites using ESPI data and inverse analysis.* In Photon02. September 2-5, 2002. Cardiff, UK. SPIE.

- Maranon, A., A.D. Nurse, and J. M. Huntley. *Characterisation of delamination in composite panels using invariant moments.* In SEM-2002. June 10-12, 2002. Milwaukee, Wisconsin, USA.

Chapter 2

LITERATURE REVIEW

Abstract This chapter reviews the other research publications which are relevant to the work reported in this thesis. The quantity of literature concerning past research into delamination, digital pattern speckle interferometry (DSPI), and damage characterisation is vast. Thus, this chapter contains a complete review of only relevant publications. This chapter is divided in three sections; first, findings of studies examining delamination cracks and its modelling is presented. Second, research concerning DSPI and its applications in detection is detailed. The last section presents the literature concerning damage characterisation in engineering structure. Subjects directly relevant to the work reported in this thesis are covered in detail. Other areas not directly related to this work are included for completeness in less detail.

2.1 Introduction

Damage, detection, and characterisation are the three key concepts that constitute the basis of a fast-evolving discipline known as damage characterisation. Damage refers to an imperfection in the material of a component that can be induced during the manufacturing or in-service operation. Detection, is a concept related to an experimental technique that permits to ascertain the presence or existence of damage in a given material or structural part. Finally characterisation refers to an analytical tool (most often a numerical one), that allows researchers and engineers to quantify the geometry and extension of damage from information derived from a detecting technique.

In the scope of this thesis, delamination in carbon composite panels is the mode of damage to be characterised, and Digital Speckle Pattern Interferometry (DSPI) is the technique used to detect such a delamination. This chapter is

divided in three sections. The first section presents a literature review on delamination and its main properties. The second section details works on DSPI and its application to detection of delamination in composites. The last section presents a review on different methodologies that have been used to characterise damage in engineering structures.

2.2 Delamination: A Mode of Damage

Fibre reinforced materials and laminated materials are being used in different structural application. However, among problems in current use of these composite materials is the separation of the interfaces of the laminate known as delamination[1]. Historically, Achenbach and Hemman [3] showed experimentally that due to the ratios of material properties on the plies in a composite laminate, large tensile and shear stresses, and subsequent edge delamination may occur at the interfaces of such laminate.

2.2.1 The genesis

During the late 1960's and early 1970's several researchers studied delamination from an analytical point of view. Pagano [4] showed that the classical laminated plate theory (CPT) provided a poor description of the state of stresses in the interface of two adjacent plies in a laminate. He hypothesized that the main limitation of the CPT could be the underestimation of the shear deformation between the laminate plied. Whitney [5] presented a modified CPT which included the effect of transverse shear deformations. However his theory did not predict accurately the large discontinuities in the slope of the shear stress at the interface of adjacent plies. A similar approach was followed by Puppo and Evenssen [6] to predict interlaminar shear stresses in tubular specimens. They suggested that delamination may not occur in tubular structures because they do not present free boundaries where the inter-laminar shear stress is not zero.

---

[1] Delamination. *Engineering.* The separation of a laminate into its basic layers. *Materials Science.* A sub critical damage to the interfaces between the plies in a laminate composite that causes a reduction in the load carrying capacity of the composite. Academic Press of Science and Technology. Edited by Christopher Morris. Academic Press, 1992.

Increasing availability of computer power during the early 1970's gave rise to the implementation of complex numerical routines to calculate states of stress and delamination in composite materials. Pipes and Pagano [7] found the solution of the theory of elasticity through a finite difference technique in order to calculate the response of a finite-width composite laminate under axial strain. They compared their solution against the one found by Puppo and Evenssen, and concluded that the Puppo-Evenssen model was not exact, especially in the region close to the free-edge of the sample.

Results from Pipes and Pagano lead researchers to investigate more in-deep the phenomenon of free-edge delaminations. Pagano and Pipes [8] studied the influence of the stacking sequence on the laminate strength. They noted that not only normal stresses but also interlaminar shear stresses are the root cause that precipitates delamination and strength degradation in composite laminates. Further investigation performed by these researchers let them to demonstrate experimentally the existence of free-edge delamination in fibrous composite laminates under uniform axial strain. They hypothesized that the stress component primarily responsible for the free-edge delamination is the inter-laminar normal stress [9]. Pagano [10] extended the work of Whitney [5] and Pagano-Pipes [9] by developing a modified plate theory that accounted for the existence of interlaminar normal stresses.

As has been described before, after a few years of research (1965 - 1975), a number of theories and models about interlaminar stresses and delamination was proposed. However these models were not supported for further and comprehensive experimental research, making their scope and predictions limited, without a solid base for design of real structures. The next section details some of the research performed during the experimental age.

2.2.2 The experimental age

Increasing application of composite materials, like in aircraft and marine structures, prompted the need for understanding of interlaminar strength and mechanical performance of composites under low-velocity impacts. Interlaminar strength properties have been necessary during the design stage in order to account for the influence of interlaminar stresses [11]. Also, researchers

turned their attention to the experimental study of low-velocity impacts, in part, due to the fact that this type of impacts can create internal delaminations with no apparent surface damage, which can lead to a catastrophic failure during in-service operation of structures and aircrafts. Garcia and Rhodes [12] studied effects of low-velocity impact on graphite polyimide laminates. They showed that the internal damage is a complex pattern of interply cracking and multilayer delamination. Additionally, they reported reductions in static compression strength of about 60 percent. Cantwell et al. [13] performed a series of impact tests on carbon/epoxy panels. They showed that composites absorb energy elastically and in fracture mechanism such as delamination, matrix cracking and fibre brakeage. Results from the C-Scan technique showed that the shape of the delamination is elliptical with the major axis of the delamination parallel to the fibre direction of the ply that is opposite to the impacted surface. His-Yung et al [14] performed similar study on graphite/epoxy panels. They found that delamination occurred only where there is a change in ply orientations. C-Scan testing on the impacted panels showed the same result that Cantwell et al. found: That the shape of the resulting delaminations is peanut-shaped. Liu [15] made and extensive study on low-velocity impacts in graphite/epoxy, glass/epoxy and kevlar/epoxy composite panels. He found that the shape of the resulting delamination is independent of the material properties of the sample, and that the area of delamination depends on the material properties and the impacting energy. A similar conclusion was formulated by Malvern et al. [16]. These authors found that there exists a linear relation between the delaminated area and the imparted kinetic energy in low-velocity impacts. Choi and Chang [17] studied the evolution of delamination during the time of impact. They showed that matrix cracking is the initial failure mode that can lead to interface delaminations.

To summarise this section it is possible to establish that research into low-velocity impact on composite laminates produced three key pieces of information. Firstly, delamination represents a major component of damage that evolves according to a definite pattern. Secondly, delamination is present only at interfaces between plies with different fibre orientation. Finally, if delamination is present, the debonded area has and oblong or peanut shape.

Having gained experimental knowledge of delamination, researchers were prepared to formulate new theoretical models to describe delamination in different composite materials and load conditions, and to take advantage of new powerful numerical tools in order to predict the onset and evolution of this mode of damage. Research in this new area is the subject of the following section.

2.2.3 The renaissance

Increasing availability of inexpensive computer power let scientist and engineers to apply numerical techniques into the solution of complex differential equations that modelled the behaviour of composite materials, and their modes of failure. Historically, distant pioneers in the application of such techniques are found in 1970. Pipes and Pagano [7], used the finite difference method to calculate interlaminar stresses in axial strained laminates. Research from 1980 has included more sophisticated tools, like the Finite Element Method (FEM), to characterise the behaviour of composites.

In order to describe different modelling techniques found in the literature, the following convention will be used from this point on in the thesis. Referring to figure 2.1, the term sub-laminates will be used to refer the two group of plies separated by the delamination. The portion of the sub-laminate above of the delamination, or the thinner portion, will be referred to as the delaminated region. The portion of the lower, or thicker portion, sub-laminate located beneath the delamination will be referred as the base region.

Literature concerning the modelling of delamination can be classified in four groups accordingly to type of interface used between the delaminated and base regions. These types are named hybrid element interface, de-equivalence crack, degraded inter-laminar layer, and sub-structure. The description of these modelling techniques is presented in the following sub sections[2].

[2]The names of the different modelling techniques are proposed by the author of this thesis.

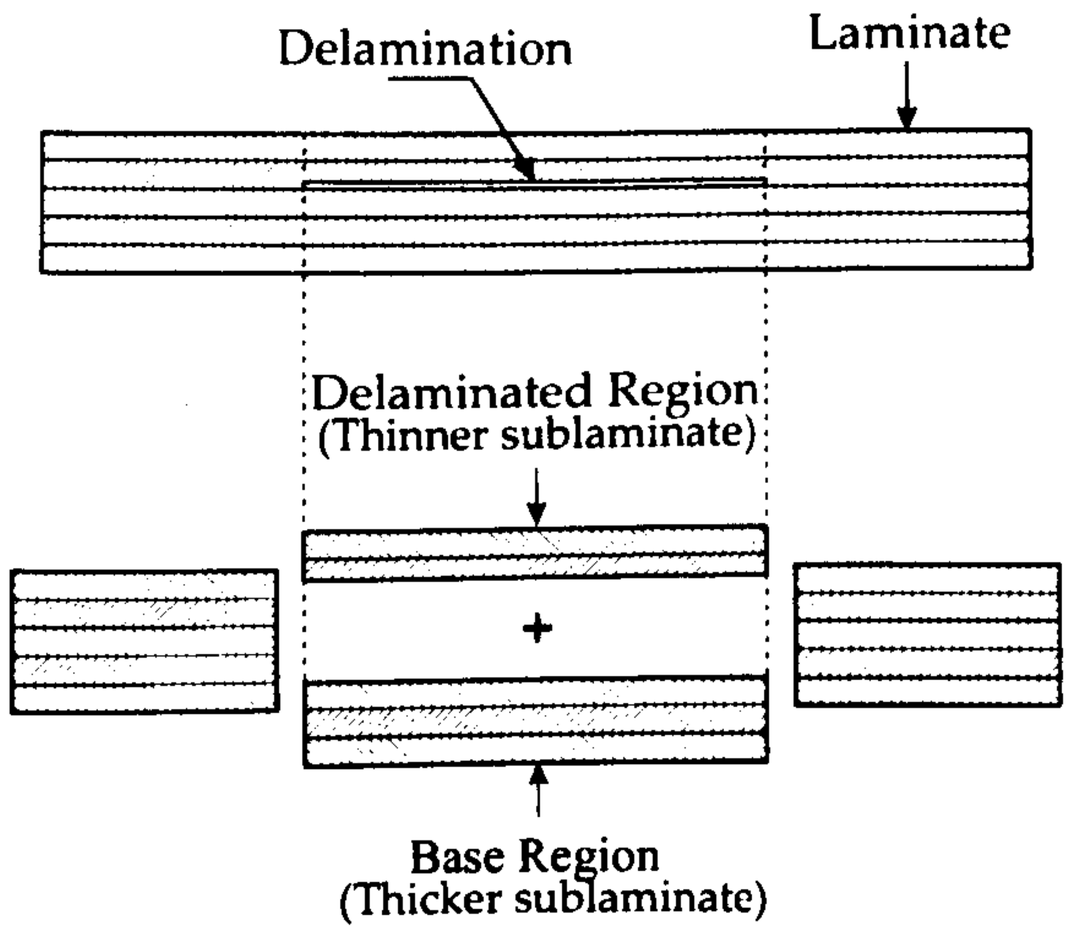

Figure 2.1. Definition of sub-laminates in the context of this thesis.

Sub-laminates refer the two groups of plies separated by the delamination. The portion of the sub-laminate above of the delamination, or the thinner portion, will be referred to as the delaminated region. The portion of the lower, or thicker portion, sub-laminate located beneath the delamination will be referred as the base region.

2.2.3.1 Delamination as hybrid element interface

In this type of modelling, finite elements in both sub-laminates are connected through beam, spring (and sometimes contact) elements in order to control the relative position of both sub-laminates or to avoid penetration of the delaminated region into the base region as is shown in figure 2.2. Reddy et al. [18] used this approach, using beam elements as interface, to study buckling and vibration in graphite/epoxy panels. They found that the finite element model (FE) provided good estimates of structural degradation. Mohammadi et al. [19] studied low-velocity impacts on graphite/epoxy panels. In their study, they used contact elements in the interface between sub-laminates to simulate the evolution of delamination during a hypothetic impact event. Borg et al. [20] used spring elements in the interface to study the fracture behaviour in composite beams. They found that there is ad dependency between the actual size of a delamination and the coarseness of the finite element mesh. They suggested that in general a highly refined sub-laminate mesh is preferable.

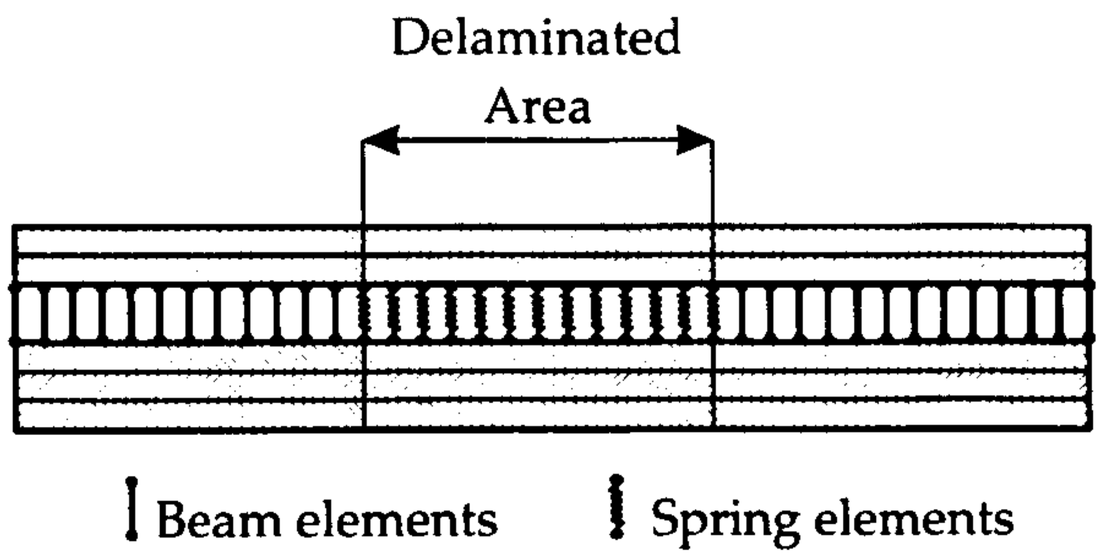

Figure 2.2. Delamination as hybrid element interface.

In this model, finite elements in both sub-laminates are connected through either beam or spring, and contact elements in order to control the relative position of both the delaminated and base regions.

2.2.3.2 Delamination as a de-equivalenced crack

In this modelling technique, finite elements in the delaminated region are not connected at all with the elements in the base region as is shown in figure 2.3. This approach has been used in some studies of laminate buckling and crack propagation where researchers do not anticipate contact or overlapping between the sub-laminates. Kim and Hong [21] studied the onset and propagation of delamination graphite/epoxy plates. In their approach the evolution of the crack's front was modelled as the introduction of new nodes at the boundaries of the delaminated region, increasing in this way the effective area of the crack. Davidson [22] studied the delamination buckling phenomenon. In his model delamination were modelled both elliptical and circular in shape. He found that for moderately sized delamination the solution of the FE model were close to the results found in the supporting experiments.

2.2.3.3 Delamination as degraded inter-laminar layer

In this modelling methodology, a thin isotropic layer is placed between plies in the laminate, and delamination is simulated as a reduction in the elastic properties of the isotropic elements that are just beneath of the delaminated region as is shown in figure 2.4. Zako and Tsujikami [23] studied the fracture of composite laminates under a single out-of-plane concentrated load. In their model, the concentrated load was incremented by small steps. In every step the normal and shear stresses of every finite element in the isotropic layer

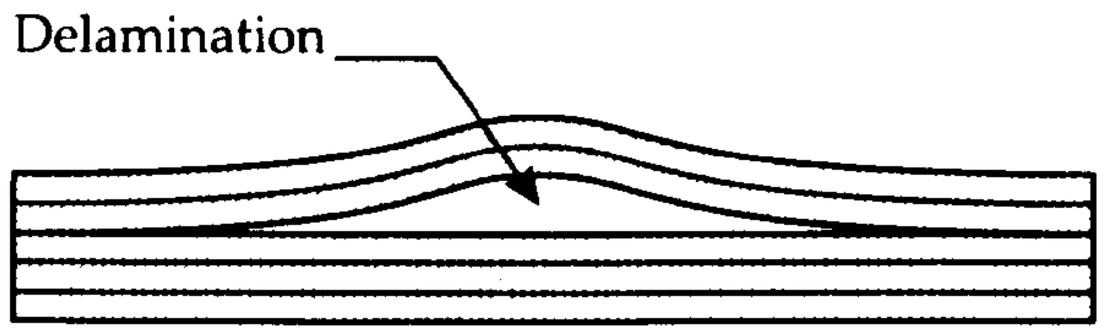

Figure 2.3. Delamination as a de-equivalenced crack.

In this modelling technique, finite elements in the delaminated region are not connected at all with the elements in the base region. This technique is based on the introduction of a crack in the composite material by a generation of new nodes in the finite element mesh, decoupling partially the degrees of freedom in the adjoining layers.

were compared against a pre-established threshold value. If the stresses in the finite element were higher that the threshold value, the elastic modulus of element was reduced. However, the exact amount of reduction is not given in the reference. Davies and Zhang [24] used a hybrid methodology to study low-velocity impact in carbon fibre laminate composites. In their study they placed spring elements between the delaminated and base regions. However, they noticed that the model's results did not agree with the experiments as expected. They showed that degrading the in-plane laminate stiffness the results from the models and the experiments agreed in a significant manner. Zou et al. [25] implemented a modified version of the Davis-Zhang's model to study low-velocity impacts. The fundamental difference with the former research is that the authors replaced the solid structure of every sub-laminate by a shell representation of it. In this way the solution times were notoriously smaller. They found that this modelling technique offered good agreement with the experiments, however the level of agreement was in general lower that the results obtained by Davis-Zhang.

2.2.3.4 Delamination as a sub-structure

In this technique, only the delaminated region is modelled. In this approach the thickness of the delaminated region is assumed to be small compared with the base region as is shown in figure 2.5.. Shivakumar and Whitcomb [26] used this approach to characterise localized buckling in isotropic (aluminium) and orthotropic (graphite/epoxy) laminates. In the proposed model, the de-

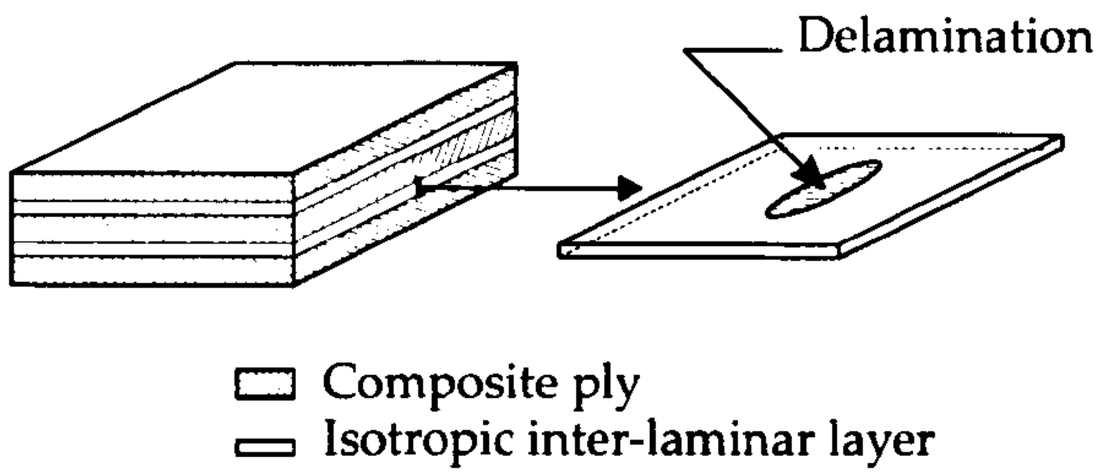

Figure 2.4. Delamination as degraded inter-laminar layer.

In this modelling technique a thin isotropic layer is placed between plies in the laminates, and delamination is simulated as a reduction in the elastic properties of the isotropic elements that are just beneath of the delaminated region.

laminated region was modelled by an elliptical shape. Shivakumar-Whitcomb work was purely theoretical, thus it is not possible to assert the validity of their model against experimental measurements. Panni [1] used a similar approach to characterise delamination in carbon reinforced composite panels. In his approach the entire group of plies above the delamination were modelled, and symmetrical boundary conditions were specified in order to take into account the effect of the base region. He showed that the solution time of this kind of FE model was much smaller than the full 3D FE models. However, again there is not an evaluation of the performance of this model against experimental values.

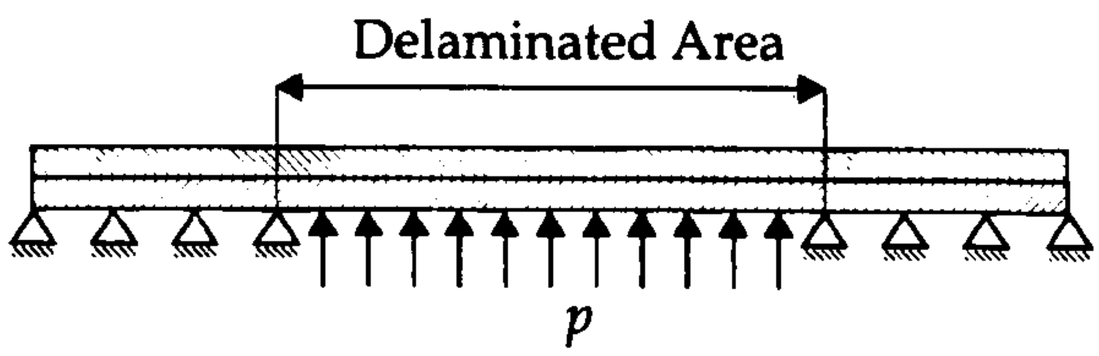

Figure 2.5. Delamination as a sub-structure.

In this technique only the delaminated region is modelled, and the base region is replaced by appropriate boundary conditions.

2.3 Digital Speckle Pattern Interferometry (DSPI)

2.3.1 Introduction

With the increasing application of composite materials in automotive and aerospace structures, the need for quality control of manufacturing, and in-service inspection has become apparent. Since damage indications can be obtained through the use of non destructive methods, a number of non destructive techniques (NDT) have been developed and tried. NDTs can be classified in two major groups. The first group contains those techniques that use only the difference in the material properties between the damaged and undamaged region to detect[3] the crack. Ultrasonic Inspection and X-ray Radiography are common examples. The second group comprises those techniques using mechanical or thermal loading to excite the damaged region. In the later, Interferometry, Digital Speckle Pattern Interferometry [4] (DSPI), Acoustic Emission, and Vibro-Thermography, are common examples. The success of these techniques to detect damage has been demonstrated by several authors [27–36].

In the scope of this thesis, the author is primarily concerned with the application of DSPI to damage detection in composite materials. Results obtained by using other NDTs are presented for comparison purposes. This section is divided in two parts. The first part research concerning DSPI to damage detection is considered. In the second part, techniques used to manipulate experimental results from DSPI are then presented.

2.3.2 DSPI and damage detection

Digital Speckle Pattern Interferometry is an NDT experimental technique that has been proved to be capable for precise measurements of displacements and strains on diffusely scattering objects. A very comprehensive description of the technique and its application can be found in the book by Rastogi [2]. Historically, Speckle Pattern Interferometry (SPI) was developed at Loughborough University in 1971 [37]. However, since its introduction till the mid-1980's

---

[3]Detect. To discover, find out, ascertain the presence or existence of something. The Oxford English Dictionary, Second Edition. Edited by J. A. Simpson. Clarendon Press, Oxford, 1989.

[4]Originally called Electronic Pattern Speckle Interferometry (ESPI) and also known by the names of Electronic Holography, Digital Holography, Phase-Shifting Speckle Interferometry and TV Holography.

the technique was confined to the laboratory and did not find much use for on-site inspection. This was mainly to two reasons. The first one was the size of the pulsed lasers used in the apparatus. The second reason was that the technique relied in upon the use of photographic film which demanded a lengthy and challenging development process. In 1985, Lokberg [38] suggested the idea of recording the holograms produced by the technique on a video camera and extracting the image by electronic processing. The resulting system was then called DSPI.

The basic principle of DSPI is described now by drawing attention on the system shown in figure 2.6. A laser beam is dived into a reference beam and an object beam. The sample object is illuminated by the object beam and the light scattered from its surface is imaged onto the charge-coupled device (CCD) array, where the reference beam is added. The resultant speckle pattern is formed by the interference of both the reference and the reflected object beam. The analogue video signal from the CCD camera is sent to an analogue-to-digital converter, where the signal recorded as a digital frame of size 512 x 512 picture elements (pixels), in the memory of a computer for a further processing. In order to measure in-plane or out-of-plane displacements, the object is first deformed causing a change in the phase of the object beam. Speckle decorrelation fringes are produced by the electronic subtraction of the intensity of the displaced surface from that of the initial surface state. Figure 2.7 shows a typical wrapped phase map of a delaminated carbon/epoxy from DSPI. Figure 2.8 shows the equivalent out-of-plane displacements.

Detection of sub-surface delaminations in composite panels using DSPI has been demonstrated by several authors now [39, 40]. Hertwige et al. [41] studied fatigued-induced delamination in carbon epoxy-panels. They showed that the area of debonding can be accurately predicted if using out-of-plane displacements from the DSPI technique. Richardson et al. [42, 43] performed a similar study to detect delaminations in glass-fibre reinforced polyester (GRP) panels in which the damage was originated from an impact test. They demonstrated that there is a linear relationship between the absorbed impact energy and the area of debonding. Tyrer et al. [44] formulated a set of rules that relate particular defect geometry and their associated surface response from DSPI.

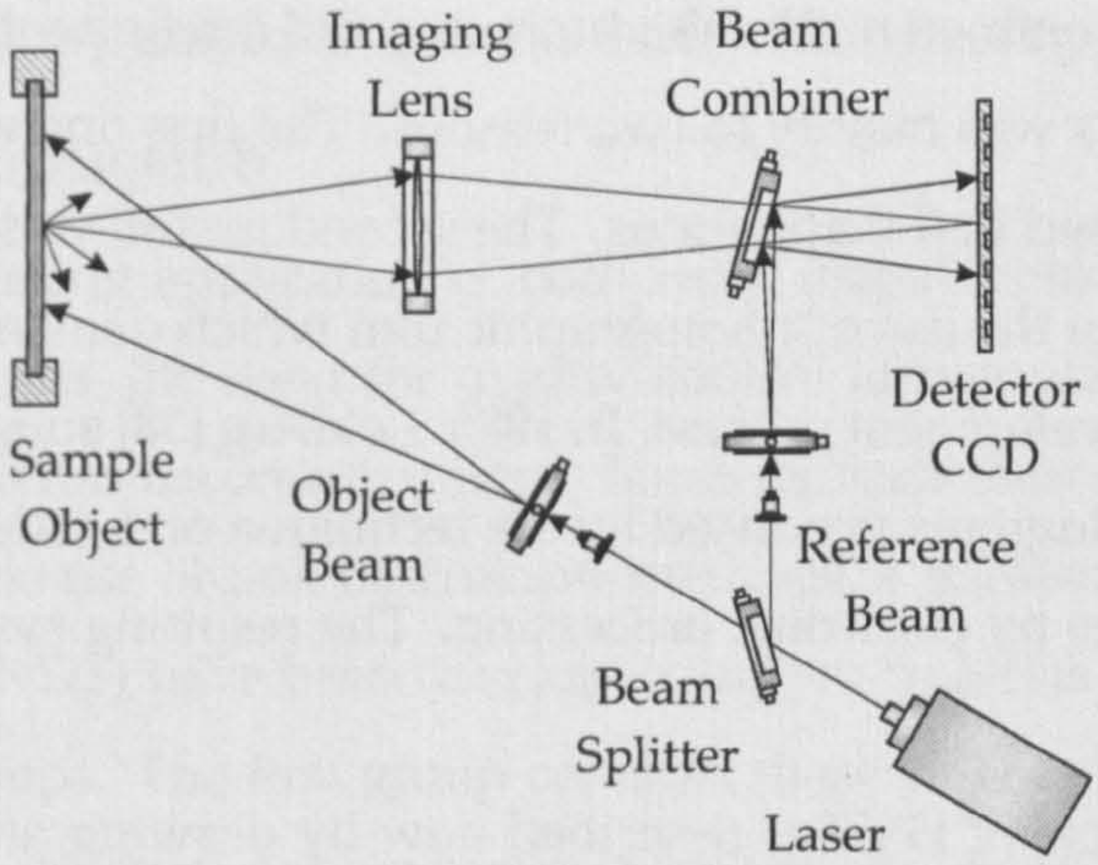

Figure 2.6. Typical Digital Speckle Pattern Interferometry (DSPI) system.

A laser beam is dived into a reference beam and an object beam. The sample object, that is simply supported, is illuminated by the object beam and the light scattered from its surface is imaged onto the charge-coupled device (CCD) array, where the reference beam is added. The resultant speckle pattern is formed by the interference of both the reference and the reflected object beam. The analogue video signal from the CCD camera is sent to an analogue-to-digital converter, where the signal recorded as a digital frame of size 512 x 512 picture elements (pixels), in the memory of a computer for a further processing.

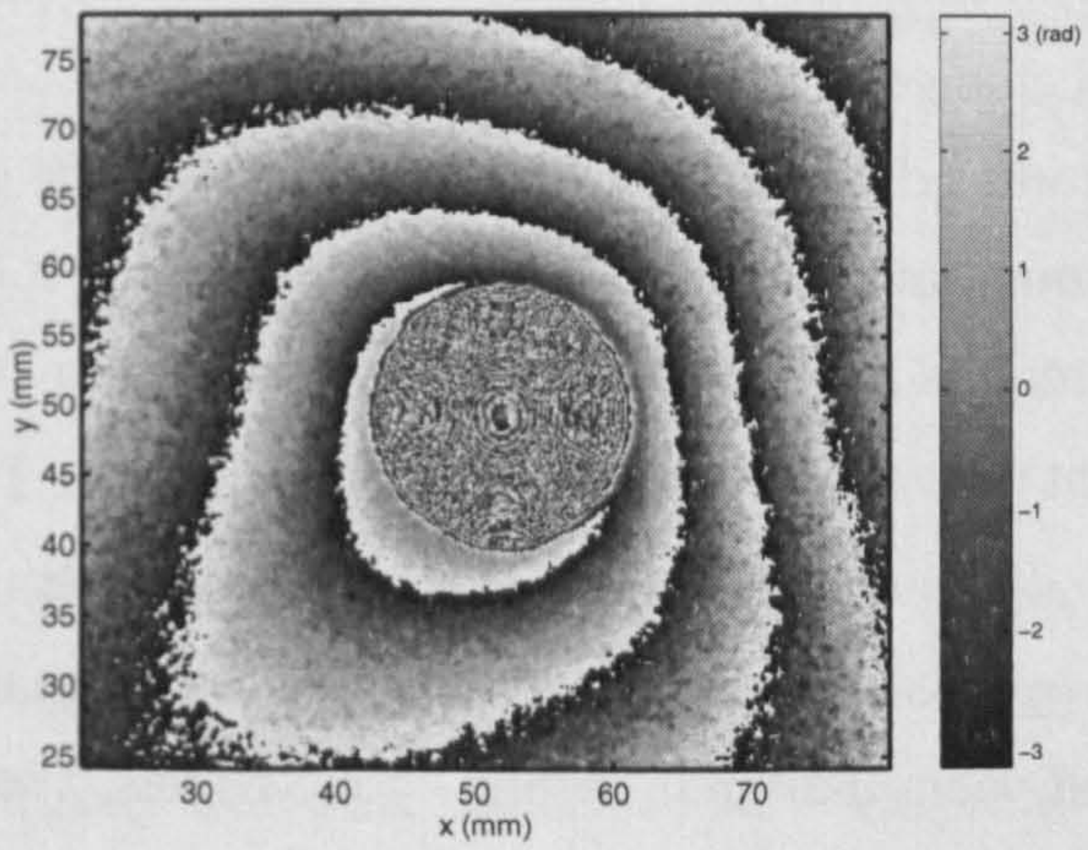

Figure 2.7. Wrapped phase map of a carbon fibre panel with delamination obtained by out-of-plane DSPI.

It was suggested that the smallest and deepest defects are difficult to detect if the inspection sensitivity of the DSPI system is poor, and the control of external loading conditions during the experiment are not optimised. Huntley et

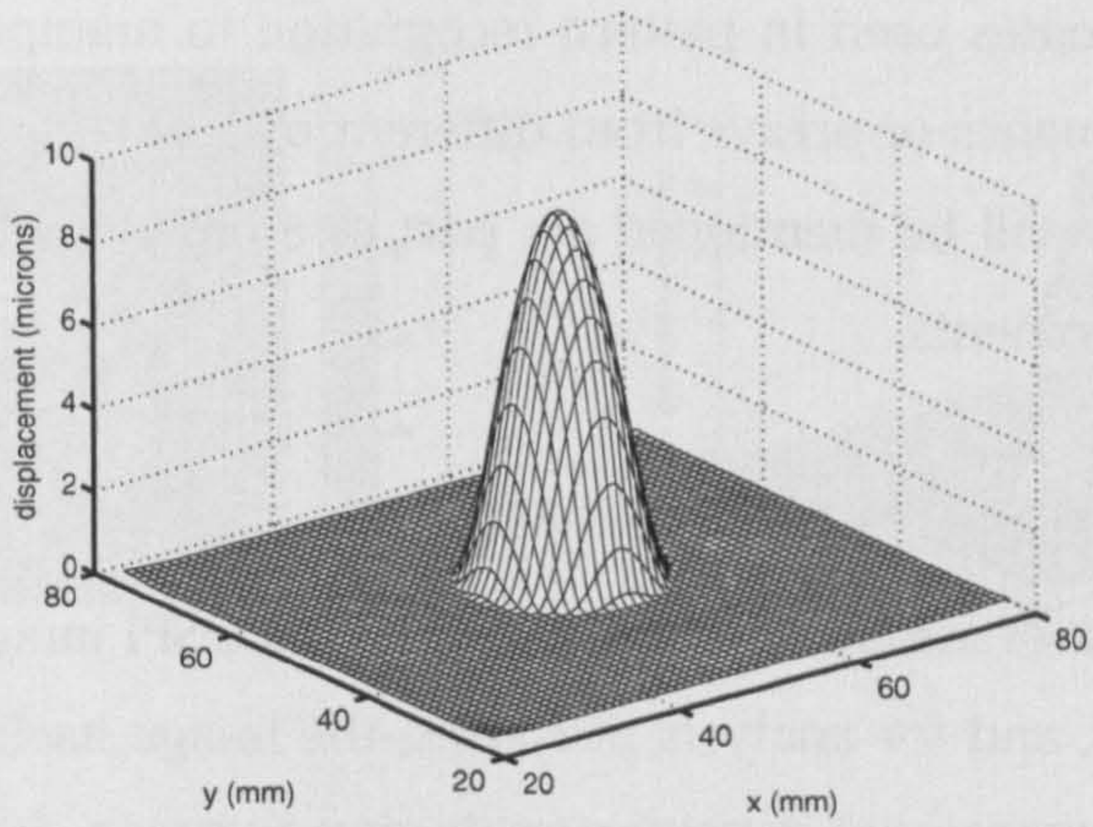

Figure 2.8. Equivalent out-of-place displacements field obtained from the wrapped phase map showed in figure 2.7.

al. [45] developed a novel DSPI system that is capable of displaying maps of displacement fields in real time. In their investigation out-of-plane displacements measured from a vacuum-loading test on a carbon/epoxy composite panel containing sub-surface delamination cracks are displayed as a series of images, every one containing 250.000 individual measurements. More recently, Davila et al. [46] used the Huntley-DSPI system to detect sub-surface delaminations. In their study, carbon fibre plates with artificial delaminations were placed in a vacuum-chamber where the damage was activated by applying a reference vacuum pressure[5]. The DSPI system was then used to measure the surface displacements field of the sample as the pressure in the chamber was increased at a rate of $2x10^4$ Pa/s. It was showed that the accuracy on the DSPI Technique is greatly affected by vibration and speckle decorrelation [47]. Techniques for dealing with these two factors are still subject of research.

DSPI measurements can be used in computerized damaged diagnostic techniques [39]. However, the main prerequisite of these techniques is to decrease the amount of data contained in the resulting image/array from DSPI measurements [48]. The problem to be considered in here is how to reduce the amount of information from DSPI maintaining, at the same time, the physical significance of such results. The next subsection details research concern-

[5]The value of the reference pressure is not mentioned in the reference.

ing with methodologies used in pattern recognition to manipulate information contained in images or arrays from different optical techniques. All the methodologies that will be mentioned are part of a broad concept known as two-dimensional moments.

2.4 Two-Dimensional Moments

Given the amount of measurements contained in a DSPI image, up to $3x10^5$ individual samples, and for analysis purposes, the image itself can be represented by a two-dimensional density distribution function $f(x, y)$ [49] as is shown in figure 2.9a and 2.9b. The general problem considered by researchers was that of manipulate efficiently the density distribution function $f(x, y)$ of the image. The solution Teague proposed is the general method of moments.

The concept of moments has been applied extensively in mechanics and statistical theory [50, 51], for example centroid position and moments of inertia. In the context of image recognition, a moment is described as a projection of the density distribution function $f(x, y)$ on to a set of base functions. The purpose of this projection is both to capture global information about the image and to replace the continuous space of $f(x, y)$ by a discrete moment-space. Although, the selection of base functions is not unique and researchers have used two principal types of functions that by extension have created the same number of moment families known as Geometric and Zernike. The following subsections present a literature review of moments and their performance to characterise images.

2.4.1 Geometric moments

Historically, Hu [52] was the first researcher to suggest that any geometrical pattern contained in an image can be represented by a set of its two-dimensional moments with respect to a fixed coordinate system. Hu used Geometric moments (GM) and combinations of these moments for recognition of characters contained in pre-designed images. Geometric moments m of order $(p+q)$, m_{pq}, have the form of a projection of the density distribution function $f(x, y)$ onto the monomial $x^p y^q$. Hu defined mathematically GM in terms of the Riemann integral as

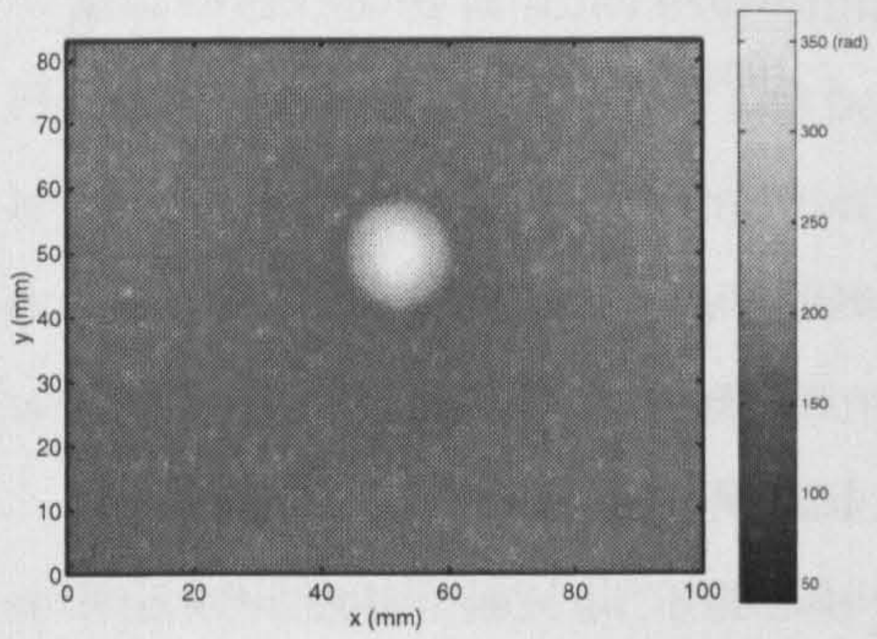

Figure 2.9a. Unwrapped phase map of a carbon fibre panel with delamination obtained by out-of-plane DSPI. Measurements were obtained from a delaminated panel placed in a vacuum chamber.

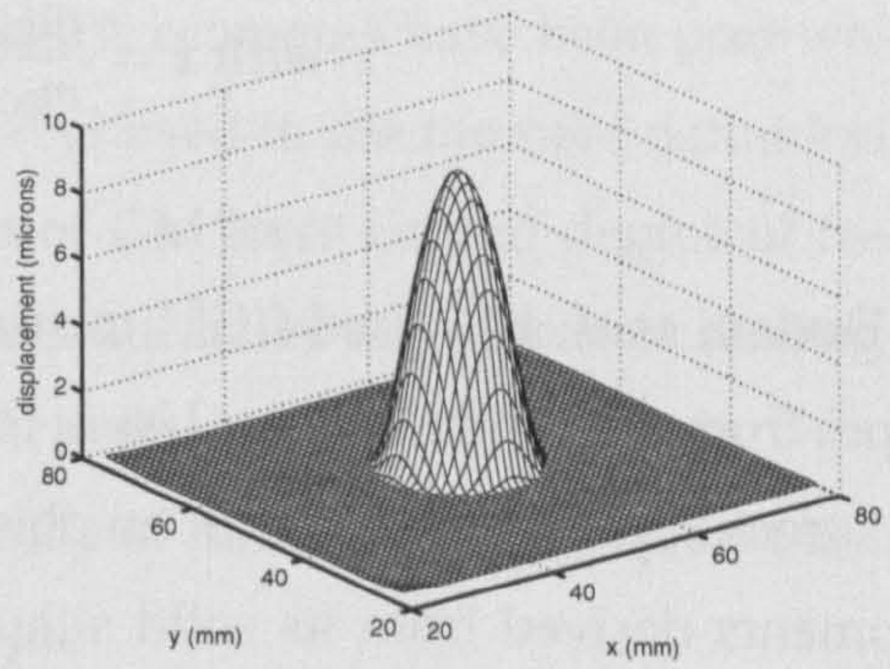

Figure 2.9b. Equivalent two-dimensional density distribution function $f(x, y)$ (out-of-plane displacements). It is possible to appreciate the bulging phenomenon that occurs on the panel's surface as a consequence of the pressure differential between the surface of the specimen and the internal delamination interface.

$$m_{pq} = \int_{-\infty}^{\infty} \int_{-\infty}^{\infty} x^p y^q f(x, y)\, dxdy, \tag{2.1}$$

where $p, q = 0, 1, 2, \ldots, \infty$. A uniqueness theorem presented by Papoulis [51] states that if $f(x, y)$ is a piecewise continuous function with a non zero values in a finite part of its domain, moments m_{pq} of all order exists, and $f(x, y)$ determines uniquely the sequence of moments.

A main property of Geometric moments is that their numerical values depend completely on the selection of the reference coordinate system used for their calculation. Hu solved this problem by introducing the concept of Central-geometric moments (CGM). These moments are equivalent to the geometric moments of a pattern that has been shifted such that the image centroid $(\bar{x}, \bar{y})$ coincides with the origin of calculation of the moments. As a consequence CGM are invariant to translations (shifts) of the image [53, 54]. Mathematically, CGM are defined as follows

$$\eta_{pq} = \int_{-\infty}^{\infty} \int_{-\infty}^{\infty} (x - \bar{x})^p\ (y - \bar{y})^p\ f(x, y)\, dxdy, \tag{2.2}$$

$$with\ \bar{x} = \frac{m_{10}}{m_{00}},\ and\ \bar{y} = \frac{m_{01}}{m_{00}}. \tag{2.3}$$

Dudani et al. [55] used CGM to study the automatic recognition of aircraft types from television images. Using low-order moments[6], they suggested that the gross structural features of an object may be better characterised by those moments derived from its solid silhouette; moreover, it was suggested that low order moments are less susceptible to noise contained in the image. Similar results were obtained by Teague [49] and Balslev [56]. Sadjadi and Hall [57] derived the mathematical extension of two-dimensional moment to three dimensions. They showed that 3D Geometric moments reduced the amount of data and processing needed for three dimensional object recognition. Reeves et al. [58] expanded the work of Dudani [55] by including scaling invariance in the definition of CGM using the following scale factor,

$$\lambda_N = {}^{1}/_{\sqrt{m_{00}}}. \tag{2.4}$$

Reeves and co-workers concluded that this approach made a significant improvement in the automatic recognition of aircraft types. Similar results were found by Hupkens and de Clippeleir [59]. Teh and Chin [60] showed that higher order moments, moments of order four and up, are more sensitive to image noise than lower order moments are. Höfling and Priber [48] suggested that CGM or functions of these moments can be used in artificial intelligence applications to characterise flaws in fringe patterns from optical interferometric techniques. They found that using three Central-geometric moments, $(\mu_{11},\ \mu_{30},\ \mu_{03})$, their classification technique yield no errors in characterising simulated flaws. Mamislov [61] continued the work of Sadjadi-Hall [57] and developed the n-dimensional Central-geometric moments theory applicable to the recognition of n-dimensional solids. A major contribution from his work is that it made possible to researchers and engineers to analyse images consisting of geometric figures and solids with curved contours and surfaces.

[6] Low order moments are moments up to third order.

The findings of studies examining Geometric moments have been positive. However, given the fact that the basis set $x^p y^q$ used in the moment definition is not orthogonal, the information content of GM have certain degree of redundancy, making these type of moments less attractive to researchers dealing with reconstruction of images from moment descriptors.

The next subsection presents another family of moments that overcome the restriction mentioned in the above paragraph.

2.4.2 Zernike moments - an orthogonal family

Historically, Teague [49] suggested the notion of orthogonal moments to recover images from a set of moments based on the theory of Zernike polynomials. Teague suggested that Zernike moments contain information about an image that is independent of the size, planar position and relative angular position. Also, it was suggested that the inclusion of third-, fourth-, and fifth-order Zernike moments may have not effect on the quality of the image reconstruction. Only with the introduction of higher order moments the definition of the recovered image is superior. The mathematical definition of Zernike moments λ of order $(p+q)$, as given by Teague, is the following,

$$\lambda_{pq} = \frac{(p+1)}{\pi} \int_0^{2\pi} \int_0^{\infty} V_{pq}(r,\theta)\ \ f(r\cos\theta, r\sin\theta)\, r\, dr\, d\theta, \tag{2.5}$$

where the general form of Zernike polynomials are defined as,

$$V_{pq}(r,\theta) = R_{pq}(r)\, e^{iq\theta}. \tag{2.6}$$

Radial polynomials in the previous equation are defined as,

$$R_{pq}(r) = \sum_{s=0}^{(p-|q|)/2} (-1)^s \cdot \frac{(p-s)!}{s!\left(\frac{p+|q|}{2}-s\right)!\left(\frac{p-|q|}{2}-s\right)!}\, r^{p-2s}. \tag{2.7}$$

Kothenzad and Hong [62] extended the work of Teague to study the influence of image's noise during the process of image recovering. They concluded that in presence of a moderate level of noise, Zernike moments performed better that the CGM. Teh and Chin [60] also studied the noise sensitivity and information redundancy of Zernike moments. They suggested that higher order

moments are more sensitive to noise than lower order moments are. However, and contradictory, higher order Zernike moments carry the fine detail of the image. Also, it was found that moments of order five and up contain information redundancy that is comparable to the one found in Geometric moments.

Kim and Kim [63] used Zernike moments as a region-based shape descriptor of images contained in large image databases. In their study, they used moments of up to order ten to classify images taking into account rotation, scale and perspective transformation. They found that the accuracy of the classification system was between 70 and 94 percent. Kan and Srinath [64] expanded the work of Kothanzad-Hong [62] by including a new scaling invariance definition. They found that this invariance permitted to Zernike moments to contain more local information about the underlying content of the images analysed. Chong et al [65] extended the mathematical theory of Zernike moments to derive translation invariants or these moments. They found that the proposed invariants can be used with both symmetrical and non symmetrical images.

To summarise this subsection, it is possible to mention that although orthogonally is one the properties of Zernike moments, another properties make them attractive to researchers in pattern recognition. These properties are rotation invariance [62], robustness to moderate levels of noise [62], and efficiency in terms of the non-redundancy provided by lower order Zernike moments [60].

The next, and final, section of this chapter details the literature concerning damage characterisation in engineering structures.

2.5 Damage Characterisation in Engineering Structures

In the literature, during the past twenty years, there has been an increase in research in the identification and prediction of damage. However, the problem of characterisation of delamination and debonding in composite materials has appeared more recently; it was prompted by the need to understand the behaviour of complex structures and systems, and to develop more accurate criteria to design such structures.

The inverse problem of delamination characterisation in laminates has been studied numerically and experimentally. This chapter covers past research and

the state of the art in the above areas. Researches relevant to delamination detection are covered detail. Other investigations in damage detection are included for completeness in loss detail. The first section presents a brief introduction to inverse problems and system identification. Then, research concerning damage detection using modal analysis is presented. Next, scientific publications that use static displacements for characterising damage are detailed. Finally, the approach of neural networks and genetic algorithms in structural damage detection are summarised.

2.5.1 Inverse problems and system Identification

Inverse problems can defined as a special kind of problems in nature where the answer of the problem is known, but not the question. Alternatively, they can be defined as problems where the detectable consequences of the nature are known, but not the cause. A typical example of inverse problems is the medical diagnosis of diseases. In this, the classical or forward problem is defined as follows: given a biological disease in a patient, predict its symptoms on the patient's body. But the more likely problem is if the doctor measures the patient's symptoms and he/she must find the causes (disease) that generated them. This is the inverse problem.

In structural mechanics, the direct of classical problem is to find the displacements and stress in a structure if both the external loads and the spatial distribution of mass are known. For example, given a truss structure or a solid body discretised into small elements, the forward problem can be posed as a matrix relationship between the unknown displacements (or stresses) $\vec{u}$, the mass distribution of the body or stiffness matrix K, and the applied boundary conditions $\vec{F}$. Mathematically, the structural direct problem can be defined as,

$$K \cdot \vec{u} = \vec{F}. \tag{2.8}$$

The classical problem presented in equation 2.8 is a well-posed problem, and represents the vast majority of structural problems that are solved through the finite element analysis. The term *well-posed problem* stems from a definition of

mathematical models of physical phenomena that have the following properties:

1 A solution exists.

2 The solution is unique.

3 The solution depends continuously on the data, in some reasonable topology.

The structural inverse problem arises when either the boundary conditions $\vec{F}$ or the mass distribution of the body K is unknown. The former problem belongs to the category of inverse problems of 1^{st} kind. The latter, belongs to the category of inverse problems of 2^{nd} kind [66]. Typically, inverse problems are ill-posed, this means that they violate one or more of the properties that defined well-posed problems. Of the three conditions for a well-posed problem it is the condition of stability of solution that is most often violated.

Inverse techniques have been applied to many engineering problems. Miniatty, et al. [67] used the finite element method and the regularisation technique to calculate the boundary conditions of an elastic body. Kubo [68] studied the problem of identifying cracks from electric potential computed tomography, and the determination of strain and stresses within a body from data of incomplete boundary conditions. He concluded that optimal structural design can be defined as an inverse problem, and that the development of such approach is being improved by the advances in computers and artificial intelligence technologies.

System identification is a branch of inverse problems in which the state of a structure is calculated from its response to a single or multiple load cases. According to the load condition, system identification techniques can be classified as either static or dynamic. Static techniques use loads from static measurements as input with stresses or strains as output. Dynamic methods (often so-called modal methods) use dynamic or vibration excitation as problem input with natural frequencies and mode shapes as responses.

The following two subsections detail research concerning dynamic and static system identification of damage. The last two sections contain a review of the

literature including artificial intelligence technologies for characterisation of flaws, in special genetic algorithms and neural networks.

2.5.2 The approach of modal analysis

Hajela and Soeiro [69] investigated the damage detection in truss structures using a combination of incomplete static displacement and eigenmodes. In the proposed approach, the analytical model was refined to minimize the difference between the predicted and measured response of the structure; treating the modulus of elasticity of each structural element, or a reduced set of elements, as an independent design variable. The authors suggested that the static load distribution in the structure affects the damage detection; if the damaged member does not play an important role in the load-bearing process, the damage detection algorithm could yield ambiguous results.

Hajela and Soeiro [70] further studied damage detection in truss structures and classify the existing parameters identification techniques in three classes that they called equation error, output error and minimum deviation approach. In the equation error approach, the equations that described the system response were explicitly stated and the minimization problem was formulated in terms of the system equilibrium equations. In the output error approach the objective function was formulated in terms of the difference in output at given notes between the analytical and theoretical model [71]. In the minimum deviation approach, changes in system parameters from initial assumed values were minimized, satisfying the system equations. The authors extended their previous work [70] and compared the output error and equation error methods of system identification. They found that for certain loading conditions these methods failed to locate damage in some structural members.

Narkis [72] studied the crack location in a simply supported beam using the natural frequencies from bending and axial vibrations. In the formulation of bending vibrations the beam was assumed to have non-material damping and the crack was simulated as a torsion spring at the damage location, and in the analysis in the axial vibrations the crack was modelled by a linear a shear spring. It was found that the ratio of relative variations of two first vibration

modes depends only on the location on the crack, and was independent of crack geometry or beam properties.

Ratcliffe [73] similarly studied the damage detection in a cantilever and free-free beams applying a Laplacian operator to the measured first bending mode shape from a damage beam. He suggested that the Laplacian function represents the curvature of the mode shape and it is proportional at the surface strain on a beam. Also, it was concluded that the mode shape data from the fundamental mode were most suited to the proposed technique.

Farrar and Jauregui [74, 75] compared five different damage identification algorithms to a modal data obtained from an undamaged and damage bridge. The methods investigated included those that examine changes in the modal strain energy, changes in mode shape curvature, changes in the flexibility coefficients derived from modal properties, changes in stiffness coefficients derived from model properties and changes in the curvature of the uniform load surface derived from model properties. They concluded that standard modal properties such as resonant frequencies and mode shapes are poor indicators of damage, and consequently the methods studied were inconsistent and did not clearly characterise the damage location when they were applied to the less severe damage cases.

Ray and Tian [76] theoretically explored the possibility of using feedback control to enhance sensitivity of modal frequencies to small changes in structure parameters and local geometry applied to finite-element model of a cantilevered beam. They proposed that instead of using a control algorithm to make the system insensitive to small changes in the system parameters, the control law could enhance or magnify the sensitivity to such changes.

Purekar and Pines [77] developed a methodology for delamination detection in beams with linear tapered geometries using active vibration control and structural waves. The proposed methodology was based on the measurement of the response of a structure when incident waves do not reflect off boundaries. They found that the damage detection using structural waves is sensitive to manufacturing tolerances, decreasing its applicability in problems where exist input noise from uncertainty in geometrical properties of the beam. Aoki and Byon [78] used the localized flexibility properties deduced from the ex-

perimentally determined global flexibility matrix to damage identification in a CFRP laminated beam affected by a reduction of the bending rigidity. They found that for damage detection based on strain flexibility their methods failed to locate damage in some elements.

Pai and Jin [79] presented a method based on the measurement of the deflection shape of a structure subjected to a single-frequency harmonic excitation to detect locations of small damage in beams and plates made of aluminium. Thornburgh and Chattopadhyay [80] developed a higher order displacement field theory to model delamination and transverse matrix cracking in composite laminates. They suggest that delamination and matrix cracking cause similar reduction in the natural frequencies of composites plates. Okafor and Dutta [81] studied the application of wavelet analysis for the purpose of quantification of the damage in a cantilevered beam. Damage was simulated by a reduction in the stiffness of one element in a finite element model. It was found that the first and the third translational modes showed the damage location clearly but the second mode was inconclusive. This result coupled the partials findings of Ratcliffe [73] and Byon [82]. Wu et al. [83] similarly studied the damage detection in anisotropic composite materials using the wavelet transform introducing the Gram-Schmidt orthogonalization algorithm to reduce the number of redundant wavelets that have little to contribute in the domain of support of the data samples. Kim and Kim [84] studied the damage detection in a circular beam with a cut perpendicular to the beam axis. The proposed method used the wavelet transform to identify the location and extend of the damage based on a simple impact excitation.

2.5.3 The approach of the static displacements

Sanayei and Nelson [85] studied the identification of stiffness parameters for linear two-dimensional elastic structures subjected to static loads. The proposed method requires displacements to be measured at the same locations that the external forces were applied, and a Monte Carlo analysis was used to estimate the effect of errors in the measurements. Damage in the structure is represented as a reduction in the cross sectional area or the bending stiffness. They found that the sensitivity to measurement error was dependent on the

structural geometry, connectivity, degree of determination, true value of parameters, and the finite element model used.

Sanayei and Scampoli [86] extended the two-dimensional solution of Sanayei and Nelson [85] to recover the constitutive matrix of the three dimensional orthotropic plate-bending elements from static data. The identified constitutive matrix was used to locate the damage areas of a reinforced concrete pier deck. They showed that the identified parameters are sensitive to measurement errors, suggesting that an accurate estimation of force and displacement is important.

Sanayei and Onipide [86] continued the study of [87] of parameter identification in truss structures. They used static applied loads at one subset of degrees of freedom (DOF) and measured displacement and another subset of DOF to detect damage in a truss and a frame model, using a condensation procedure. They suggested that, although structural damage is a non-linear behaviour, the use of loads of small magnitudes result in structures behave only in their elastic range. Also, it is suggested that if the finite element errors are very small, they can be considered as a part of the measurement errors.

Banan et al. [88, 89] suggested two new algorithms for estimating the constitutive properties of a finite element model in bowstring truss structures. The first method was based on minimizing the error in nodal forces between the finite element model and the measurements; the second minimized the errors in nodal displacements. The damage was represented as a reduction in the cross sectional areas. They found that in presence of noise in the measurements, both force and displacement error estimators were biased.

Liu and Lin [90] proposed a method that employed the finite element analysis together with the least squares method to identify the flexural rigidity of non-uniform aluminium beams, using the static longitudinal strains of the beam as input data. They suggested that the identification of the beam properties could be formulated as an optimisation problem in which the error norm of the equilibrium equation is minimized. However, the proposed methodology is sensitive to the position of the strain gages in the beam reducing its effectiveness to locate damage in real structures.

Sanayei and Saletnik [91, 92] extended the work of Sanayei and Onipide [86] to the parameter estimation of linear-elastic structures using static strain measurements, preserving the structural connectivity. It was found that for certain loading and displacement conditions their algorithms did not run due to an ill conditioning of the sensitivity matrix. The non-destructive testing that support the investigation in [91, 86] was presented by Sanayei et al. [93].

Liu and Chian [94] extended the beam solution of Liu and Lin [90] to the identification of element properties of truss structures using the measured axial strains. They found that is difficult to identify the rigidity of an element accurately if the axial force of the element is nearly zero in every test, and suggest that this problem could be avoided by performing a preliminary stress analysis on the truss and designing the test based on its results.

Fukunaga et al. [95] studied the damage identification on laminated composite structures by using bending deflect under static loading. The method was based on the minimization of a vector norm of the residual forces using a non-linear optimisation technique. The damage was modelled as a 50% reduction of all bending stiffness component within an element in the finite element division.

2.5.4 The approach of neural networks

Neural networks (NNs) are computing mechanisms made of a large number of simple, highly interconnected processing elements, which manipulate information by their dynamic state response to external inputs. One of the properties of the neural networks is its ability to learn and generalise from examples and to adapt with changing scenarios. NNs are able to map causal models - for estimation and prediction-, and inverse mapping -from effect to possible cause. In their design, NNs try to mimic some of the learning activities of the human brain.

The training process in NNS involves the presenting a set input patterns with known outputs. The system adjusts the weights of the internal connections to minimise the error between the network output and target output. A back-propagation network architecture is shown in figure 2.10. After the neural

network is trained, it is able to generalise rules being able to respond to input data to predict a required output.

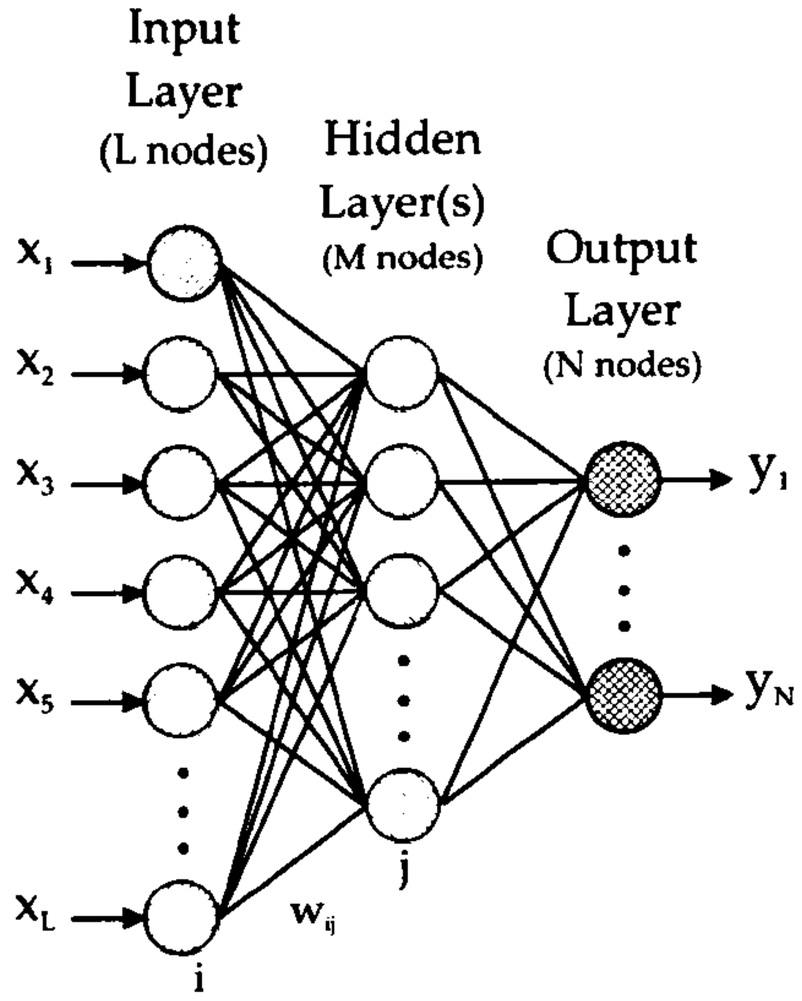

Figure 2.10. Three layer neural network.

The input, output and hidden layers have L, M, and N processing nodes respectively. The weight w_{ij} between nodes i and j is also shown. For a given input pattern $X = (x_1, x_2, \ldots, x_N)$ the output of the neural network is $Y = (y_1, y_2, \ldots, y_N)$.

Neural networks have been used in several knowledge areas like finance [96], civil engineering [97] and materials science [98]. Literature concerning neural networks and damage detection is overwhelming[7], thus this section details key research publications in this area.

2.5.4.1 Neural networks and damage characterisation

Wu et al. [99] investigated the problem of damage detection in a three-story frame when the structure was subjected to earthquake acceleration based on response spectrum data. The damage in the structure was represented by a percentage reduction in stiffness in one structural member, and the resulting Fourier spectrum of the acceleration time histories was used as input to a neural network with one hidden layer consisting of 10 neurons. They suggested that based on the generalization capability of neural networks, only

[7] At February 2004, a simple search in http://www.sciencedirect.com using the keywords "neural network and damage or crack or delamination' produced a list of 4633 articles.

several variations for damage state for selected key structural member may be sufficient in order to adequately train the neural network. However, they questioned the exact number of damage states that must be presented to the network before it gains adequate prediction performance.

Kudva et al. [100] studied the damage size and location in a sixteen bay aluminium-stiffened panel under uniaxial compression. The damage was modelled as circular holes of different sizes and at different locations. The neural network was trained using measured strain measurements at discrete locations from finite element analysis. And it was arranged using two hidden layers with forty neurons each; the hidden layers permit non-linear modelling of the input-output relationships. They found that it was easier to predict damage location than size, since location is a discrete variable and size output is a continuous variable. However, they stated that there were no established procedures for choosing the optimal number of hidden layers and neurons per layer.

Islam and Craig [101] investigated the delamination detection in composite beams using piezoelectric materials. The delamination was modelled as two beams, made of solid elements above and below the plane of delamination, and spring elements were used two connect the beams in the non-delaminated region and gap elements were used to connect the beams in the delaminated region. A back propagation neural network was trained with the frequencies of the first five modes obtained from model analysis data from piezoceramic sensors. The network architecture consisted of three layers with one hidden layer made off three neurons. They suggested that the back propagation algorithm was not well suited for numbers that are close together, so another method, fuzzy sets, could be needed to provide more information to the network.

Szewczyk and Hajela [102] studied the damage detection in planar and spatial truss structures. Damage was modelled by fifty percent reduction in the stiffness of the structural elements, and a modified counter propagation neural network was used to relate the stiffness of individual structural elements and the global static displacements under a test loads. The neural network was composed of one hidden layer where the learning of the neurons was based on the minimum disturbance principle. The authors found that counter propagation neural network function as a fast look-up table with generalization capa-

bilities and suggest that the performance of the networks decline gradually in the presence of noisy or incomplete input data.

Rhim and Lee [103] used a multilayer perceptron (MLP), a class of neural networks that can be used as a nearest neighbourhood classifier, for damage classification in cantilever graphite/epoxy laminate beams with delaminations. The damage was modelled divided the beam in two parts. Each part was modelled separately by beam elements and then assembled into a global finite element model. The models for structures with various damages were organised into pattern classes according to the location and severity of the damage, and a three layer MLP was trained with a conventional back propagation algorithm. The authors found that damage identification based on MLP technique was robust to measurement noise and distortion of input patterns.

Ceravolo et al. [104] studied the damage detection in a simply supported beam from structural responses to an impulse load applied to mid span. The damage was simulated through a constant reduction in the moment of inertia, and a two level hierarchical neural network was trained using the displacement and acceleration cross correlograms to identify a single fault in the structure. They suggest that a first level network could be used to estimate the severity of the damage on the basis of a statistical classification, and a second level network specialized in a particular type of damage identify the position of the fault by using mapping capabilities.

Okafor et al. [105] investigated the delamination size prediction in a composite glass/epoxy beam with built in piezoelectric sensors. The damage was modelled using the procedure developed by Islam and Craig [101]. A feed forward back propagation neural network with one hidden layer was trained with the first four model frequencies of the delaminated beam. They found that for the beams investigated, neural networks predicted dimensionless delamination size between 0.22 and 0.82 but under predicted sizes below 0.08.

Byon and Nishi [82] proposed a method to damage detection in a CFRP laminated beam using hierarchical neural networks. The damage in the beam was modelled as a partial reduction in the bending stiffness, and the natural frequencies and the third mode shape were obtained from a finite-element model.

The authors suggested that the third natural frequency mode is more sensitive to damage than the first or the second mode.

Tsai and Hsu [106] studied the damage detection in reinforced concrete structures. The damage was modelled by a reduction in material strength for concrete, and decreasing in the cross sectional area of steel members. The neural network was trained with the displacement time history of three degree of freedom separately. They suggested that the neural network could be used in two ways: Firstly in the so-called category identification the neural network was used to identify if the damage occurred in steel member or in concrete only, or both. Secondary the network was used to identify the damage machine condition in detail.

Ni et al. [107] proposed a methodology to design input patterns to neural networks, using a hierarchical identification strategy [104], for damage location and severity in a two-story steel frame affected with a reduction in rotational stiffness at a specific joint. A hierarchical neural network with one hidden layer was trained using the natural frequencies and a modal vector value of the frame. The authors found that when the damage location and extent were identified using independent networks with the same configuration of input and output patterns, the training efficiency was improved but the capacity to detect multi-damaged cases was less accurate.

Chang et al. [108] investigated the damage detection on a clamped-clamped reinforced concrete T beam. The fault was modeled as a reduction in the flexural bending of each element. An iterative neural network model with two hidden layers was trained with the first three natural frequencies and the first mode shape curvature changes. They suggested that the change of the mode curvature is a good indicator for damage identification. Also it is addressed that using orthogonal array to generate the combinations of input parameter changes could significantly reduce the number of training data.

Valoor and Chandrashekhara [109] extended the delamination prediction in composite beams by using model analysis of Okafor et al. [105] to damage detection in a thick composite beam that took into account the Poisson effect and the transverse shear deformation. They suggested that in symmetrical structures, the network could only predict the location of delamination in each sym-

metrical segment, although the incorporation of mode shapes was proposed as a solution to differentiate between locations.

Otieno et al. [110] presented an initial method for isolating fringes in shearographs of poor quality in order to detect and characterise damage in laminated composites. The methodology comprised the median filtering of the fringe patterns, and neural networks complemented by a fuzzy inference system were used to classify each image. The authors found that the classification accuracy was low when neural networks were used alone. However, shearograph images could be classified when the networks were combined with a fuzzy decision-making system.

Ishak et al. [111] studied the identification of interfacial delaminations in carbon/epoxy composite using the strip element method and adaptive multilayer perceptron networks. The strip element method was used to compute the theoretical dynamic responses of laminated beam composites containing a delamination that penetrates through the width of the beam, and these theoretical responses were used as the training data for a multiplayer perceptron network with two hidden layers. It was found by the authors that the proposed method predicts accurately the length of the damage. However, the neural network was not accurate to identify the location and depth of the damage.

Zapico et al. [112] presented a methodology to located and quantify damage in framed structure. Their approach used two neural networks to calibrate the undamaged structure, and to predict the damage respectively. Damage in the structure was modelled as a reduction in the effective elastic modulus of the affected element in the frame. They found that neural networks predictions were accurate when the structure was either completely damaged or undamaged.

2.5.5 The approach of genetic algorithms

Genetic algorithms (GAs) are optimisation techniques based on the concept of natural selection and genetics. A comprehensive reference of the nature and use of them can be found elsewhere [113–115]. GAs are designed to exploit efficiently large, non-linear, and highly complex search spaces where traditional gradient-based methods may fail. Figure 2.11 shows the fundamental structure of the genetic algorithm.

First, a population of individuals is randomly generated. The population then evolves toward better regions of the search space by means of process of selection, crossover and mutation. During the selection step, couples of parents are chosen from base population according to their fitness. In the crossover step, parent individuals breed offspring's individuals by combining information from parent individuals. The mutation forms new individual by making large alteration with small possibility to the offspring individuals regardless of their inheriting information. With the evaluation of fitness for all individuals, the selection favourably selects individual of higher fitness to reproduce more often that those of lower fitness. These reproductions form a new generation of the evolutionary process. The previous steps are repeated until a given terminal criterion is reached.

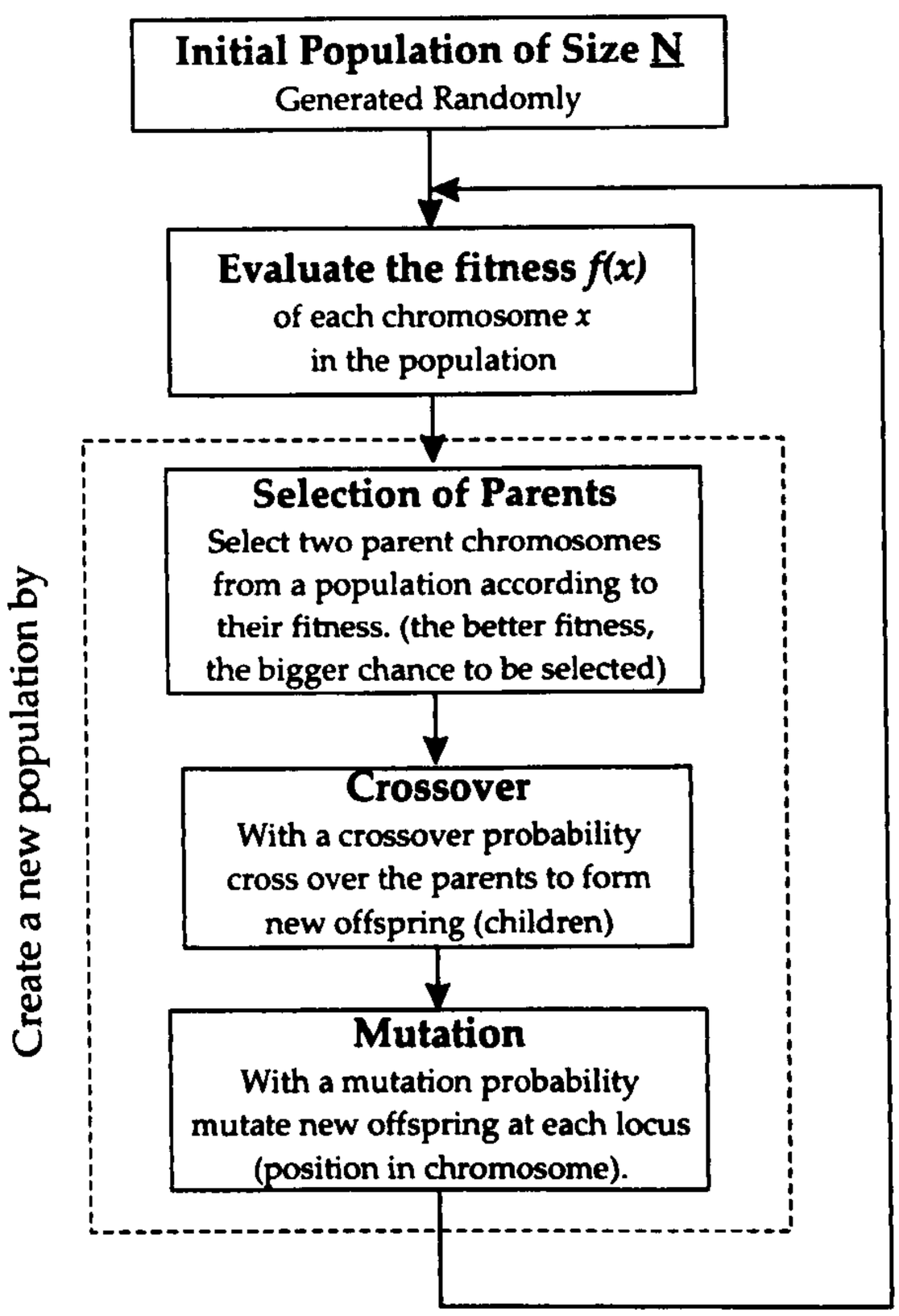

Figure 2.11. A basic genetic algorithm.

The four stages in every genetic algorithm are: generation of a new population, selection, crossover, and mutation

Genetic algorithms have been used in different areas of science and engineering. Roth and Levine [116] used GAs for extracting geometric primitives[8] from geometric sensor data. In their study they compared the performance of GAs versus random sampling. They found that the more complex the geometric sensor data, the better the GA performed in comparison to random search. Doyle [117] developed a GA-based force location method on aluminium beams. He proposed a new genetic algorithm where the position of the impact on the beam was encoded as a real number. He found that GAs were computational inefficient to characterise the damage. However, he pointed out that this deficiency could be mitigated by using computers with multiple (parallel) processors. An implementation of Doyle's idea was performed by Oyama et al. [118]. They implemented an adaptive range genetic algorithm (ARGA) for three dimensional shape optimisation of aircraft wings in a parallel computer with 166 processors. They reported that the parallel implementation made a corresponding turnaround time almost 1/64 of the evaluation time taken by a single processor implementation (7000 hours).

During the last then years, interest in GAs have developed by the increasing advances in computer processing power, and moderately price reduction of workstations [1]. However, the availability of commercial GA software is somewhat limited, in particular due to the fact that GAs are problem specific, thus imposing on researchers the need for coding their own algorithms. In structural engineering, GAs have been used for two main areas: structural optimisation [119–123] and damage characterisation. The following subsection covers published research in the latter area.

2.5.5.1 Genetic algorithms and damage characterisation

To identify location and depth of flaws in structures, researchers have used several minimisation techniques to optimise the difference between on-site testing measurements and proposed mathematical models that describe the structure. Typical minimisation techniques include gradient-based algorithms, ge-

[8] A geometric primitive is a curve or surface which can be described by an equation with a number of free parameters.

netic algorithms, and neural networks. In the present subsection, literature concerning GAs and damage characterisation is presented.

Cracks that occur in structural elements causes local variations in its stiffness that affects the static and dynamical behaviour of such structures [31]. Researchers trying to locate the depth and position of such cracks have used GAs to characterise structures' material stiffness as a way to reveal damage. Suh and Shim [124] used a GA to characterise cracks in clamped-free beams. In their approach, the difference between the eigenfrequencies of the real and finite element model (FEM) of the beam was minimised. They showed that this approximation produced accurate stiffness predictions with an error estimated within 5 percent. Krawczuk and Ostachowicz [125] performed a similar study where they took into account the depth of the crack. They showed that the depth of the crack did not have any effect on the accuracy of the characterising technique.

He et al. [126, 127] characterised cracks in rotor-bearing systems. In their approximation, location, depth and arc length of cracks in rotating shafts were the variables to reveal. They found that the depth of the crack was the factor that presented less accuracy with an error estimated in 12 percent. Liu and collaborators [128, 129] studied flaw characterisation in sandwich plates. They modelled the damage as a reduction in percent in the elastic modulus of the sandwich's core. They found that their algorithm did not predict accurately the area of damage, and instead of giving a unique solution for the problem, their algorithm generated a number of candidates for damaged elements in the core.

Sherrat el al. [130] presented a novel approach to characterise progressive-tearing in box-sectioned composites that were subjected to impact events. They suggested that genetic algorithms might be better suited for the application at hand, because of the discrete nature of the damage parameters to identify (the number of elements in a FE mesh that exhibited cracks). Xia and Hao [131] studied damage detection in portal frames. Their method was based on the fact that structural damage causes changes in the vibration characteristics of a frame (frequencies, mode shapes and modal damping). They found that er-

rors existing in the measured mode shapes of the structure produced highly inaccurate results in the prediction of damage location.

2.6 State of the Art - David Panni's Research

This section presents the results of the research performed by Panni [1, 132]. His work is the most relevant to this thesis as he was one of the first researchers to investigate the characterisation of delamination in carbon fibre panels by using optical interferometric data.

Panni, in his PhD thesis, proposed a generalised approach to integrate simulated displacements from DSPI with a finite element model to characterise a single delamination in carbon fibre panels. The core of the solution method was the development of an integrated finite element model - genetic algorithm tool for the automatic recognition of delamination. Panni's method exploited the bulging phenomenon that occurs on the surface of a delaminated panel when placed in a vacuum chamber (figure 2.9a and 2.9b). He argued that the bulging is a consequence of a pressure differential between air trapped inside of the delamination, and the negative pressure inside of the vacuum chamber.

Panni suggested that the characterisation method should not assume a-priori the shape of the delamination. As a consequence, in his theoretical model, delamination footprint was defined in terms of pixels that allow the representations of generic shapes as is shown in figures 2.12a and 2.12b. It was argued that the advantage of this type of modelling is the use a single finite element mesh to study multiple delaminations shapes.

2.6.1 The finite element model

Panni proposed a method that assumed that a FE model of a delaminated panel in a vacuum chamber might be represented using the sub-structure approach[9], using a single layer of composite shell elements (LUSAS QTS8) as is shown in figure 2.12c. The entire area of the panel was discretised into a 16x16 mesh of elements, mimicking the pixelated output from the DSPI technique as is shown in figure 2.12d. It was suggested that this type of modelling pre-

[9]The sub-structure approach is discussed in subsection 2.2.3.4.

sented the best compromise between the ability to resolve delaminations (with circular shape) and the reduction in the computer power required by the characterisation technique.

Panni suggested that any shape of delamination or combination of delaminations in composite plates may be represented by assigning each element in the mesh to one of two sates - delaminated or not delaminated. Thus in the FE model, each node in the mesh was assigned a boundary conditions in terms of either force (delaminated) or a zero displacement (not delaminated).

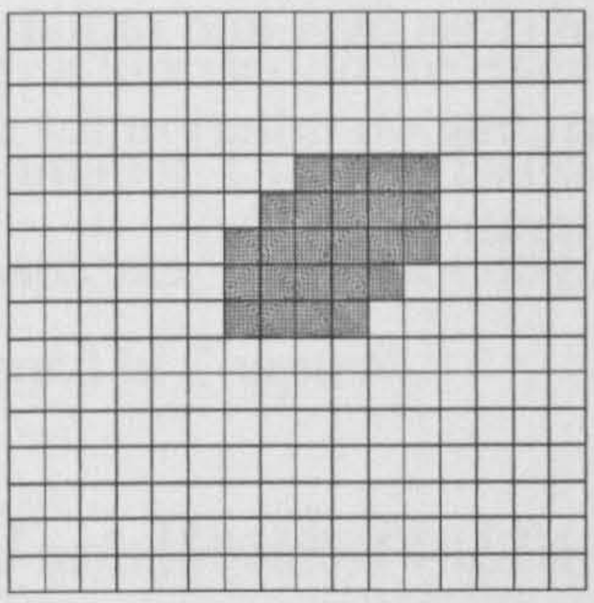

Figure 2.12a. Pixelated representation of an elliptical delamination in a 16 x 16 bitmap grid.

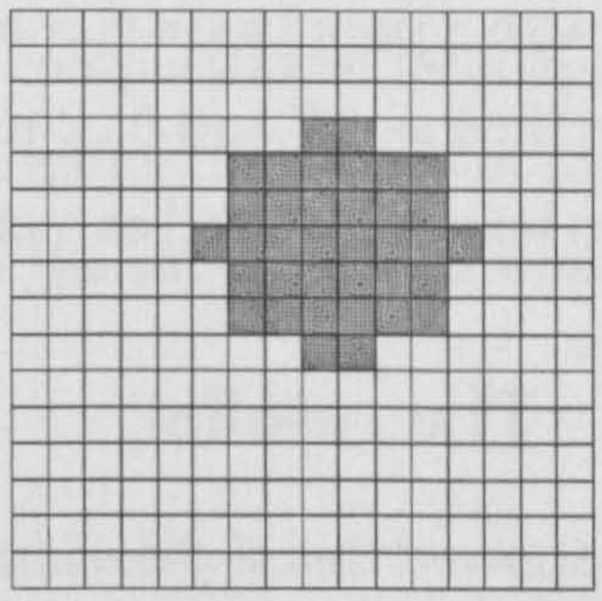

Figure 2.12b. Pixelated representation of a circular delamination in a 16 x 16 bitmap grid.

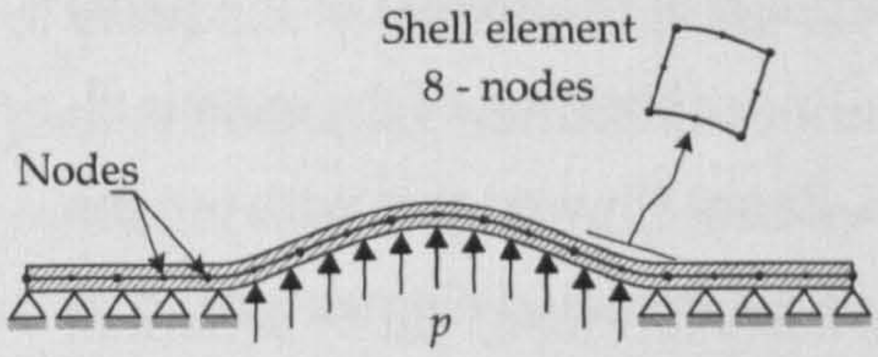

Figure 2.12c. Section through reduced thick FE shell model used by Panni to simulate a delamination in carbon-fibre panels. This model can be classified as a substructure delamination modelling.

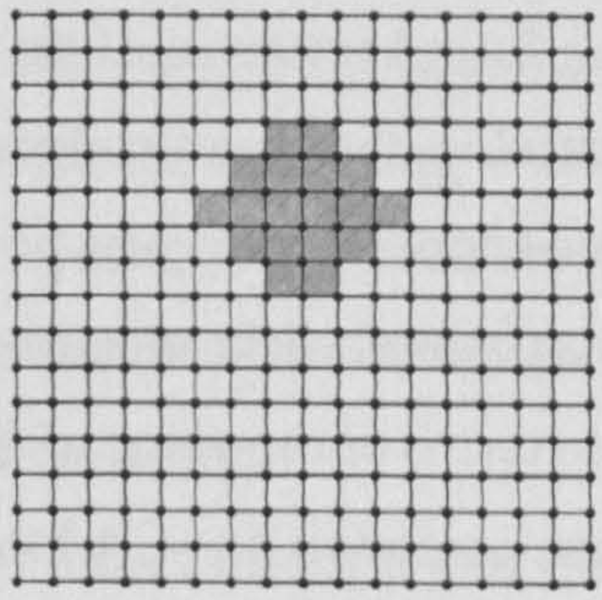

Figure 2.12d. Top view of the FE model proposed by Panni. It is possible to appreciate the pixelated representation of the delamination.

2.6.2 The genetic algorithm

Panni developed a binary coded genetic algorithm were every delaminated stated was represented by an array of 257 elements, 256 of them representing the delaminated/not delaminated state of every node in the 16x16 mesh, and the last location representing the depth of the delamination as an integer. The fitness of each model was determined by how accurate it minimises the objective function representing the difference between the simulated DSPI data and the response from the FE model.

The proposed genetic algorithm operated on an elitist, single point crossover strategy with a population size of 25. Probabilities of cross over and mutation were specified as 0.7 and 0.02 respectively. The termination criterion for the algorithm was established as a prefixed number of iterations (400).

2.6.3 The results

Panni showed that if the shape of the damage was fully resolved, then the depth of the delamination was found with total accuracy. In fact, even if the genetic algorithm did not converge to a good solution, the shape and approximate size of the delamination were resolved with some accuracy. Critical problems were found in terms of the amount of a-priori knowledge needed to be incorporated in the genetic algorithm. Some of the information required for a successful convergence was both the specification of the area(s) of the panel that did not contain delaminations, and the on-line calibration of the genetic algorithm in terms of the value of its parameters. Panni showed that with out the previous information, the GA located erroneous delaminated elements beyond the closed boundary of the flaw.

2.7 Summary and Conclusions

During the past forty five years, the use of composite materials have expanded to many applications, including aircraft, automotive and aerospace structures, and many other products. Unfortunately, the manufacturing process and the in-service operation of composites may result in the presence or introduction of unwanted defects and damage.

Although much research has been done to date, it is clear from the literature that more studies need to be conducted to characterise delamination in composite panels. In particular, to reduce the gap in the understanding in the simulation of composite debonding through finite element analysis, and inverse techniques based on neural networks and genetic algorithms to locate and size delaminations. Delamination characterisation is not only an industrial interest but also an academic one. The future development of aerospace, automotive and many other industries rely on the understanding of failure modes and the assessment of structural integrity.

The ultimate objective of this chapter was to solve the research question one, which addressed to the state-of-the art of both computational techniques for delamination characterisation, and DSPI for detection of damage in composite materials. The following paragraphs answer the sub-questions what were designed in Chapter 1.

2.7.1 Research Question 1

Delamination modelling techniques Historically two main approaches have been used to model delamination in composite laminates: the classical laminated plate theory and the theory of elasticity. The former was deprecated during the 80's as a consequence of (a) its inability to predict accurately the shear stresses in the interface of the laminate and (b) the increasing availability of computer power during the early 70's, that opened the possibility to implement complex numerical routines needed to calculate the solutions of the constitutive equations provided by the theory of elasticity.

Solutions to the theory of elasticity have been found through two different approaches: Finite Differences (FD) and the Finite Element Method (FEM). Finite differences have been used to solve problems of stress and strains in laminates, however it lacks the flexibility of FEM to deal with complex laminate shapes. Research on modelling of delamination since 1980 has included, as a general rule, some form of finite element simulation.

To date, finite element models of delamination take advantage of three important conclusions derived from the studies on low-velocity impact during the 70's and 80's: Firstly, delamination represents a major component of dam-

age that evolves accordingly to a definite pattern. Secondly, delamination is present either at interfaces between plies with different fibre orientation or at the edges of composite panels. Finally, if delamination is present, the debonded area has an elliptical or peanut shape. The precise shape of the delamination is dependant on the number of crack in the panel. If a single crack is present then the delamination is elliptical in shape.

Literature concerning the modelling of delamination through the FEM can be classified in four groups accordingly to the type of interface used between the delaminated and base regions. They are the hybrid element interface, de-equivanlenced crack, degraded inter-laminar layer, and sub-structure.

In the hybrid element interface technique, both sub-laminates are connected through a combination of spring and beam elements. It has been successfully used in studies of low-velocity impact. However, a major drawback in its implementation is the dependency between the size of the delamination and the coarseness of the FE mesh. Another disadvantage is that the solution of the FE model requires large amounts of CPU time. The de-equivalenced crack technique has been used to model buckling in composite laminates where there are not overlapping between the sub-laminates. Researchers using this technique have reported a good agreement between the predictions of the FE model and experimental measurements.

The degraded inter-laminar layer model is the most simple of all the models. However, it is the one with less agreement with experimental data. In this technique, the delamination is simulated through a reduction in the elastic properties of the elements that are just beneath of the delaminated region. The last technique is labelled as delamination as sub-structure where the model include only the delaminated region. This is the most cost-effective technique in terms of CPU solution time; however, there is not research available on the evaluation of the performance of this model against experimental data.

Digital Speckle Pattern Interferometry (DSPI) This is an experimental technique that has been proved to be capable for precise measurements sensitivity of the order of the wavelength of light from diffusely scattering objects. DSPI produces real-time fringe patterns that typically represent contours of

constant displacement component depth. However, fringe patterns provide visual information to the trained eye, but they are generally noisy. Loss of accuracy in the technique is due to systematic and random errors.

Systematic errors appear form the effect of higher harmonics , miscalibration and vibration. Higher harmonics can be produced for non-linearities in the detector array. Miscalibration represented by a poor alignment of the device or motion of the specimen while the experiment is being carried. Vibration and other environmental disturbances such air currents can cause significant errors. Random errors are introduced due to variations of the laser output power or electronic noise in the detector camera.

Researchers using DSPI to detect delamination in laminates have found that small and deep delaminations are difficult to detect if the sensitivity of the system is poor, or there is not strict control on the pressures inside of the vacuum chamber.

Compact representation of DSPI data The theory of two dimensional moments is a paradigm that is widely used by researchers on pattern recognition. By using moments, it is possible to reduce large sets of experimental data into small arrays containing the convolution of the experimental data with a suitable base-function family. Two types of moments are commonly used by researchers: Zernike and Geometric.

Zernike moments appeal researchers by their properties like orthogonally, rotation invariance, robustness to moderate levels of noise, and efficiency in terms of the non-redundancy provided by lower order moments. However, some of these properties make them not useful to characterise damage. Zernike moments contain information about an image hath is independent of the size, planar position and relative angular orientation.

On the other hand, central geometric moments offer attributes that make them attractive to be used in the characterization of delamination. Firstly, they are sensitive to the location of the crack that is given by the equation 2.3. Secondly, this type of moments are sensitive to the size of the image that are representing. Finally, the orientation of the flaw can be discriminated using CGM,

because these moments are function of the angle of orientation of the features of the image.

Characterization of damage Progress has been made to understand and identify the damage of truss structures. Some authors suggested that the static load distribution in the structure affects the damage detection, and indicated that although structural damage is non-linear in behaviour, the use of loads of small magnitudes result in structures behave only in their elastic ranges. It was showed also those standard modal properties such as resonant frequencies and mode shapes are poor indicators of damage, and consequently the methods studied were inconsistent and did not clearly characterise the damage location.

Having developed an understanding for damage identification in truss structures, researchers have turned their attention to characterise flaws in composite materials. It has been found that the damage detection using structural waves is sensitive to manufacturing tolerances, decreasing its applicability in problems where exist input noise from uncertainty in geometrical properties. Also it has been showed that for damage detection based on strain flexibility methods failed to locate damage in some elements.

The findings of studies examining the use of neural networks and genetic algorithms in composite panels have been mixed. It was stated that it was easier to predict damage location than size due to location is a discrete variable and size out put is a continuous variable. However, there were no established procedures for choosing the optimal number of hidden layers in neural network architectures, or for choosing the operators and its values in genetic algorithms. Also it has been mentioned that the performance of both neural networks and genetic algorithms decline gradually in the presence of noisy or incomplete input data and they were not accurate to identify the location and depth of the damage. Moreover, studies using genetic algorithm using experimental data have not provided accurate predictions of damage in terms of shape, size and position. Of the two approaches, genetic algorithms offers some advantages when used it in-service where the exact nature of laminate lay up, and materials properties is not known *a-priori.* This is due to the fact that genetic algorithms operate on mathematical models that can be updated on-line. As

a consequence, any variation in the physics of the modelled process can be incorporated into the genetic algorithm as a change in one of its variables.

Genetic algorithms have shown to be effective at searching large domains for a global optimal point by sampling a small fraction of the total solution space. This ability has made them attractive for researchers working in the solution of inverse problems and optimisation.

Latest research on characterisation of delamination in composites The latest and closest research linked to this thesis was performed by David Panni at Loughborough University (2002). Panni developed a general method to integrate a FE model with genetic algorithm in order to design and optimise composite structures. As an extension of his research, he showed that at, least theoretically, is possible to characterise delamination in laminates. He showed that if the shape of the delamination could be fully resolved, then the depth of the delamination was found with total accuracy. Panni concluded that problems in his model existed in terms of the *a-priori* knowledge needed to be incorporated, like for example the areas of the laminate that did not contain delaminations, and the on-line calibration of the genetic algorithm in terms of the value of its parameters.

Chapter 3

A FINITE ELEMENT MODEL FOR EMBEDDED DELAMINATION

Abstract The basic approach to the characterisation of delamination is the parameterisation of the expected flaws. It is proposed that an embedded delamination can be approximated as an elliptical-shaped crack with by six parameters: the coordinates of the centre in the plane of the laminate, the length of the delamination, the width of the flaw, the angle of orientation, and the depth below the measured surface of the laminate. Also, it is proposed that from a computationally point of view, a delamination can be introduced in a finite element (FE) mesh using the sub-structure technique. Finally, the interpretation of the integro-differential equation that relates the out-of-plane displacements on the laminate during a DSPI test, and the pressure of the air trapped in the delamination is presented.

3.1 Introduction

Computational modelling of delamination requires a compromise between two (often conflicting) objectives (a) effective representation of the damage, and (b) rational use of CPU time to solve the numerical model. Firstly, the numerical model must reflect accurately the geometry and physics of the damage. Geometrically, a delamination is an irregular but it can be idealized as elliptical in shape [12–15]. Physically, delamination is a separation of the individual plies in a bonded structure, which has been modelled using four different approaches: hybrid element interface [19, 20], de-equivalenced crack [21, 22], degraded inter-laminar layer [23, 24], and sub-structure [26, 1]. Secondly, the computational model must be cost-effective. In terms of the modelling technique, it was showed in Chapter 2 that FE analysis is the favoured tool used by researchers in the field. Then, in order to optimise the solution time taken

by the FE model it is necessary to make a trade-off between resolution of the mesh, and the accuracy of the expected results.

An additional factor to take into account during the modelling of delamination is the scope of the model. For example, to simulate low velocity impacts in a laminate the hybrid element interface technique is the best choice in terms of the physics of the problem, but this choice may not be the best one when modelling buckling of laminates. In the context of this research, the finite element model to be designed is constrained by the experimental technique used to detect the damage, in this case DSPI. In the literature only a few researchers have tried to close the gap between delamination modelling and DSPI [1].

Although much research on modelling of delamination has been done to date, it is clear from the literature that more studies need to be conducted to design a cost-effective FE model that can be used to simulate the behaviour of delamination in the context of the DSPI technique.

3.2 Problem Statement

In order to ascertain the presence of delamination in a composite panel using the DSPI technique, the laminate is placed in a vacuum chamber at atmospheric pressure $P_{atmospheric}$, as shown in Figure 3.0a. Once the chamber is completely sealed, the main vacuum pump is activated until the chamber reaches a reference pressure $P_{chamber}$ (Figure 3.0b). If the laminate contains a delamination, the DSPI device may detect the bulging effect that is produced as a consequence of the pressure differential that exists between the pressure in the chamber and the pressure of the air trapped inside of the delamination. Provided that a DSPI device with high sensitivity is used, the output of the technique is an array of measurements that corresponds to the out-of-plane displacements of the surface of the laminate between the deformed and the non deformed state. Figure 3.1 shows a typical DSPI post-processed output from a delaminated panel in the conditions described above.

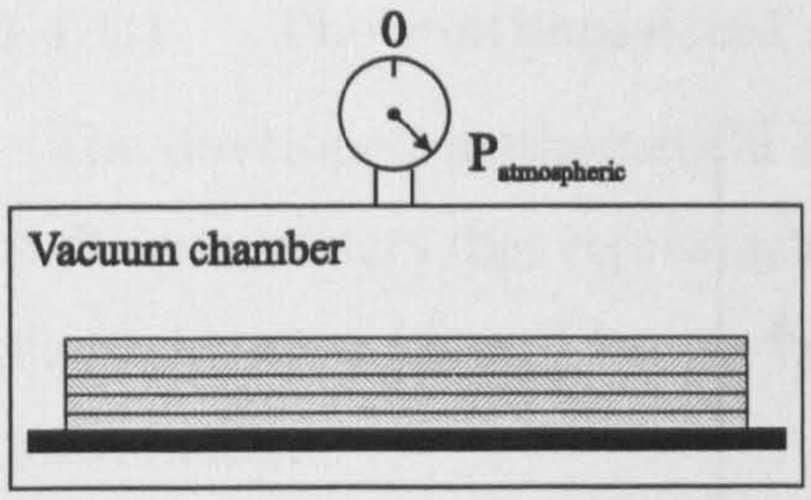

Figure 3.0a. Laminate in a vacuum chamber when the chamber is not in operation.

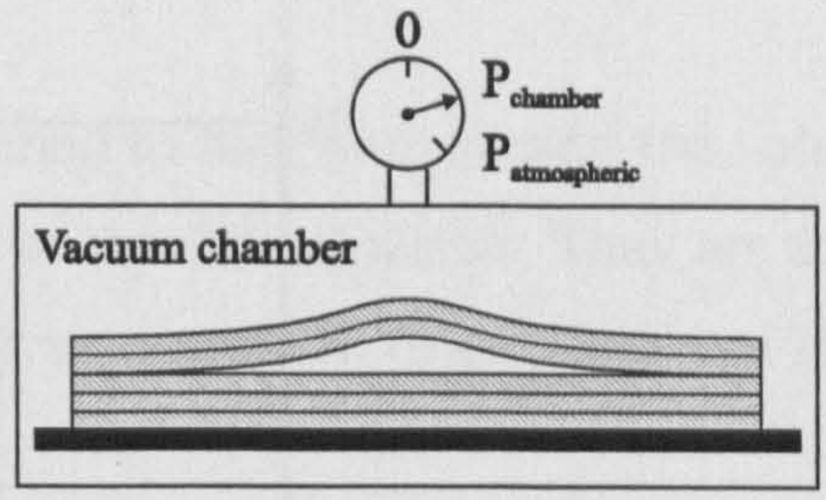

Figure 3.0b. Laminate in the same chamber when a vacuum pressure $P_{chamber}$ is applied. Note the bulging effect.

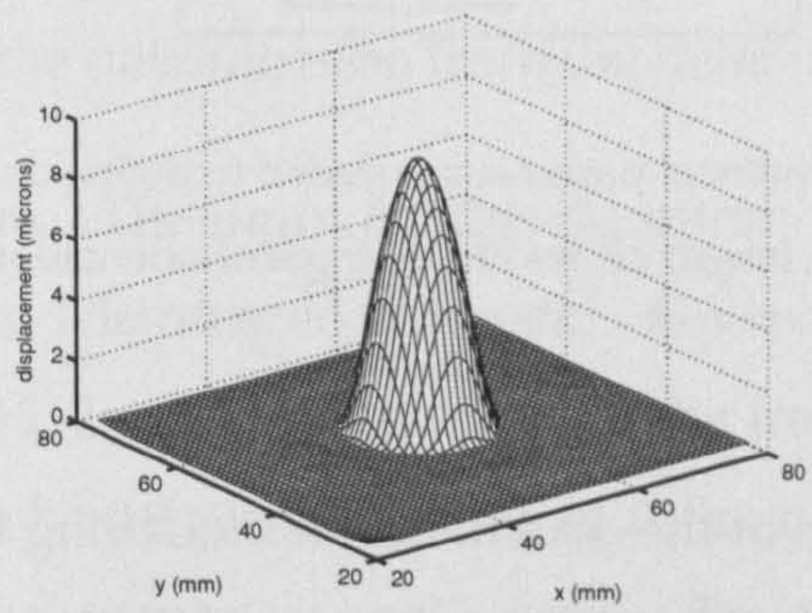

Figure 3.1. Typical out-plane-displacements field obtained from a carbon fibre panel with a circular delamination.

3.3 Objectives and Research Questions

From the previous paragraphs is clear that there is a need for a delamination modelling technique that can be applied in the context of optical interferometric experimental techniques. The main objective of this chapter is stated as:

Given the bulging effect that experiences a delaminated composite panel during a DSPI experiment, design a FE model that simulates accurately the physics of the problem.

This objective can be satisfied if the following research questions are solved:

1 **Subquestion A:** How can an embedded delamination be modelled mathematically in geometrical terms? (Parametric issues).

2 **Subquestion B:** What is the ideal configuration of a FE mesh to represent delamination? (FE resolution) .

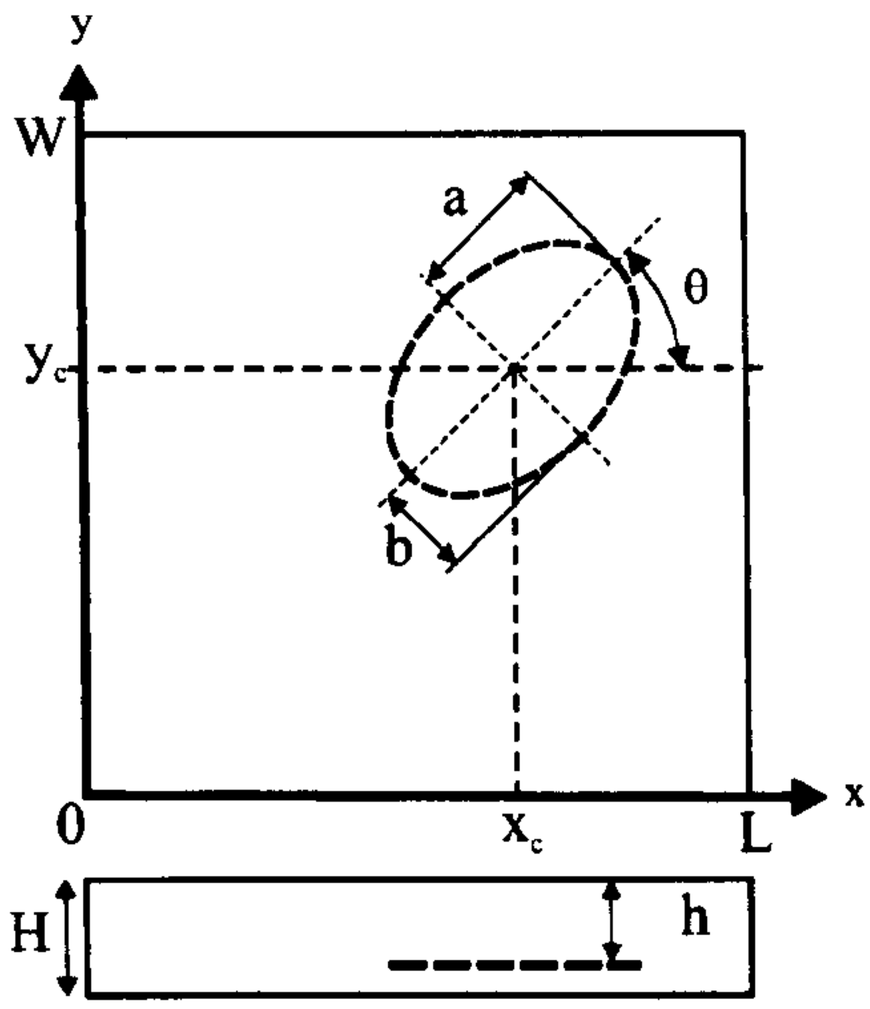

Figure 3.2. Geometrical parameters needed to define delamination. Planar location (x_c, y_c), length $2a$, width $2b$, angle of orientation θ, and depth h.

3 **Subquestion C:** Which of the delamination modelling techniques available in the literature describes better the physics of the problem at hand? (Delamination modelling).

4 **Subquestion D:** What are the boundary conditions for this problem.(FE constrains) .

The following section details the methodology and experimental setup used to solved the previous research questions.

3.4 Methodology and Experimental Setup

3.4.1 Subquestion A

A mathematical model was developed for the geometrical definition of delamination (shape). The model is based upon the previous studies (Chapter 2) that conclude that a delamination can be idealized as elliptical in shape which implies that the flaw can be represented by six parameters: (1,2) the planar location (x_c, y_c), (3) length $2a$, (4) width $2b$, (5) angle of orientation θ, and (6) depth h, as is showed in Figure 3.2.

3.4.1.1 The mathematical model

The developed mathematical method aimed to find numerically the value of the parameters that represent the shape of the delamination. They are the planar location (x_c, y_c), length $2a$, width $2b$, and angle of orientation θ of the delamination.

The mathematical model is divided in two parts. The first part uses the laplacian and the variance of the surface displacement, like the one shown in Figure 3.1, to detect the borders of the bulge. The second part of the model uses a second order minimization method to calculate numerically the planar position and shape of the delamination from the detected edges.

Detection of borders The input for the algorithm is the out-of-plane displacement field from a delaminated laminate[1]. Given the fact that DSPI provides an array of $512x512$ measurements, it can be treated as an image composed of the same number of pixels. Therefore techniques that are relevant in the context of image analysis can be applied here. The description of the model corresponds to the one presented in reference [133].

The first step in the analysis is to establish an upper limit for the surface displacement that are taken into account in the analysis. In the present development this limit was set (by trial and error) at 10% of the maximum surface displacement in the model.

The second step is to calculate the laplacian of the surface displacement field $z(x, y)$ using a finite difference formulation. The laplacian of $z(x, y)$ in position $(n1, n2)$ of the DSPI array is given by equation 3.1.

$$\begin{aligned} \nabla^2 z(n_1, n_2) &= z(n_1 + 1, n_2) + z(n_1 - 1, n_2) + \ldots \\ &\ldots z(n_1, n_2 + 1) + z(n_1, n_2 - 1) - 4 \cdot z(n_1, n_2) . \end{aligned} \tag{3.1}$$

In the same way, the variance of the laplacian is calculated using equations 3.2 and 3.3.

[1] In this chapter simulated out-of-plane displacements fields are used

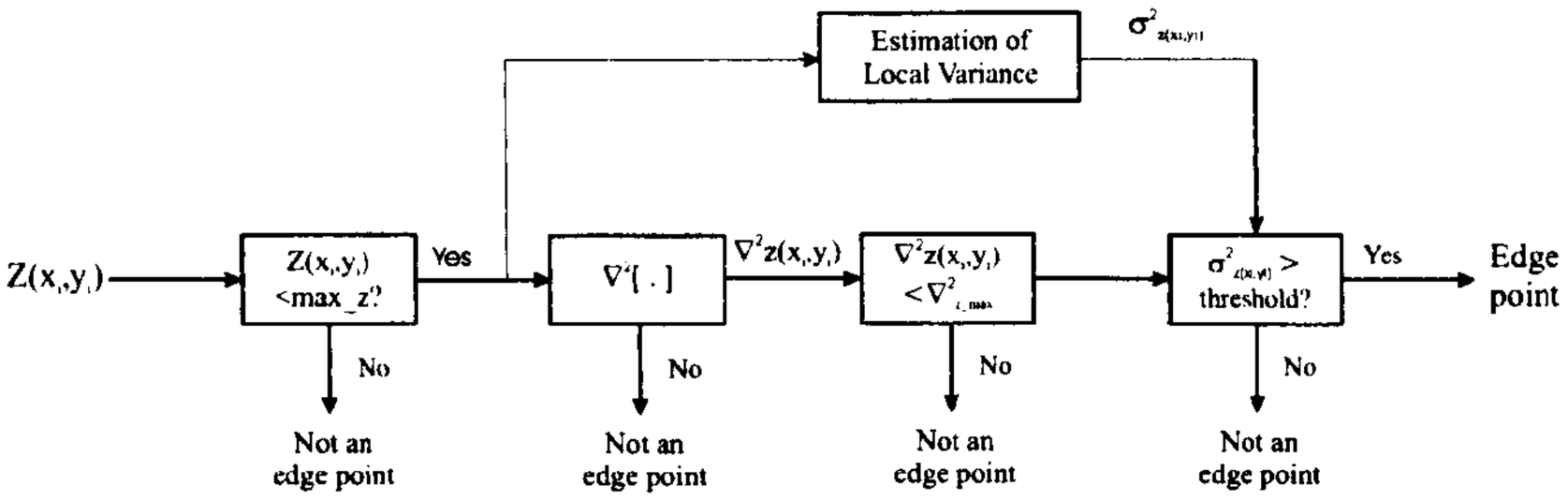

Figure 3.3. Edge detection algorithm.

It uses three main steps: the calculation of the laplacian and the variance of the laplacian from the image, compare the laplacian against a preset threshold, and finally compare the variance of the laplacian against a second threshold.

$$\sigma_z^2(n_1,n_2) = \frac{1}{(2M+1)^2} \sum_{k_1=n_1-M}^{n_1+M} \sum_{k_2=n_2-M}^{n_2+M} [z(k_1,k_2) - m_z(k_1,k_2)]^2, \qquad (3.2)$$

where,

$$m_z(k_1,k_2) = \frac{1}{(2M+1)^2} \sum_{k_1=n_1-M}^{n_1+M} \sum_{k_2=n_2-M}^{n_2+M} z(k_1,k_2) \quad with \quad M \approx 2. \qquad (3.3)$$

The third step in the analysis is to compare the laplacian of point $(n1, n2)$ with a pre-established threshold (0.95 by trial and error). If the laplacian is less or equal to the threshold then this point could be and edge of the delamination.

The last step consists in compare the variance of the laplacian in point (n1,n2) with a threshold (0.01 by trial and error). If the variance is less or equal to the threshold, then the point $(n1, n2)$ is an edge of the delamination. Figure 3.3 shows the flow diagram of the edge detection routine.

Calculation of elliptical parameters The elliptical damage can be described using polar coordinates as seen in Figure 3.4. For every point in the boundary (x_k, y_k), the equation of the ellipse is given as,

$$\sqrt{1-(1-\varepsilon^2)\cdot\cos^2(\zeta-\theta)}\cdot r_k = b \qquad (3.4)$$

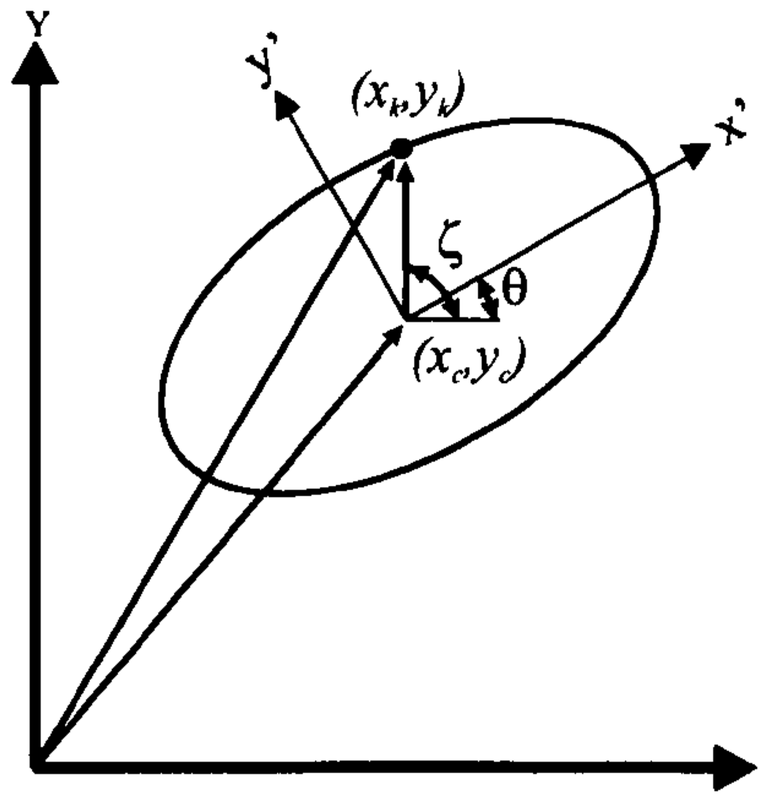

Figure 3.4. Geometrical parameters of an ellipse in polar coordinates.

In equation 3.4 ε is the relation between the width and length of the ellipse (b/a), ζ is the angle of the relative position vector as is shown in Figure 3.3. The magnitude of the vector from the centre of the ellipse (x_c, y_c) to the point (x_k, y_k) is r_k. If points (x_k, y_k) are not in the boundary of the delamination, then an error function for each point can be defined as,

$$\varphi_k = \sqrt{1 - (1 - \varepsilon^2) \cdot \cos^2(\zeta - \theta)} \cdot r_k - b. \tag{3.5}$$

In order to find the optimal values of (x_c, y_c), ε, θ and b in equation 3.4 a second order Newton-Raphson minimisation process [134] using the least squares methodology is implemented to solve an inconsistent non linear equations of the form:

$$\Gamma = \sum_{k=1}^{m} (\varphi_k)^2 \tag{3.6}$$

In which m is the number of points in the boundary of delamination. It is clear that if function $\Gamma = \Gamma(\theta, b, \varepsilon, x_c, y_c)$ possesses partial derivates of low order, then at any point $x = (\theta, b, \varepsilon, x_c, y_c)$ a gradient vector $G(x)$ is defined with components,

$$G_i(x) = \frac{\partial \Gamma(x)}{\partial x_i}, \tag{3.7}$$

and also is possible to define a Hessian Matrix $H(x)$ with components,

$$H_{ij}(x) = H_{ji}(x) = \frac{\partial^2 \Gamma(x)}{\partial x_i \partial x_j}, \tag{3.8}$$

where $G(x)$ is a vector of five components and $H(x)$ is a $5x5$ matrix. Using the gradient and the Hessian matrix, it is possible to write a quadratic Taylor series for Γ in the following manner,

$$\Gamma(x+h) = \Gamma(x) + G(x)^T h + \frac{1}{2} h^T H(x) h. \tag{3.9}$$

To find the minimum of the quadratic function in equation 3.9 it is necessary calculate the first partial derivates with respect to *hi* and equate them to zero. The result is expressed as,

$$H(x)h = -G(x). \tag{3.10}$$

The convergence of the second-order Newton-Raphson method is very fast if the initial search point of the algorithm $x_o = (\theta_0, b_0, \varepsilon_0, x_{c0}, y_{c0})$ is close the global minimum, that is the case of this work

The second-order Newton-Raphson method enjoys a certain amount of popularity between researchers because of its fast convergence in a sufficiently small neighbourhood of the global minimum value. Convergence is quadratic, which means that the number of significant digits double after each iteration. In comparison, the convergence of Steepest Descent method is at best linear and for the Conjugate Gradients method it is superlinear [135].

The following is the iterative procedure for locating a minimum point of the function Γ:

1 Start with a point $x_o = (\theta_0, b_0, \varepsilon_0, x_{c0}, y_{c0})$ that is an estimate of the minimum point.

2 Compute the gradient and Hessian matrix in the point x_o.

3 Solve the matrix equation 3.10.

4 Find the error in the analysis as the norm l_2 of h.

5 If the error is lower than a prescribed criteria (0.0001), then x_o is the minimum point.

6 If the error is not lower, then calculate $x_o = x_o + h$ and return to step 1.

3.4.1.2 Numerical implementation

Three simulated DSPI out-of-plane displacements[2] were used to verify the mathematical model outlined above. The first model corresponded to results from an embedded circular delamination with radius 15 *mm*, planar location (x_c, y_c) equal to $(37.5, 37.5)$ *mm*. The second model used results from an elliptical delamination, with parameters $(2a, 2b)$ equal to $(40, 20)$ *mm*, θ equal to 90 degrees, and planar location (x_c, y_c) equal to $(37.5, 37.5)$ *mm*. The third model contained an elliptical delamination with same length, width, and planar location of model two, with θ equal to 45 degrees.

The mathematical model was implemented in MATLAB 5.3, and was solved in a DELL Inspiron 8100 Pentium III computer. The source code of the implementation is included in the CD room that is attached to this thesis under the directories tree */SRC/Border Detection/*.

3.4.2 Subquestion B

The goal of this question was to study the effect of the type of meshing on the representation of delamination by comparing the two possible paradigms that can be applied, either mapped or free meshing. Effective representation of an idealized elliptical delamination can be met if the model satisfies two basic rules: (1) a detailed representation of the boundary, and (2) a refined mesh in the zones of high gradients, which is inside of the flaw boundaries in the case of the work reported in this thesis.

The problem is then to think about whether a mapped mesh or a free mesh satisfies the rules presented above. A free mesh has no restrictions in terms of element shapes, and has no specified pattern applied to it.

---

[2]The procedure used to generate these simulations is the one presented in reference [1].

On the other hand, a mapped mesh is restricted in terms of the element shape that it contains and the pattern of the mesh. A mapped area mesh contains either only quadrilateral or only triangular elements, while a mapped volume mesh contains only hexahedron elements. Additionally, a mapped mesh typically has a regular pattern, with obvious rows of elements.

To tackle the problem, the procedure followed in this thesis consisted in represent delamination using both paradigms of meshing, and then both models were evaluated by comparing only their ability to do an effective representation of the flaw. The following paragraphs describes the details of the methodology that was used.

3.4.2.1 Basic assumptions

It is assumed that the parameters of the damaged region are planar location (x_c, y_c), length of delamination $2a$, with $2b$ and angle of orientation θ, that these parameters satisfy the following restrictions:

1 The length of the delamination $2a$ (parallel to x' in Figure 3.4) is equal or greater than the width $2b$. If a penny shaped delamination is desired, then $a = b$.

2 The coordinates of the centre of the delamination in the plane of the laminate, (x_c, y_c), must be inside the area of the panel.

3.4.2.2 Mapped meshing

A two dimensional model of a typical mapped meshing is shown in Figure 3.5. This mesh is composted of 100 quadrilateral elements. On top of the mesh, a contour of the delamination that the mesh intends to represent is plotted. Clearly, the problem in here is how determine the nodes that lie both on the boundary and inside of the flaw. Of course, it is arguable that a densely populated mesh would represent properly such boundary. However, the main counter-argument is that the solution time of a FE model increases approximately with the cubic power of the number of the elements that are contained in the mesh [136].

In order to determine the nodes of the FE mesh that define the delamination, the following methodology is proposed.

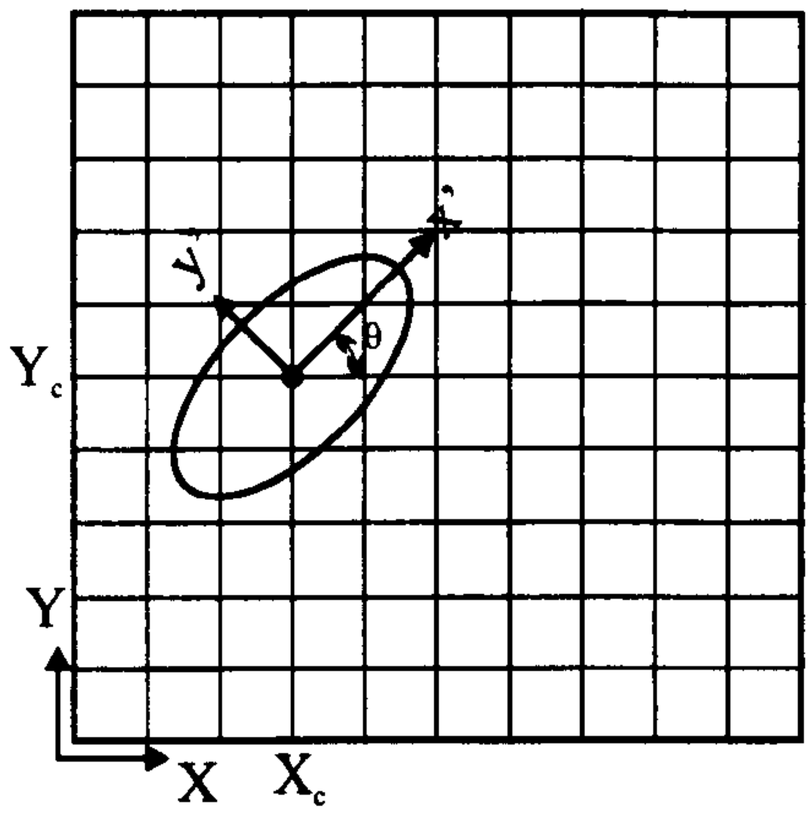

Figure 3.5. Two dimensional model of a mapped mesh of a model containing an elliptical delamination.
The shape of the delamination is shown on top of the model.

Nodes belonging to delaminated area In the rotated (local) system of coordinates (x', y') showed in Figure 3.5, the boundary of the elliptical damage could be represented using the following equation,

$$\frac{x_i'^2}{a^2} + \frac{y_i'^2}{b^2} = 1. \tag{3.11}$$

In the global Cartesian system of coordinates (X, Y), the boundary of the damage, expressed in equation 3.11, could be stated as,

$$Ax^2 + Bxy + Cy^2 + Dx + Ey + F = 0, \tag{3.12}$$

where x and y are defined in the following way,

$$\begin{bmatrix} x \\ y \end{bmatrix} = \begin{bmatrix} \cos\theta & -\sin\theta \\ \sin\theta & \cos\theta \end{bmatrix} \cdot \begin{bmatrix} x' \\ y' \end{bmatrix} + \begin{bmatrix} x_c \\ y_c \end{bmatrix}. \tag{3.13}$$

Equation 3.13 establish a relationship between the local system of coordinates (x', y') and the global system of coordinates (X, Y). Nodes that are inside of the oval area satisfy so-called *belonging criteria*. This criteria establishes that

a node i in position (x_i, y_i) in the global system of coordinates belongs to the delaminated area if the following statement is true.

Given, (x_c, y_c) in (X, Y), (x_i, y_i) in (X, Y), and θ, if $F(x_i, y_i) \leq 1$ then the node i in position (x_i, y_i) belongs to the delamination.

In the above statement $F(x_i, y_i)$ is given by equations 3.14 and 3.15,

$$F(x_i, y_i) = \frac{x_i'^2}{a^2} + \frac{y_i'^2}{b^2}. \tag{3.14}$$

$$\begin{bmatrix} x_i' \\ y_i' \end{bmatrix} = \begin{bmatrix} \cos\theta & \sin\theta \\ -\sin\theta & \cos\theta \end{bmatrix} \cdot \begin{bmatrix} x_i - x_c \\ y_i - y_c \end{bmatrix} \tag{3.15}$$

Numerical implementation In order to show the ability of mapped meshes to represent elliptical delamination, three numerical examples were developed as follows:

1 In this example, the objective was to introduce a penny shaped delamination with a radius of 16.5 *mm* in a finite element mesh composed of 100 elements. The centre of the delamination (x_c, y_c) was $(37.5, 37, 5)$ *mm*. The length of the sides of the laminate were fixed at 80 *mm*.

2 In this example, an elliptical shaped delamination with a length of 40 *mm*, width of 20 *mm* and angle of ration of 45^o was inserted in the same conditions of example one.

3 In this example, In this example, an elliptical shaped delamination with a length of 40 *mm*, width of 20 *mm* and angle of ration of 45^o was inserted in a finite element mesh composed of 100 elements. The centre of the delamination (x_c, y_c) was $(20, 30)$ *mm*.

The mathematical model was implemented in MATLAB 5.3, and was solved in a DELL Inspiron 8100 Pentium III computer. The source code of the implementation is included in the CD room that is attached to this thesis under the directories tree */SRC/Belonging Criteria/*.The master file is *DETECTION.m*.

3.4.2.3 Free meshing

A free mesh is designed in order to insert parametrically a delamination in a FE mesh. At first sight, there should not be much difference between a mapped mesh and a free mesh. However, their philosophies are different. To appreciate the difference, let's define the process that both of the meshing styles applies when representing delamination:

DEFINITION 3.1 (MAPPED MESH) *Given a set of desired delamination parameters, then (1) mesh the laminate with quadrilateral elements, and (2) identify nodes that are to be delaminated using a suitable criterion, like the one presented in the previous section.*

DEFINITION 3.2 (FREE MESH) *Given a set of desired delamination parameters, then (1) build the geometry of the laminate taking into account the relevant boundaries of the flaw, and (2) mesh the laminate with irregular elements.*

The implications of using the mapped meshing technique will be presented in the results of this chapter, but for now it is possible to say that using this type of meshing generates an overhead in time, that is due to the fact that mesh must be inspected (node by node) in order to determine the delaminated region. Indeed, the previous description of the process is similar to the one followed by inverse problems! Given the consequences, then try to find a suitable initial model that reproduces such consequences.

On the other hand, free meshing behaves like a classical or direct problem that is, given the problem, find a suitable solution. This only argument is enough to justify that free meshing is a cost-effective methodology, in terms of time, to represent delamination.

The proposed method to represent delamination in a FE model using free meshing is as follows.

1 Define the geometry of the laminate. In this case a panel.

2 Superpose on the base geometry the desired delamination.

3 Divide the compound geometry in order to isolate regions of high gradients from regions with no displacements. In the case of samples testes through DSPI the critical regions are those inside of the delamination.

4 Select an appropriate coarseness of the mesh by defining the appropriate size of the elements in the model. This was done using a standard FE convergence analysis.

5 Mesh the model using a free mesh.

Numerical implementation In order to show the ability of free meshes to represent elliptical delamination, two examples are presented where the methodology outlined above was applied:

1 In this example, the objective was to generate a penny shaped delamination with a radius of 10 *mm* in a composite laminate of sides equal to 100 *mm*. The centre of the delamination (x_c, y_c) was $(65, 40)$ *mm*.

2 In this example, an elliptical shaped delamination with a length of 40 *mm*, width of 30 *mm* and angle of ration of 45^o, and planar location $(65, 65)$ *mm* was generated.

The results the previous methodology will be delayed until the presentation of the results at the end of the chapter.

3.4.3 Subquestion C

Two out of the four methodologies found in the literature are the best suited to model the mechanical behaviour of delamination, these are: de-equivalenced crack and sub-structure. The hybrid element interface is not cost-effective for two reasons. The first is that imposes an overhead of CPU time due to the non-linearities that arise by the introduction of spring/beam elements at the interface between sub laminates. The second reason is that this technique is mainly used in studies of impact on composites, where there is possibility of interpenetration between the sub laminates. The degraded inter-laminar layer has one main drawback: to effectively simulate delamination, a reduction of the 100 percent in the elastic modulus is necessary to achieve a behaviour that correlates with reality, but in a finite element model it is impossible to set an elastic constant to zero for the model becomes ill-conditioned and no solution is obtained.

Then the question is whether the de-equivalence crack or the sub-structure model is more appropriate to simulate the physics involved in the testing of delamination through DSPI. The answer is simple, from a physical point of view both models are equally appropriate[3].

Meanwhile, it is possible to say that that if *physics* is not the attribute that discriminates between the different modeling techniques, then the only attribute left is cost-efficiency in term of solution *time*. The modelling technique that proves to be solved in a faster time will be the appropriate for the problem at hand.

A logic argument will be presented that will conclude that sub-structure model is the most cost-efficient to simulate the physics of delamination in the context of DSPI. Once again, the argument will be presented in the *results* section of this chapter.

3.4.4 Subquestion D

Boundary conditions (BC) refers to the combination of both displacement constraints and external loads. Displacement constraints of the FE model in the context of DSPI analysis is a problem that has been already solved for de-equivalence crack and sub-structure modelling [1]. In the case of sub-structure modelling, the appropriate displacement constraints are pictured in Figure 2.12c from Chapter 2.

The second component of BC is the external loads that act on the model. The development of this research question will try to persuade the reader of two points. First, that when testing delaminated panels through DSPI is not possible to determine analytically the external loads that act on the sample. Second, if there is not experimental knowledge about the external loads, the inverse problem of characterising delamination in composites panels from interferometric it ill-conditioned.

In order to prove the statements above a mathematical model was developed for the evaluation of the external forces on the delaminated region of the

[3]The explanation of why both models are appropriate to model the mechanical behavior of delamination will be delayed until the end of the chapter.

laminate. The model is based on the supposition that the theory of slender beams can be applied. The model will be presented in the *results* section.

3.5 Results and discussion

3.5.1 Parametric representation of delamination

This subsection addresses to the methodology developed for subquestion *A* posed in this chapter. Three verification models were developed with the aim of (1) to detect the *edge* of a delamination from the simulated results of DSPI out-of-plane displacements, and (2) to numerically calculate the parameters of the elliptical flaw from the borders detected in (1).

First model Figure 3.6 displays the results of the computation of the flaw parameters for an embedded circular delamination with radius 15 *mm*, located at $(37.5, 37.5)$ *mm*. The laplacian-based edge detection technique detected a set of uniform distributed edge points along the border of the delamination bulge, as is indicated with white points in sub-figure (b). Clearly, the edge is not unique, and it seems that three different layers of edge points are present as follows. Referring to sub-figure (c) it is possible to observe that the inner-layer of edge points is located on the dashed line, the second is located between the former and the solid line, and the third one is located just outside of the solid line. This findings may indicate that some of the detected edge points are false. Lim [133], indicated that this is possible in when laplacian-based filter methods are used.

The second part of the model, the characterisation of the parameters of delamination is showed in sub-figure (b). Identification of the planar location of the circular flaw is achieved (black diamond in the center of the image), however the size of the predicted delamination is slightly bigger (dashed line) than the expected flaw. This, again, can be explained by the influence of the false positives reported during the edge detection phase.

3.5.1.01 Second model. Figure 3.7 shows the Edge detection and delamination parameters for an embedded elliptical delamination with major axis 15 *mm*, located at $(37.5, 37.5)$ *mm* and θ 90 degrees. As in the previous

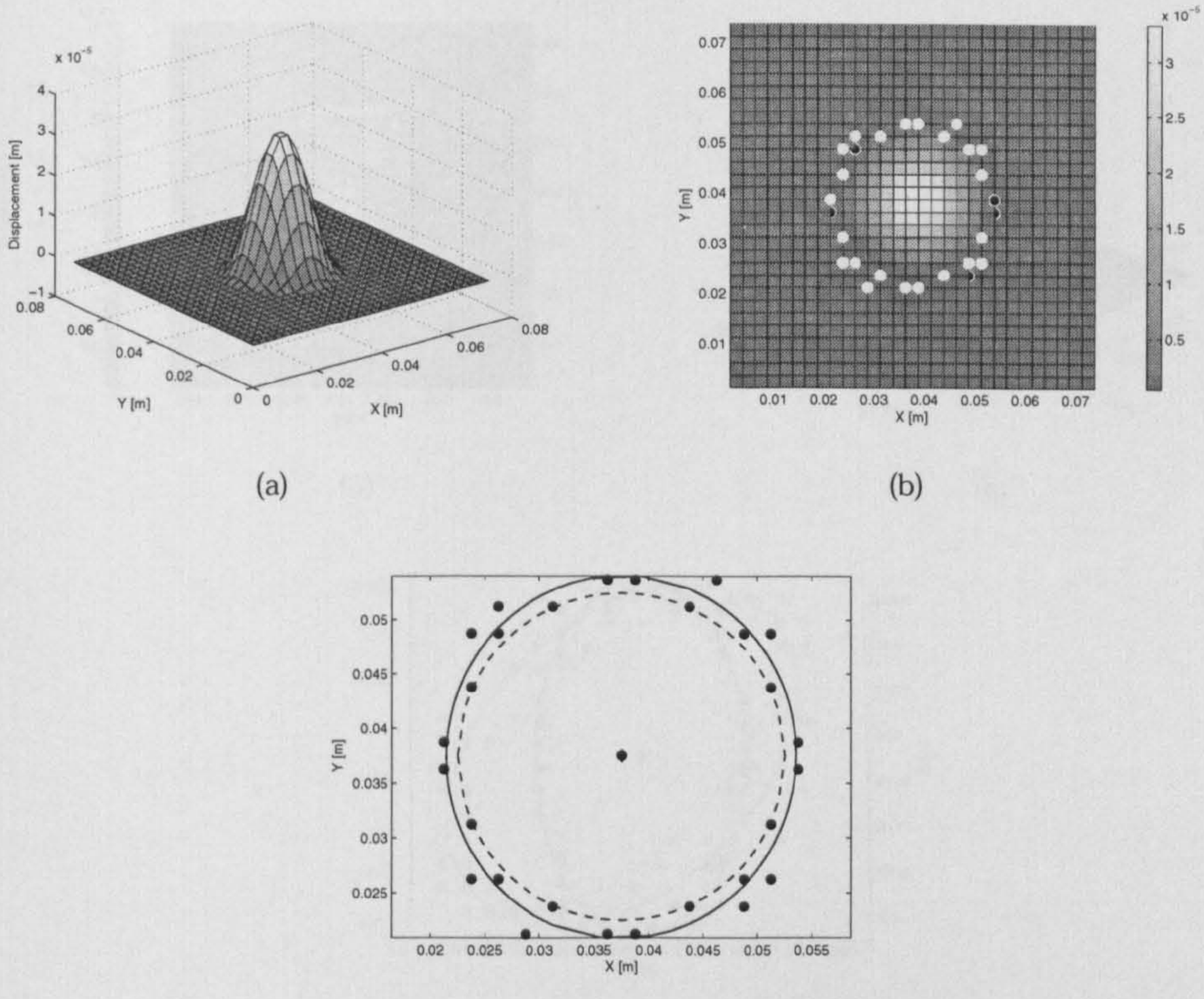

Figure 3.6. Edge detection and delamination parameters for an embedded circular delamination with radius 15 *mm*, located at $(37.5, 37.5)$ *mm*.
(a) Simulated out-of-plane displacements; (b) edges of the delamination bulge (white points); (c) comparison of the flaw parameters between the delamination that generated the original displacement field (dashed lines) and the one obtained using the proposed mathematical model (solid line).

model, the laplacian technique detected a uniform distribution of edge points along the border of the delamination. Indeed, the same three layers of edge points are present (sub-figure(b)), then the same conclusions as in the previous case can be drawn.

However, there exists a significant difference with respect to the fist model, and this is on the characterised size of the delamination. While in the first model the predicted delamination was scaled in both axes, in this model the scaling only occurred along the $x-axis$. Although, the trend is that characterised delaminations have a slightly larger area in comparison the original flaw.

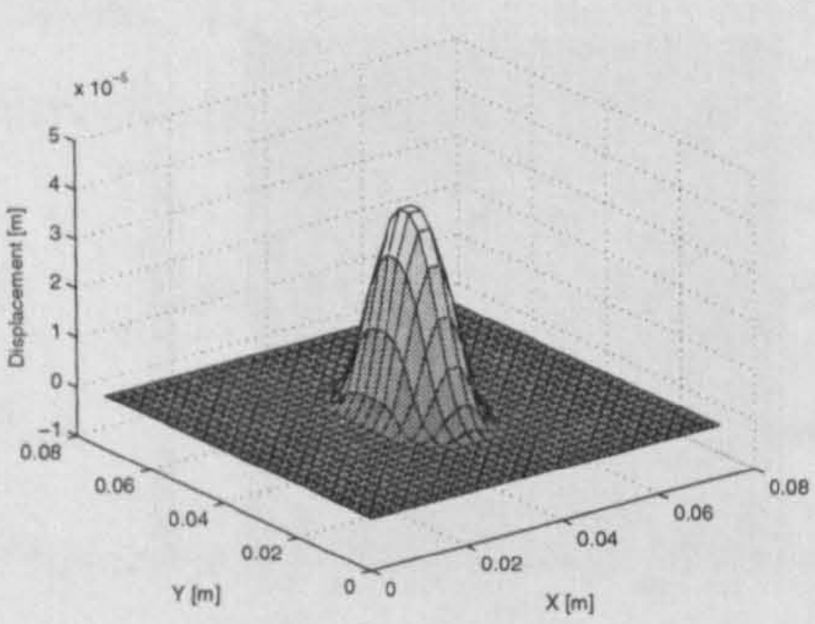

(a)

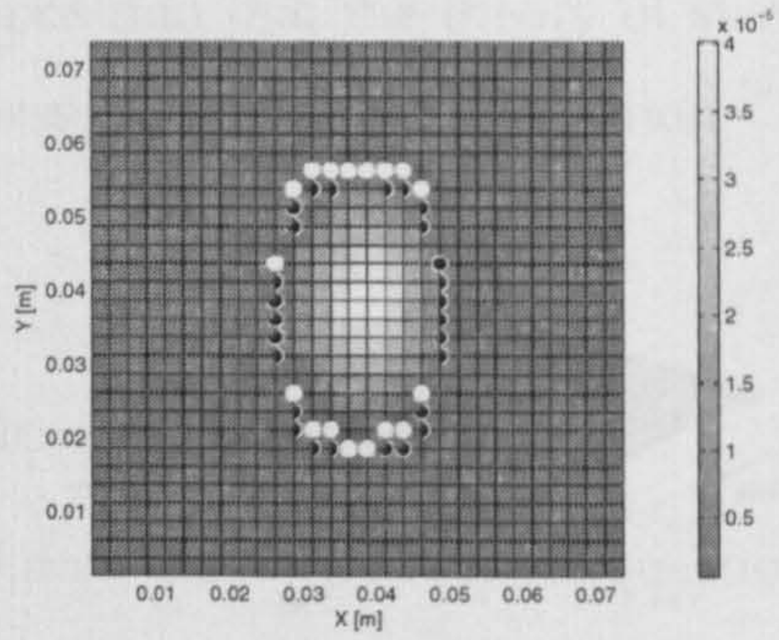

(b)

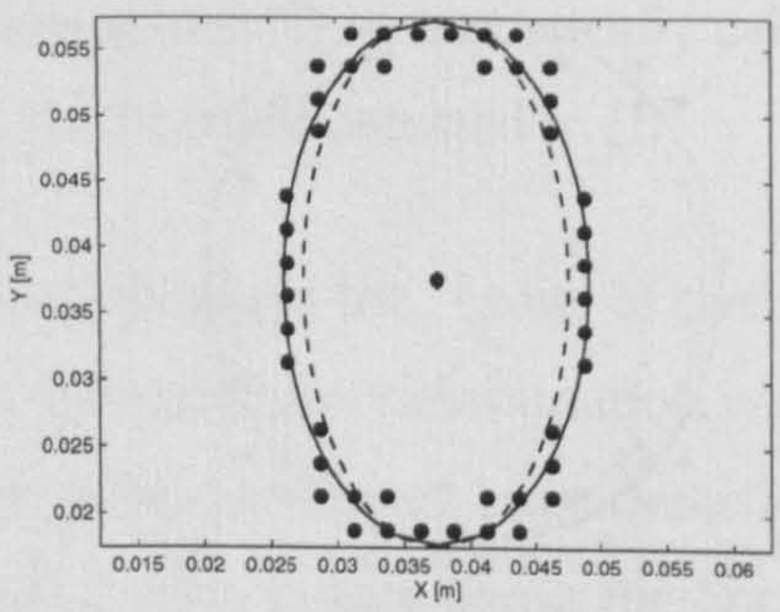

(c)

Figure 3.7. Edge detection and delamination parameters for an embedded elliptical delamination with radius 15 *mm*, located at $(37.5, 37.5)$ *mm* and θ 90 degrees.
(a) Simulated out-of-plane displacements; (b) edges of the delamination bulge (white points); (c) comparison of the flaw parameters between the delamination that generated the original displacement field (dashed lines) and the one obtained using the proposed mathematical model (solid line).

Third model Figure 3.8 shows the edge detection and delamination parameters for an embedded elliptical delamination 40x20 *mm*, located at $(37.5, 37.5)$ *mm* and θ 45 degrees. Sub-figure (a) shows the edge points detected. In comparison with models one and two, a larger dispersion of this points is present, especially in the direction of the minor axis of the delamination. Clearly, edge points continue to be allocated in three different layers as was explained in model one.

Although the size of the characterised delamination is bigger than the expected (sub-figure (c)), its behaviour is a combination between model one and two. This is, the scaling effect occurs in both axis of the delamination (as in

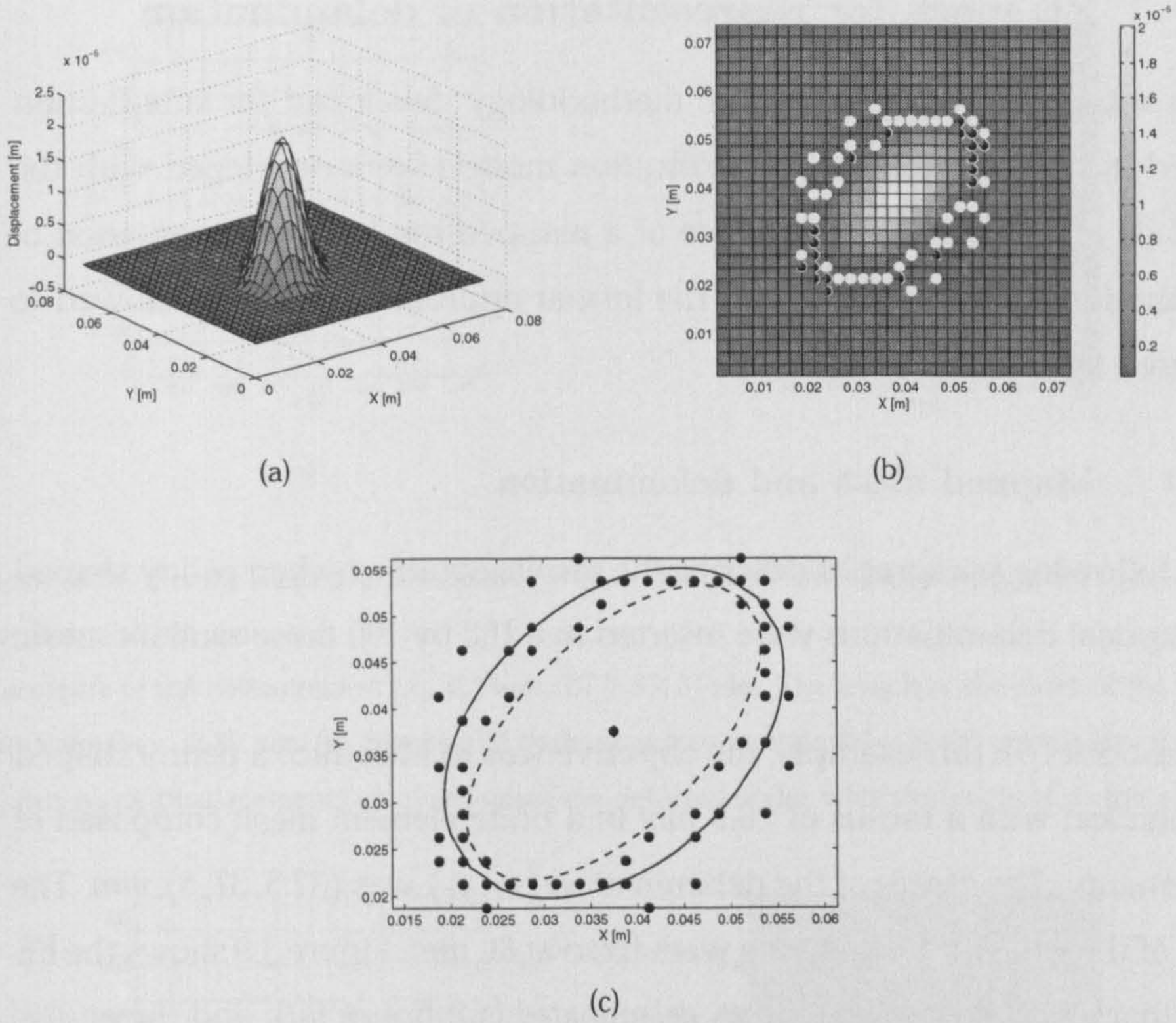

Figure 3.8. Edge detection and delamination parameters for an embedded elliptical delamination 40x20 *mm*, located at $(37.5, 37.5)$ *mm* and θ 45 degrees.
(a) Simulated out-of-plane displacements; (b) edges of the delamination bulge (white points); (c) comparison of the flaw parameters between the delamination that generated the original displacement field (dashed lines) and the one obtained using the proposed mathematical model (solid line).

model one), but the effect is stronger along the shorter axis of the delamination, like in model two.

Remark To conclude this section, it is possible to say that, in general, the laplacian based technique used to detect the edge points of the delamination, provides satisfactory results. The only issue to be addressed in future studies is how to either improve this technique or find another one that could provide better edge points. The second part of the model, that is the size characterisation, also showed promising results, no only in terms of the accuracy of the results, but also in the computational economy derived from its use.

3.5.2 FE mesh for representation of delamination

This subsection addresses to the methodology developed for subquestion *B* posed in this chapter. Three verification models were developed with the aim of (1) evaluate the performance of a mapped mesh for representation of delamination, and (2) to compare the former approach with one followed to generate a free mesh.

3.5.2.1 Mapped mesh and delamination

The following paragraphs describe the results obtained when penny shaped and elliptical delaminations were inserted in a 100 by 100 finite element mesh.

First model In this example, the objective was to introduce a penny shaped delamination with a radius of 16.5 *mm* in a finite element mesh composed of 100 elements. The centre of the delamination (x_c, y_c) was $(37.5, 37, 5)$ *mm*. The length of the sides of the laminate were fixed at 80 *mm*. Figure 3.9 shows the FE nodes that could be considerate as *delaminated* (subfigure (a)), and the equivalent out-of-place displacements that could be obtained from such FE mesh. In this case the centre of the delamination was located at one of the nodes of the FE mesh, on the other hand the edge of the delamination did not intersect any of the nodes. Results from the criteria outlined in the methodology part of this chapter, show that distribution of the nodes belonging to the delamination are even, and that they represent in a sensible way the boundaries of the flaw. Sub-figure(b) shows the equivalent out-of-plane displacements obtained when the mesh in (a) is used. Clearly, the contours represent a circular flaw. However, the boundary of the delamination is not well represented, displaying a behaviour of a polygonal flaw.

Second model The second model aimed to represent an elliptical shaped delamination with a length of 40 *mm*, width of 20 *mm* and angle of ration of 45^o. The centre of the delamination was placed at $(37.5, 37, 5)$ *mm*. Figure 3.10 shows the detected delaminated nodes using the belonging criteria (a), and (b) the equivalent out-of-plane displacements. As in model one, the centre of the delamination was intentionally placed in one of the nodes of the mesh. In

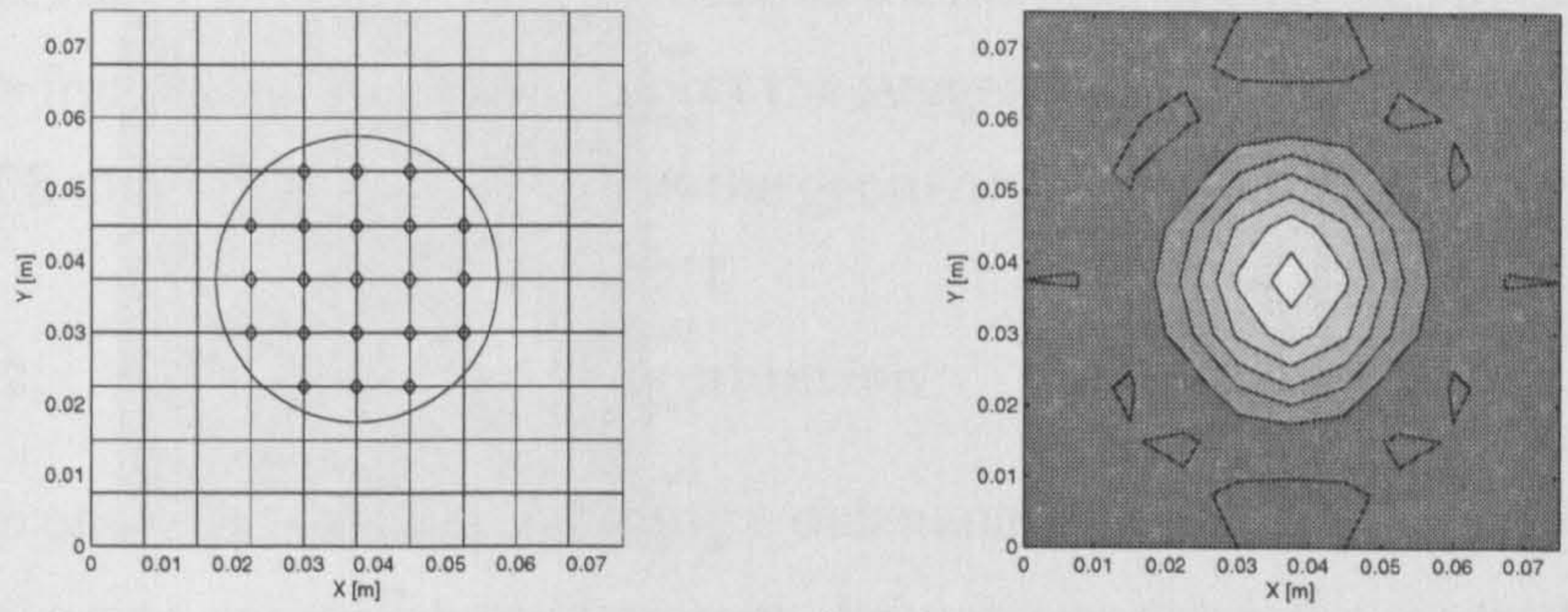

(a) (b)

Figure 3.9. Penny shaped delamination with a radius of 16.5 *mm* in a finite element mesh composed of 100 elements.
The centre of the delamination (x_c, y_c) was $(37.5, 37, 5)$ *mm*. The length of the sides of the laminate were fixed at 80 *mm*. (a) detected FE nodes that represent the flaw in the mapped mesh, and (b) out-plane-displacements obtained when the detected nodes were delaminated in the mesh.

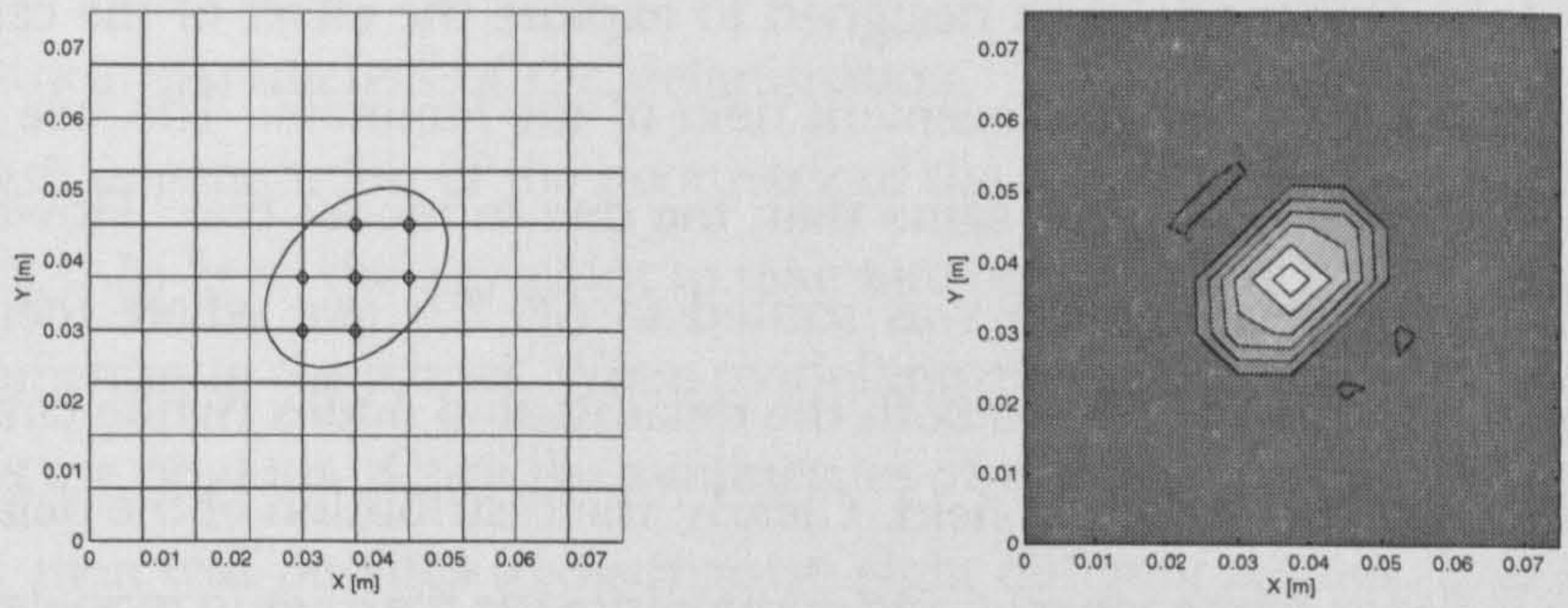

(a) (b)

Figure 3.10. Elliptical shaped delamination with a length of 40 *mm*, width of 20 *mm* and angle of ration of 45^o. The centre of the delamination was placed at $(37.5, 37, 5)$ *mm*.
(a) detected FE nodes that represent the flaw in the mapped mesh, and (b) out-plane-displacements obtained when the detected nodes were delaminated in the mesh

this condition, the resulting delaminated nodes fairly represents the area of the flaw. However, the displacement field for this delamination displays common similarities with model one. The boundary of the delamination appears polygonised. Indeed, this representation of the flaw introduces significant errors in the calculation of the displacement field. The problem is even more important when elliptical delaminations with high aspect ratio are used for the representation.

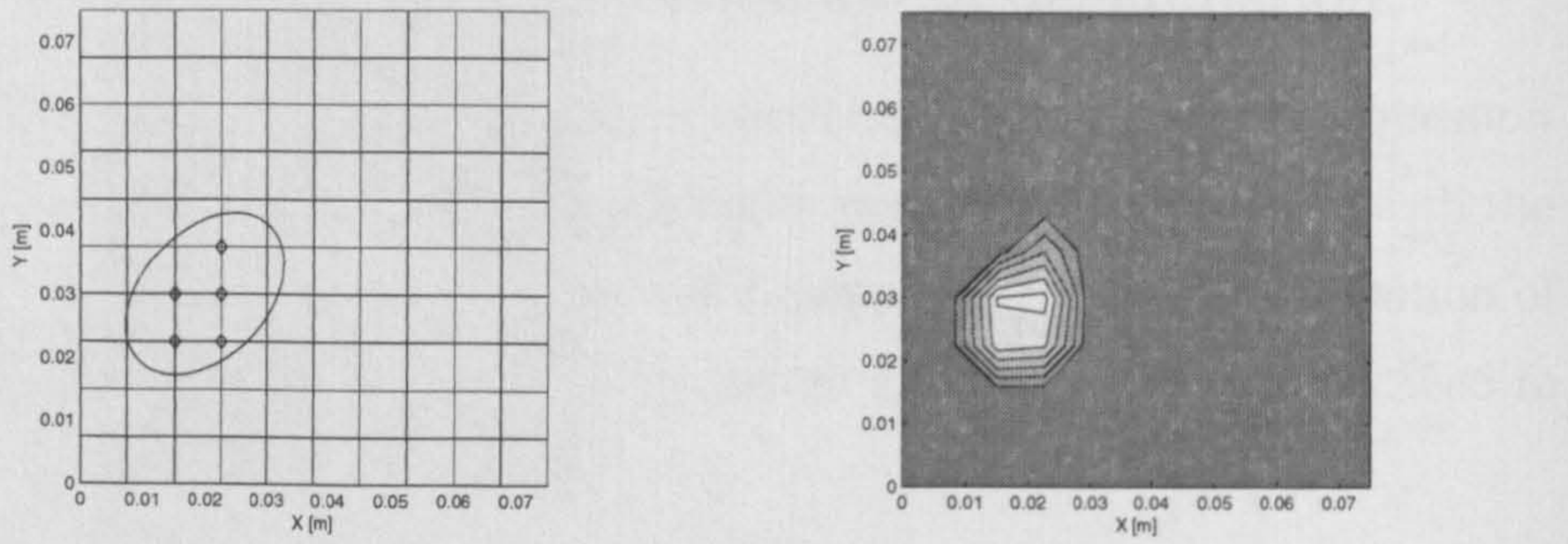

(a) (b)

Figure 3.11. Elliptical shaped delamination with a length of 40 *mm*, width of 20 *mm* and angle of ration of 45^o. The centre of the delamination was placed at $(20, 30)$ *mm*.
(a) detected FE nodes that represent the flaw in the mapped mesh, and (b) out-plane-displacements obtained when the detected nodes were delaminated in the mesh

Third model This model was designed to explore the effect of the centre of the delamination on the displacement field of the laminate. The size and orientation of the flaw were the same than the one in model two. However the location of the delamination was shifted to $(20, 30)$ *mm* where there is not a FE node. Figure 3.11 shows both the delaminated nodes (white circles) and the equivalent displacement field. Clearly, the distribution of the delaminated nodes is not as homogeneous and symmetrical as the ones in model two. Nodes at $(30, 30)$ and $(30, 40)$ *mm* are to close to the boundary of the flaw that, if they are *delaminated*, then the area of the delamination would be increased in at least forty percent. As a consequence of location of the centre of the delamination, the displacement field does not appear to reflect the fact that an elliptical delamination is inserted in the model.

Remark Given the results derived from the previous models, it is possible to conclude that mapped meshing is a paradigm that is not adequate to represent embedded delamination in composites. The only possibility to use mapped meshing would be refining the size of the mesh, at such degree that FE nodes are located on the boundary of the delamination. However this approach goes in opposition to the goals of design a cost-efficient FE model for embedded delamination, as the computing time necessary to solve the finite element model

increases approximately with the cube of the number of elements in the model. Results from this subsection support the suggestion from Panni [1], that a *pixelated* FE model does not represent the geometry of delamination.

3.5.2.2 Free mesh and delamination

A second alternative for meshing a delaminated panel is using a free mesh. The following paragraphs will present, through examples, the methodology to generate a free mesh that represents in an appropriate manner the geometry of delamination.

3.5.2.21 First example. In this example, the process followed to generate a free mesh representing a penny shaped delamination with a radius of 10 *mm* located at $(65, 40)$ *mm* was developed. Figure 3.12 shows the three main steps involved in the generation of the free mesh. Sub-figure (a) shows the geometrical parameters of the delamination. The first step in the design of the mesh is generation of the geometry of the model, this is showed in subfigure (b). In here, the key point to take into consideration is the exploitation of symmetries in the model. When modelling circular delaminations, the symmetries are obvious. Once the symmetries of this model were merged to the model, then was possible to distinguish eight different regions, four inside of the delamination, and four outside of it. The second step, was the determination of the regions with high displacement gradients. When modelling the bulging effect produced by delamination these areas are the ones that contains the mentioned bulge. Then, the model is further divided to delimitate the regions of interest as is shown in subfigure (c). The final step was the meshing of the model. This was accomplished in two steps. (1) a FE convergence analysis to determine the optimum size of the elements, and (2) generate the mesh. The first step was accomplished by following standard procedures for the calibration of FE meshes, that is, the number of divisions in the boundary of the flaw were sequentially incremented until the average displacement of the model displayed an asymptotic behaviour [136]. results from this methodology indicates that the optimum number of nodes in the boundary of the delamination is sixteen, and that this value is independent of the size and geometry of the

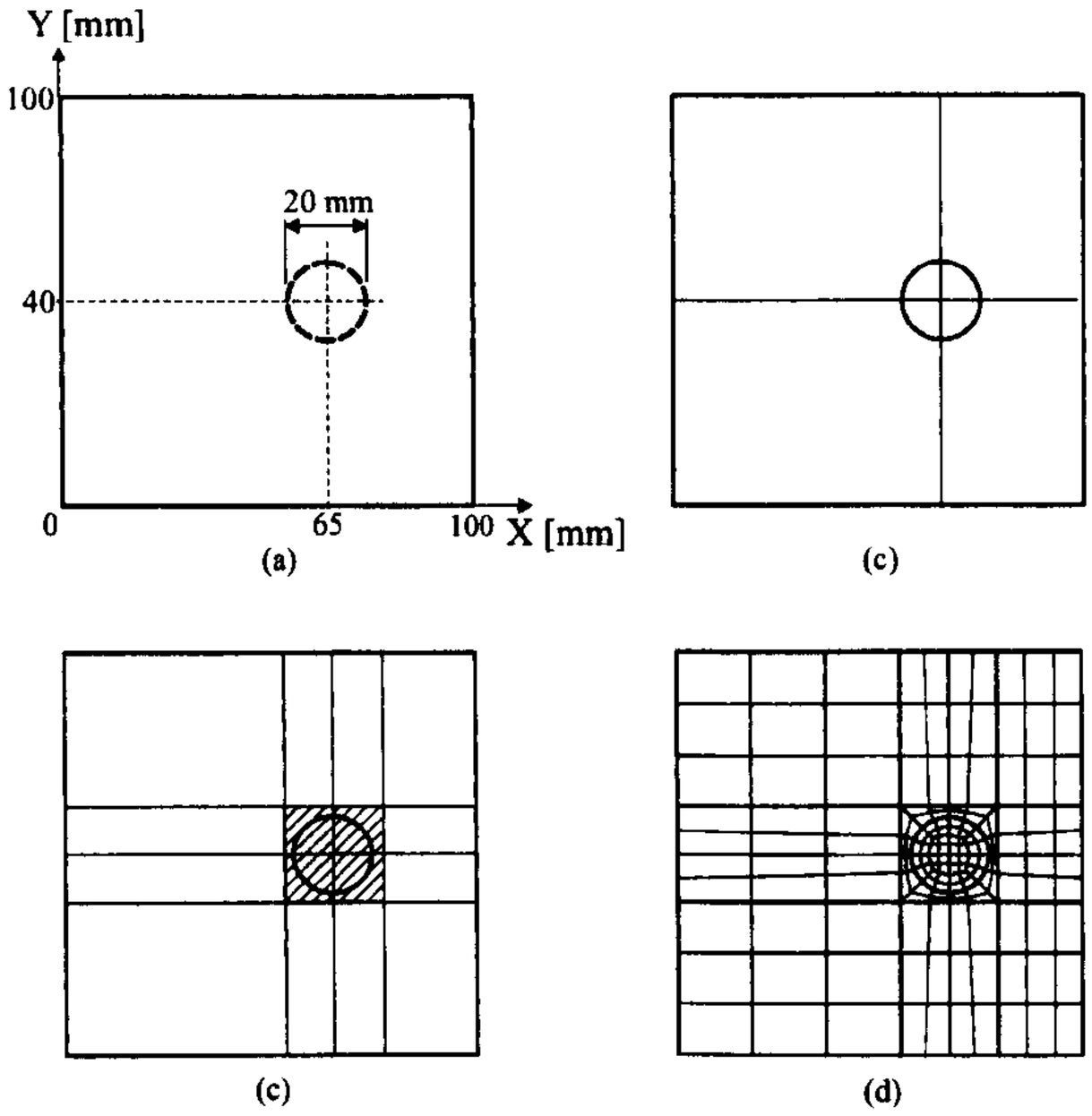

Figure 3.12. Process followed to generate a free mesh representing a penny shaped delamination with a radius of 10 *mm* located at $(65, 40)$ *mm*.
(a) desired parameters of circular delamination, (b) design of the geometric model exploiting symmetries, (c) a further refining of the geometry to isolate regions with high displacement gradients, and (d) select an appropriate coarseness of the elements and meshing of the model.

delamination. The second step is the meshing of the model. In here, the FE software package ANSYS was used to generate the mesh, as is shown in sub-figure (d).

3.5.2.22 Second example. In this example, the process followed to generate a free mesh representing an elliptical shaped delamination with a length of 40 *mm*, width of 30 *mm*, angle of orientation of 45^o, and planar location $(65, 65)$ *mm* was developed. Figure 3.13 shows the three equivalent steps involved in the generation of the mesh. All the steps, but the first, followed the same reasoning presented in model one, so their details are not included in here. In the first step of the methodology it is necessary to exploit the symmetries of the model. When modelling elliptical delaminations that can have arbitrary angles of orientation, the proper selection of the points of symmetry are not obvious. The findings of this study concluded that the best manner to tackle the problem is choosing these points as is shown in sub-figure(b). In this

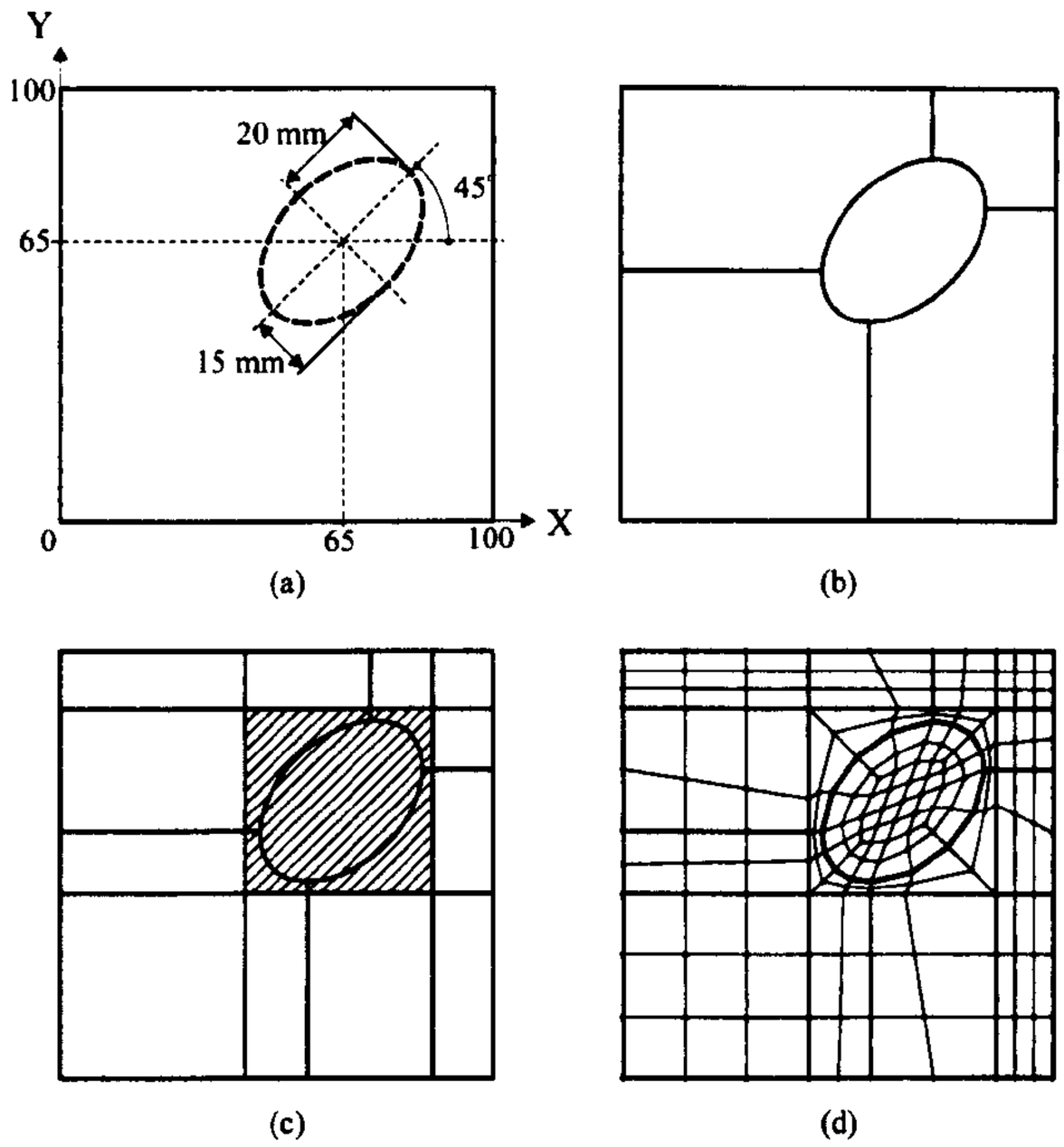

Figure 3.13. Process to be followed to generate an elliptical shaped delamination with a length of 40 *mm*, width of 30 *mm*, angle of orientation of 45^o, and planar location $(65, 65)$ *mm*. (a) desired parameters of circular delamination, (b) design of the geometric model exploiting symmetries, (c) a further refining of the geometry to isolate regions with high displacement gradients, and (d) select an appropriate coarseness of the elements and meshing of the model.

points the parametrical equation of the ellipse has derivates equal to zero, that is $\frac{dy}{dx} = 0$ for the lower and upper points, and $\frac{dx}{dy} = 0$ for the left and right-hand points. In this manner, the basic geometry of the geometric model is composed of five areas; four outside of the delamination, and one inside of it.

Remark From the previous description of the methodology it is seems clear that the use of free mesh is both flexible and straightforward. Firstly, there is not need of mathematical model to determine which nodes of the FE mesh are either inside or outside of the delamination. Secondly, the representation of the boundary is exact, hence the simulations displays correct displacement fields. Finally, the number of elements used for this model is minimal. In the model one FE model contained 106 elements, and model two contained 180 elements. To the knowledge of the author, there are not other studies in the literature that address the problem of the type of FE mesh for the modelling of delamination.

Then, further work on this topic could be done, to not only understand in deep the interaction between meshing and accuracy of the simulations, but also to developed FE models to predict the remaining life and strength of delaminated composite panels.

3.5.3 Delamination model

The problem under consideration in here is whether the de-equivalenced crack model or the sub-structure approximation are more appropriate to simulate the physics involved during the detection of delamination through the DSPI technique. In the following paragraphs an argument will be presented that will try to convince the reader that both approximations represent in a reasonable manner the physics of the process. Additionally, it will be argued that from a perspective of cost-efficiency the approach of sub-structures is superior to the de-equivalenced model. The argument will develop as follows. Firstly, a brief description of the every model will be provided. Secondly, based on the background, conclussions will be drawn in terms of a fair comparisons between the approaches. This section addresses subquestion *C* of this chapter.

3.5.3.1 The de-equivalenced crack model

Delaminations can be represented by de-equivalencing the mid-side node between two elements in a FE mesh as is shown in Figure 3.14(a). A longer crack can be considered as a series of adjacent de-equivalenced node cracks in line, as is showed in sub figure(b). The starting point for the application of this model is the a meshed FE model of the laminate, and the damage parameters that the analyst wishes to include in the model, as is Figure 3.15a. Then the analyst coded a computational routine that allow him to inspect the FE mesh, and determine which nodes must be de-equivalenced. Then, using another routine, or a mouse if he is using a graphic interface, nodes that are meant to be de-equivalenced are cloned, and new elements are created. The final de-equivalenced mesh is pictured in sub figure (b).

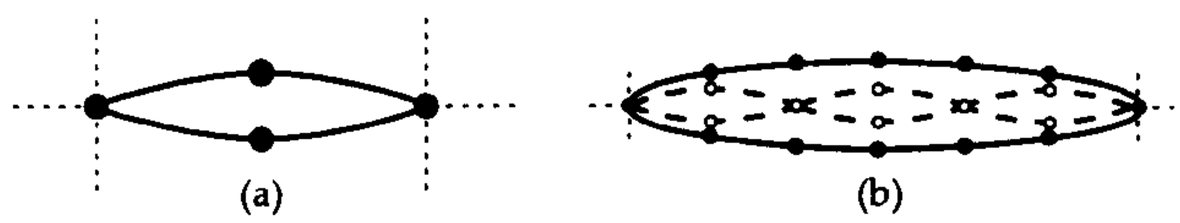

Figure 3.14. Delamination representation in a FE model by de-equivalencing the mid-side nodes. (a) Single de-equivalenced node crack. (b) Longer de-equivalenced crack.

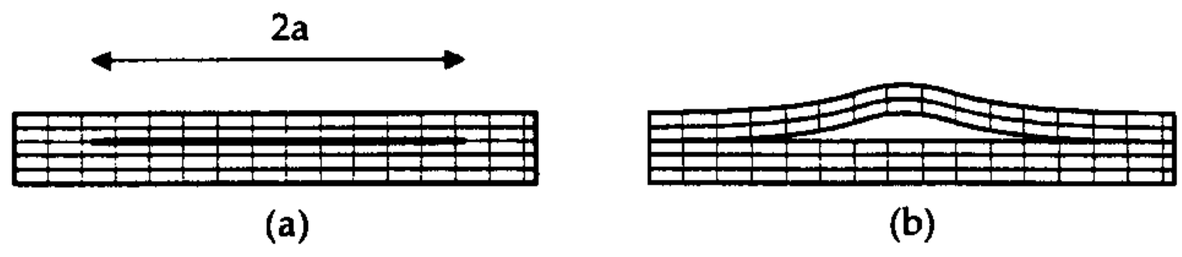

Figure 3.15. Process in the generation of a de-equivalenced crack. (a) FE mesh, with the parameters of the delamination to be included: length $2a$ and depth represented by the solid line. (b) de-equivalenced mesh.

3.5.3.2 The sub-structure model

A second alternative to model delamination is by considering that a delaminated plate is composed of two regions: (1) the base, and (2) the delaminated region as is showed in Figure 3.16. Delamination is represented as the FE model of the delaminated region in conjunction with a prescribed boundary conditions. This model describes the physics involved in the process of testing delaminated panels using the DSPI technique; two principal justifications exists. The first reason is that during the experiment there is not contact between sub laminates. The second reason is that the displacements of the delaminated panel are of the order of magnitude of the wavelength of light. Then, under this circumstances the delaminated region can be considered as cantilever-cantilever beam.

The starting point for the application of this sub-structure modelling is the geometric model of the laminate, and the damage parameters that the analyst wishes to simulate. That is the geometry of the laminate in Figure 3.16. Then the analyst implement the geometry of the delaminated region in the pre-processor of a FE software package, and then, he/she meshes model using the tools available in such software.

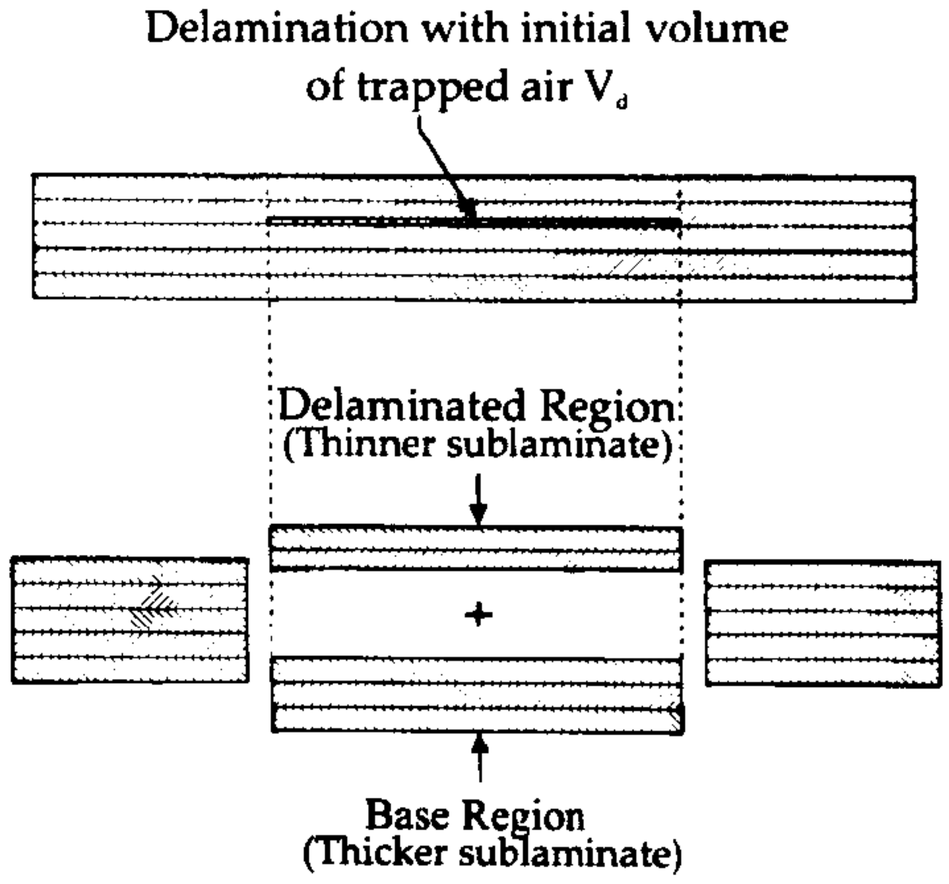

Figure 3.16. Definition of sub-laminates in the context of this thesis.

Sub-laminates refer the two groups of plies separated by the delamination. The portion of the sub-laminate above of the delamination, or the thinner portion, will be referred to as the delaminated region. The portion of the lower, or thicker portion, sub-laminate located beneath the delamination will be referred as the base region.

3.5.3.3 Closing discussion

There exists a close symmetry between the problem of choosing a model to simulate the behaviour delamination, and specifying the type of mesh to represent the flaw (see research question 2). The fundamental relation between both the de-equivalenced model and sub-structure is the same that exists between inverse and classical problems. The de-equivalenced model starts with FE mesh, and then external routines are used to modify the problem in such way that satisfy the requirements of the analyst. On the other hand, the sub-structure analysis presents a direct approach to solve the problem. That is, the analyst specifies what he/she wants, and then a simple routine implements the FE model.

Another point of connection between both problems, geometric representation and physics of the problem, is that ideally the de-equivalenced model can be used with mapped meshes, whilst the sub-structure approach is deeply connected with a free mesh. The de-equivalenced approach requires node searching routines that are more easily implemented when the mesh if mapped, on the other hand the sub-structure approach take advantage of the classical approach of free meshing.

From the previous paragraphs seems clear that both delamination models can represent the physics of delamination, however, from a computational point of view the sub-structure approach is cost-effective for two reasons: (1) it does not need routines to find the nodes that are to meant delaminated, and (2) the finite element model contains much less elements as the only part of the model that is implemented is the sub laminate that is on top of the delamination.

3.5.4 Boundary conditions

In was showed in the previous section that the sub-structure approach is the best suited to model delamination in a cost-effective way. The following step is to determine the boundary conditions for that represent the delamination physics during a DSPI test. Boundary conditions refers to the combination of displacement constraints and external forces applied to the model.

The displacements constraints for the sub-structure model have been widely studied in the literature [1]. On the other hand, the author of this thesis believes that there are no studies on the external forces that act on the delaminated region during a typical DSPI experiment. This section develops a mathematical model that can be used to predict the load condition on the sub laminate. Although at the of writing this model has not been solved, due to the great complexity of the mathematics involved, it is possible to conclude that when testing delaminated panels through DSPI is not possible to determine analytically the external loads that act on the sample. Second, if there is not experimental knowledge about the external loads, the inverse problem of characterising delamination in composites panels from interferometric is ill-conditioned. This section addresses subquestion *D*.

3.5.4.1 The mathematical model

The following mathematical model is based Euler-Bernoulli Beam Equation. The structure of the model is the following. First the objective of the model is presented. Second, the limitations and suppositions of the analysis are presented. Third, the free body diagram of the delaminated region at the beginning and the end of the DSPI experiment is presented. Fourth the results from

the equations of equilibrium are presented. Fifth the integral equation that relates the external forces on the sub laminate is showed. Finally, the conclusions that can be derived from this model are presented.

Objective of the model The objective is two-fold: (1) calculate out-of-plane displacements of a beam representing the delaminated sub laminate, and (2) understand the interaction between the displacements and the external loads applied to the model.

Limitations The Euler-Bernoulli Beam Equation is applicable to two dimensional representation of beams. On the other hand, delamination in the context of DSPI is three dimensional problem. Then, although the scope of the Euler-Bernoulli equation is not extensive to the problem studied in this thesis, it provides a insight on relation between displacements and external forces. Another limitation is that the model is developed for an isotropic material, but in reality this study is centered in composite laminates.

Suppositions The following are the suppositions made during the development of this model.

- The ideal gas law is applicable to this problem.
- The initial volume of air trapped inside of the delamination is known.
- The initial pressure of the air trapped inside of the delamination is known.

Free body diagram Figure 3.17 shows the free body diagrams of the delaminated sub laminate at the beginning and the end of a typical DSPI experiment. The initial state is defined by the no operation of the vacuum chamber (sub figure (a)), then on the sub laminate act two opposing forces, (1) a force due to the atmospheric pressure P_c that tries to tight together the laminate, and (2) a force due to the pressure of the air trapped in the delamination P_d that tries to *open* the crack. Given the fact that most composite laminates are manufactured in sub atmospheric environment, then $P_c > P_d$.

In the final stage of the DSPI experiment, the delamination is in equilibrium as is showed in sub figure (b). In this position, the chamber has change its pres-

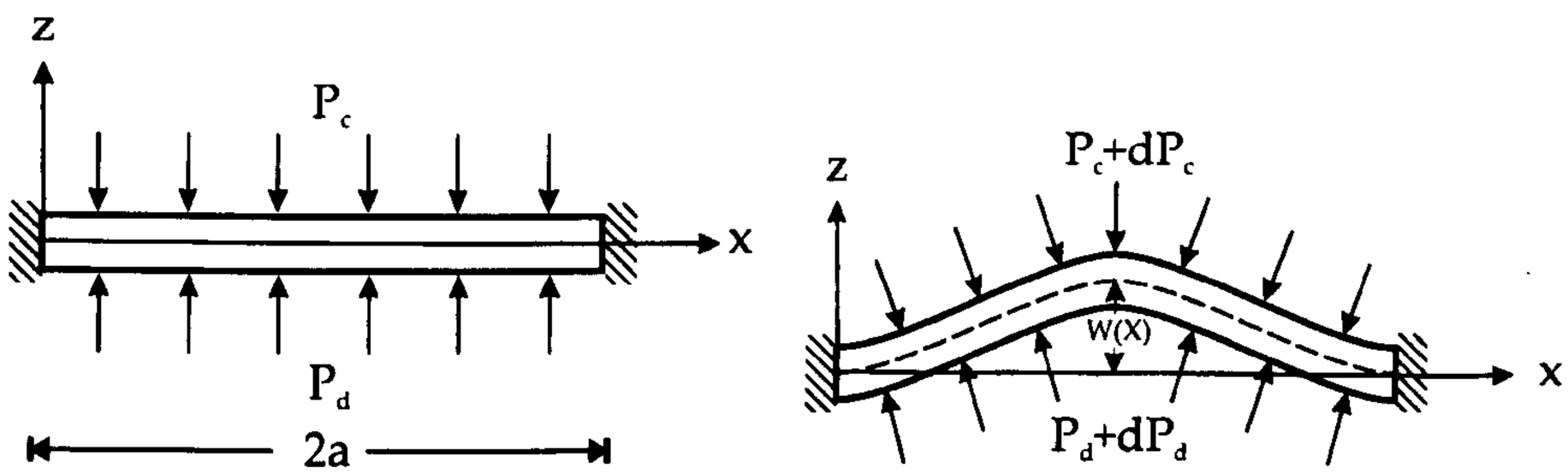

Figure 3.17. Free body diagram of the delaminated region. (a) at the beginning of the experiment, and (b) at the end of the DSPI test.

sure to $P_c + dP_c$ where $dP_c < 0$, and it is a known parameter. At the same time the pressure inside of the delamination changes to $P_c + dP_d$ due to an increase of the volume of air contained in the delamination. If the initial volume of air contained inside of the cavity is v_d, then the final volume is expressed by the following equation,

$$v_f = v_d + \int_0^{2a} w(x)\,dx, \tag{3.16}$$

where $w(x)$ is the function that represents the out-of-plane displacements of the delamination. If the ideal gas law is applied, then the final pressure of the air trapped in the delamination is as follows,

$$P_f = \frac{P_d \cdot v_d}{v_d + \int_0^{2a} w(x)\,dx}. \tag{3.17}$$

Equations of equilibrium The equations of equilibrium are obtained from the diagram of the forces acting on a differential portion of the delamination when it has reached its position of rest (Figure 3.18). Equilibrium of forces along the $z-axis$ and equilibrium of moments around point O provide the following two equations,

$$\frac{dq}{dx} = P^* - P_f, \tag{3.18}$$

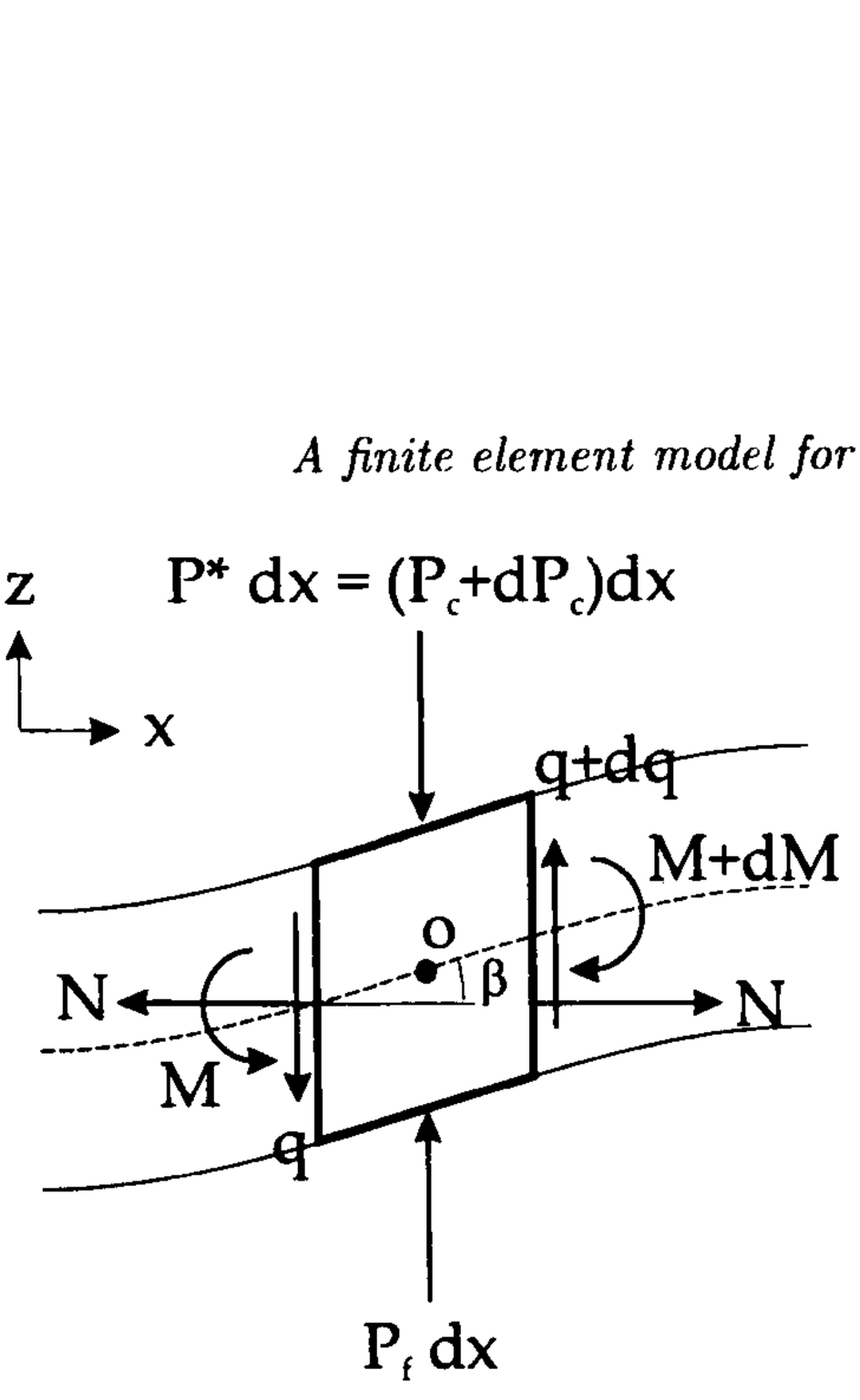

Figure 3.18. Forces on a differential portion of the delamination at its final position.

$$dM = Vdx, \tag{3.19}$$

where q is the internal shear force, M is the internal bending moment, and P^* is the final pressure in the vacuum chamber $P_c + dP_c$.

Integral equation The final step of the model uses the bending equation 3.20 to assemble the both equilibrium equations 3.18 and 3.19. The bending equation is,

$$M = -EI\frac{d^2w}{dx^2}, \tag{3.20}$$

where E is the Young's modulus of the delaminated sub laminate, and I is the area moment of inertia of the sub laminate's cross section. The final expression for the Euler-Bernoulli equation is then,

$$EI\frac{d^4w}{dx^4} = \frac{P_d \cdot V_d}{V_d + \int_0^{2a} w(x)\,dx} - P^*. \tag{3.21}$$

Equation 3.21 is a so-called integro-differential equation because it includes integrals and derivates of the of the function to be solved.

Conclusion A mathematical model was presented that correlates the out-of-plane displacements with the external forces acting on the surface of the delaminated sub laminate when a DSPI experiment is performed. This model can be examined through two different points of view (1) as a classical or forward model, and (2) as an inverse of backward problem.

The direct problem is as follows: given the pressures inside of the delaminated sublaminate, the pressure inside of the vacuum chamber, and the initial volume of air trapped in the delamination, calculate the out-of-plane displacements of the sub laminate. This problem might be solved with the application of the mathematics of integro-differential equations.

The second point of view is the following. Given the out-of-plane displacements, for example from the DSPI technique, and the change of pressure in the vacuum chamber, determine the change of pressure of the air inside of the delamination. Based on equation 3.21, two possible interpretations exists. The first one, comes from the fact that a delamination generated by a low impact event has area but not volume. It is simply a new surface that is created inside of the laminate. If this is true, then the mentioned equation predicts that the surface of the sub laminate remains flat, and in consequence the delamination can not be detected. The second interpretation, is that for some reason, air is trapped inside of the delamination, generated for example in the process of vulcanisation of tyres, then in order to know the change of pressure inside of the bulge, it is necessary to know precisely the amount of air that is present in it.

The previous argument poses a source of ill-conditioning in the process of damage characterisation from measurements from DSPI. If a complete characterisation of damage is required, then the analyst must know the exact volume of air that is contained in the delamination at the beginning of the experiment. If the information is not available or not computable, then the problem is ill-posed, and only partial characterisation is possible.

3.6 Conclusion

This chapter addresses the research question two included in Chapter one. The main question to be solved is as follow, *which of the delamination modelling*

techniques available in the literature are accurate and efficient enough to describe computationally an embedded delamination? How can these techniques be adapted?

The methodology implemented to solve the above question involved splitting the question in four sub questions (A to D). This sub questions pointed to the geometric representation of delamination, FE representation of delamination in terms of the type of mesh, and delamination model that model the physics of delamination, and the FE boundary conditions. The following sub sections provides the main conclusions to these questions.

3.6.1 Parametric representation of delamination - Subquestion A

Delamination represents a major component of damage that evolves according to a definite pattern. Geometrically, delamination can be approximated an elliptical-shaped crack with with six parameters: (1,2) the planar location, (3) length of the delamination, (4) width, (5) angle of orientation, and (6) depth below the measured surface of the laminate. The findings of laplacian-based techniques for the detection of edges in out-of-plane displacements from the DSPI technique, indicate that is possible to determine the size and orientation of flaw, but in general this approach will provide results that over predict the area of the delamination.

3.6.2 Type of FE mesh to represent delamination - Subquestion B

Two possible FE meshing paradigms can be applied for the geometric representation of delamination in a FE model. These are mapped and free meshing. The findings from numerical experiments indicate that a mapped mesh is not flexible enough to cope with the geometry of elliptical delaminations. The principal reasons for this are that (1) in order to accurately represent the boundary of the flaw, it is necessary to increase the resolution of the mesh, increasing at the same time the CPU time needed to solve the FE model, and (2) complex, and not always precise, routines are needed to search the mesh in order to determine which nodes must be delaminated.

On the other hand, free meshing is a flexible and cost-efficient paradigm to represent the geometry of damage. This paradigm is parallel to the solution of classical or forward problems in the sense that the FE mesh is generated in a geometric model a laminate after the flaw is merged with laminate model. The findings indicate that using a well designed free mesh it is possible to represent a parametric delamination with high accuracy, and with low computational cost in terms of the number of FE elements needed in the model.

3.6.3 Delamination model - Subquestion C

Studies in the literature concerning the simulation of the physics in the literature provide two models that can be used to represent the physics of delamination during a DSPI experiment. These are the de-equivalenced crack and the sub-structure model. The former has an element of intuitiveness that could make them attractive to use in the following manner: once the FE mesh of a laminate composite has been implemented, then search and de-equivalence the nodes of the mesh that are inside of the delaminated region. The findings indicate that although this technique could represent the physics of delamination, it is not cost-effective in terms of the computational time required to both de-equivalenced the mesh, and solve the FE model.

On the other hand, the sub-structure approach is not intuitive, but it provides a direct connection between the physics of the delamination and the type of mesh required in the analysis. Findings indicate that this delamination model works best with free meshing, satisfying multiple objectives simultaneously: (1) accurate representation of the geometry (boundary) of the flaw, and (2) compact FE models that are cheap to run.

3.6.4 Boundary conditions - Subquestion D

Boundary conditions refer to the combination of both displacement constraints and external loads on a FE model. If the delamination model to use is sub-structure, then the displacement constraints have defined presented in the literature. They are (1) cantilever-cantilever around the boundary of the delaminated sub laminate. On the other hand, the determination of the external

loads that act on the delaminated region during a DPSI experiment is rather complex.

The two main forces on the delaminated region are the pressure in the vacuum chamber and the pressure of the air inside of the delamination. The findings of the interpretation of the integro-differential equation that correlates the out-of-plane displacements and the pressures on the delaminated region, indicate that in order to calculate the pressure of the air inside of the delamination, it is necessary to know the exact volume of air contained inside of the bulge. If this volume is not known, then the problem of characterisation of delamination from DSPI measurements is ill-posed, and in consequence, a unique determination of the parameters of the delamination is not possible.

Chapter 4

A THEORETICAL BACKGROUND ON INVERSE PROBLEMS, OPTIMISATION AND GENETIC ALGORITHMS

Abstract This chapter presents a theoretical background of the problem of delamination characterisation in composite laminates. The non-destructive crack problem is formulated as an inverse problem using the output error criterion, that leads to the definition of a non-differentiable, non-convex optimisation problem that minimise the difference between the central geometric moments calculated from the DSPI technique and the moments computed from the surface displacements of a FE model with a trial delamination. It is proposed that the determination of the minimum of the optimisation problem can be performed through the use of a genetic algorithm.

4.1 Introduction

This chapter presents a theoretical background to the subject of inverse problems and genetic algorithms in the context of delamination characterisation in composite laminates. The objective here is to present the formulation of the crack identification problem, and to explain how this problem could be solved with the aid of genetic algorithms. Chapter six will show the practical implementation of the concepts derived in here.

The discussion will begin with the statement of the problem of crack identification in terms of an inverse problem, and the solution of an adjoint optimisation problem. This is followed by the presentation of the research subquestions that are tackled in this chapter. Next, the methodology followed to answer these research subquestions is presented. Finally, the development of the ideas proposed in the methodology section is presented, and the conclusion to this chapter is detailed.

Definitions about the structures, operators and convergence of genetic algorithms presented in section 4.5.3 are widely known in the GA research community. However, the author of this thesis believes their inclusion is important for the completeness of this work. Readers interested in the mathematical treatment of GAs are addressed to reference [137].

4.2 Problem Statement

Direct (or classical) problems in structural mechanics look for the response of a structure to a known set of prescribed forces and/or displacements, where the geometric parameters of the structure are suppose to be known. The adjoin inverse problem seeks to determine the unknown geometric parameters of the structure from the partially (or complete) known displacements.

In this work, the structure is a composite laminate with a known lay-up and material mechanical properties, with the geometric parameters of an embedded delamination as the unknown parameters. The response of this laminate to a partially known force (Chapter 3) is given by a measurable set of boundary displacements. The identification problem that is under investigation, seeks to recover both the geometric parameters of an idealised elliptical flaw, and the pressure of the air trapped inside of the crack from out-of-plane displacements and vacuum pressure measurements using the DSPI technique.

Identification (inverse) problems of this kind have been treated in the literature under the name of *non-destructive crack identification problems.* [70]. However, it is believed that the inverse problem of characterisation of delamination, under the conditions described in this thesis, has not been formally treated in the literature. Therefore, a re-definition of the inverse crack identification problem should be reformulated.

In general, inverse problems are formulated as optimisation problems for the difference between the either measured or computed, and the desired responses within the search space defined by the range of the variables that are being identified. In the process of solving an inverse problem by any of the numerical optimisation techniques, it is necessary to solve many times the associate direct problem, as it is required by the algorithm of optimisation. Hence, the computational time necessary to solve a particular inverse problem can

increase dramatically depending of the complexity of both the computational model used to represent the direct problem, and the efficiency of the optimisation algorithm.

Crack identification problems are ill-posed [138], since small variations of the geometric parameters of the flaw might lead to (1) large variations in the static response of the structure, and (2) multiplicity of the solutions for the inverse problem. The latter arises always that an incomplete or small number of boundary conditions is used. This ill-posseness leads to non-smooth and non-convex optimisation problems. The numerical solution of these optimisation problems has proved to be a difficult one, especially by the presence of local minima that can not be avoided by local optimisation techniques. Is it in here that global optimisation techniques, like genetic algorithms, ant colonies, and neural networks, can display their immense power to explore efficiently the search space. In the context of this thesis, genetic algorithms is the global optimisation technique used to solve the inverse problem.

4.3 Objectives and Research Questions

The purpose of this chapter is to provide a framework for the solution of the inverse problem of characterisation of delamination. From the previous paragraphs, it is clear that it is necessary to (1) give a formal definition of the inverse problem under consideration, and (2) characterise the solution of the inverse problem in terms of the optimisation technique used with this aim. The principal objective of this chapter is,

> *Provide a formulation of the inverse problem of damage characterisation, and provide its solution through the use of genetic algorithms.*

This objective can be satisfied if the following research questions are answered:

1 **Subquestion A:** How can the inverse problem of characterisation of delamination be formulated? (Formulation of the inverse problem).

2 **Subquestion B:** Does the previous formulation leads to a cost-effective solution of the inverse problem? If not, how can this problem be re-formulated? (Cost-effective reformulation of the inverse problem).

3 **Subquestion C:** How can the solution of the problem of characterisation of delamination be expressed in terms of a genetic algorithm? (Solution of the inverse problem)

The following section details the methodology and experimental setup used to solved the previous research questions.

4.4 Methodology and Experimental Setup

4.4.1 Subquestion A

The inverse problem is formulated as an optimisation problem for a scalar performance error function. The formulation is based upon the output-error criterion developed by Hajela and Soeiro [70] which relates the measured and predicted displacements of a structure. The advantage of this criterion is that it transforms a multiobjective optimisation problem to a classical single-objective one. The process for the development of the formulation of the inverse problem starts by the definition of the set of parameters that characterise an ideal elliptical delamination. Then, a definition of the external loads on the system is provided in terms of the known pressures in the vacuum chamber and the unknown pressure of the air trapped inside of the delamination. Finally, the inverse problem is formulated a as minimisation problem that involves the parameters of the delamination, and the external loads.

4.4.2 Subquestion B

Even though the formulation of the characterisation problem provided in subquestion *A* adheres to the classical treatment of inverse problems, it is not cost-effective in terms of computation time needed to solve it. The main reason that supports this statement is the following. In a given step of the optimisation process it is necessary to calculate the difference between the measured displacements from the DSPI technique and the displacement obtained from a finite element model that contains a trial delamination. Typically, DSPI provides and array of upwards $3x10^5$ measurements. Hence, a computational routine that usually uses the L^2 norm must be implemented to find the difference between the measured and predicted displacements. The process involves five operations: (1) square the measured displacements in a given point, (2) inter-

polate the solution provided by the FE model to find the predicted displacement in a particular location, (3) square the predicted displacement from the FE model, (4) find the difference between the squared values of the displacements, and finally, (5) calculate the squared root of the mention difference. For example, the time taken to process the five operations for $3x10^5$ measurements is about fifteen minutes [1]. It is clear that time consumed in the comparison is excessive, and that another form of comparison must be found.

DSPI measurements could be used in computerised damage diagnostic techniques like genetic algorithms, neural networks or fuzzy classification. However, the main prerequisite for these techniques is to decrease the amount of data contained in the resulting image/array from DSPI. The problem to be considered in here is how to reduce the size of the array containing the DSPI measurements maintaining, at the same time, the physical significance of such results.

Central geometric moments (CGM) can be used as the basis of comparison between the out-of-plane displacement of a delaminated panel from the DSPI technique, and the displacement field from a finite element model with a trial flaw. It was showed (in Chapter 2) that these moments are the best suited to represent DSPI results because they are sensitive to the size, and orientation of the features of the bulge immersed the DSPI results.

It is proposed that the CGM can be used to *represent* the information contained in the DSPI data. This is not a new idea in the field of optical interferometric techniques, and it is a concept that is widely used. In consequence, the author believes that it is not necessary to describe in-deep the technique. If the reader is interested, the book by Mukundan and Ramakrishnan [139] presents a comprehensive treatise on the theory and applications of moment functions in image analysis. The present analysis of CGM will be concerned with their numerical implementation on a free FE mesh.

Given the fact that DSPI measurements (and results from any other optical interferometric technique) can be represented by a set of CGM, it is necessary

---

[1]The test was performed on a supercomputer SGI Origin 2000, with 4 CPU, 1 GB RAM, 128 GB HD located at the Advanced Computer Center *MOX* at Los Andes University in Bogota - Colombia.

to re-examine and re-define the formulation of the inverse problem given in subquestion *A*. The output-error criterion is used, but instead of using the measured and computed displacements, the CGM representation of them are included in the formulation.

4.4.3 Subquestion C

The formulation of the inverse problem of characterisation of damage leads to a scalar performance error function that is not smooth, and in general non convex. Global optimisation techniques must be used to find the solution (optimum point) of the inverse problem. The purpose of this section is to introduce genetic algorithms, and to show how to integrate the parameters of the inverse problem in the formulation of a typical genetic algorithm (GA). The process carried out is the following. First, a short background on genetic algorithms will be presented. Then, the genetic structures and operators will be introduced, showing how the inverse problem parameters are merged into the GA structures. Finally, a discussion on the convergence of GAs will be presented.

4.5 Results and discussion

4.5.1 Output-error formulation of the inverse problem

The inverse problem of characterisation of delamination in composite laminates can be formulated as an optimisation problem using the output error criterion [70]. This section addressees research subquestion *A* of this chapter.

Consider a composite laminate which contains an unknown delamination during a session of a DSPI test. Let $\tilde{u}_0(p_c, p_d)$ stands for the vector field of *measured* out-of-plane displacements at specific locations (x_i, y_i) during such a test, where p_c is the known pressure inside of the vacuum chamber, and p_d is the *unknown* pressure of the air trapped inside of the delamination.

Now, consider a FE model representation of the laminate in the vacuum chamber which contains a known trial-delamination. The delamination is characterised by the set of geometric parameters,

$$\vec{z} = [x_c, y_c, a, b, \theta, h]^T, \tag{4.1}$$

where (x_c, y_c) is the planar location of the trial flaw, $2a$ is the length , $2b$ is the width, θ is the angle of orientation , and h is the depth of the flaw. In Chapter 3, it was showed that these are the appropriate parameters for the identification of an embedded delamination.

Let $\tilde{u}(\vec{z}, p_c, p_d^t)$ stands for the vector field of *computed* out-of-plane displacements (at the same specific locations (x_i, y_i) used in the DSPI experiment), from a FE model with a *trial* set of delamination parameters $\vec{z}$, where p_c is the known pressure inside of the vacuum chamber, and p_d^t is a *trial* pressure of the air trapped inside of the delamination.

The typical inverse problem associated with the above descriptions is as follows:

> ***Given*** *(as data)* $\tilde{u}_0(p_c, p_d)$ *and* p_c, ***find*** *the parameters of the delamination* $\vec{z}$, *and the pressure of the air trapped in the delamination* p_d.

In ideal circumstances, the solution to this inverse problem could be posed as the solution of the following non-linear and non-explicit system of equations,

$$\tilde{u}(\vec{z}, p_c, p_d^t) = \tilde{u}_0(p_c, p_d). \tag{4.2}$$

However, the system shown in equation 4.2 is often undetermined, and it is usually restated as the least-squares minimisation problem for a scalar performance function $\Phi_{err}\left(\vec{z}, p_d^t\right)$ as follows,

$$\Phi_{err}\left(\vec{z}, p_d^t\right) = \left\| \tilde{u}\left(\vec{z}, p_c, p_d^t\right) - \tilde{u}_0\left(p_c, p_d\right) \right\|, \tag{4.3}$$

where $\| \cdot \|$ is the l^2 norm (least square identification). It is worth remarking that, although the least square formulation might solve problems of existence and uniqueness associated with the original problem stated in equation 4.2, in general the least square solution is less stable with respect to perturbations and noise in the input data $\tilde{u}_0\left(p_c, p_d\right)$.

Before attempting the solution of the optimisation problem in equation 4.3 is worth to mention some of the difficulties that may arise.

First, the response of the FE model $\tilde{u}(\vec{z}, p_c, p_d^t)$ is a non differentiable function of the damage parameters $\vec{z}$. This can be explained if it is considered that the flaw parameters do not appear explicitly in the FE formulation, they are represented by a combination of displacements constraints in the FE model. Secondly, the scalar performance function $\Phi_{err}\left(\vec{z}, p_d^t\right)$ is in this case a generally non-differentiable and non-convex function, since this function is expressed in terms of the function $\tilde{u}(\vec{z}, p_c, p_d^t)$ that it is not differentiable.

In light of the complexity of the nondifferentiable optimisation problem is equation 4.3, the problem in tackle by a derivate free optimisation procedure which is based on genetic algorithms.

4.5.2 Cost-effective reformulation of the inverse problem

4.5.2.1 Two dimensional geometric moments

The two dimensional geometric moments of order $p+q$ of a function $f(x, y)$ are defined as,

$$m_{pq} = \int_{-\infty}^{\infty} \int_{-\infty}^{\infty} x^p y^q f\,(x, y)\, dxdy, \tag{4.4}$$

where $p,\ q\ =\ 0,\ 1,\ 2,\ \ldots,\ \infty$. Note that the monomial product $x^p y^p$ is the basis function for this moment definition.

A set of n moments consists of all m_pq for $p+q<n$, that is the set contains $\frac{1}{2}(n+1)(n+2)$ elements.

Considering the fact that an image segment has finite area or in the worst case is piecewise continuous, moments of all orders exist and a complete moment set can be computed and used uniquely to describe the information contained in the image. However, in order to obtain all of the information contained in an image requires an infinite number of moment values. Therefore, to select a meaningful subset of the moment values that contain sufficient information to characterize the image for a specific application becomes very important.

4.5.2.2 Two dimensional central geometric moments

The central geometric moments of $f(x, y)$ are defined as,

$$\eta_{pq} = \int_{-\infty}^{\infty} \int_{-\infty}^{\infty} (x - \bar{x})^p \ (y - \bar{y})^p \ f(x, y) \, dx dy, \tag{4.5}$$

$$with \ \bar{x} = \frac{m_{10}}{m_{00}}, \ and \ \bar{y} = \frac{m_{01}}{m_{00}}. \tag{4.6}$$

Geometric central moments defined in equation 4.5 are invariant under the transformation of coordinates. The lower order moments represent some well known fundamental geometric properties of the underlying image functions.

Volume The definition of the zero-th order geometric moment m_{00} represents the total mass of the given function or image $f(x, y)$.

Centre of mass The first two geometric moments m_{10} and m_{01} are proportional to the centre of mass of the image $f(x, y)$. The centre of mass is the point where all the mass of the image could be concentrated without changing the first moment of the image about any axis. The coordinates of the centre of mass in the two dimensional Cartesian space is given by equation 4.6.

4.5.2.3 Numerical computation of geometric moments

The inverse problem to be solved involves the comparison between and image/array of experimental data, and the displacements from a finite element model. Therefore, two different algorithms that must be implemented to calculate the moments in both circumstances are presented in this section.

Moments from DSPI measurements If the image function $f(x, y)$ from the DSPI technique is thought as an MxN array of pixels, the double integration in equation 4.5 can be approximated by a double summation as follows,

$$m_{pq} = \sum_{i=1}^{M} \sum_{j=1}^{N} x_i^p y_j^q f(x_i, y_j) \Delta x \Delta y, \tag{4.7}$$

where Δx and Δy are the sampling intervals in the x and y directions. Equation 4.7 predicts accurate results when applied to lower order moments, that is moments up to order three. For higher order moments an extended Simpson's rule must be used. The reason for this is that the approximation error in equation 4.7 increases out of control when the order of m_{p+q} increases [140].

Moments from a FE model The out-of-plane displacement function $u(x, y)$ from a FE model could be thought as the equivalent of the image function $f(x, y)$ from the DSPI technique. However, given the fact that a free mesh is used in the FE model, the function $u(x, y)$ can not be integrated using the same exact rule as for $f(x, y)$, but it can be adapted. Using Figure 4.1 as a reference, the procedure to calculate the CGM from $u(x, y)$ is as follows.

Consider a composite laminate that is discretised by a FE mesh with Q finite elements. The FE mesh has been setup to be coarse in areas of low gradients, and highly refined in the zones were the trial delamination is modelled. In this circumstance, every finite element e in the mesh could be thought as the equivalent to one *pixel* in the image function $f(x, y)$.

Given an element e, the finite element analysis provides the out-of-plane displacements in local element's nodes i, j, k, and l. That is, $u_s(x_s, y_s)$ for $s = [i, j, k, l]$ where x_s and y_s are the coordinates of the element's nodes in the Cartesian coordinate system. If the FE mesh has been *well* designed, then it is possible to say that the average displacement $\tilde{u}_e(x_e, y_e)$ is representative of the nodal element displacements $u_s(x_s, y_s)$, where x_e and y_e stand for the Cartesian coordinates of the centroid of the element. If Δ_e represents the area of element e, then the element geometric moments m^e_{pq} of order (p+q) can be calculated using the following equation,

$$m^e_{pq} = x^p_e y^q_e \tilde{u}_e(x_e, y_e)\Delta_e. \tag{4.8}$$

If the FE mesh is composed of Q elements, then the geometric moments m_{pq} of the FE out-of-plane displacements can be approximated as,

$$m_{pq} = \sum_{e=1}^{Q} x^p_e y^q_e \tilde{u}_e(x_e, y_e)\Delta_e. \tag{4.9}$$

4.5.2.4 Numerical computation of central moments

Central moments are geometric moments that have their origin of coordinates in the centroid of the image function. Then, the numerical calculation of equation 4.5 can be expressed in function of geometric moments. Equation 4.10 shows the general expression for central geometric moments η_{pq} as a function of both the equivalent geometric moments m_{pq}, and the centroid of the image function $(\bar{x}, \bar{y})$.

$$\eta_{pq} = \sum_{i=0}^{p} \sum_{j=0}^{q} (-1)^{p+j-i-j} \begin{pmatrix} p \\ i \end{pmatrix} \begin{pmatrix} q \\ j \end{pmatrix} \bar{x}^{p-i} \bar{y}^{q-j} m_{ij}. \tag{4.10}$$

4.5.2.5 Similarity measure

Geometric central moments (GCM) can be used as the basis of comparison between the out-of-plane displacement of a delaminated panel from the DSPI technique, and the displacement field from a finite element model with a trial flaw. With this aim, a similarity measure is introduced that represents a distance in the seven-dimensional moment space between the CGM calculated from the DSPI array of measurements, and the surface displacements from a FE model with a trial delamination.

If the CGM from the DSPI measurement are considered to be arranged in the form of the vector:

$$\vec{\eta}_0 = \left[\eta^0_{20}, \eta^0_{02}, \eta^0_{11}, \eta^0_{30}, \eta^0_{12}, \eta^0_{21}, \eta^0_{03}\right]^T, \tag{4.11}$$

and the CGM from the FE model with a trial delamination is in the form of the vector:

$$\tilde{\eta} = \left[\eta^t_{20}, \eta^t_{02}, \eta^t_{11}, \eta^t_{30}, \eta^t_{12}, \eta^t_{21}, \eta^t_{03}\right]^T, \tag{4.12}$$

then, the seven-moment representation from the DSPI measurements and the FE model can be compared using the following similarity measure:

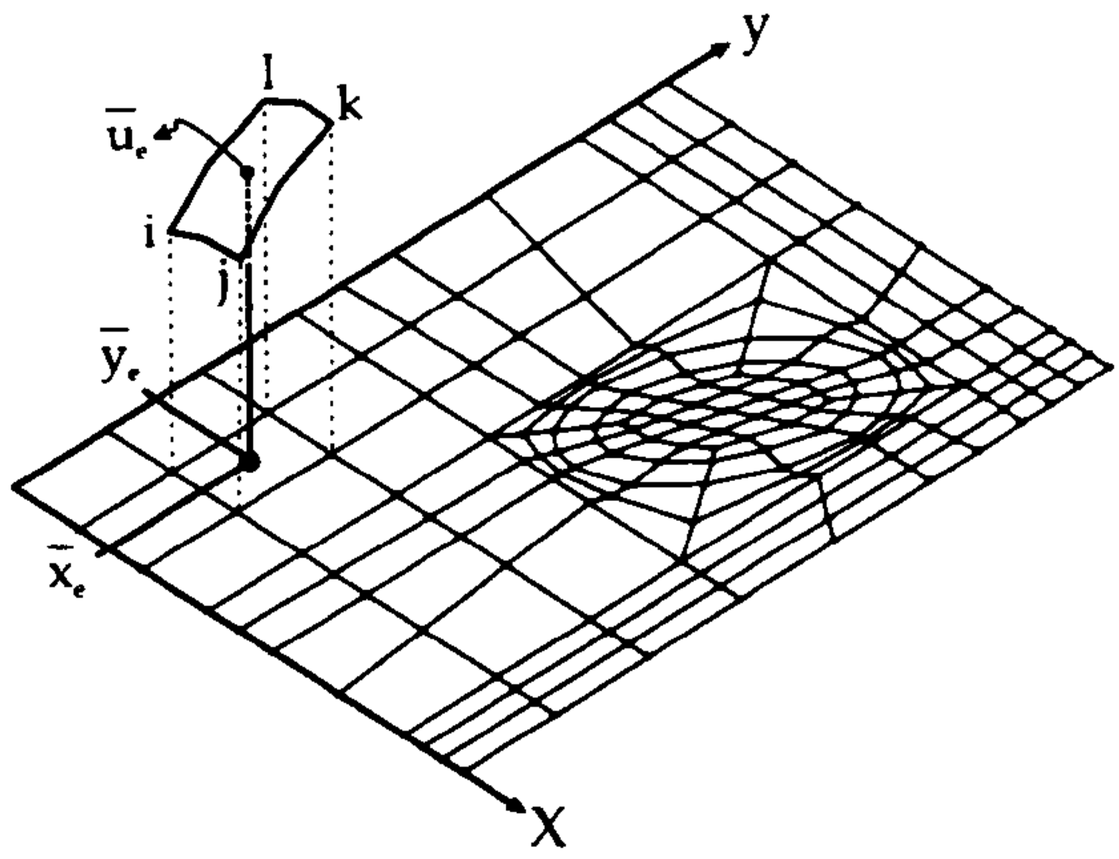

Figure 4.1. Calculation of geometric moments in a FE mesh.

For an element e in the FE mesh, x_e and y_e are the centroids of the area, and $\bar{u}_e$ is the average out-of-plane displacement. Geometric moments are calculated using equation 4.9, where Q is the number of elements that define the surface of the model, and Δ_e is the area of the element.

$$\|\tilde{\eta} - \vec{\eta}_0\|\,, \tag{4.13}$$

where $\|\cdot\|$ is usually the l^2 norm.

Only one question remains in the formulation of CGM as an effective representation of out-of-plane displacements. This is, why only moments up to order three and not higher are used to represent the image field? The answer to this question came in 1988 when Reeves, A. P [58] was studying the characterisation of military airplanes from photographies.

He concluded that a truncated set of moments up to order three offers a more convenient and economical representation of essential characteristics of images. This result was supported by Teh, C. [60], who concluded that geometric moments of order four and higher are more sensitive to the noise immerse in the image, and contain a higher information redundancy compared to low order moments.

4.5.2.6 Reformulation of the inverse problem

In the previous section was showed that it is possible to represent the large amount of data from a DSPI experiment through the use of a seven-dimensional moment space vector $\vec{\eta}$ (equation 4.11). In this section, the inverse problem of

characterisation of delamination will be re-examined in order to take into account the new compact representation of the displacement field vector.

Consider a composite plate which contains an unknown delamination during a session of a DSPI test. Let $\vec{\eta}_0(p_c, p_d) = \left[\eta^0_{20}, \eta^0_{02}, \eta^0_{11}, \eta^0_{30}, \eta^0_{12}, \eta^0_{21}, \eta^0_{03}\right]^T$ stands for the central geometric seven-dimensional moment space *representing* the *measured* out-of-plane displacements field during such a test, where p_c is the known pressure inside of the vacuum chamber, and p_d is the *unknown* pressure of the air trapped inside of the delamination.

Now, consider a FE model representation of the laminate in the vacuum chamber which contains a known trial-delamination. The delamination is characterised by the set of geometric parameters,

$$\vec{z} = \left[x_c, y_c, a, b, \theta, h\right]^T, \tag{4.14}$$

where (x_c, y_c) is the planar location of the trial flaw, $2a$ is the length , $2b$ is the width, θ is the angle of orientation , and h is the depth of the flaw.

Let $\tilde{\eta}(\vec{z}, p_c, p^t_d) = \left[\eta^t_{20}, \eta^t_{02}, \eta^t_{11}, \eta^t_{30}, \eta^t_{12}, \eta^t_{21}, \eta^t_{03}\right]^T$ represents the vector of *computed* central geometric moments, from a FE model with a *trial* set of delamination parameters $\vec{z}$, where p_c is the known pressure inside of the vacuum chamber, and p^t_d is a *trial* pressure of the air trapped inside of the delamination.

The re-examined inverse problem associated with the descriptions presented above is as follows:

> ***Given** (as data) $\vec{\eta}_0(p_c, p_d)$ and p_c, **find** the parameters of the delamination $\vec{z}$, and the pressure of the air trapped in the delamination p_d.*

In ideal circumstances, the solution to this inverse problem could be posed as the solution of the following non-linear and non-explicit system of equations,

$$\tilde{\eta}(\vec{z}, p_c, p^t_d) = \vec{\eta}_0(p_c, p_d). \tag{4.15}$$

However, the system shown in equation 4.2 is, as the original formulation, undetermined, and it is usually restated as the least-squares minimisation problem for a scalar performance function $\Psi_{err}\left(\vec{z}, p^t_d\right)$ as follows,

$$\Psi_{err}\left(\vec{z}, p_d^t\right) = \left\|\tilde{\eta}\left(\vec{z}, p_c, p_d^t\right) - \tilde{\eta}_0\left(p_c, p_d\right)\right\|, \tag{4.16}$$

where $\|\cdot\|$ is the l^2 norm (least square identification).

The previous reformulation of the inverse problem contributes to the solution of the optimisation problem in a cost-effective manner. The main reason for this is that once the FE model of the laminate has been solved, it is not necessary to map (interpolate) the FE mesh on to the locations where the DSPI technique made its measurements.

4.5.3 Delamination characterisation and genetic algorithms

Genetic algorithms (GAs) are optimisation techniques based on the concept of natural selection and genetics. GAs are designed to exploit efficiently large, non-linear, and highly complex search spaces where traditional gradient-based methods may fail. From a computational point of view, the implementation of GAs is simple. A GA consist of four basic steps (Figure 4.2). First, a population of individuals is created randomly or by a random perturbation of an input chromosome. The population then evolves toward better regions of the search space by means of processes of selection, crossover and mutation. During the selection step, couples of parents are chosen from base population according to their fitness. In the crossover step, parent individuals breed offspring's individuals by combining information from parent individuals. The mutation forms new individual by making large alteration with small possibility to the offspring individuals regardless of their inheriting information. With the evaluation of fitness for all individuals, the selection favorably selects individual of higher fitness to reproduce more often that those of lower fitness. These reproductions form a new generation of the evolutionary process. The previous steps are repeated until a given terminal criterion is reached. The following sub-sections provide the terminology and theoretical foundation of genetic algorithms.

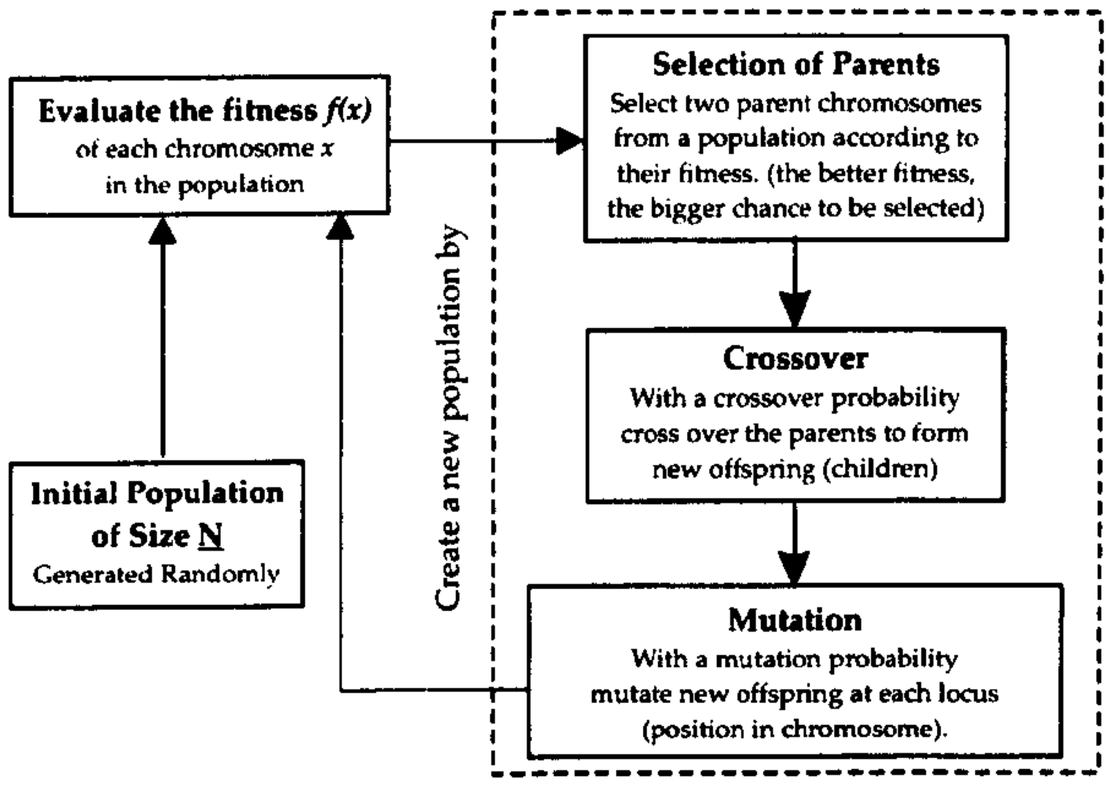

Figure 4.2. A basic genetic algorithm. The four stages in every genetic algorithm are: generation of a new population, selection, crossover, and mutation

4.5.3.1 Genetic Structures

Having laid the foundation of genetic algorithms in the previous section, the definitions of the structures related with genetic algorithms are presented here; e.g. gene, chromosome, individual, population and generation.

DEFINITION 4.1 (GENE) *A gene γ is a structure that contains a specific item of information encoded in a suitable form.*

A gene is the smallest structure of a GA that forms the inherited information from generation to generation. The optimal type of parameter encoded in a gene depends on the definition of the problem. In general, any problem parameters could be encoded using one of two representations: binary strings or real-valued vectors.

Binary strings have been the traditional way to encode variables in genetic algorithms. The data structure of the optimisation parameters are represented by a binary string of length L. Using binary encoding implies the use of auxiliary decode functions to map the binary representation of a gene into a specific floating number.

A more recent approach to encode information in genes is the use of pseudo-real numbers. Thus, a direct representation of the real values of the parameters to optimise is used.

Remark In the problem of delamination characterisation there exist seven genes (unknowns). Six of them representing the damage parameters:

$$\vec{z} = [x_c, y_c, a, b, \theta, h]^T,$$

and one representing the pressure of air inside of the delamination p_d.

There are not rules or methodologies to choose a *correct* type of encoding for these genes. In general, this decision is problem specific, hence encodings that work with some problems are found to be disruptive in others. The only recommendation in the literature is that the decision on the encoding must be motivated by the appeal of the analyst to it, or more specifically, the analyst must use the Occam's Razor which establishes that of alternate possibilities, the simpler one must be chosen.

In this thesis genes were encoded using real numbers. Motivations for this are: (1) the floating point representation is robust, accurate, and efficient because it is conceptually closest to the real value of the unknowns of the problem, and (2) there is usually a discrepancy between the binary representation space and the actual problem space. For example, two points close to each other in the real space might be far away in the binary-represented space.

In conclusion, in the problem of characterisation of delamination there exist seven genes, $\gamma_1 = x_c$, $\gamma_2 = y_c$, $\gamma_3 = a$, $\gamma_4 = b$, $\gamma_5 = \theta$, $\gamma_6 = h$, and $\gamma_7 = p_d$, which are encoded using real numbers.

DEFINITION 4.2 (ALLELE) *An allele is an allowed value of a gene. Complete set of alleles from the valid range of the genes.*

An allele is thus a specific value of a specific gene within a specific time. An important issue is that of the allowed range of the values of an allele. Theoretically, there must be a finite, or at least a denumerable number of possible values. The main reason for this is that the search space must be contained, in such a way that the optimisation problem do not diverge into unknown or undesired regions.

Remark In this work the possible (allowed) value of the genes that encodes the problem are determined by the geometry and physics of the problem. The following argument will use Figure 4.3 to illustrate this point.

Genes $\gamma_1 = x_c$, and $\gamma_2 = y_c$ represent the planar location of the centre of the delamination in the plane of the laminate. Their values could vary from 0 until the length of the panel L. However, a more reasonable approach exist. It was showed in this chapter that central geometric moments are immersed in their definition the centre of mass the bulge that represent the delamination, equation 4.6. Therefore, it is suggested that a *reasonable* range of values for this genes can be given by the following equations,

$$\begin{aligned} [\min(\gamma_1), \max(\gamma_1)] &= [(1-\varepsilon)\bar{x}, (1+\varepsilon)\bar{x}], \\ [\min(\gamma_2), \max(\gamma_2)] &= [(1-\varepsilon)\bar{y}, (1+\varepsilon)\bar{y}], \end{aligned} \tag{4.17}$$

where ε is number in the range $(0, 1)$.

Genes $\gamma_3 = a$, and $\gamma_4 = b$ encode the size of the delamination to be characterized. Their values are not known a priori; however, it is possible to use the *laplacian edge detection technique* developed in Chapter 3 to *predict* a suitable allele range for these genes. For example, if the edge detection technique predicts that the size, and with of the delamination are $\bar{a}$ and $\bar{b}$, then it is suggested that a *possible* range of values for this genes can be given by the following equations,

$$\begin{aligned} [\min(\gamma_3), \max(\gamma_3)] &= [(1-\lambda)\bar{x}, (1+\lambda)\bar{x}], \\ [\min(\gamma_4), \max(\gamma_4)] &= [(1-\lambda)\bar{y}, (1+\lambda)\bar{y}], \end{aligned} \tag{4.18}$$

where λ is number in the range $(0, 1)$.

Gene $\gamma_5 = \theta$ encodes the angle of orientation of the delamination. The possible allele of this gene are not in the continuous space. Possible values for the angle of delamination are determined by the angle of the orientations of the composite laminate. For example if the specification of an eight ply plate is given by $(90, 0, +45, -45)_s$, then the possible values of gene five are given by $\gamma_5 = [-45, 45, 90, 0]$. Indeed, the alleles of gene five are based on the assumption that in the event of a low velocity impact, the longest axis of an embedded delamination is usually parallel to the orientation of the ply that is just beneath of the delamination [13].

Gene $\gamma_6 = h$ encodes the depth of the delamination measured from the surface of the laminate that is closest to the DSPI detector. Delamination is present

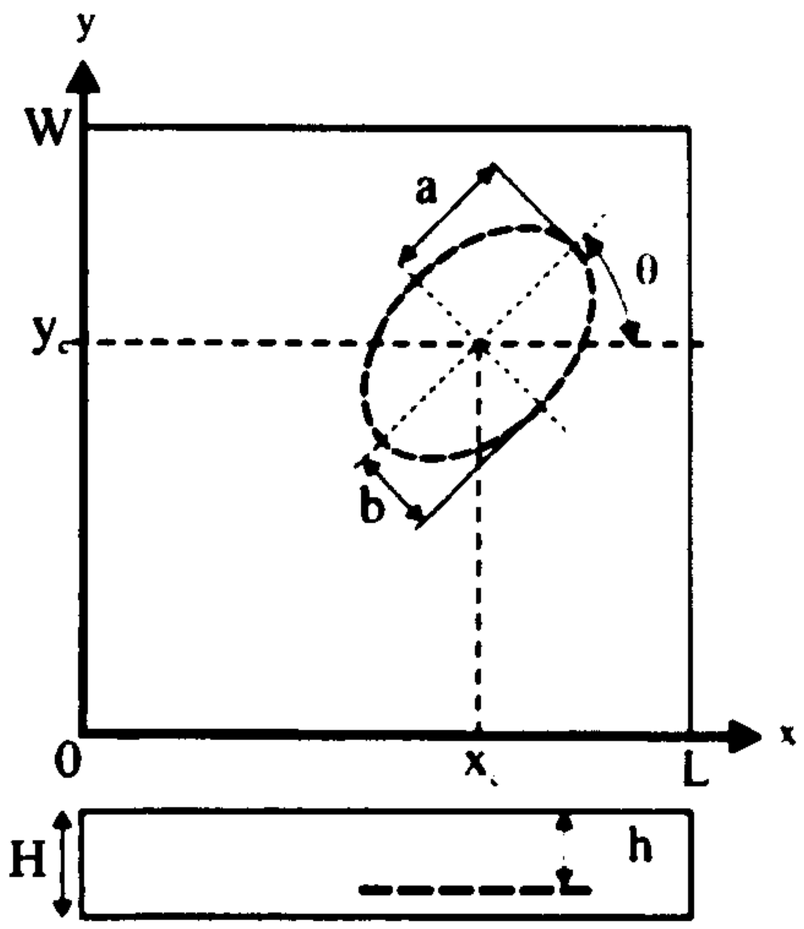

Figure 4.3. Geometrical parameters needed to define delamination.
Planar location (x_c, y_c), length $2a$, width $2b$, angle of orientation θ, and depth h.

only at the interfaces of the laminate, hence the possible alleles of gene six are in a discrete space that represents the thickness of the delaminated region. For example, given a six ply laminate with a ply thickness of 0.125 mm, the possible alleles of gene six are $\gamma_6 = [-0.125, -0.25, -0.375, -0.5, -0.625]$. In this case, it is not possible to constraint further the alleles of γ_6. If a n ply laminate is given, then there exists $(n-1)$ possible values where the delamination could be located.

Gene $\gamma_7 = p_d$ encodes the pressure of the air trapped in the delamination when the DSPI test take place. At the time of writing, the precise range of values of this pressure is unknown. The explanation so far, it is that the pressure in equal or greater than zero, and lower than the atmospheric pressure. Hence, the possible range values for this allele is $(0, p_{atm})$.

DEFINITION 4.3 (CHROMOSOME) *A chromosome ξ is a vector of genes. Mathematically,*

$$\xi = \langle \gamma_1, \gamma_2, \ldots, \gamma_n \rangle . \tag{4.19}$$

where n is the length of the chromosome.

Genes are positional; such position is called a *locus* in genetics. This means that, although two genes may look the same, they *encode* for different infor-

mation if they are at different *loci*. Often the concept of genes is omitted in the literature on genetic algorithms, and chromosomes are used exclusively. In this case the chromosome is though as a string of bits encoding the problem at hand.

Remark In this thesis a chromosome is understood as the tuple $(\vec{z}, p_d)$ composed by the delamination parameters and the unknown pressure of the air inside of the delamination. Explicitly, a chromosome is the vector ξ of genes one to seven expressed in the following way,

$$\xi = \langle x_c, y_c, a, b, \theta, h, p_d \rangle \,. \tag{4.20}$$

DEFINITION 4.4 (INDIVIDUAL) *An individual α is a tuple*

$$\alpha = \langle \xi, \tau \rangle \,, \tag{4.21}$$

where ξ is a chromosome and τ is the actual generation number.

Sometimes the term *individual* is replaced by *member of the population* especially when it is important to emphasise the membership.

Example Suppose that the damage parameters of a delamination are $x_c = 0.05$ mm, $y_c = 0.03$ mm, $a = 0.01$ mm, $b = 0.005$ mm, $\theta = +45$, and $h = -0.125$ mm. Moreover, suppose that the pressure inside of the delamination is $p_d = 10000$ Pa. Additionally, say that the actual generation number is three, and the individual under consideration is the number five. Then, the fifth individual with genes encoding the damage parameters, and the pressure inside of the delamination in the third generation of a genetic algorithm can be expressed as,

$$\alpha_5 = \langle \langle 0.05, 0.03, 0.01, 0.005, 45, -0.125, 10000 \rangle, [3] \rangle.$$

DEFINITION 4.5 (GENETIC FITNESS) *An individual's genetic fitness ϕ is the probability to propagate its genes to next generation:*

$$\phi(\xi, \tau) = p(\alpha_\tau) \,, \tag{4.22}$$

where α_τ is an individual with chromosome ξ within the generation τ.

Genetic fitness is what connects the individual to the problem under investigation. Genetic fitness (or fitness as is used in the literature) is expressed in terms of a *function fitness function* $p(\alpha_\tau)$ that essentially determines how difficult the optimisation space is to search.

In most numerical problems, the fitness function is explicitly given by a mathematical equation. However, many real world problems are usually not well-defined and their representation is up to the designer of the GA. The primary criterion is that the fitness function properly ranks the individuals so the most desirable solution is assigned to the best fitness (maximization or minimization). Otherwise, selection will choose the wrong individuals when forming the next generation.

In addition to the ranking criterion, a number of properties of fitness functions exist. These are not strict requirements, but issues that should be considered when designing the fitness function, because the search performance depends on the topology of the fitness landscape. First, the fitness landscape should not contain plateaus. Selection fails on plateaus, because all individuals have the same fitness in such a scenario. Consequently, a genetic algorithm essentially degrades to random search when the landscape mainly consists of plateaus. Second, the fitness landscape should be somewhat smooth. This is, adjacent solutions in the search space should have similar fitness values. Searching a very irregular landscape corresponds to finding a particular grain of sand in the ocean, and no algorithm can do this any better than random search. Third, ridges in the search space may pose an additional challenge to the algorithm, because a ridge in the fitness landscape corresponds to correlation between the parameters in the search space. In the vicinity of a ridge, any movement in the search space that is not in the direction of the ridge orientation will lead to a fitness reduction. Fourth, local optima may attract the population of the algorithm and lead to a premature convergence of the search.

Remark In the previous section it was showed that the inverse problem of characterisation of delamination could be posed as the *minimization* of the scalar performance function $\Psi_{err}(\vec{z}, p_d^t)$ (equation 4.16). This function could be

rewritten to take into account the language used in genetic algorithms as follows,

$$\Psi_{err}(\vec{z}, p_d^t) = \Psi_{err}(\alpha_\tau). \tag{4.23}$$

If at some generation during a genetic algorithm an individual is close to the global minimum of the problem, the performance criteria $\Phi_{err}(\alpha_\tau)$ would be close to zero. Moreover, if the purpose of the genetic algorithm is *reward* fittest individuals, the fitness function $p(\alpha_\tau)$, should be somehow inversely proportional to the performance criteria (if the performance criteria lowers, the fitness function increases). Taking into account the restrictions to the design of a suitable fitness function, researchers have come up with the following equation,

$$p(\alpha_\tau) = \frac{k}{k + \Phi_{err}(\alpha_\tau)}. \tag{4.24}$$

In this equation k is a scaling parameter, that is usually fixed at 1.0. Equation 4.24 shows that there is a one-to-one correspondence between the genetic fitness of an agent, and the solution of the inverse problem.

DEFINITION 4.6 (POPULATION) *The population Ω of a genetic algorithm is the set of all individuals within a generation τ.*

In a genetic algorithm, the initial population specifies the starting points of the search. The initial population can be created in a number of ways The most common setup is the random initialization where the chromosomes are randomly assigned, preferably using a uniform distribution. The goal is to create a population with a good coverage of the search space, and consequently have a gene pool with good potential for breeding better solutions. Alternatively, chromosomes can be evenly scattered over the whole search space according to a regular grid-layout. A third approach is to incorporate expert knowledge into the initialization. In some cases, it is possible to assign the initial search space positions based on specific knowledge about the objective function.

Other aspect of the population is its size. Large number of individuals in a population allow a comprehensive search of the optimisation space. However, large populations induce overhead penalties in computing time. For example,

consider a problem where the solution of a single FE model takes two minutes. If the population size is twenty, then the evaluation of the fitness function for a single population would take about forty minutes. If the genetic search evolves for a hundred generations (this being quite common), then the whole optimisation would take about three days.

Remark In the initial stages of this research large number of individuals (20) were used. Typical running times were about 4.5 days, time that is prohibitive if it is taking into account that a four processor supercomputer was used. A particular finding in this thesis is that it is possible to work with populations composed of as little as five individuals.

DEFINITION 4.7 (ELITE POPULATION) *An elite population is part of a population that is automatically included in the population of the next generation because the fitness function of its individuals exceeds an elite threshold.*

This is the only structure in the definition of genetic algorithms that do not follow any principles of natural evolution. For example, elite populations may or may not participate in the reproduction, and in fact it works like time machine that is capable of sending *good* individuals into the future. The effects of elitism on the convergence of a genetic algorithm can or cannot be beneficial; in the implementation of some applications is desired to retain the best individual found so far, then elitism is implemented. However, not always elitism is beneficial, and sometimes it leads to a non convergence of a genetic algorithm [141].

DEFINITION 4.8 (GENERATION) *A generation τ is an ordinal number used to indicate the current stage of evolution in a particular genetic algorithm.*

4.5.3.2 Genetic Operators - Operators affecting genes

DEFINITION 4.9 (MUTATION) *The gene-specific genetic operator of mutation $\omega_{\gamma,m}$ is a deterministic function transforming an allele of a gene ω_P to another ω_Q by adding a small perturbation δ with a low probability p_m.*

$$\omega_{\gamma,m} : \gamma_Q = \gamma_P + \delta \tag{4.25}$$

During the evolution of genetic algorithms, individuals in a population tend to migrate and concentrate around spots of local minima, and consequently there is a reduction in the genetic diversity of the population that lead to a premature convergence. Furthermore, if the initial population did not contain some *beneficial* gene, then the algorithm may be prevented to explore a region of the optimisation space. The mutation operator introduces new *traits* into the population that allows the genetic algorithm to overcome local minima.

Example Consider a chromosome that encodes the damage parameters $x_c = 0.025$ mm, $y_c = 0.035$ mm, $a = 0.015$ mm, $b = 0.010$ mm, $\theta = 90$, and $h = -0.250$ mm, and the pressure inside of the delamination is $p_d = 1000$ Pa. Now, select a random locus on the chromosome, and mutate it by adding ten percent of its value. Suppose that the randomly selected locus is three, then the chromosome before and after the mutation step is given as follows,

$$\textit{Before mutation}: \quad \langle 0.025, 0.035, \underline{0.0150}, 0.010, 90, -0.250, 1000\rangle$$
$$\textit{After mutation}: \quad \langle 0.025, 0.035, \underline{0.0165}, 0.010, 90, -0.250, 1000\rangle.$$

DEFINITION 4.10 (RANGE ADAPTATION) *The operator of range adaptation* $\omega_{\gamma,\Delta}$ *is a function that transform the range of the alleles* $[\min(\gamma_P), \max(\gamma_P)]$ *for a gene* γ_P. *Formally,*

$$\begin{aligned} &\omega_{\gamma_P,\Delta} : [\min(\gamma_P), \max(\gamma_P)]_{i-1} \mapsto [\min(\gamma_P), \max(\gamma_P)]_i \\ &\textit{where} \quad (\max(\gamma_P) - \min(\gamma_P))_{i-1} \geq (\max(\gamma_P) - \min(\gamma_P))_i \end{aligned} \tag{4.26}$$

Fast convergence to a local minima and loss of diversity are common problems of real-coded genetic algorithms. A tentative solution to this issue is by re-generating the entire population every M $(M > 1)$ generations using the following procedure [142],

1 Every M $(M > 1)$ generations the average $\mu_{i,sampling}$ and the standard deviation $\sigma_{i,sampling}$ of each delamination parameter p_i are calculated by sampling the top half of the previous generation.

2 A new average and standard deviation for each parameter p_i are obtained updating the previous values according with equation 4.27, where ω_μ and ω_σ are relaxation factors that provide robustness during the range adapta-

tion.

$$\mu_{i,new} = \mu_{i,present} + \omega_\mu \left(\mu_{i,sampling} - \mu_{i,present}\right)$$
$$\sigma_{i,new} = \sigma_{i,present} + \omega_\sigma \left(\sigma_{i,sampling} - \sigma_{i,present}\right) \tag{4.27}$$

3 The new search range of each parameter p_i is re-defined using Eq. 4.28, where κ $(1 \leq \kappa \leq 6)$, determines the degree of overlapping between the sampled top half population and the new generation.

$$p_{i,min} = \mu_{i,new} - \kappa\, \sigma_{i,new}$$
$$p_{i,max} = \mu_{i,new} + \kappa\, \sigma_{i,new} \tag{4.28}$$

4 All but two individuals (the first and second-best-fitness individuals) are discarded and then a new population is generated randomly according to the new parameter range.

The essence of this operator is to adapt the population toward promising regions during the optimisation process, which enables efficient and robust search while keeping the length of the chromosome short. This characteristic makes this operator especially attractive when real number encoding is used.

Additionally, this operator could eliminate the need for a prior definition of search boundaries since this operator distributes solution candidates according to the normal distribution of the design variables in a given population [118].

Remark In this study, the range of the planar location, the length, and the width of the delamination was fixed using knowledge from the DSPI results in the form of geometric moments and a laplacian edge detection technique. Results in Chapter 6 will show that this operator increase the speed in the prediction of these parameters.

4.5.3.3 Genetic Operators - Operators affecting chromosomes

DEFINITION 4.11 (CROSSOVER) *Crossover is a function transforming a set of chromosomes to a chromosome.*

$$\omega_\xi : \xi_P \mapsto \xi_Q. \tag{4.29}$$

Crossover is an operator that leads to the almost exponential convergence of the optimisation problem when using genetic algorithms. In this operator, two

parents are chosen according with their fitness, and then allowed to breed in order to produce offspring. The probability of cross over is relative high, and values of 0.6 to 0.8 are reported in the literature [143].

A number of different crossover mechanisms exists, that can be applied or not depending on the type of encoding that is used. If the genes are encoded using a binary representation, the following mechanisms are available: (1) single-point crossover, (2) multi-point crossover, (3) uniform crossover, (4) shuffle crossover, and (5) crossover with reduced surrogate.

For real number encoding the following mechanisms are available: (1) discrete recombination, (2) intermediate recombination, and (3) line recombination. In this study real number encoding is used.

Discrete recombination During a discrete recombination there is an exchange of corresponding genes between two individuals. Consider the following two individuals that encode two particular sets of damage parameters, (this two individuals will also be used in the following examples on other types of real number mechanisms of recombination. Also note that the generation number is omitted in the definition of the individual),

$$\alpha_1 = \langle 0.05, 0.03, 0.01, 0.010, 45, -0.125, 10000 \rangle$$
$$\alpha_2 = \langle 0.07, 0.04, 0.02, 0.005, 90, -0.250, 2500 \rangle.$$

For each locus in the chromosome the parent who contributes its genes to the offspring is chosen randomly with equal probability. This means that two arrays called *donors* are randomly created, where every position in it has a random value of either one or two as follows,

$$donor_1 = \langle 1, 2, 2, 1, 1, 1, 2 \rangle$$
$$donor_2 = \langle 1, 1, 2, 1, 2, 2, 1 \rangle.$$

The procedure to create the offspring is simple, for the first offspring the array $donor_1$ is chosen, then the value stored in every location j of $donor_1$ indicates which parent inherits its gene to the offspring in loci j. The process to create the second offspring is the same. Using the previous definitions, the new two offspring are defined as,

$$offspring_1 = \langle 0.05, 0.04, 0.02, 0.010, 45, -0.125, 2500 \rangle$$
$$offspring_2 = \langle 0.05, 0.03, 0.02, 0.010, 90, -0.250, 10000 \rangle.$$

Intermediate recombination During intermediate recombination, the alleles of the genes of offspring are chosen somewhere around and between the genes alleles of the two individual-parents using the following rule,

$$offspring_j = \alpha_1 + \beta_j(\alpha_2 - \alpha_1), \tag{4.30}$$

where β is a random scaling factor chosen over a predefined interval $(-r, 1 + r)$. In intermediate recombination $r = 0$, for extended intermediate recombination $r > 0$. Typical values of r found in the literature are around $r = 0.25$. Each gene in the offspring is the result of combining the parents genes according to the above expression with a new β chosen for each gene.

Considering individuals α_1 and α_2 defined above. Two new arrays called *beta* (β) are created with the same number of positions as genes in the parents. When using intermediate recombination every position in the β array is filled with a random number in the range (0,1) as follows,

$$\beta_1 = \langle 0.86, 0.85, 0.59, 0.50, 0.90, 0.82, 0.64 \rangle$$
$$\beta_2 = \langle 0.82, 0.66, 0.34, 0.29, 0.34, 0.53, 0.73 \rangle.$$

The procedure to create the offspring is as follows, for the first offspring the array β_1 is chosen, then the offspring is created according to equation 4.30. The process to create the second offspring is the same. Using the previous definitions, the new two offspring are defined as,

$$offspring_1 = \langle 0.0672, 0.0386, 0.016, 0.008, 90, -0.250, 5163.2 \rangle$$
$$offspring_2 = \langle 0.0660, 0.0366, 0.013, 0.008, 45, -0.250, 4546.7 \rangle.$$

The application of this type of crossover mechanism in this study has some implications for genes five and six, which encode the angle of orientation and depth of the delamination. Firstly, intermediate recombination generates values for the angle of orientation that may not be aligned with the angle of fibres in the laminate. In that case, the resultant is rounded to closest valid angle of orientation. Secondly, a similar situation occurs with the depth of the delamination. In this case too, the resultant depth is rounded to the closest valid value.

Line recombination During line recombination, the alleles of the genes of offspring are chosen somewhere around and between the genes alleles of the two individual-parents using the following rule,

$$offspring_j = \alpha_1 + \beta(\alpha_2 - \alpha_1), \tag{4.31}$$

The difference between line and intermediate recombination, is that for line recombination only two single scaling parameters β are used.

Considering individuals α_1 and α_2 defined above. Two new parameters called β_1 and β_2 are randomly created in the range (0,1) as follows,

$$\beta_1 = 0.5$$
$$\beta_2 = 0.25$$

The procedure to create the offspring is as follows, for the first offspring the scaling parameter β_1 is chosen, then the offspring is created according to equation 4.31. The process to create the second offspring is the same. Using the previous definitions, the new two offspring are defined as,

$$offspring_1 = \langle 0.060, 0.0350, 0.0150, 0.0075, 45, -0.125, 6250 \rangle$$
$$offspring_2 = \langle 0.055, 0.0325, 0.0125, 0.0088, 90, -0.125, 8125 \rangle.$$

The same procedure followed for intermediate recombination is used in here to correct the alleles from genes five and six.

4.5.3.4 Genetic Operators - Operators Affecting Populations

Selection is the only operator that operates on entire populations. Selection determines which individuals are chosen for reproduction (recombination). A formal definition of selection is the following:

DEFINITION 4.12 (SELECTION) *The population-specific genetic operator ω_Π is a mapping transforming a population Π_P of individuals into another population Π_Q of individuals.*

$$\omega_\Pi : \Pi_P \mapsto \Pi_Q. \tag{4.32}$$

Selection is accomplished through two successive steps. The first step is fitness assignment by using either proportional fitness assignment [113, 115] or

rank-based fitness assignment [144, 145]. Then, the proper selection method is performed. Parents are selected according to their fitness by means of one of the following methods: roulette-wheel selection [146, 147], stochastic universal sampling [146], local selection [148, 149], truncation selection [150], or tournament selection[151].

Proportional fitness assignment In proportional fitness assignment, the individuals in a population are sorted according to their objective function. The fitness assigned to each individual depends only on the actual value of its objective function. The main problem associated with proportional selection is that it is scale sensitive. At some stage of the genetic algorithm, some individuals will have a fitness that is much larger that the fitness of the remaining population. This implies that over-fitted individuals will reproduce more frequently, leading the GA to a premature convergence.

Rank-based fitness assignment In this fitness assignment method, the individuals in the current population are sorted into descending order according to the objective function values. The fitness assigned to each individual depends only on its relative position in the individual rank. Ranking simplifies the mapping from the objective function to the fitness function and also eliminates the fitness scaling problem exhibited by the proportional fitness assignment. However, a major drawback of ranking is that it ignores the information about the relative difference between individuals narrowing the search space slowly.

Roulette wheel selection Before the selection step, proportional fitness assignment is used such that the probability of selecting and individual for reproduction is proportional to the individual's fitness. The sampling procedure is referred to as the roulette wheel selection, because the probability distribution can be represented as a roulette wheel on which every slice has an area according to the individual's selection probability. This selection algorithm provides zero bias[2] but does not guarantee minimum spread[3].

---

[2]Absolute difference between an individual's fitness and its expected probability of reproduction

[3]Range of possible values for the number of offspring of an individual

Stochastic universal sampling Stochastic universal sampling overcomes the limitations of the roulette wheel selection method. In this method, the probability distribution is mapped on to a roulette wheel, but N equal spaced pointers are used to determine which individuals will be selected. This selection method is more efficient than the roulette wheel method because it ensures a generation of offspring that is closer to their parents.

Local selection In local selection every individual of the population resides inside a constrained set called the local neighbourhood. Individuals only interact with other individuals inside the constrained set. The first step in local selection is choosing a half of the mating parents using proportional or ranking-based methods. Then, a local neighbourhood is defined for every chosen individual, and inside of this space the other mating parent is selected using any of the selection methods described in this section. The size of the neighbourhood determines the speed of propagation of genes between individuals inside of the population.

Truncation selection In truncation selection individuals are sorted according to their fitness. Only the best individuals in the population are then selected to mate, producing a random offspring. Typically, only the 10% to 50% of the top fitness individuals is chosen to generate offspring, leaving the less fitted individuals without possibility of recombine. Then, truncation selection leads to a higher loss of diversity and much smaller selection variance compared to the other selection methods.

Tournament selection In tournament selection a group of M individuals is chosen randomly from the population. Then, these chosen individuals take part in a tournament where the fitness value are compared between the M individuals and the best individual is selected. This process is repeated to select all the parents, and this will lead to a high individuals' spread. An advantage of this method is that is invariant under scaling.

4.5.3.5 Convergence and stopping criteria

Genetic algorithms are typically required to determine a satisfactory solution to a problem where other search techniques have failed or can not be applied. The required parameters for the convergence of the algorithm are specified before the genetic algorithm is executed. When an individual in the population achieves the parameters of convergence, the algorithm stops.

On the other hand, some times genetic algorithms are required to find the best solution to an optimisation problem. While a genetic algorithm can not guaranteed to find a global minimum, it usually finds suitable solutions in a reasonable period of time. In this circumstances, the stopping criteria is generally specified as the number of generations since the last improvement in fitness was found.

4.6 Conclusion

This chapter addresses the research question three included in Chapter one. The main question that this chapter aimed to be solved is as follows, *How can the problem of characterisation of delamination in composite laminates be formulated and solved?*

The methodology employed to solve the above question involved splitting the research question in three sub questions (A to C), which pointed to the formulation of the characterisation problem in terms of a classical inverse problem. Next, the reformulation of the inverse problem in terms of central geometric moments that allowed a more efficient algorithm of solution, and finally, genetic algorithms as a global optimisation tool for the solution of the inverse problem. The following sub sections provides the main conclusions to these questions.

4.6.1 Formulation of the inverse problem - Subquestion A

The problem of characterisation of delamination in composite laminates can be formulated as an inverse problem where the measured response of the surface of the laminate is used to predict the geometric parameters of the flaw. Mathematically, the inverse problem can be formulated using the output error

criterion that relates the measured response of the laminate from DSPI and the displacements obtained from a FE model with a trial debonding.

The output error criterion leads naturally to an optimisation problem where the objective function is written as the minimisation of the difference between the measured and computed FE displacements, and the variables to optimise are the geometric parameters of an idealised delamination in a FE model.

4.6.2 Reformulation of the inverse problem - Subquestion B

The classical formulation of the inverse problem leads to non-efficient solution algorithms as a consequence of the number of measurements that are provided by the DSPI technique. The large amount of data contained in the array of experimental results can be represented by a finite set of central geometric moments.

Central geometric moments are able to represent accurately the physical content of the experimental results because they are sensitive to the size, location, and orientation of the displacement field contained in both the DSPI measurements, and the FE model that encapsulates the delamination to be characterised. These moments are equivalent to geometric moments that are calculated from the centroid of the out-of-plane displacement field.

The computation of geometric moments involves the calculation of a convolution of the out-of-plane displacements with a predefined family of monomial functions. In case of the measurements from DSPI, geometric moments can be computed replacing the integral of area for a double summation. In the case of the FE model, a formula that also uses a double summation was developed in order to take advantage of the design of the FE mesh.

Out-of-plane displacements from both the DSPI technique and a FE model can be compared using a seven-moment similarity measure, which is based in low order central geometric moments. A comparison of this condition is cost-effective because it reduces the time of computation used in such comparison.

The use of central geometric moments involves the reformulation of the delamination characterisation problem, as an inverse problem where the central geometric moments computed form the measured response of the surface of

the laminate is used to predict the geometric parameters of the flaw. This new version of the inverse problem can be formulated using the output error criterion that relates the central geometric moments from DSPI and the moments obtained from the displacements of a FE model with a trial crack.

The output error criterion is written as an optimisation problem where the objective function is written as the minimisation of a seven-moment similarity measure.

4.6.3 Solution of the inverse problem - Subquestion C

The formulation of non-destructive crack identification problems leads naturally to non-differentiable, non-convex optimisation problems. Traditional local minimisation techniques can not be used to solve such optimisation because (1) they usually converge to local minima close to the starting point of search, and (2) they require the information about the derivates of the objective function. Thus, a global optimisation method is required for the numerical solution of the optimisation problem.

In a genetic algorithm, the set of unknown delamination parameters are represented as a chromosome of genes using real number encoding. Furthermore, due to the stochastic nature of genetic algorithms, a initial population of trial delaminations is assumed. For each set of alleles of the genes in the chromosome of an individual, the error function $\Psi_{err}(\vec{z}, p_d^t)$, that is the difference between measured and calculated central geometric moments, is calculated. In accordance to the terminology used in genetic algorithms, the minimisation problem is transformed into a maximisation problem. Therefore, instead of an error (or objective) function, a fitness function is introduced.

The mechanism of work of genetic algorithms is inspired on the concepts of natural selection and genetics. In the selection step, individuals with higher fitness function values are chosen to breed and to inherit their characteristics to the next generation. A cross over operator allows to interchange genetic content between individuals within the reproduction step. Finally, random genes in individuals are randomly mutated during the creation of a new generation.

Chapter 5

DELAMINATION IDENTIFICATION USING A LOW-POPULATION GENETIC ALGORITHM

Abstract A novel identification technique based on a low-population genetic algorithm for quantitative characterisation of a single delamination in composite laminated panels is presented in this chapter. The damage identification procedure is formulated as an inverse problem through which system parameters are identified. The input of the inverse problem, the central geometric moments (CGM), is calculated from the surface out-of-plane displacements measurements of a delaminated panel obtained from DSPI. The output parameters, the planar location, size and depth of the flaw, are the solution to the inverse problem to characterise an idealised elliptical flaw. The inverse problem is then reduced to an optimisation problem where the objective function is defined as the L_2 norm of the difference between the CGM obtained from a finite element (FE) model with a trial delamination and the moments computed from the DSPI measurements. The optimum crack parameters are found by minimising the objective function through the use of a real-coded low-population genetic algorithm. DSPI's measurements of ten delaminated T700/LTM-45EL carbon/epoxy laminate panels are used to validate the methodology presented in here.

5.1 Introduction

The use of composite materials has expanded to many applications in recent years, including automotive, aircraft, and aerospace structures. These structures are often under the influence of heavy mechanical loads during their manufacturing and in-service operation, having them to be regularly controlled in order to check their serviceability. Systematic non-destructive inspections are normally scheduled in order to detect early signs of damage. When damage is detected, composite structures have to be subjected to both stringent

maintenance and structural integrity analysis to insure their capacity for continued use.

The increased complexity in the design of structures made of composite materials has lead to the continuous development of more sophisticated non-destructive techniques (NDT) for the detection of damage. These techniques, like DSPI, are more efficient, faster and accurate than traditional inspection techniques like X-rays or Thermography. However, results from these new NDT are less intuitive for human interpretation, often requiring experts to decode the information obtained from such techniques.

Although much research on detection of delamination in composite laminates has been done to date, it is clear from the literature that more studies need to be performed to design and test methodologies for the automatic identification of such damage from measurements obtained from non-destructive techniques.

5.2 Problem Statement

Identification of damage in structures made of composite materials must meet at least two, often conflicting, objectives: *speed* and *accuracy*. Firstly, the time consumed to post-process data from NDT into meaningful flaw's geometrical parameters must be minimum. Secondly, engineers and researchers on-field need to know accurately the location and extent of damage in order to predict remaining strength and life span of structural components. In the literature concerning damage identification, however, most researchers have been concerned with the ability to characterise damage in an accurate way, leaving apart the implications of speed in the characterisation process.

Although the amount of research on damage detection and identification is vast, much of it only presents theoretical results obtained from simulations that do not agree completely with the reality of on-field experimentation. Studies that validate experimentally the approaches suggested by researchers are the exception rather than the rule.

5.3 Objectives and Research Questions

To the knowledge of the author of this thesis, there are not studies reported in the literature that suggest, and validate experimentally, a methodology for the identification of delamination in composite laminates. The main objective of this chapter is stated as follows,

> *Design a computational methodology for delamination identification, and examine its validity using experimental data from Digital Speckle Pattern Interferometry (DSPI).*

This objective can be satisfied if the following research sub questions are solved:

1 **Sub question A:** How can the concepts of finite element analysis, geometric moments, inverse problems, and genetic algorithms be incorporated into a single computational methodology that can be used to identify delamination in composite laminates? (Formulation).

2 **Sub question B:** Does the experimental validation of the methodology leads to a cost-effective (in terms of *speed* and *accuracy*) solution of the identification problem? (Validation).

The following section details the methodology and experimental setup used to solved these research questions.

5.4 A Methodology for Identification of Delamination - Sub question A

A six-step computational methodology for the characterisation of delamination from DSPI measurements is presented in this section. Based on Figure 5.1 the basic steps in the methodology are as follows:

1 Edges of the bulge present in DSPI measurements are determined using a Laplacian-based filter (Chapter 3).

2 Initial parameters that define the size and orientation of the delamination are calculated from the detected edges in step one (Chapter 3).

3 Reduction of the amount of data in DSPI measurements is obtained by using central geometric moments of up to order three (Chapter 4).

4 A finite element (FE) model with a trial delamination parameters is assembled in order to compare its response, in terms of displacements, against the response of the real laminate during a DSPI test. (Chapter 3).

5 Central moments computed from the FE response are used as a base of comparison with the moments calculated from DSPI (Chapter 4).

6 A genetic algorithm is used to minimise the difference between the central geometric moments computed from a FE model with a parametric trial crack, and moments from DSPI measurements (Chapter 4).

Even though every one of the previous steps have been detailed in previous chapters, a brief summary is now presented in order to establish the context of this chapter.

5.4.1 Laplacian-based edge detection - Step 1

When loaded in a vacuum chamber, the surface of a laminate containing a delamination will tend to bulge. DSPI detects such bulging effect, and produces a number of displacement measurements of the plate surface. The first step in the identification methodology is to *locate* the area of the panel where the bulge is present.

A laplacian-based edge detection technique is used to define a boundary that separates the bulge form the regions of low (or zero) displacements. This technique uses both the laplacian and the variance of the laplacian calculated from the surface displacement measurements of the panel $\tilde{u}_0(x, y)$. Given a particular planar position on the surface of the panel (x_i, y_i), the laplacian of $\tilde{u}_0(x_i, y_i)$ is computed. If the laplacian is less or equal to a predefined threshold, then the variance of the laplacian is calculated in that point. If the variance in (x_i, y_i) is higher than a second threshold, then (x_i, y_i) is considered as an edge point.

The process described in the previous paragraph is repeated for every measured position of the panel. The output of this technique is an array of points (x_i, y_i) that define the boundary of the experimental bulge.

5.4.2 Determination of initial parameters of delamination - Step 2

The solution of the inverse problem of characterisation of delamination is equivalent to the solution of a minimisation problem arising in the application of the output error criterion (Chapter 4). Cost-effective solution of optimisation problems can be obtained if a *good* starting point for the search is predefined. The second step in the identification methodology aims to provide such starting point by post processing the data, from the detected edges in step one, into a set of meaningful delamination geometrical parameters.

A second order minimisation technique is used to *map* the Cartesian coordinates of the detected edges (step 1) into numerical values that define a parametric ellipse. The technique starts by defining the equation of an ellipse in polar coordinates. Then, the partial derivates of this equation are obtained to construct the gradient vector and the Hessian matrix of the parametric ellipse. Finally, the gradient vector, and the Hessian matrix are used in a second order Newton-Raphson method to find the optimum parameters of the ellipse that minimise the distance between the points in the edge of bulge, and the points along the boundary of the ellipse.

The output of this technique is a set of values that represent the size and orientation of the delamination that can be used as starting point for the solution of the inverse problem studied in this thesis.

5.4.3 Central geometric moments from DSPI measurements - Step 3

Among non-destructive techniques, DSPI shows potential to be used in identification of damage in composite laminates. This technique is able to make non-contact, whole-field , and real-time measurements of out-of-plane static displacements that can be used to evaluate the existence of internal damage. Typically, DSPI provides an unequivocal set of experimental data in the form of an array that contain up to 300000 individual measurements. Even though this technique has several advantages for crack identification, the vast quantity

of data must be reduced, with minimal loss of quality, in order to be used in an efficient way.

In this thesis central geometric moments (CGM in Chapter 4) are used to represent DSPI measurements. These moments allow reducing the amount of data from DSPI maintaining at the same time the physical significance of such results. The numerical computation of CGM from the experimental data is somewhat simple.

The array of measurements from DSPI can be considered as a two dimensional array of pixels in an image. In this way, the integrals involved in the calculation of the moments are reduced to a double summation that relates the measurements at a given Cartesian point with the area of the *pixel* that contains such a point.

The output of this step is an array of seven central geometric moments (up to fourth order moments), which represents DSPI measurements.

5.4.4 FE representation of a delaminated laminate - Step 4

Solution of the crack identification problems seeks for the minimisation of the difference between measured responses of a structure, and a the response from a FE model that contains a trial flaw. If the inverse problem is posed as an optimisation search, the FE model with multiple trial cracks must be solved as needed by the optimisation algorithm. The computer time consumed for solving such models can make them prohibitive in practice.

A free-mesh-based FE model is used in this thesis (Chapter 3) to account for two main factors: (1) effective representation of the boundary of the damage, and (2) short computer time used in its solution. The FE model is discretised in such a way that regions with low displacement gradient are meshed using coarse elements. Regions close and inside of the delaminated area are meshed using refined elements.

Computer time consumed in the solution of the FE model can be optimised not only by *sizing* the mesh, but also by choosing and adequate model that represents the physics of delamination during a DSPI experiment. In here the

sub-structure modelling technique was the one chosen because it balances both criteria.

5.4.5 Central geometric moments from FE response - Step 5

Surface displacements calculated from the FE model must be compared with the CGM derived from DSPI measurements. To do this, CGM are computed from the response of the FE Model (Chapter 4). The technique used to do this involves the assumption that every element in the two-dimensional mesh of the FE model can be considered as *pixels* in an image. In this way, CGM are calculated in the same way as it is described in step 3.

5.4.6 Delamination identification through a genetic algorithm - Step 6

The formulation of non-destructive crack identification problems leads naturally to non-differentiable, and non-convex optimisation problems. Local minimisation techniques can not be used to solve such optimisation because they usually converge to local minima close to the starting point of search, and they require the information about the derivates of the search space. Therefore, a global optimisation method is required for the numerical solution of the optimisation problem.

A low-population genetic algorithm is used as the global optimisation technique to solve the inverse problem. In this genetic algorithm, the set of unknown delamination parameters are represented as a chromosome of genes using real number encoding. Furthermore, due to the stochastic nature of genetic algorithms, an initial population of trial delaminations is assumed. For each set of alleles of the genes in the chromosome of an individual, the error function that represents the difference between measured and calculated central geometric moments, is calculated.

The output of the genetic algorithm is the geometric parameters of the delamination that is embedded in the composite laminate.

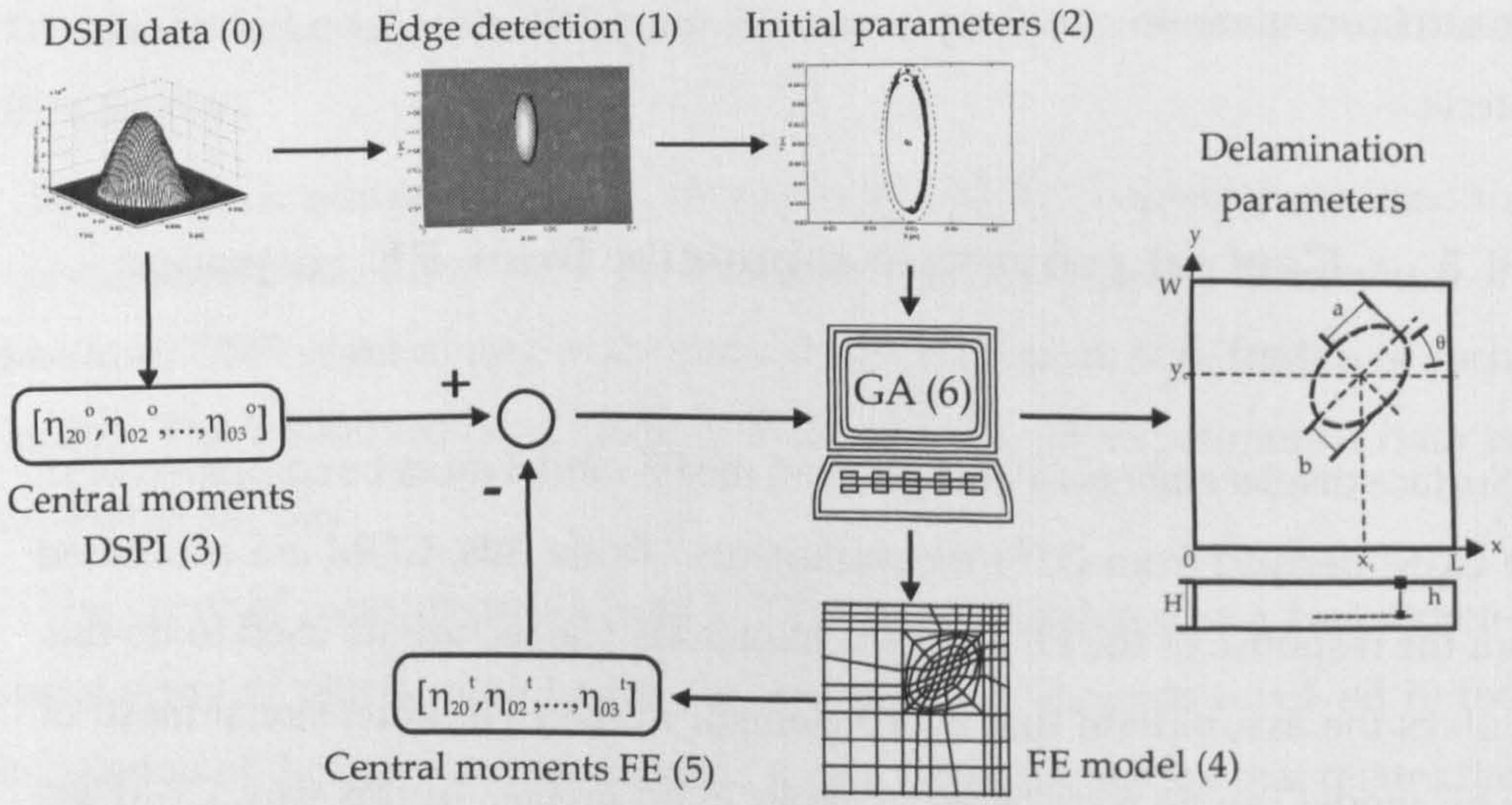

Figure 5.1. Methodology of identification of delamination from DSPI measurements. Determination of edges of the bulge present in DSPI measurements (1). Initial calculation of the geometrical parameters that define the size and orientation of the delamination from the previous step (2). Representation of DSPI data using central geometric moments (3). A finite element (FE) model is used to represent the composite laminate with a trial flaw (4). Displacements from FE analysis are represented through central geometric moments (5). A genetic algorithm is used to minimise the difference between the moments from DSPI and FE analysis (6).

The following section presents the methodology and procedures followed for the experimental validation of the methodology that was presented in the previous sections.

5.5 Experimental Validation - Sub question B

This section presents a description of the procedural steps, materials, and tools employed for the experimental validation of the methodology presented above. Firstly, the description of the experimental samples provided for validation in this work is given. Secondly, the specific configuration of the variables of the models used in this validation is provided. Finally, the methodology followed to present the results of the validation is described.

5.5.1 Experimental Samples

A group of ten experimental out-of-plane displacement field measurements were used as test cases for the damage identification technique. The author

of this thesis did not have any participation in the preparation of the samples nor in the DSPI sessions where the measurements were obtained. However, in order to give completeness to this thesis, and to provide a consistent methodology for replication of the procedures developed in this work, the following two subsections describe the manufacturing of the samples and the process followed during the DSPI experiments. Both sections are based on personal communications with Mr Luis Rivera (manufacturer of the samples at the laboratories of Automotive and Aeronautical Engineering - Loughborough University), and Dr Pablo Ruiz (DSPI experimenter at the Wolfson School - Loughborough University).

5.5.1.1 Manufacturing of composite laminates

The process carried out for manufacturing preconditioned composite panels included cutting of individual plies, lay-up, delamination embedment, curing and trimming. Laminate panels were fabricated from T700/LTM-45EL carbon/epoxy unidirectional (UD) prepreg. The UD mechanical properties of this composite system were determined as $E_{11} = 127\ GPa$, $E_{22} = 9.1\ GPa$, $G_{12} = 5.6\ GPa$ and Poisson's ratio $\nu_{12} = 0.31$. The ply thickness was determined as 0.125 mm. Prepreg was cut using a sharp blade, following a cutting plan to minimise waste. Once the individual plies were cut, they were stacked in a cross ply symmetric lay-up sequence. The lay-up was $(90/0/90)_S$ for a final 6-ply laminate.

Artificial delamination was embedded into the laminate, in the form of a double layer of thermoplastic fluonnate ethylene propylene (FEP) film of 0.051 *mm* thick. Between the two layers of FEP, a silicon grease ring was applied along the edge, to trap the air inside and avoid any interaction between the inclusion and the resin during the curing process. The two FEP layers were first cut with a scalpel by placing either circular or elliptical steel templates on a large piece of FEP thermoplastic film. Size of circular inclusions were 40, 20, 10 and 5 *mm* in diameter. Elliptical inclusions were 40 and 20 *mm* major axis with 3 : 1 aspect ratio. After cutting, the inclusions were carefully cleaned, prepared with the silicon ring and centrally located onto the specimen, stacked

Table 5.1. Experimental composite laminates used for validation.

Number	*Name*	*Shape*	*Length [mm]*	*Width [mm]*	*Angle (degrees)*	*Depth [mm]*
1	10C12D	Circular	10	10	-	-0.125
2	10C23D	Circular	10	10	-	-0.250
3	20C12D	Circular	20	20	-	-0.125
4	20C23D	Circular	20	20	-	-0.250
5	40C12D	Circular	40	40	-	-0.125
6	40C23D	Circular	40	40	-	-0.250
7	E2012D90	Elliptical	20	6.67	90	-0.125
8	E2023D0	Elliptical	20	6.67	0	-0.250
9	E4012D90	Elliptical	40	13.33	90	-0.125
10	E4023D0	Elliptical	40	13.33	0	-0.250

between the 1st and 2nd, the 2nd and 3rd, and the 3rd and 4th plies. Table 5.1 shows a specimen list.

All the panels were cured in an autoclave using the manufacturer's recommended curing cycle of 18 hours at 60^oC at 80 *psi*, with an initial ramp rate of $2^oC/min$. No vacuum was used, so the air trapped the delamination would remain inside the laminate. After curing panels were trimmed down using a diamond coated wheel trimmer. The nominal in-plane dimensions of all the panels were 100 *mm* wide by 100 *mm* long.

5.5.1.2 DSPI experimental setup

Figure 5.2 shows the speckle interferometer used to measure the surface deformation of the carbon composite laminates as the embedded delaminations expanded inside them due to vacuum loading. The beam from a frequency-doubled CW Nd:YVO4 laser ($\lambda = 532nm$) was divided into object and reference arms by a 90 : 10 beam splitter. The reference beam passed through a Pockels cell and recombined with the speckle pattern formed by the scattered object beam using a second 90 : 10 beam splitter in front of the camera objective. The Pockels cell was driven by a staircase waveform generator that produces one out of a set of four equally-spaced voltage levels, which were

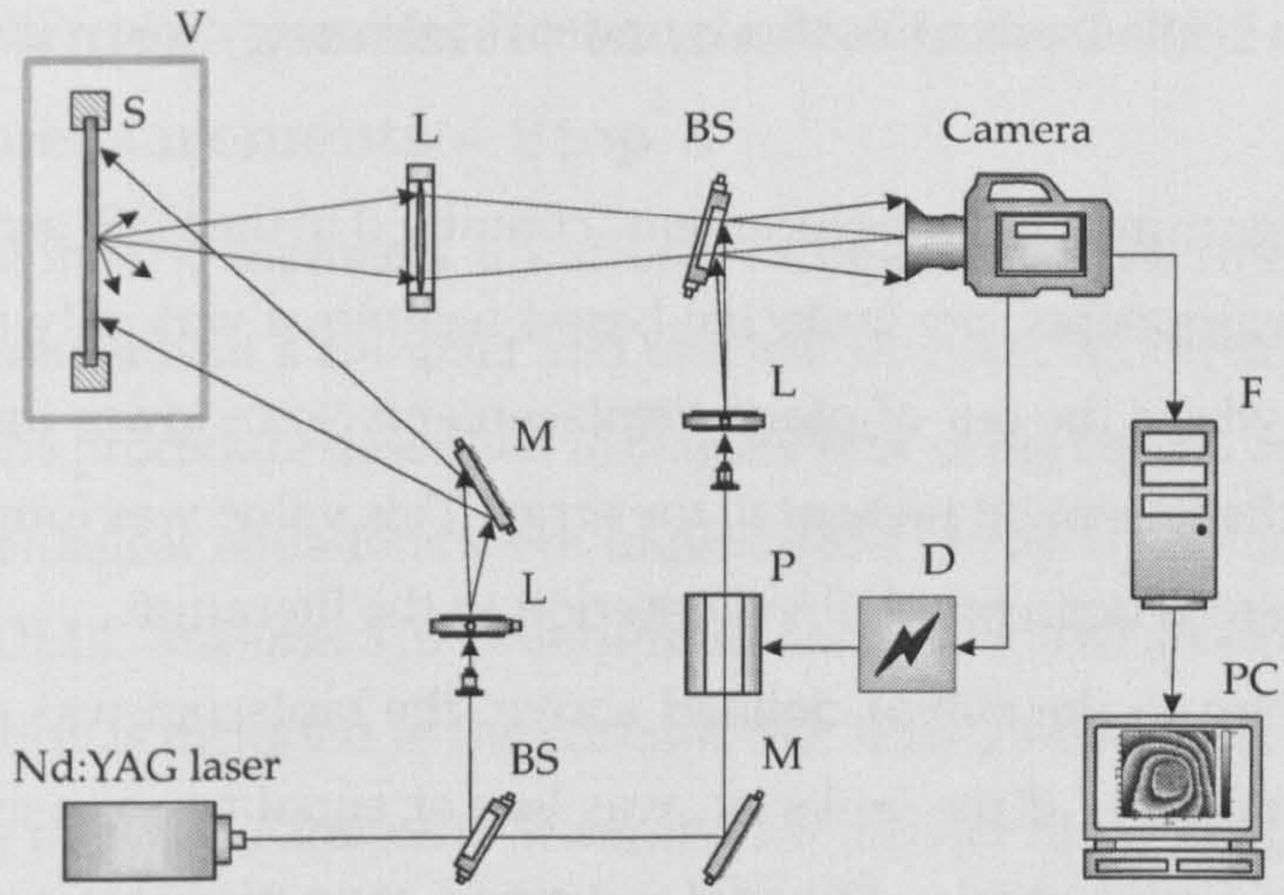

Figure 5.2. Optical set-up of the high-speed out-of-plane speckle interferometer. Personal computer (PC), frame store (F), pulse conditioner and high-voltage amplifier (D), Pockels Cell (P), 90 : 10 beam splitter (BS), mirrors (M), lenses (L), carbon fibre specimen (S) and vacuum chamber (V).

clocked cyclically in response to the rising edges of the strobe signal from the camera (VDS HCC-1000). In this way, the camera acted as the master clock for the whole system and a different phase step was introduced at the start of every new frame.

The laminates were placed in a vacuum chamber and imaged through a built-in transparent Perspex window. The initial relative pressure was -900 mbar, which caused the air trapped inside the delamination crack to expand and to deform the laminate. Air was allowed slowly into the chamber to release the load over the laminate and when the pressure reached -800 mbar, the camera started recording a sequence of 1024 phase-stepped interferograms, which is the maximum that can be stored in the camera's available memory.

5.5.2 Laplacian-based edge detection - Step 1

DSPI experimental results were given in arrays of 512 by 631 elements. The detection of the borders of the bulge contained in the DSPI array was performed according to the steps presented in chapter 3. The mathematical model was implemented in MATLAB 5.3, and was solved in a DELL Inspiron 8100 Pentium III computer. The source code of the implementation is included in

the cdroom that is attached to this thesis under the directory tree /SRC/Border Detection.

Given the large number of measurements contained in the DSPI array, 323.072 individual measurements, the laplacian-based technique was only applied to such positions where the out-of-plane displacements were lower than 10% of the maximum displacement present in the array. This value was found by trial and error, as there is not a pre-defined criterion in the literature.

For every point in the subset defined above, the laplacian was calculated using the equation 3.1. If the laplacian was less or equal to a pre-established threshold of 0.95 (value obtained by trial and error), then the point under analysis was considered as a border candidate.

Finally, for every point in the border candidate subset, the variance of the laplacian was calculated using the equation 3.2. If the variance was less or equal to a pre-established threshold of 0.01, then the point under consideration was labelled as part of the border of the DSPI bulge.

5.5.3 Determination of initial parameters of delamination - Step 2

Given the set of points that defined the boundary of the DSPI bulge obtained in step one, a second-order Newton-Raphson minimisation technique was used to determine the best set of numerical values that represented mathematically the aforementioned boundary. The process that was used is described in chapter three. The mathematical model was solved in the same computer as the algorithm presented in step one.

The initial values for the minimisation process were chosen in the following manner. The centre of the ellipse was fixed as the average of the coordinates of the points that were present in the boundary of the DSPI bulge. The initial value of the major axis of the delamination was pre-defined as the absolute difference between the maximum and minimum coordinate along the $x-axis$. Similar procedure was followed for the minor axis of the ellipse. The initial angle of orientation of the ellipse was pre-fixed as zero degrees.

The source code of the implementation is included in the cdroom that is attached to this thesis under the directory three /SRC/Border Detection.

5.5.4 Central geometric moments from DSPI measurements - Step 3

Central geometric moments up to order three were used to represent the DSPI measurements in a compact and efficient manner. Moments were calculated using the procedure described in chapter four using equations 4.7 and 4.10. These mathematical equations were implemented in MATLAB 5.3, and were solved in a DELL Inspiron 8100 Pentium III computer. The source code of the implementation is included in the cdroom that is attached to this thesis under the directory tree */SRC/Geometric Moments*. The master file is *MAIN.m*.

5.5.5 FE representation of a delaminated laminate - Step 4

The mathematical modeling of delaminated panels was performed through a specifically designed FE model, as was described in chapter three. The software used to implement the FE model was ANSYS 8.3. FE models were solved on a supercomputer SGI Origin 2000, with 4 CPU, 1 GB RAM, 128 GB HD located at the Advanced Computer Center *MOX* at Los Andes University in Bogota - Colombia.

The stages involved in the specification of the FE model were: (1) build the model, (2) apply boundary conditions and solve the model. These stages are described in the following paragraphs.

Build the model. The first step in building the FE model was the specification of the element type to be used. The ANSYS software element library contains more than 150 different element types. For composite materials, ANSYS offer one three dimensional element, SOLID46. This is a layered element designed to model layered thick shells or solids, which provides three degrees of freedom, that is displacements along x, y, z coordinates. The element is defined by eight nodes, layer thicknesses, layer material direction angles, and orthotropic material properties. Shear moduli GXZ and GYZ must be within a factor of 10.000 of each other.

Parametric models in ANSYS are implemented using the ANSYS Parametric Language (APDL), which is a scripting language that is used to either automate

tasks or build FE models in terms of variables. APDL is an extension of the FORTRAN programming language that form the core of the ANSYS software.

The specification of the element type SOLID46 using APDL can be found in the attached cdroom under the directory tree */SRC/FE Model/ELEM.txt*.

The second step in building the model is the definition of the *element real constants*. These are properties that depend on the element type SOLID46, like the number of plies, fibre orientation, and material properties of each ply. The number of plies is a model specific, at it is used to determine the depth of the delamination as it was explained in chapter three. The APDL subroutine that defines the real constants for the element SOLID46 can be found in the attached cdroom under the directory tree */SRC/FE Model/CONSTREAL.MAC*.

The third step during the setup of the FE model is the definition of material properties. The material properties used in the FE model correspond to the ones showed above, which correspond to T700/LTM-45EL carbon/epoxy $E_{11} = 127\ GPa$, $E_{22} = 9.1\ GPa$, $G_{12} = 5.6\ GPa$ and Poisson's ratio $\nu_{12} = 0.31$. The APDL script that contains the definition of the mechanical properties of the laminate can be found under the directory tree */SRC/FE Model/VAR.txt* and */SRC/FE Model/MAT.txt*.

Once the material properties have been defined, the fourth step in the analysis is generating the FE model (nodes and elements) that describes the geometry of a composite laminate with a trial delamination. The method that generates the FE model used in this thesis was *solid modelling*. In this approach, the geometry of the model is generated first (as it was described in chapter three), then the ANSYS program automatically meshes the geometry with nodes and elements. The advantages of *solid modelling* are as follows: (1) it is appropriate for 3D models of solid volumes, (2) it allows geometric boolean operations like *extrusion* and *subtraction of volumes*, (3) APDL scripting can be incorporated, (4) it readily allows modifications to geometry. The complete process to generate the FE model was described in chapter three. The APDL subroutines that incorporate such process can be found under the directory tree */SRC/FE Model/*.

Boundary conditions. Once the FE model is generated, the following step is to define the boundary conditions and the external loads on the FE model.

Given the physics involved during a DSPI test[1], a static structural analysis was performed, where DOF constraints and surface loads were applied onto the FE model.

Degrees of freedom (DOF) constraints were specified as zero displacements around the boundary of the composite panel, and the surface load corresponded to a trial pressure inside of the delaminated area, as it is shown in figure 3.17. After the boundary conditions are defined, the complete model is solved using the ANSYS Solver routine.

5.5.6 Central geometric moments from FE response - Step 5

Central geometric moments up to order three were used to represent the out-of-plane displacements obtained from the FE model described in the previous section. These moments were calculated using the procedure described in chapter four using equations 4.9 and 4.10. These mathematical equations were implemented in using APDL, and The source code of the implementation is included under the directory tree */SRC/FE Model/CANMOMENT.MAC.*

5.5.7 A low-population adaptive-range genetic algorithm (LARGA) - Step 6

As it was shown in chapter four, identification of delamination can be formulated as an inverse problem with the crack's extension and location as the system parameters to be determined. This inverse problem can be reformulated as an optimisation search with the objective function defined as the difference between a set of two-dimensional central geometric moments (CGM), calculated from finite element (FE) model with a trial parameter set, and the extended CGM calculated using the DSPI out-of-plane measurements from the panel with a single delamination having unknown geometrical parameters. The inverse problem is redefined as the least-squares minimisation problem for a scalar performance function $\Psi_{err}\left(\vec{z}, p_d^t\right)$ as follows,

[1] See chapter three for the discussion of the physics involved during a DSPI test.

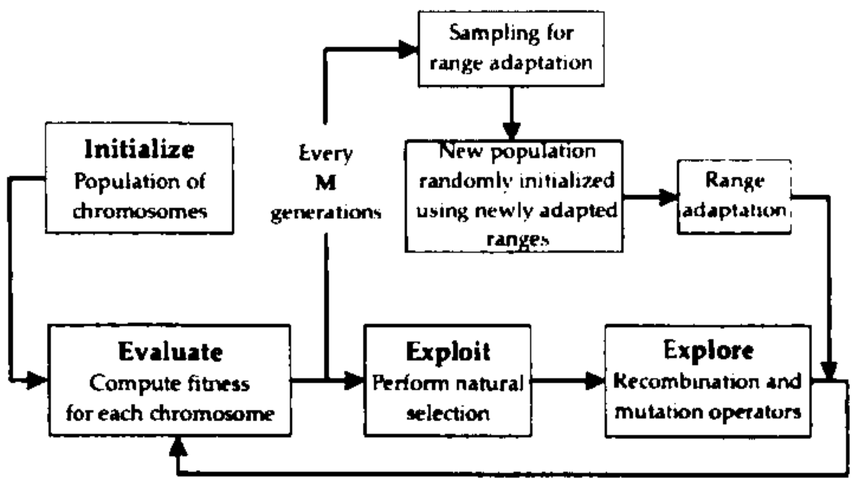

Figure 5.3. Adaptive-range Genetic Algorithm (ARGA) flowchart.

$$\Psi_{err}\left(\vec{z}, p_d^t\right) = \left\|\tilde{\eta}\left(\vec{z}, p_c, p_d^t\right) - \tilde{\eta}_0\left(p_c, p_d\right)\right\|, \tag{5.1}$$

where $\|\cdot\|$ is the l^2 norm (least square identification). It was shown in chapter four, that this minimisation problem could be solved through the use of a genetic algorithm.

Finding the global optimum in the discrete domain for the scalar performance function in Eq. 5.1 is challenging even for common GA implementations. Adaptive range genetic algorithms (ARGA) [118] integrate the ideas of stochastic GAs and the use of dynamic real-code representations for exploring a large search space more efficiently. ARGAs incorporate three new steps onto the structure of the conventional GA, as it is shown in Fig. 5.3. First, every M generations the top half of the previous generation is selected into a subset, and the average and standard deviation of this subset is calculated. Then, in the second step (range adaptation), a new search range for every gene in the chromosome is calculated using the average and the standard deviation calculated in the first step. In the third step (regeneration), all but one individual in the population are generated randomly according to the new gene's range. Here, the process overlaps with the structure given for the conventional GA, and the process continues as described in the chapter four.

However, a main disadvantage of GAs is the computational time consumed to find the minimum of a given function. The main reason for this, is that typically GAs use a large number of individuals (population) in a given generation (iteration). This author of this thesis proposes the use of a novel low-population adaptive-range genetic algorithm (LARGA) that provides a sound

balance between *speed* and *accuracy* for the identification of delamination from DSPI measurements.

The feasibility and utility of the proposed low-population LARGA is investigated through numerical simulations involving the characterisation of a circular and elliptical delaminations. In this work two separate studies are reported as follows. In the first study (Theoretical feasibility study), out-of-plane displacements are obtained from FE simulations and using different levels of white noise, the performance of the LARGA to characterise damage is evaluated. In the second study (Experimental validation study), real measurements from DSPI are used to evaluate again the performance of LARGA. The next subsections presents the results of these studies and the description of methods and materials used. Finally, the complete methodology described in this chapter (steps one to six) is applied to the characterisation of delamination from the ten experimental samples outlined above.

5.5.7.1 LARGA Evaluation - Materials and methods

The finite element representation of the physical model consist of a clamped eight-ply T300/5208 $(45^0/-45^0/0^0/90^0)_s$ graphite epoxy panels with size 0.1 by 0.1 by 0.003 m. The material properties of the layers are $E_x = 132\,GPa$, $E_y = 10.8\,GPa$, $\nu_{xy} = 0.24$, $\nu_{yz} = 0.49$, $G_{xy} = 5.6\,GPa$, $G_{yz} = 3.38\,GPa$. In the physical model the plate is into a vacuum chamber that is used to excite the damaged region by separating the adjacent delaminated layers. A parameterized re-meshing technique is used to modify the FE models automatically during the LARGA procedure. In this technique, the mesh of every FE model is regenerated when the delamination's parameters are changed, allowing a smooth transition in the size and aspect ratio of the elements in the mesh.

The LARGA algorithm was coded in-house using the ANSYS Parametric Language (APDL). The code is approximately 1000 lines including specific configuration files. The complete code is available in the cdrom attached to this thesis under the directory tree */SRC/LARGA* except for the experimental DSPI data, which is copyrighted by Loughborough University. The main file of the LARGA implementation is *gaLARGA.MAC* which loads every step of the genetic algorithm.

As it was shown in chapter four, the problem of identification of delamination can be encoded using seven genes. Six of them representing the damage parameters $\vec{z} = [x_c, y_c, a, b, \theta, h]^T$, and one representing the pressure of air inside of the delamination p_d. These genes are encoded using real numbers. The alleles of the genes were specified as follows.

- Alleles of genes $\gamma_1 = x_c$, and $\gamma_2 = y_c$, that represent the planar location of the centre of the delamination in the plane of the laminate, were defined by equation 4.17. The value of the parameter ε was set as 0.1 by trial-and-error.

- Alleles of genes $\gamma_3 = a$, and $\gamma_4 = b$, that encode the size of the delamination to be characterised, are defined by equation 4.18. The value of the parameter λ was set as to 0.2 by trial-and-error.

- Allele of gene $\gamma_5 = \theta$, that encodes the angle of orientation of the delamination in the composite panel, was set as the pair $[0, 90]$ that are the angles of orientation of the fibres in the laminate.

- Allele of gene $\gamma_6 = h$, that encodes the depth of the delamination measured from the surface of the laminate that is closest to the DSPI detector, was set a the array of discontinuous values $\gamma_6 = [-0.125, -0.25, -0.375, -0.5, -0.625]$. These values correspond to vertical coordinates of the interface between every ply in the composite laminate.

- Allele of gene $\gamma_7 = p_d$, that encodes the pressure of the air trapped in the delamination when the DSPI test take place. It was fixed as the range $(0, 3000Pa)$ by trial-and-error. However, it must be noted that this range is not the optimal one, as it is not possible to determine, neither experimentally (using DSPI) nor analytically, the change of pressure of the air inside of the delamination.

Roulette wheel selection was applied to select the parents for the crossover step. The algorithm used the following parameters: probability of crossover $p_c = 1.0$, probability of mutation $p_m = 0.1$. The range adaptation operator, equations 4.27 and 4.28 were set with parameters $M = 4$, $\omega_\mu = 0.75$, $\omega_\sigma = 0.75$, and $\kappa = 3$. Parents crossover was performed using intermediate recombina-

tion, equation 4.30. The LARGA algorithm converged when the best-fit individual in the current population reached a threshold value of 0.998, or when the algorithm was not capable to find better fitness regions for a period of seven generations.

5.5.7.2 LARGA Evaluation - Theoretical feasibility study

The objective of this study is to determine the accuracy and speed of the LARGA under a controlled environment. The input for the genetic algorithm, the Geometric Central Moments (GCM), are calculated from a FE model of the delaminated panel. The FE model was set up with an ideal circular delamination of 20 *mm* of diameter located 0.25 *mm* beneath the surface. In order to evaluate the solution time and accuracy of LARGA versus the population size, LARGAs with populations of 5, 10, 15 and 20 individuals were used. To take into account the influence of noise in the input CGM, three types of models with random-white noise equivalent 0%, 5% and 10% of the maximum displacement were also implemented. Finally, to account for the influence of the initial population in the efficiency and effectiveness of LARGA, ten replications of every model were performed using randomly-generated initial population.

5.5.7.3 LARGA Evaluation - Experimental validation study

The objective of this study is to determine the accuracy and speed of the LARGA using real out-of-plane DSPI measurements. The reference composite panel was prepared with a 20 *mm* diameter delamination located 0.25 *mm* beneath the surface. The damage characterisation was performed using a LARGA with five individuals, and twenty replications were performed using a different randomly-generated initial population.

5.6 Results

5.6.1 LARGA Evaluation - Theoretical feasibility study

Figure 5.4a shows the comparison of the convergence of LARGA for five different replications using a population of five individuals and white-noise of 0%. The accuracy of the analysis was found to be inversely proportional of the number of generations used by LARGA to converge to the global optimum.

These results may be explained by considering that if the initial population contained a better genetic content, then the search procedure may be shorter. The solution time of the LARGA was found to be inversely proportional to the population size (Figure 5.4b and 5.5b). The predicted delaminated area using LARGA was found to be significantly closer to the real value used in the original FE model as shown in Figure 5.5a.

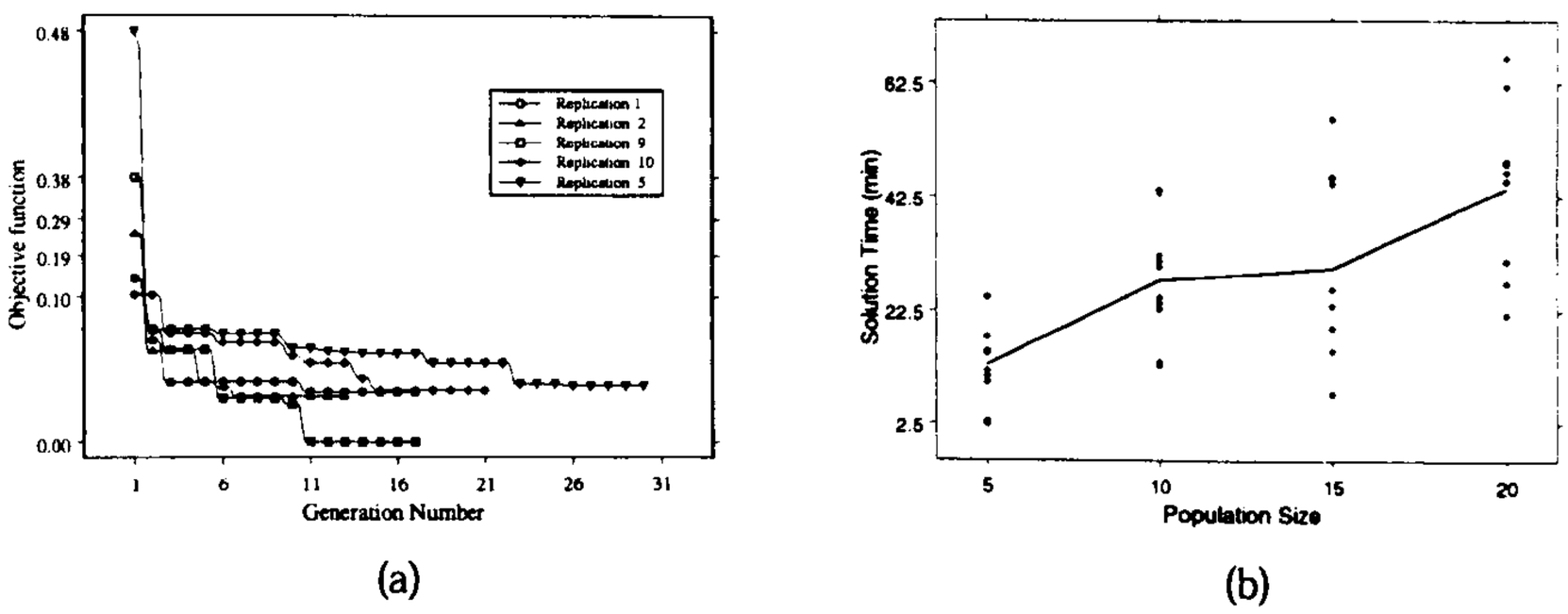

Figure 5.4. (a) Comparison of convergence histories of five model replications for simulated out-of plane displacements. Noise 0%, population = 5. Figure not at scale. (b) Comparison of convergence time of five model replications for simulated out-of plane displacements. Noise 0%, population = 5, 10, 15 and 20.

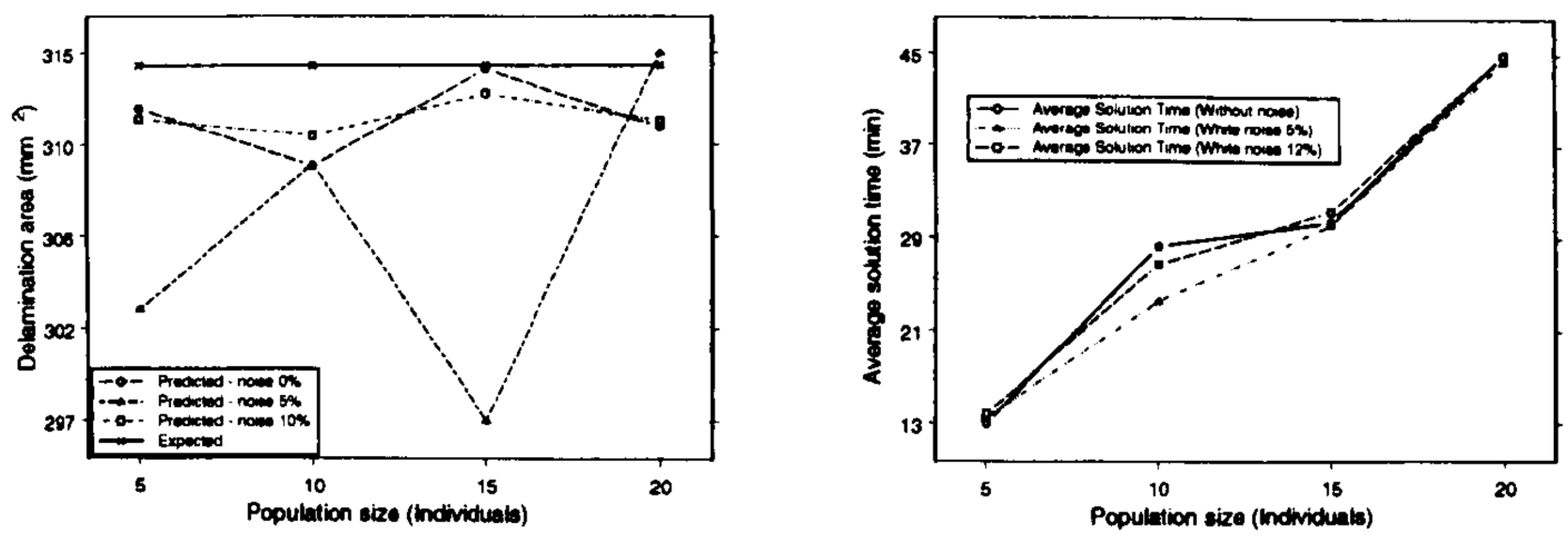

Figure 5.5. (a) Comparison of predicted delamination area for simulated out-of plane displacements. Noise 0%, population = 5, 10, 15 and 20. (b) Comparison of average solution time for simulated out-of plane displacements. Noise 0%, population = 5, 10, 15 and 20.

5.6.2 LARGA Evaluation - Experimental validation study

The average solution time of LARGA using DSPI measurements was found to be in consistency with those reported in the theoretical study (Figure 5.6a and 5.5b). At a difference with the theoretical study, LARGA over predicted the delaminated area as is shown in Figure 5.6b. Also it was found that using real experimental data, LARGA predicted the correct delamination depth in 18 of 20 replications (Figure 5.7. In the theoretical study the prediction rate was of 100%. These results may be explained by taking into account the complex noise pattern that is present in DSPI.

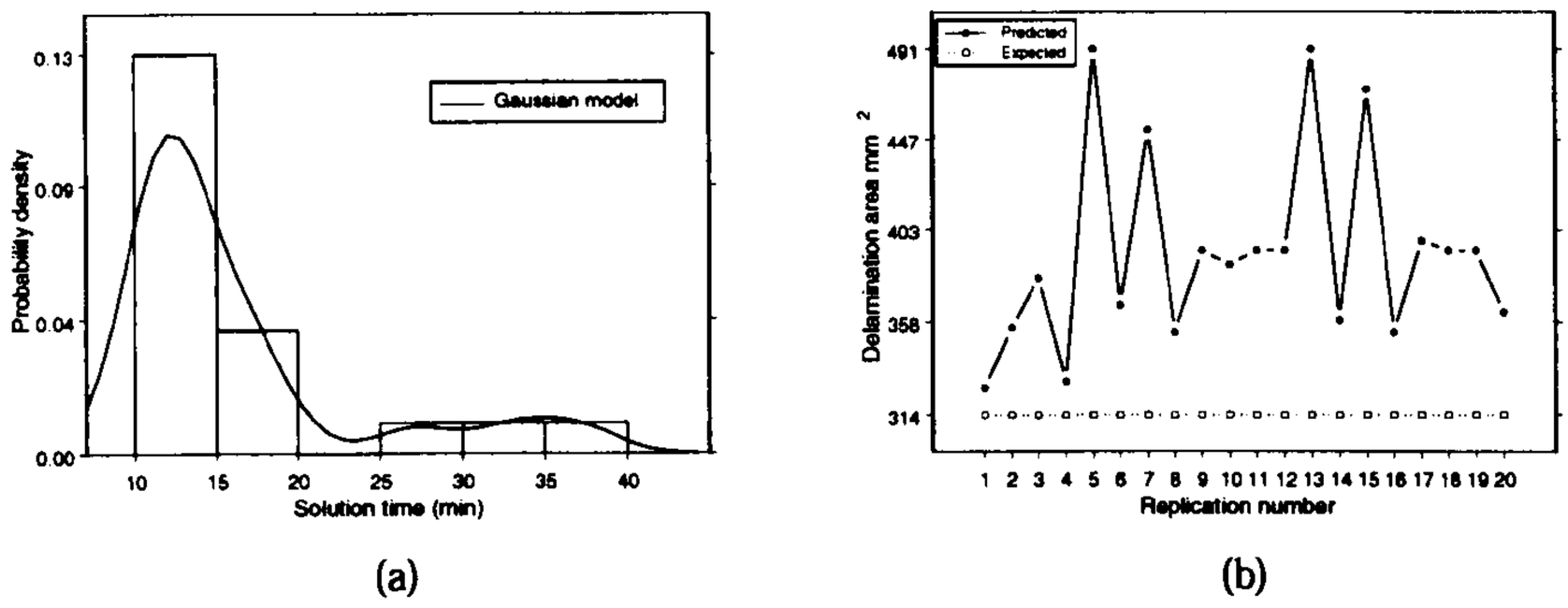

Figure 5.6. (a) Probability density plot of solution time for real DSPI measurements. (b) Comparison of predicted delamination area of twenty model replications for real DSPI measurements. Population = 5.

The following subsections present the results obtained from the delamination identification methodology proposed in this thesis. A summary of the results presented for all the experimental samples is included in tables 5.2 to 5.6.

5.6.3 Identification Methodology: Sample 1 - 10C12D

Figure 5.8 presents the findings of the identification methodology for sample one. Experimental data from DSPI were for a circular delamination with diameter 10 *mm* located at (50, 50) *mm* from the bottom left corner of the panel, and with a depth of 0.125 *mm*.

Laplacian-based edge detection. Subfigure (b) shows the detected borders of the bulge showed in (a). The border of the bulge is irregular, and it

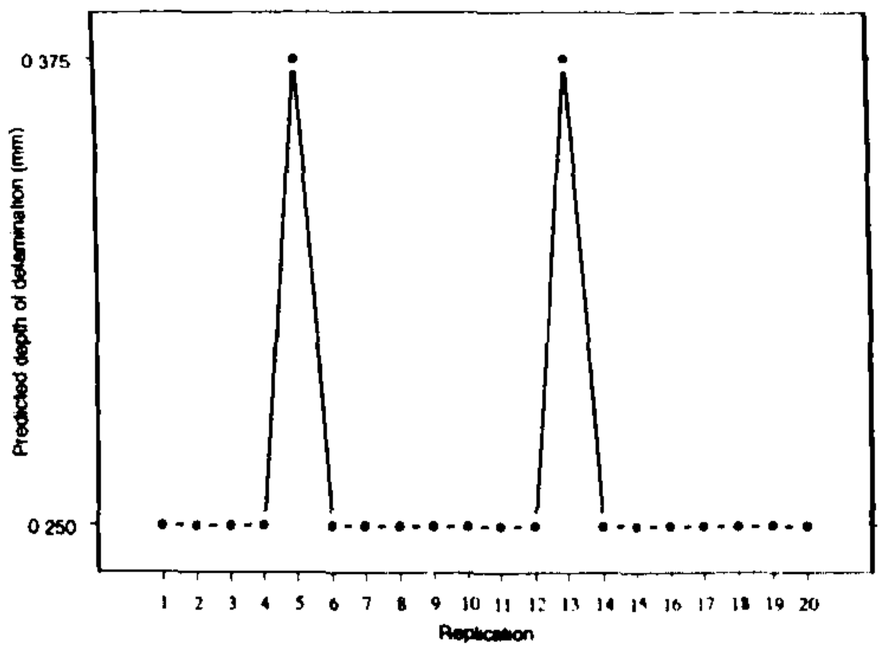

Figure 5.7. Comparison of predicted delamination depth of twenty model replications for real DSPI measurements. Real delamination depth is 0.25 mm. Population = 5.

is not present around its whole perimeter. A tentative interpretation might be that experimental results present a discontinuity where the border is not detected, as it can be seen in (a).

Initial parameters of delamination. Subfigure (c) shows the identified initial parameters of the ellipse from the edges detected above. The effective borders of the bulge were found to cover a little more of 180 degrees of the bulge. The identified ellipse (continuous line) is significantly smaller than the current delamination in the laminate, the area of the ellipse is around one-half of the original crack. Also the location of the centre of the ellipse displayed an offset of 5 percent in relation with the original damage.

Convergence of the genetic algorithm. Subfigure (d) shows the history of convergence for five replications of the genetic algorithm with different random initial population. Replication three and four converged to a minimum of the objective function in the four generation. After this point, the algorithm could not find another region for exploration, and consequently it terminated eight generations later. Replications two and five did converge to a local minima of the objective function around generation three of the algorithm. Successive attempts to re-initiate the population using the operator of range adaptation failed to help to move the population toward other regions of the search space. On the other hand, replication one was able to move to another region of

the domain, but it landed in another local minima. The average solution time for the replications was 711 seconds, with an average of eleven generations per replication.

Identified parameters of the delamination. Subfigure (e) shows the comparison between the size and location of the identified laminate, and the equivalent variables in the physical laminate. The relative error in the planar location of the laminate is 4.72%, the area of the predicted crack is 2.21% bigger. Two out of the five GA replications converged to the correct depth of delamination. The average change of the pressure of the air trapped inside of the delamination was 41 *Pa*.

5.6.4 Identification Methodology: Sample 2 - 10C23D

Figure 5.9 presents the results of the identification methodology for sample two. Experimental measurements from DSPI were for a circular delamination with diameter 10 *mm* located at $(50, 50)$ *mm* from the bottom left corner of the panel, and with a depth of 0.250 *mm*.

Laplacian-based edge detection. The detected edge of the bulge showed in subfigure (b) was not complete, it expanded to an angle of around 180 degrees of the circumference due mainly to the effects of the experimental results, as it was suggested in the previous sample.

Initial parameters of delamination. Subfigure (c) shows the identified initial parameters of the ellipse from the edges detected above. The identified ellipse was smaller than the current delamination in the laminate, the area of the ellipse was around one fifth smaller than the original crack. Also the location of the centre of the ellipse displayed an offset of 4 percent in relation with the original damage.

Convergence of the genetic algorithm. Subfigure (d) shows the history of convergence for five replications of the genetic algorithm with different random initial population. All five replications converge to a region of the search space where the objective function was similar, however, three of the replica-

tions (2,3,5) converged to the incorrect local minima of the function. Replications one and four converged to the correct minima of the function, but the algorithm took more than six generations to find it. The average computer time used by the replications was 275 seconds, and the average number of iterations was twelve.

Identified parameters of the delamination. Subfigure (e) shows the comparison between the size and location of the identified laminate, and the equivalent variables in the physical laminate. The relative error in the planar location of the laminate was 3.79%, the area of the predicted crack is 23% larger. Two out of the five GA replications converged to the correct depth of delamination. The average change of the pressure of the air trapped inside of the delamination was 695 *Pa*.

5.6.5 Identification Methodology: Sample 3 - 20C12D

Figure 5.10 presents the findings of the identification methodology for sample three. Experimental data from DSPI were for a circular delamination with diameter 20 *mm* located at (50, 50) *mm* from the bottom left corner of the panel, and with a depth of 0.125 *mm*.

Laplacian-based edge detection. Subfigure (b) shows the detected borders of the bulge showed in (a). The border of the bulge is regular, and it is present around the entire perimeter. As a difference with samples one and two, the bulge on from the experimental data is well defined.

Initial parameters of delamination. Subfigure (c) presents the identified initial parameters of the ellipse that were calculated from the edge detected above. The initial size of the delamination was 30 percent smaller than the actual delamination in the panel. Also, it was found that the centre of the identified ellipse was offset to the right by five percent.

Convergence of the genetic algorithm. Subfigure (d) shows the history of convergence for five replications of the genetic algorithm with different random initial population. Replications three and four converged to a point close

to the global minima in the ninth generation of the algorithm. The rest of the replications converged to a local minimum around generation twelve. The average solution time for each replications was 1220 seconds, with an average of 17 generations per replication.

Identified parameters of the delamination. Subfigure (e) shows the comparison between the size and location of the identified laminate, and the equivalent variables in the physical laminate. The best individual in all the replications displayed a relative error in the planar location of the laminate of 4.60%, the area of the predicted crack was 0.06% bigger. Two out of the five GA replications converged to the correct depth of delamination (0.125 *mm*) with an average change of the pressure of the air trapped inside of the delamination of 65 *Pa*.

5.6.6 Identification Methodology: Sample 4 - 20C23D

Figure 5.11 presents the results of the identification methodology for sample four. Experimental measurements from DSPI were for a circular delamination with diameter 20 *mm* located at $(50, 50)$ *mm* from the bottom left corner of the panel, and with a depth of 0.250 *mm* measured from the top of the laminate.

Laplacian-based edge detection. The laplacian-based edge technique detected accurately the borders of the bulge from the experimental data as is shown in subfigure (b). This is due to the symmetric nature of the bulge from DSPI measurements.

Initial parameters of delamination. Subfigure (c) shows the identified initial parameters of the ellipse from the edges detected above. The identified ellipse was smaller than the current delamination in the laminate, the area of the ellipse was around thirty percent smaller than the original crack. Also the location of the centre of the ellipse displayed an offset of 3 percent to the right of the original delamination.

Convergence of the genetic algorithm. Subfigure (d) shows the history of convergence for five replications of the genetic algorithm with different ran-

dom initial population. All five replications did not converge to the global minimum of the objective function, but to a local one. The average computer time used by the replications was 475 seconds, and the average number of iterations was 18.

Identified parameters of the delamination. The genetic algorithm detected a delamination with an area 9.8% bigger than the current crack in the laminate. The centre of the delamination was predicted with an accuracy of 3.92%. Five out of five replications converged to a delamination closer to the surface.

5.6.7 Identification Methodology: Sample 5 - 40C12D

Figure 5.12 presents the findings of the identification methodology for sample five. Experimental data from DSPI were for a circular delamination with diameter 40 *mm* located at (50, 50) *mm* from the bottom left corner of the panel, and with a depth of 0.125 *mm* measured from the top surface of the laminate.

Laplacian-based edge detection. The experimental data from DSPI were smooth and symmetrical as it is showed in subfigure (a). The laplacian-based technique identified properly the points around the central bulge of the displacement measurements as it is shown in subfigure (b).

Initial parameters of delamination. The initial size and position of the ellipse representing the damage were closed to the real parameter damages. The area predicted was 8% smaller, and the centre of the delamination was identified with a relative error of less than 1%.

Convergence of the genetic algorithm. Subfigure (d) shows the history of convergence for five replications of the genetic algorithm with different random initial population. Replications two to five converged to a point close to the global minima between the eighth and eleventh generation of the GA. Replication one converged to a local minimum in the 13th generation of the algorithm. The average solution time for each replications was 1128 seconds, with an average of 16 generations per replication.

Identified parameters of the delamination. Subfigure (e) shows the comparison between the size and location of the identified laminate, and the equivalent variables in the physical laminate. The best individual in all the replications displayed a relative error in the planar location of the laminate of 2.67%, the area of the predicted crack was 5.35% bigger. Four out of the five GA replications converged to the correct depth of delamination (0.125 *mm*) with an average change of the pressure of the air trapped inside of the delamination of 99 *Pa*.

5.6.8 Identification Methodology: Sample 6 - 40C23D

Figure 5.13 presents the findings of the identification methodology for sample six. Experimental data from DSPI were for a circular delamination with diameter 40 *mm* located at (50, 50) *mm* from the bottom left corner of the panel, and with a depth of 0.250 *mm*.

Laplacian-based edge detection. Subfigure (b) shows the detected borders of the bulge showed in (a). The border of the bulge is regular, and it is present around the entire perimeter. The bulge from the experimental data is well defined, but there is a spurious small bulge located to the right of the main dome. A feasible explanation for this extra bulge is a localized defect during the manufacturing of the sample. However, the abnormality does not affect the initial detection of the bulge's shape.

Initial parameters of delamination. Subfigure (c) presents the identified initial parameters of the ellipse that were calculated from the edge detected above. The initial size of the delamination was five percent smaller than the actual delamination in the panel. Also, it was found that the centre of the identified ellipse was offset to the right by six percent.

Convergence of the genetic algorithm. Subfigure (d) shows the history of convergence for five replications of the genetic algorithm with different random initial population. Replications one, two, four and five converged to a point close to the global minima in the seventh generation of the algorithm. The remaining replication converged to a local minimum around generation

seventh. The average solution time for each replications was 1226 seconds, with an average of 17 generations per replication.

Identified parameters of the delamination. Subfigure (e) shows the comparison between the size and location of the identified laminate, and the equivalent variables in the physical laminate. The best individual in all the replications displayed a relative error in the planar location of the laminate of 1.60%, the area of the predicted crack was 0.42% bigger. Four out of the five GA replications converged to the correct depth of delamination (0.250 *mm*) with an average change of the pressure of the air trapped inside of the delamination of 270 *Pa*.

5.6.9 Identification Methodology: Sample 7 - E2012D90

Figure 5.14 presents the results of the identification methodology for sample seven. Experimental measurements from DSPI were for an elliptical delamination with length 20 *mm*, width 6.67 *mm*, orientation of 90 degrees, located at (50, 50) *mm* from the bottom left corner of the panel, and with a depth of 0.125 *mm*.

Laplacian-based edge detection. The detected edge of the bulge showed in subfigure (b) was not complete, it expanded to an angle of around 240 degrees of the circumference due mainly to an incomplete set measurements from DSPI.

Initial parameters of delamination. Subfigure (c) shows the identified initial parameters of the ellipse from the edges detected above. The identified ellipse was smaller than the current delamination in the laminate, the area of the ellipse was around one forty percent smaller than the original crack. Also the location of the centre of the ellipse displayed an offset of ten percent in relation with the original damage.

Convergence of the genetic algorithm. Subfigure (d) shows the history of convergence for five replications of the genetic algorithm with different ran-

dom initial population. All five replications converge to a region of the search space where the objective function was similar, however, none of the replications converged to the global minima of the function. The average computer time used by the replications was 1262 seconds, and the average number of iterations was seventeen.

Identified parameters of the delamination. Subfigure (e) shows the comparison between the size and location of the identified laminate, and the equivalent variables in the physical laminate. The relative error in the planar location of the laminate was 0.63%, the area of the predicted crack is 2.82% larger. None of the five GA replications converged to the correct depth of delamination.

5.6.10 Identification Methodology: Sample 8 - E2023D0

Figure 5.15 presents the findings of the identification methodology for sample eight. Experimental data from DSPI were for an elliptical delamination with length 20 *mm*, width 6.67 *mm*, orientation of 0 degrees, located at (50, 50) *mm* from the bottom left corner of the panel, and with a depth of 0.250 *mm*.

Laplacian-based edge detection. The experimental data from DSPI was discontinuous, incomplete and asymmetrical as it is showed in subfigure (a). The laplacian-based technique identified a suitable set of points around the central bulge of the displacement measurements as it is shown in subfigure (b).

Initial parameters of delamination. The initial size and position of the ellipse representing the damage were closed to the real parameter damages. The area predicted was 15% larger, and the centre of the delamination was identified with a relative error of less than 13%.

Convergence of the genetic algorithm. Subfigure (d) shows the history of convergence for five replications of the genetic algorithm with different random initial population. None of the replications converged to the global minimum of the objective function. The average solution time for each replications was 2983 seconds, with an average of 14 generations per replication.

Identified parameters of the delamination. Subfigure (e) shows the comparison between the size and location of the identified laminate, and the equivalent variables in the physical laminate. The best individual in all the replications displayed a relative error in the planar location of the laminate of 2%, the area of the predicted crack was 5.66% bigger. None of the five GA replications converged to the correct depth of delamination (0.250 *mm*).

5.6.11 Identification Methodology: Sample 9 - E4012D90

Figure 5.16 presents the results of the identification methodology for sample nine. Experimental measurements from DSPI were for an elliptical delamination with length 40, width 13.33 *mm*, orientation of 90 degrees, located at (50, 50) *mm* from the bottom left corner of the panel, and with a depth of 0.125 *mm*.

Laplacian-based edge detection. The detected edge of the bulge showed in subfigure (b) was not complete, it expanded to an angle of around 260 degrees of the circumference due to an incomplete set of measurements from DSPI.

Initial parameters of delamination. Subfigure (c) shows the identified initial parameters of the ellipse from the edges detected above. The identified ellipse was smaller than the current delamination in the laminate, the area of the ellipse was around twenty percent smaller than the original crack. Also the location of the centre of the ellipse displayed an offset of less than one percent in relation with the original damage.

Convergence of the genetic algorithm. Subfigure (d) shows the history of convergence for five replications of the genetic algorithm with different random initial population. Two out of five replications converged to a region of the search space where the objective function was similar. The average computer time used by the replications was 294 seconds, and the average number of iterations was fourteen.

Identified parameters of the delamination. Subfigure (e) shows the comparison between the size and location of the identified laminate, and the equivalent variables in the physical laminate. The relative error in the planar location of the laminate was 1.8%, the area of the predicted crack is 7.90% larger. Two out of the five GA replications converged to the correct depth of delamination (0.125 *mm*) with an average change of the pressure of the air trapped inside of the delamination of 77 *Pa*.

5.6.12 Identification Methodology: Sample 10 - E4023D0

Figure 5.17 presents the results of the identification methodology for sample ten. Experimental measurements from DSPI were for an elliptical delamination with length 40, width 13.33 *mm*, orientation of 0 degrees, located at (50, 50) *mm* from the bottom left corner of the panel, and with a depth of 0.250 *mm*.

Laplacian-based edge detection. The detected edge of the bulge showed in subfigure (b) was not complete, it expanded to an angle of around 270 degrees of the circumference. However, the shape of the bulge is not as distorted as in samples seven to nine.

Initial parameters of delamination. Subfigure (c) shows the identified initial parameters of the ellipse from the edges detected above. The identified ellipse was smaller than the current delamination in the laminate, the area of the ellipse was around twenty five percent smaller than the original crack. Also the location of the centre of the ellipse displayed an offset of five percent in relation with the original damage.

Convergence of the genetic algorithm. Subfigure (d) shows the history of convergence for five replications of the genetic algorithm with different random initial population. Three out of five replications (1, 2, 5) converged to a region of the search space where the objective function was similar. The average computer time used by the replications was 385 seconds, and the average number of iterations was sixteen.

Table 5.2. Laplacian based edge detection for all experimental samples.

In general the edges of the bulge were not detected completely, most of the times due to gaps of discontinuities contained in the DSPI data.

Sample	*Name*	*Shape*	*Was the edge complete?*	*Was the edge symmetrical?*
1	10C12D	Circular	No	No
2	10C23D	Circular	No	No
3	20C12D	Circular	Yes	Yes
4	20C23D	Circular	Yes	Yes
5	40C12D	Circular	Yes	Yes
6	40C23D	Circular	Yes	No
7	E2012D90	Elliptical	No	No
8	E2023D0	Elliptical	No	No
9	E4012D90	Elliptical	No	No
10	E4023D0	Elliptical	No	No

Identified parameters of the delamination. Subfigure (e) shows the comparison between the size and location of the identified laminate, and the equivalent variables in the physical laminate. The relative error in the planar location of the laminate was 11%, the area of the predicted crack was 11% larger. Three out of the five GA replications converged to the correct depth of delamination (0.250 *mm*) with an average change of the pressure of the air trapped inside of the delamination of 1425 *Pa*.

5.7 Discussion and Conclusion

This chapter addresses the research question four included in chapter one. The main question that this chapter aimed to solved is as follows, *How can experimental DSPI measurements be incorporated into a fast and accurate validated computational methodology for the identification of delamination in composite laminates, that can be used in-service, where size, mechanical properties, and lay up of laminates are not known a priori?*.

The methodology employed to solve the above question involved splitting the research question in two sub questions (A and B). These sub questions

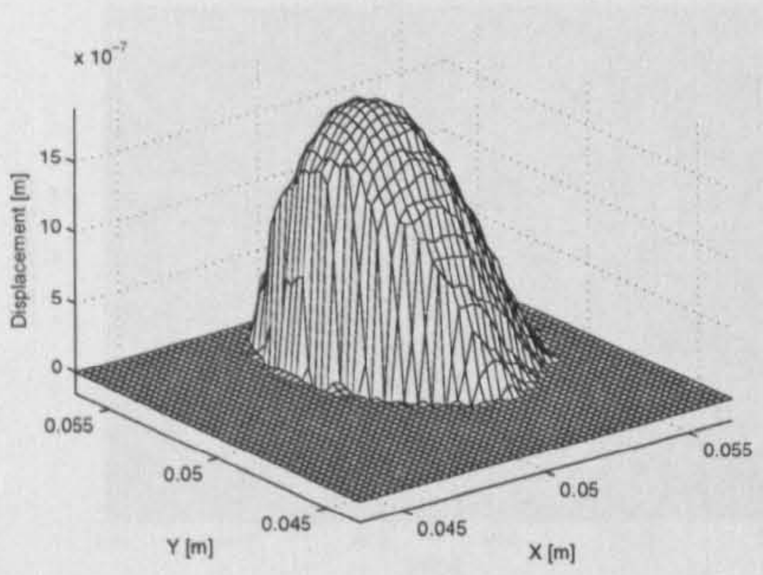

(a)

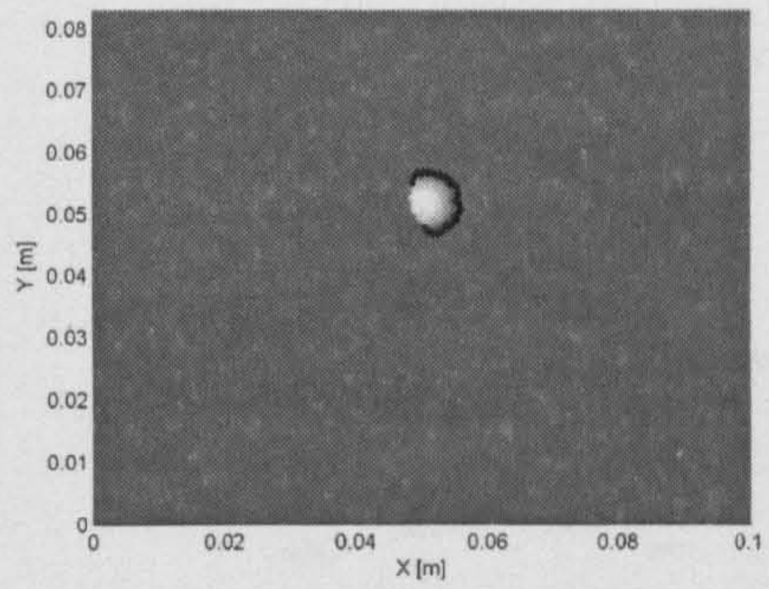

(b)

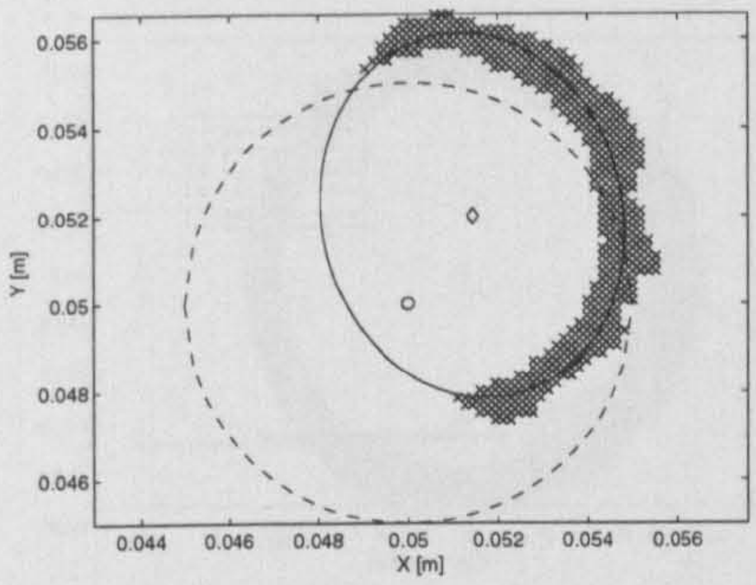

(c)

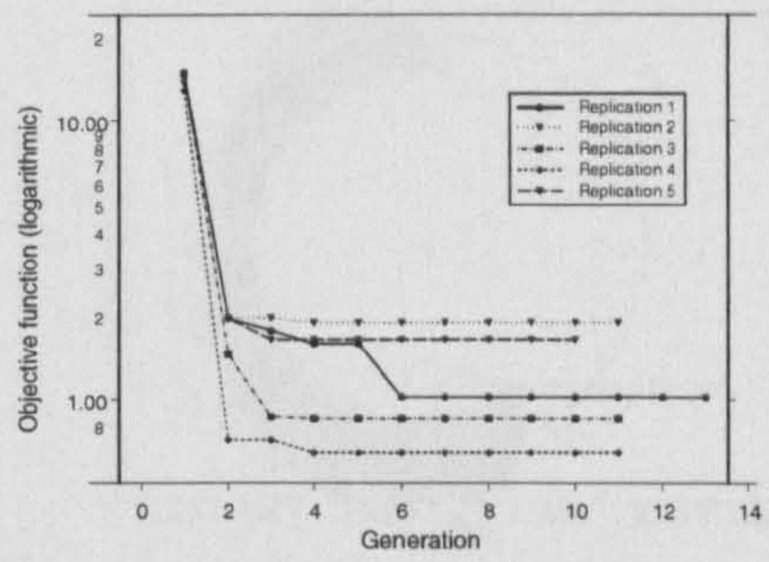

(d)

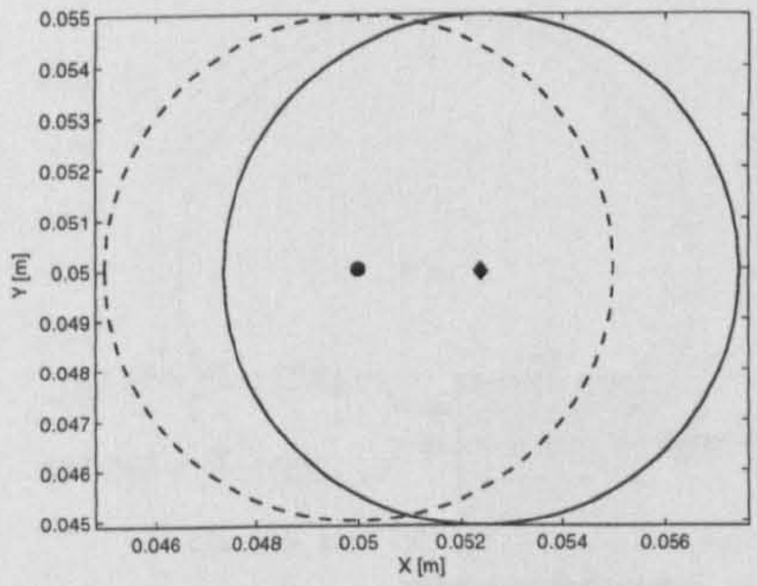

(e)

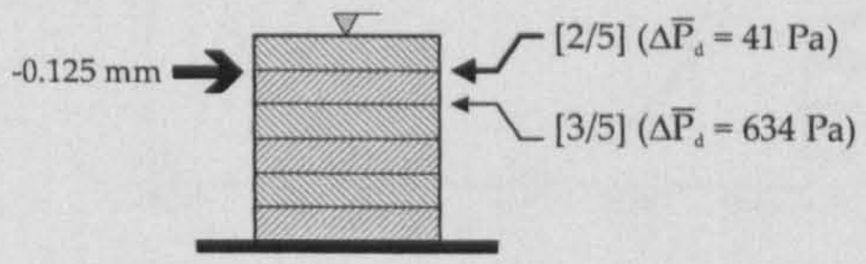

(f)

Figure 5.8. Results of damage characterisation for a sample one (10C12D).

(a) Zoomed DSPI's out-of-plane displacements; (b) detection of the edge of the bulge using a laplacian filter (black points); (c) initial estimation of delamination parameters using the detected edges (—-) versus original flaw in the sample (−−); (d) convergence history from genetic algorithm (GA) after five replications with random initial population; (e) planar location, size and orientation of delamination predicted from GA (—-) versus original flaw in the sample (−−); (f) predicted depth of the flaw from the GA, thick black arrow on the left indicates the depth of the delamination in the experimental sample. Arrows on the right indicate the predicted depth, and the computed average pressure $\bar{p}_d$ of the air trapped inside of the delamination. Note that numbers in square brackets indicate the relative frequency that the GA predicted a particular depth during five replications.

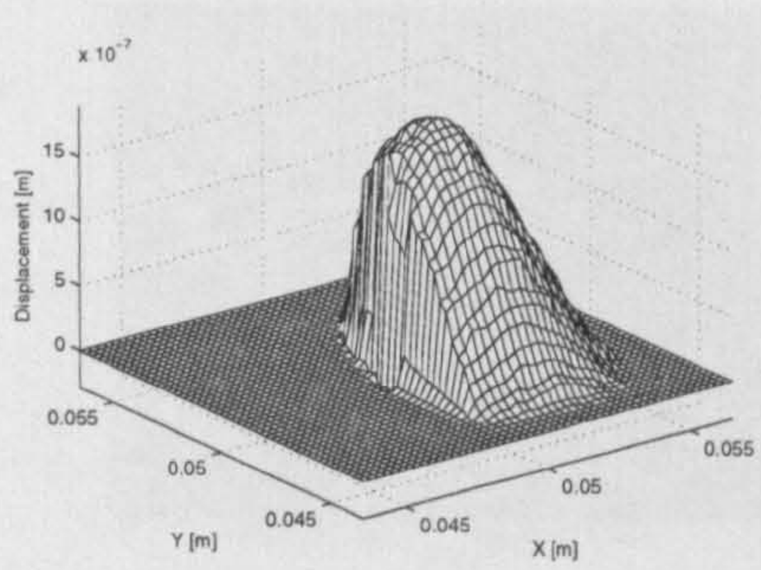

(a)

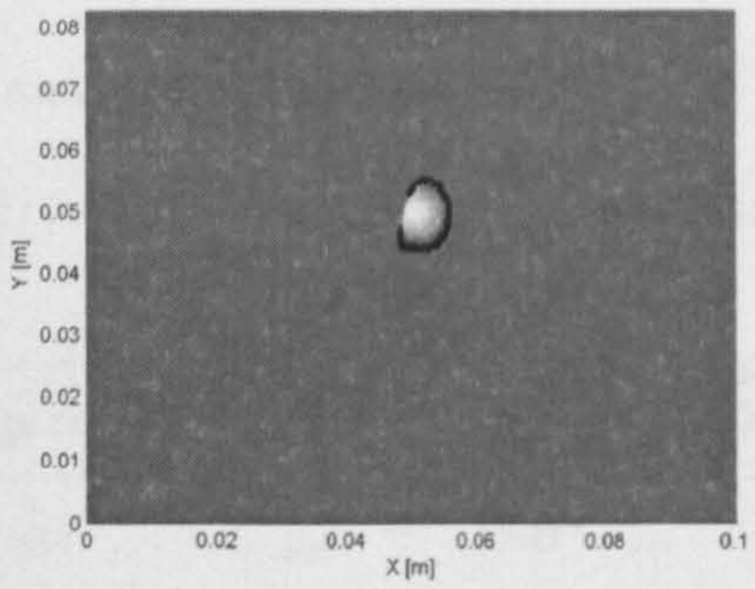

(b)

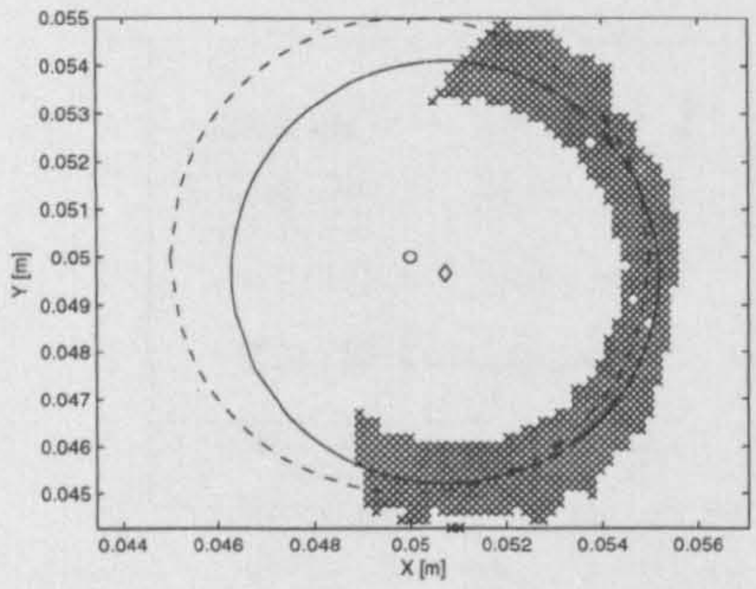

(c)

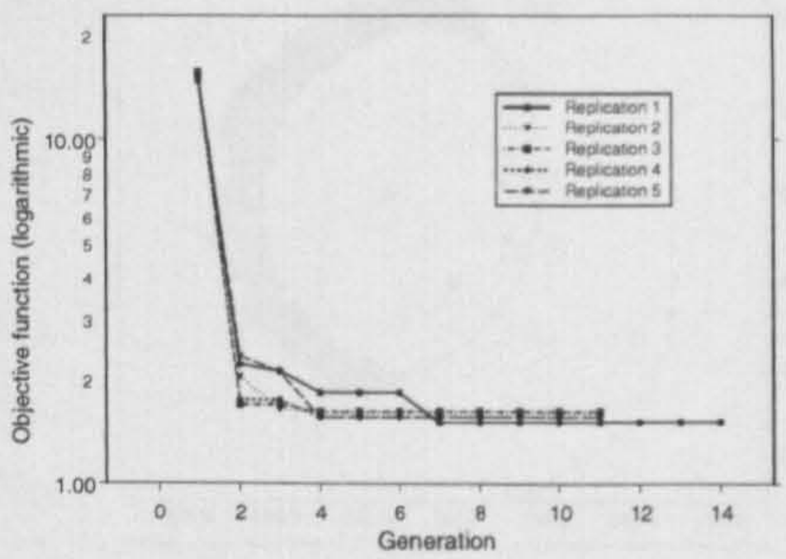

(d)

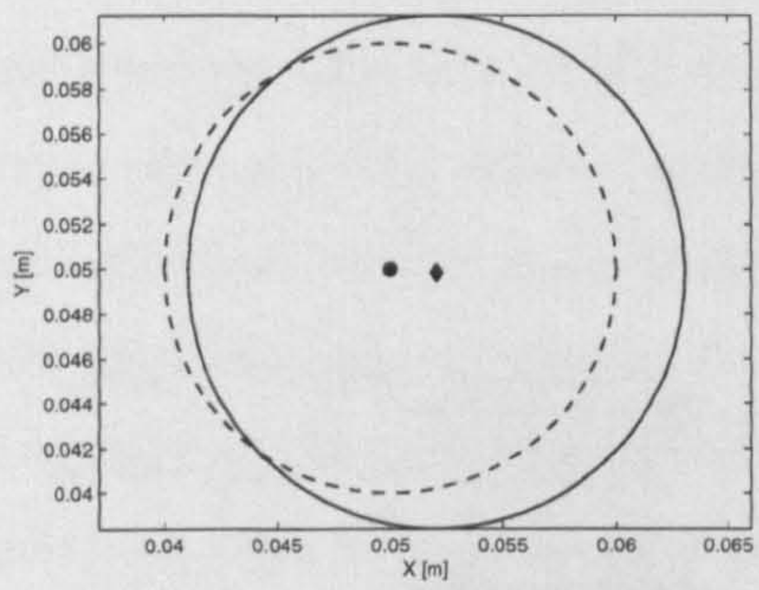

(e)

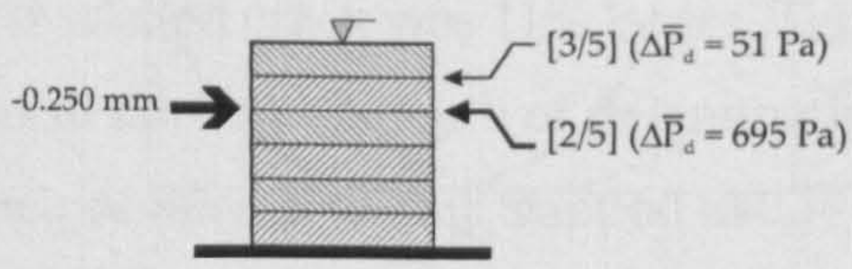

(f)

Figure 5.9. Results of damage characterisation for a sample two (10C23D).
(a) Zoomed DSPI's out-of-plane displacements; (b) detection of the edge of the bulge using a laplacian filter (black points); (c) initial estimation of delamination parameters using the detected edges (—) versus original flaw in the sample (– –); (d) convergence history from genetic algorithm (GA) after five replications with random initial population; (e) planar location, size and orientation of delamination predicted from GA (—) versus original flaw in the sample (– –); (f) predicted depth of the flaw from the GA, thick black arrow on the left indicates the depth of the delamination in the experimental sample. Arrows on the right indicate the predicted depth, and the computed average pressure $\bar{p}_d$ of the air trapped inside of the delamination. Note that numbers in square brackets indicate the relative frequency that the GA predicted a particular depth during five replications.

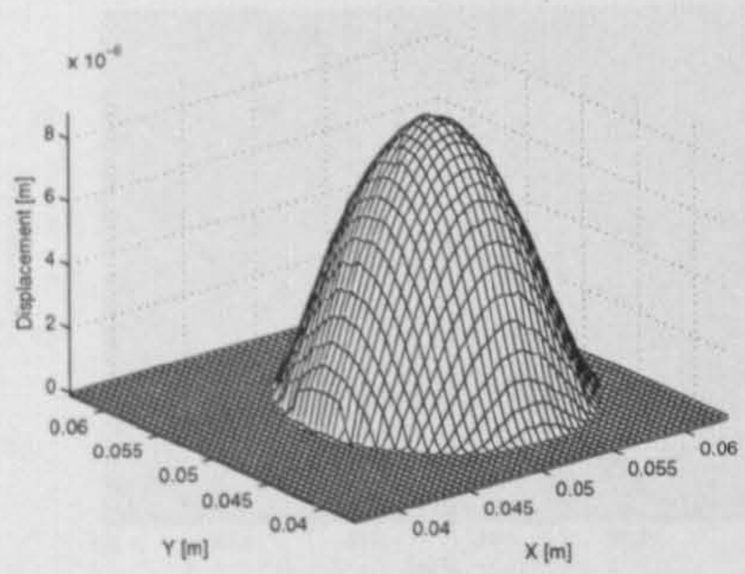

(a)

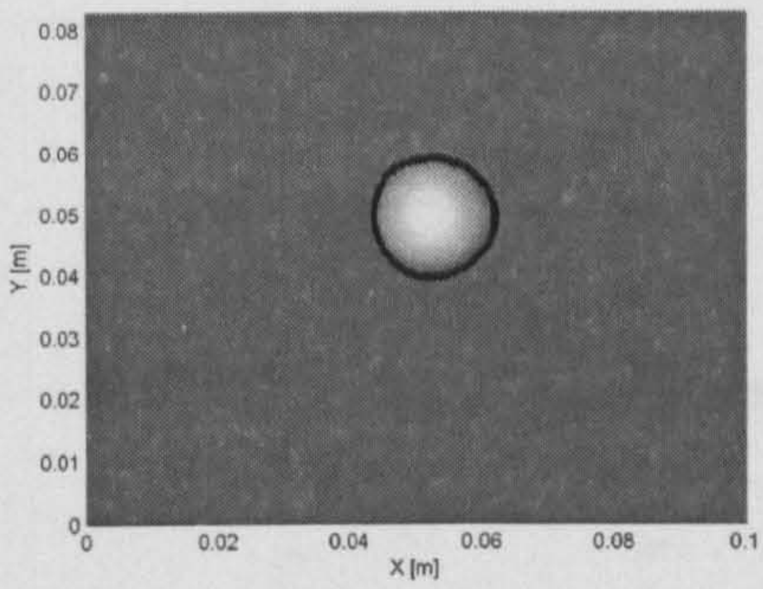

(b)

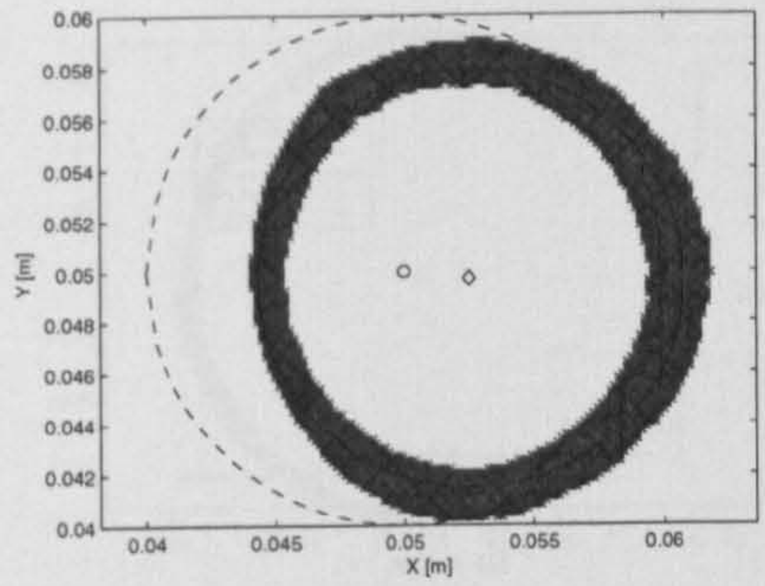

(c)

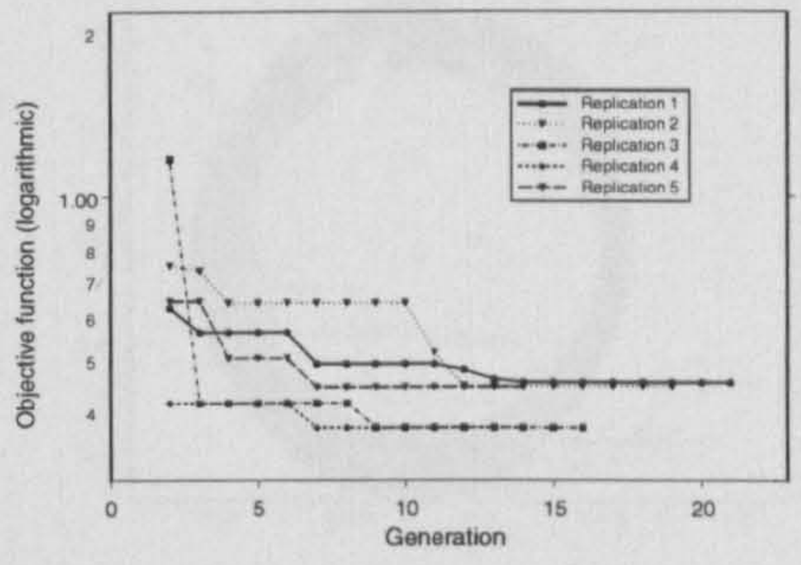

(d)

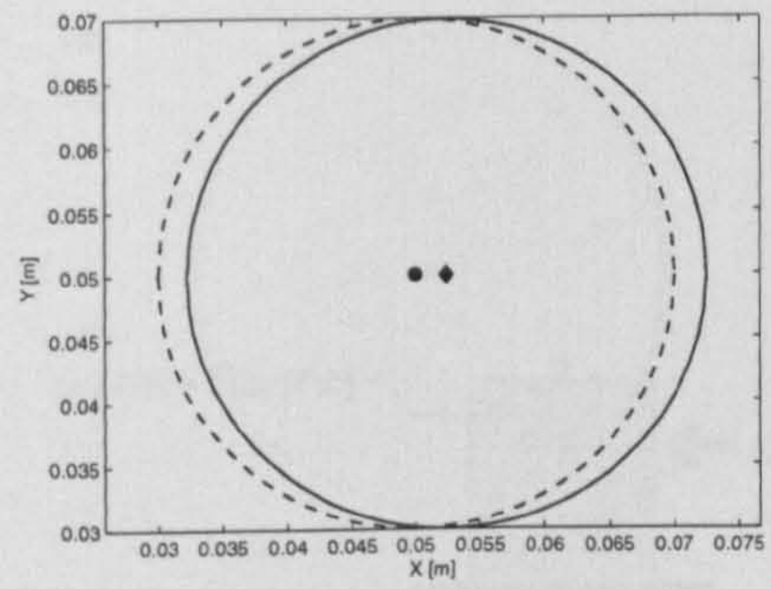

(e)

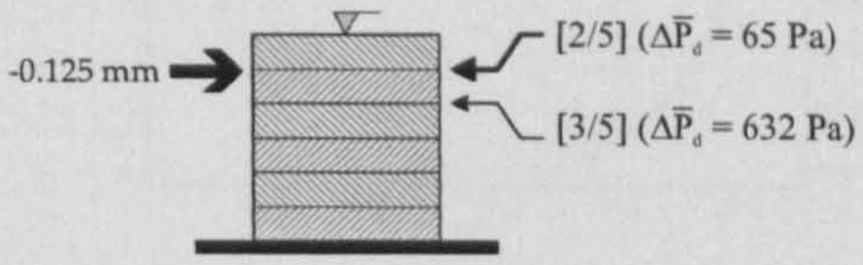

(f)

Figure 5.10. Results of damage characterisation for a sample three (20C12D). (a) Zoomed DSPI's out-of-plane displacements; (b) detection of the edge of the bulge using a laplacian filter (black points); (c) initial estimation of delamination parameters using the detected edges (—-) versus original flaw in the sample (−−); (d) convergence history from genetic algorithm (GA) after five replications with random initial population; (e) planar location, size and orientation of delamination predicted from GA (—-) versus original flaw in the sample (−−); (f) predicted depth of the flaw from the GA, thick black arrow on the left indicates the depth of the delamination in the experimental sample. Arrows on the right indicate the predicted depth, and the computed average pressure $\bar{p}_d$ of the air trapped inside of the delamination. Note that numbers in square brackets indicate the relative frequency that the GA predicted a particular depth during five replications.

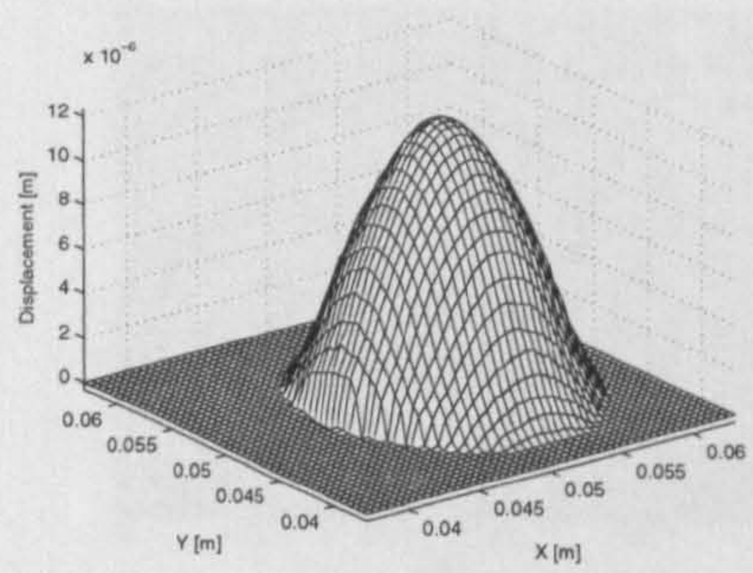

(a)

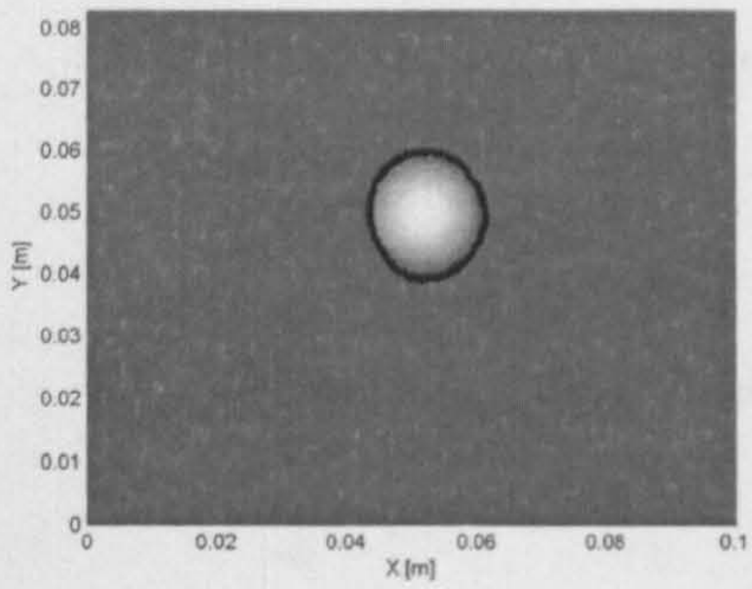

(b)

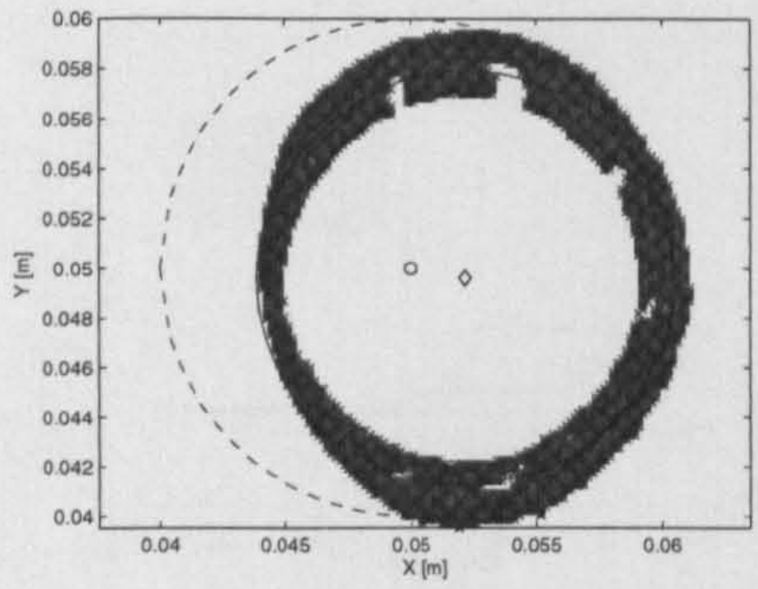

(c)

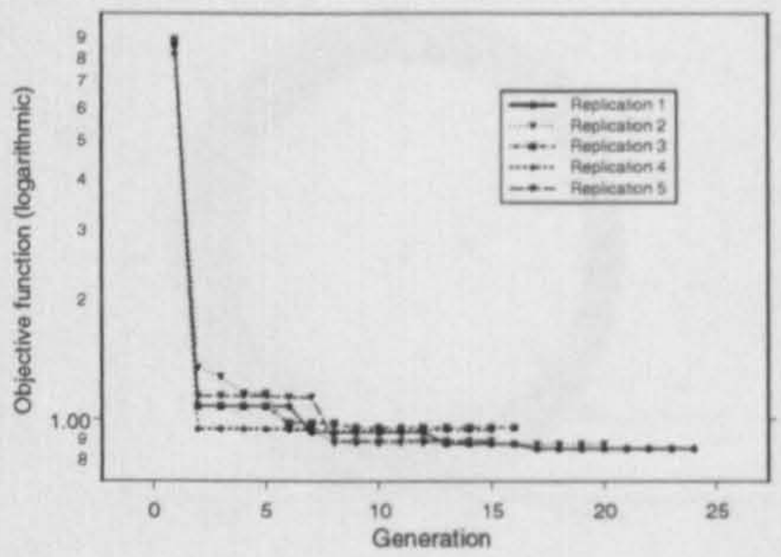

(d)

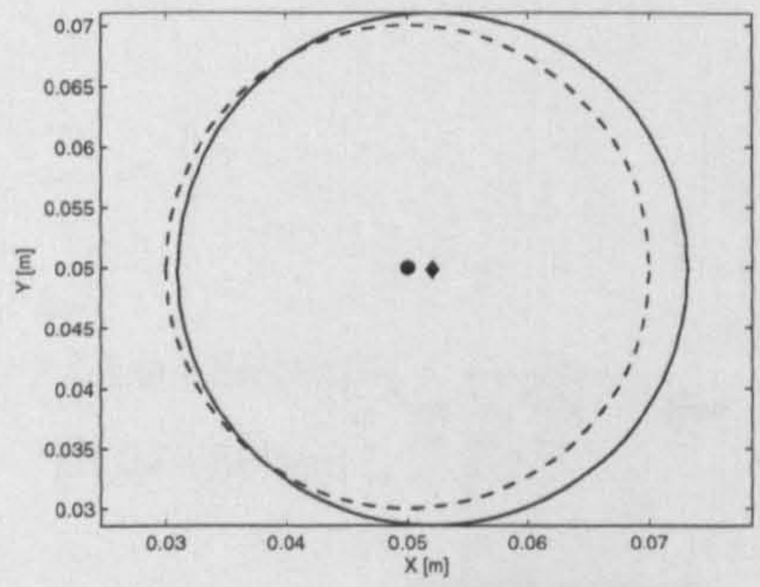

(e)

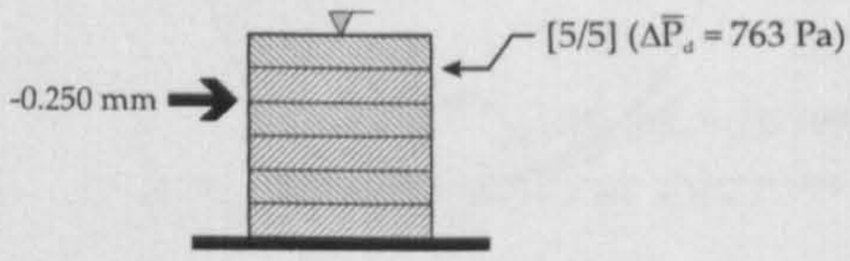

(f)

Figure 5.11. Results of damage characterisation for a sample four (20C23D). (a) Zoomed DSPI's out-of-plane displacements; (b) detection of the edge of the bulge using a laplacian filter (black points); (c) initial estimation of delamination parameters using the detected edges (—) versus original flaw in the sample (– –); (d) convergence history from genetic algorithm (GA) after five replications with random initial population; (e) planar location, size and orientation of delamination predicted from GA (—) versus original flaw in the sample (– –); (f) predicted depth of the flaw from the GA, thick black arrow on the left indicates the depth of the delamination in the experimental sample. Arrows on the right indicate the predicted depth, and the computed average pressure $\bar{p}_d$ of the air trapped inside of the delamination. Note that numbers in square brackets indicate the relative frequency that the GA predicted a particular depth during five replications.

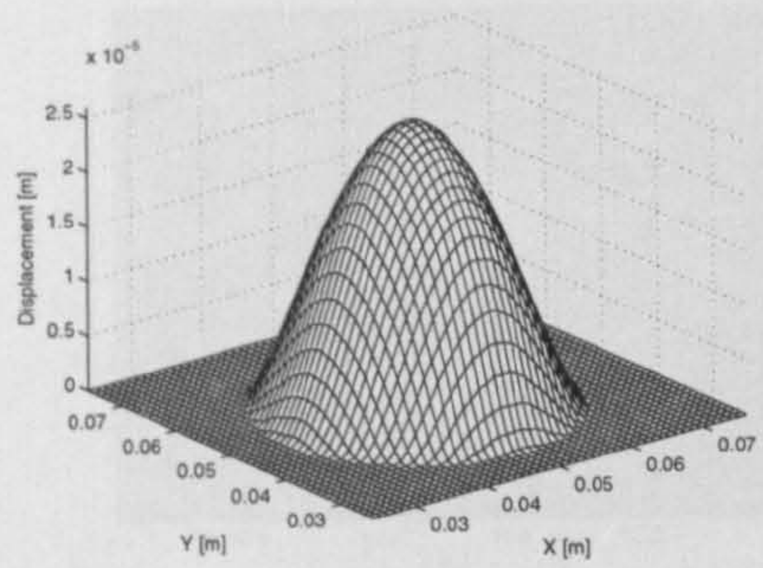

(a)

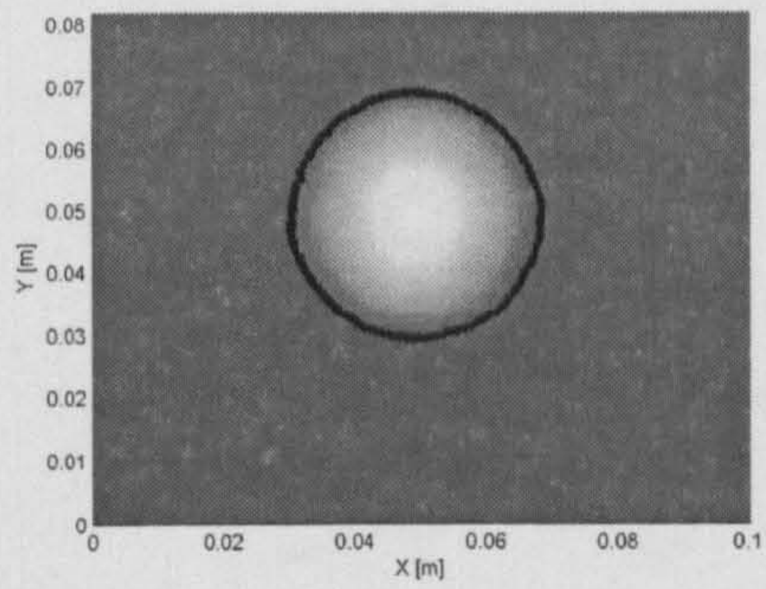

(b)

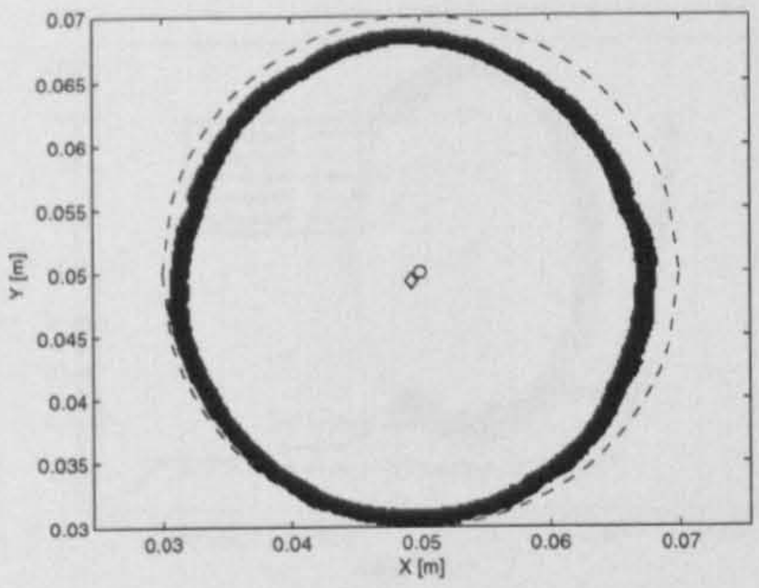

(c)

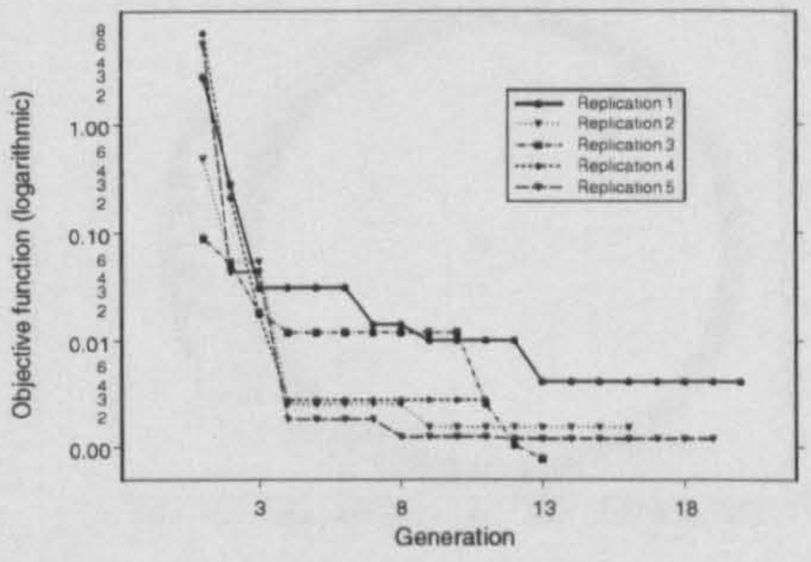

(d)

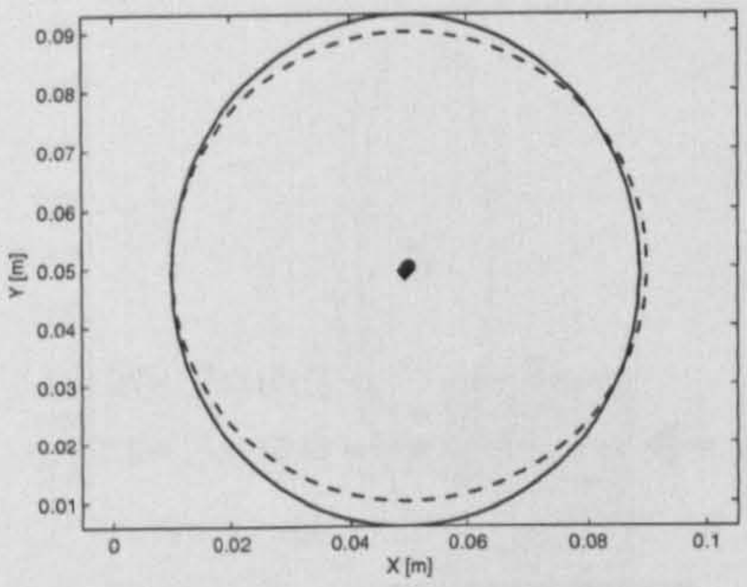

(e)

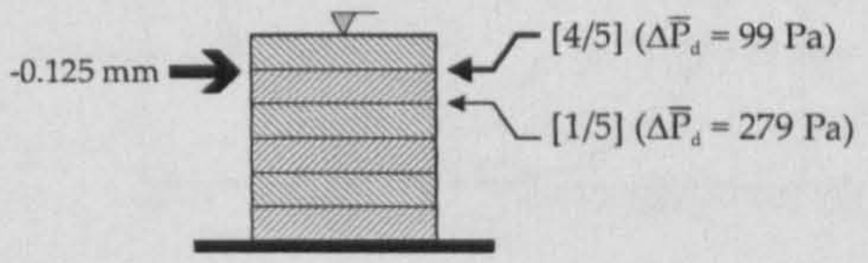

(f)

Figure 5.12. Results of damage characterisation for a sample five (40C12D).

(a) Zoomed DSPI's out-of-plane displacements; (b) detection of the edge of the bulge using a laplacian filter (black points); (c) initial estimation of delamination parameters using the detected edges (—) versus original flaw in the sample (– –); (d) convergence history from genetic algorithm (GA) after five replications with random initial population; (e) planar location, size and orientation of delamination predicted from GA (—) versus original flaw in the sample (– –); (f) predicted depth of the flaw from the GA, thick black arrow on the left indicates the depth of the delamination in the experimental sample. Arrows on the right indicate the predicted depth, and the computed average pressure $\bar{p}_d$ of the air trapped inside of the delamination. Note that numbers in square brackets indicate the relative frequency that the GA predicted a particular depth during five replications.

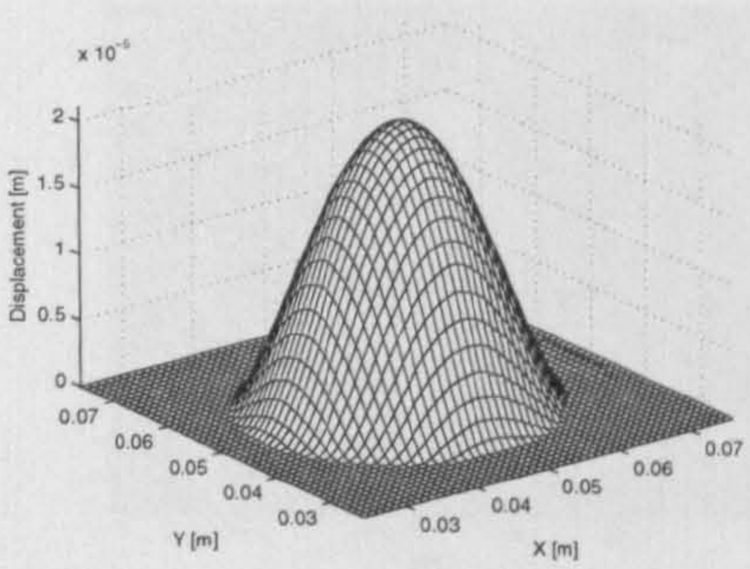

(a)

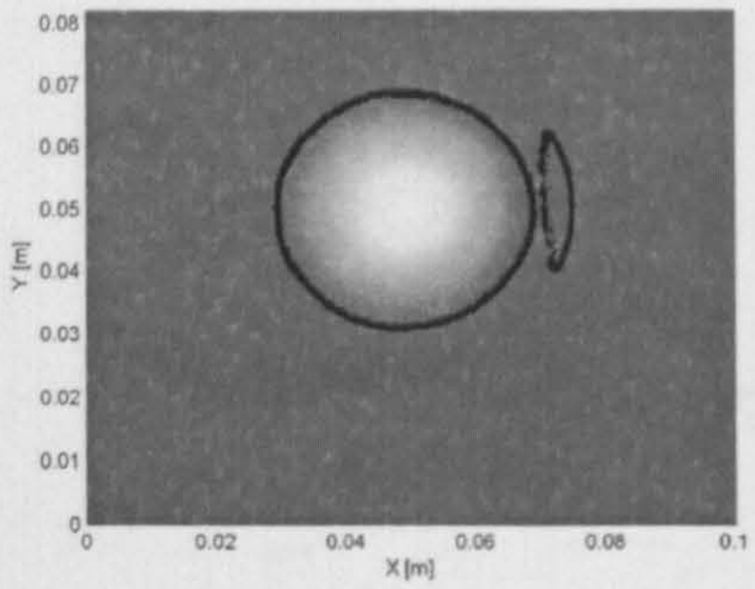

(b)

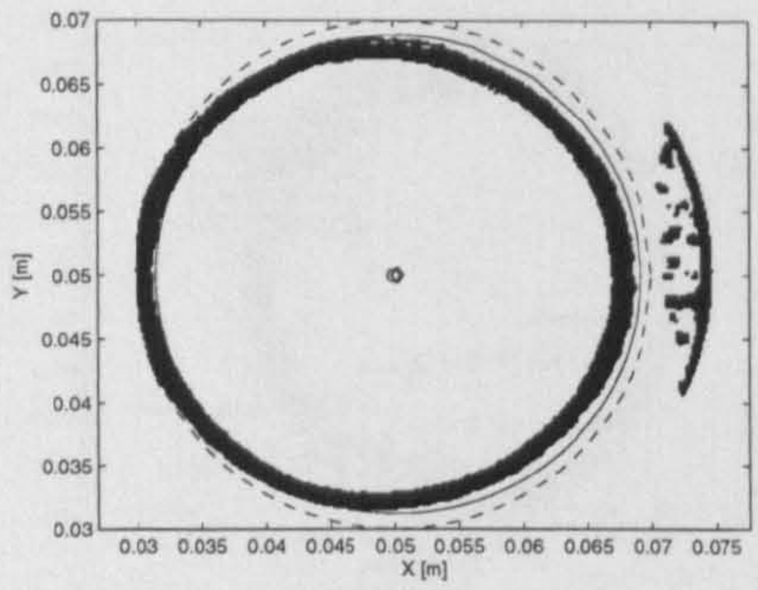

(c)

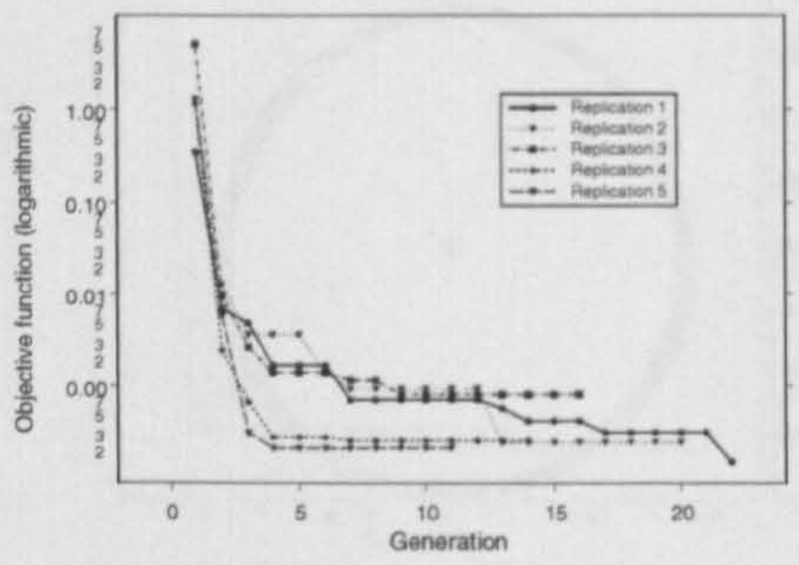

(d)

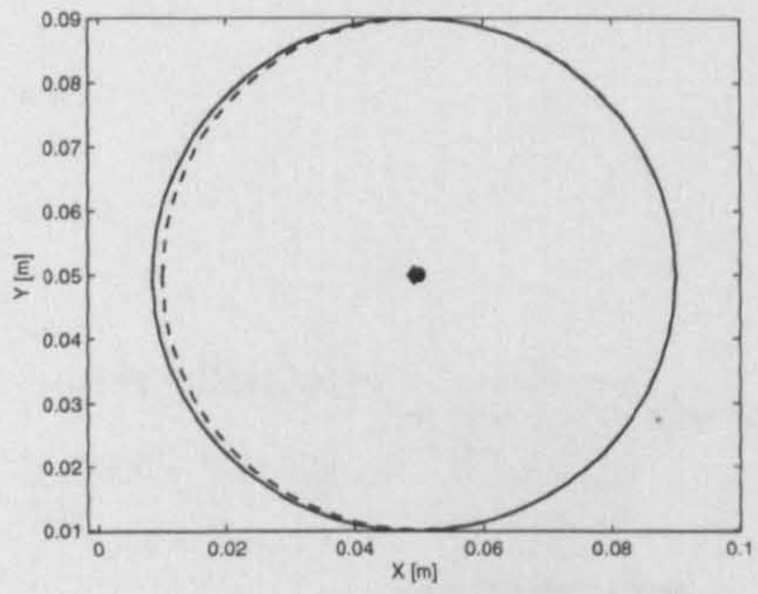

(e)

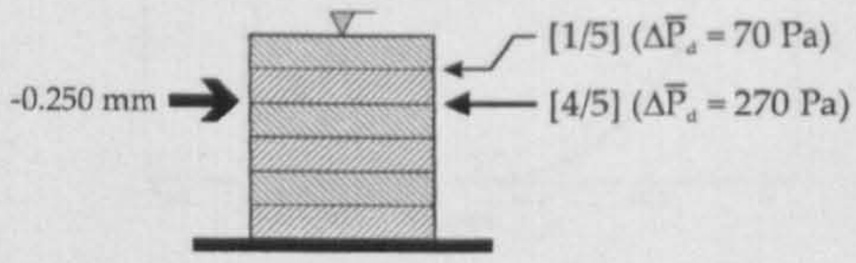

(f)

Figure 5.13. Results of damage characterisation for a sample six (40C23D).
(a) Zoomed DSPI's out-of-plane displacements; (b) detection of the edge of the bulge using a laplacian filter (black points); (c) initial estimation of delamination parameters using the detected edges (—-) versus original flaw in the sample (−−); (d) convergence history from genetic algorithm (GA) after five replications with random initial population; (e) planar location, size and orientation of delamination predicted from GA (—-) versus original flaw in the sample (−−); (f) predicted depth of the flaw from the GA, thick black arrow on the left indicates the depth of the delamination in the experimental sample. Arrows on the right indicate the predicted depth, and the computed average pressure $\bar{p}_d$ of the air trapped inside of the delamination. Note that numbers in square brackets indicate the relative frequency that the GA predicted a particular depth during five replications.

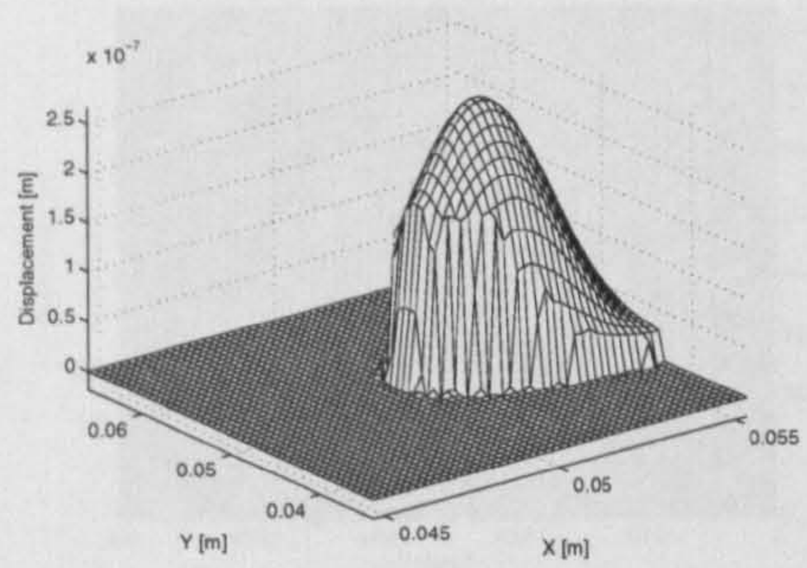

(a)

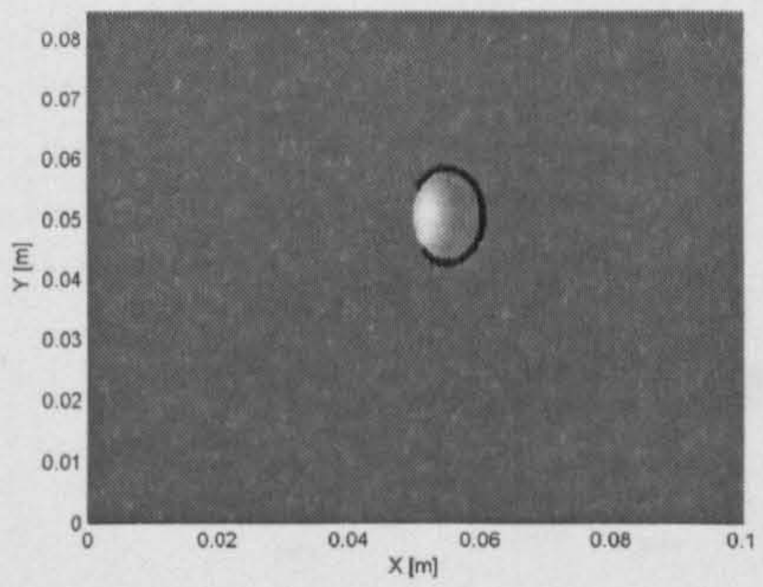

(b)

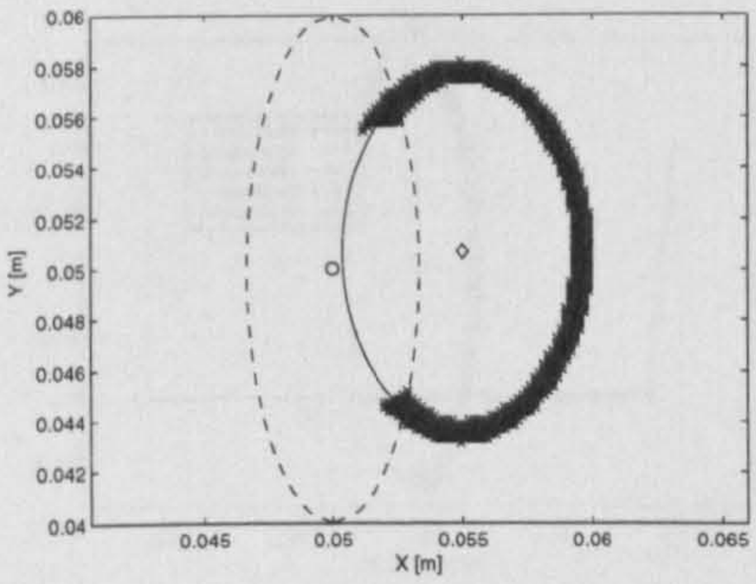

(c)

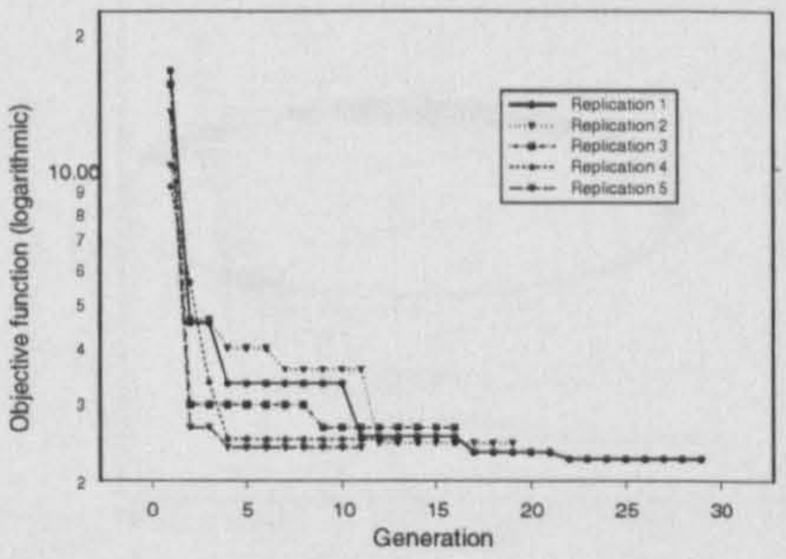

(d)

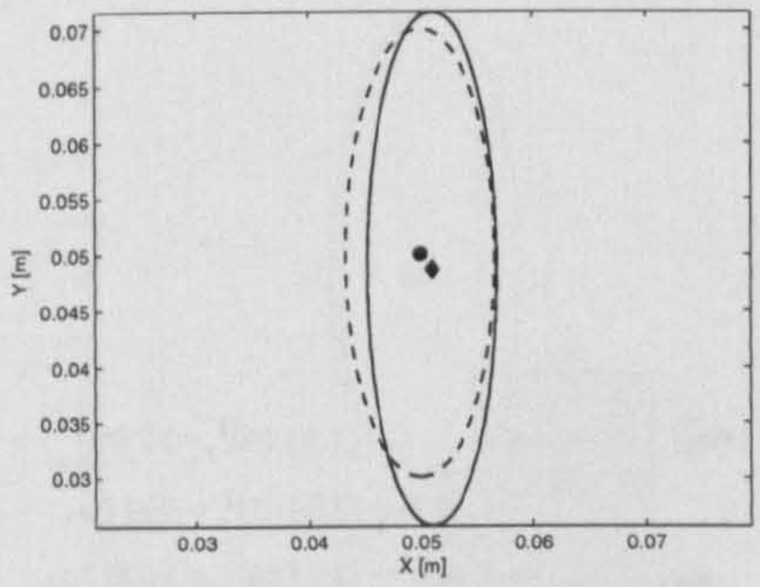

(e)

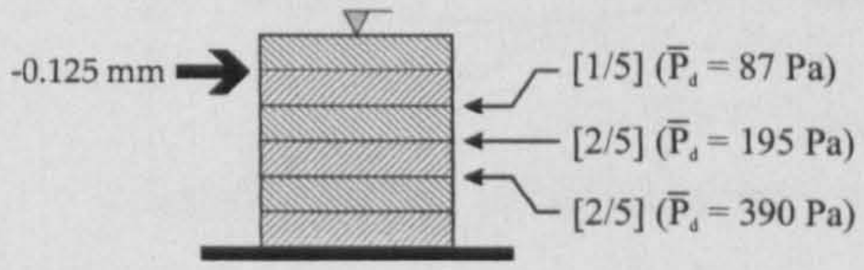

(f)

Figure 5.14. Results of damage characterisation for a sample seven (E2012D90). (a) Zoomed DSPI's out-of-plane displacements; (b) detection of the edge of the bulge using a laplacian filter (black points); (c) initial estimation of delamination parameters using the detected edges (—-) versus original flaw in the sample (−−); (d) convergence history from genetic algorithm (GA) after five replications with random initial population; (e) planar location, size and orientation of delamination predicted from GA (—-) versus original flaw in the sample (−−); (f) predicted depth of the flaw from the GA, thick black arrow on the left indicates the depth of the delamination in the experimental sample. Arrows on the right indicate the predicted depth, and the computed average pressure $\bar{p}_d$ of the air trapped inside of the delamination. Note that numbers in square brackets indicate the relative frequency that the GA predicted a particular depth during five replications.

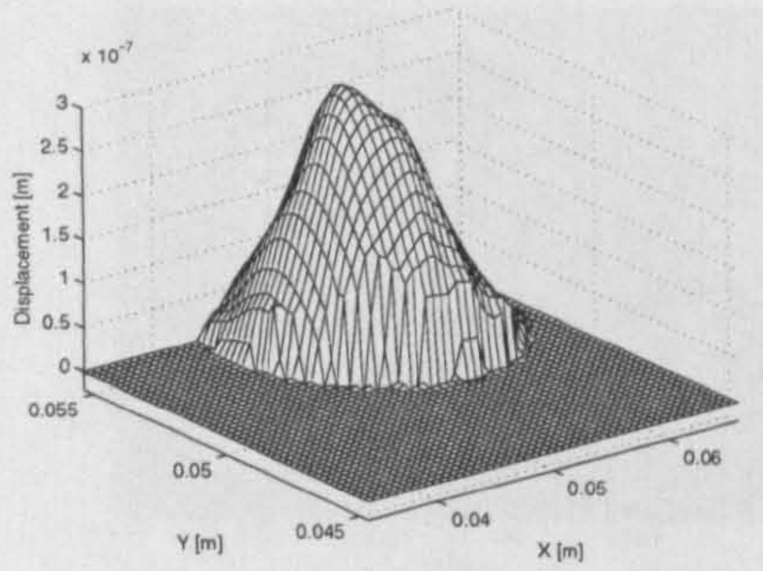

(a)

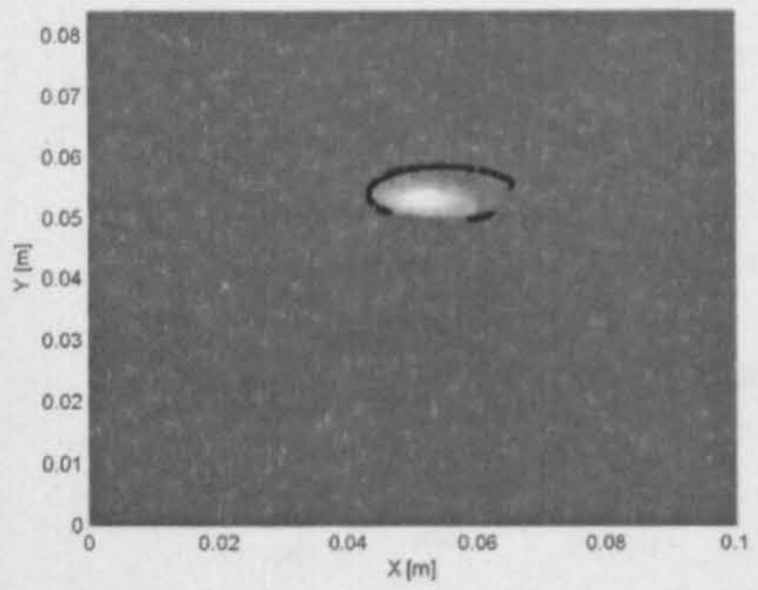

(b)

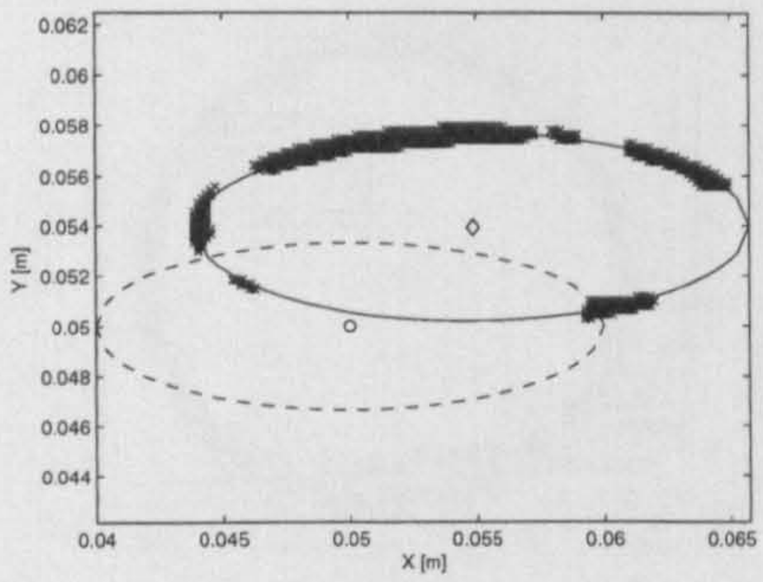

(c)

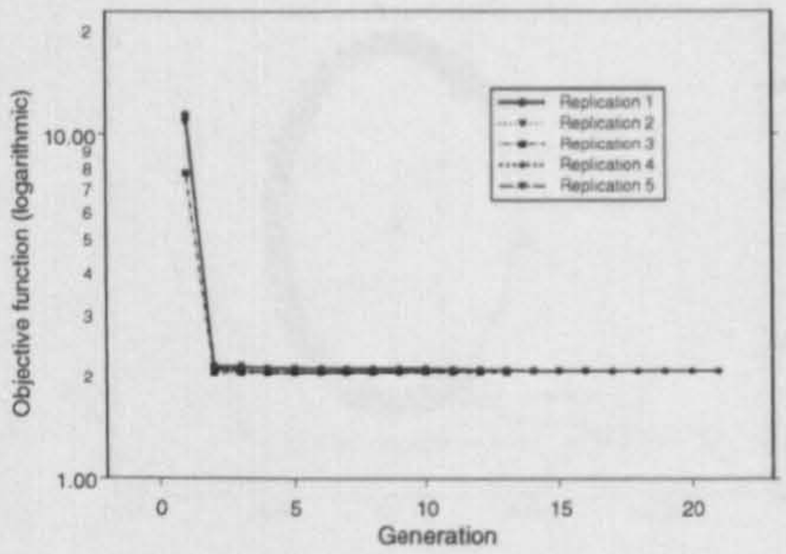

(d)

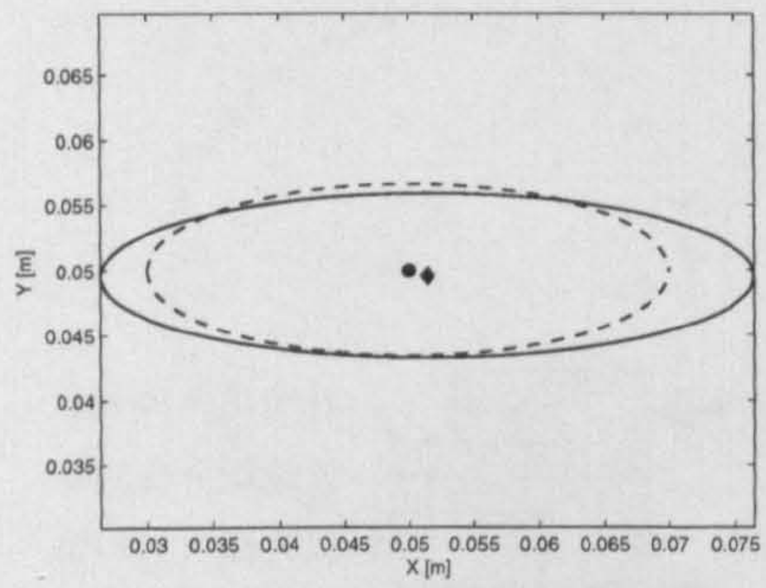

(e)

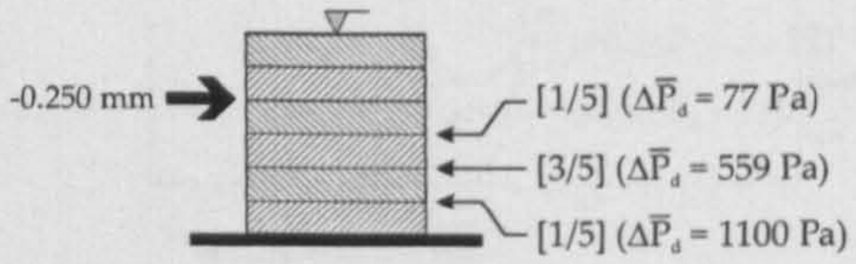

(f)

Figure 5.15. Results of damage characterisation for a sample eight (E2023D0). (a) Zoomed DSPI's out-of-plane displacements; (b) detection of the edge of the bulge using a laplacian filter (black points); (c) initial estimation of delamination parameters using the detected edges (—-) versus original flaw in the sample (−−); (d) convergence history from genetic algorithm (GA) after five replications with random initial population; (e) planar location, size and orientation of delamination predicted from GA (—-) versus original flaw in the sample (−−); (f) predicted depth of the flaw from the GA, thick black arrow on the left indicates the depth of the delamination in the experimental sample. Arrows on the right indicate the predicted depth, and the computed average pressure $\bar{p}_d$ of the air trapped inside of the delamination. Note that numbers in square brackets indicate the relative frequency that the GA predicted a particular depth during five replications.

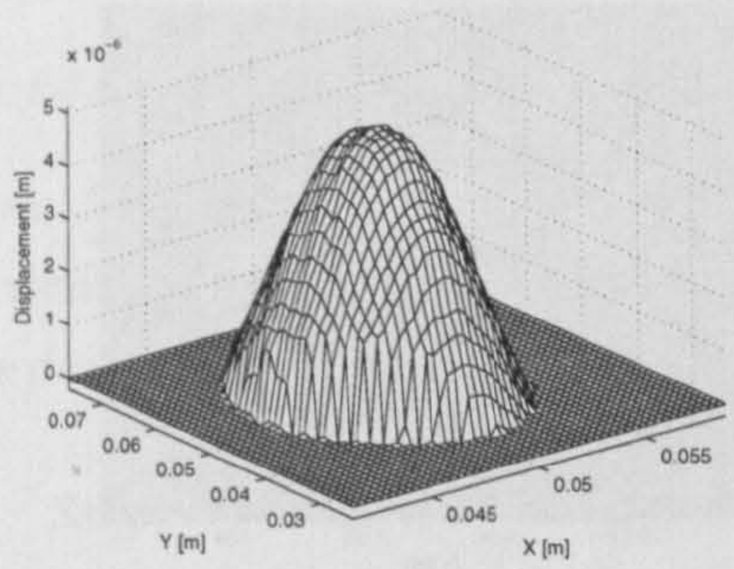

(a)

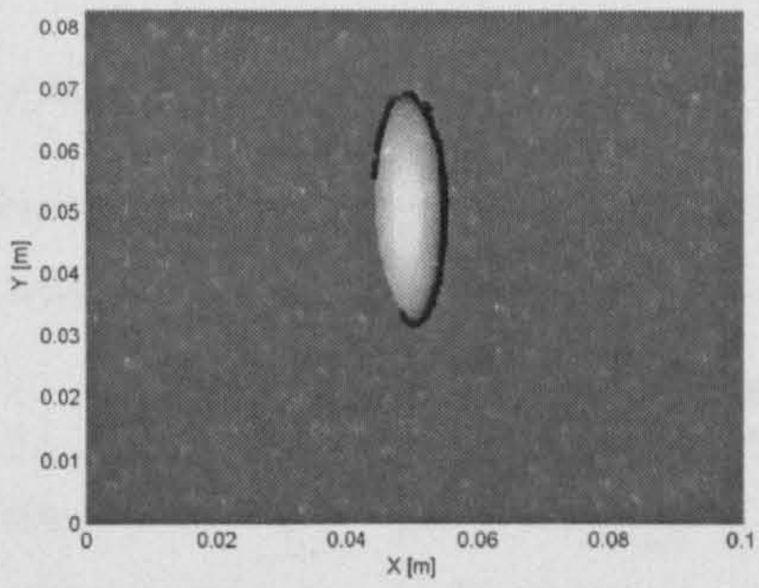

(b)

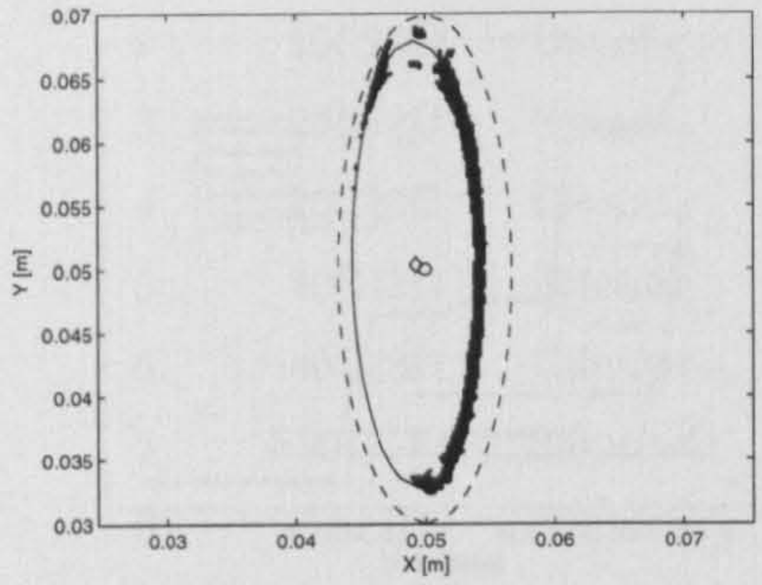

(c)

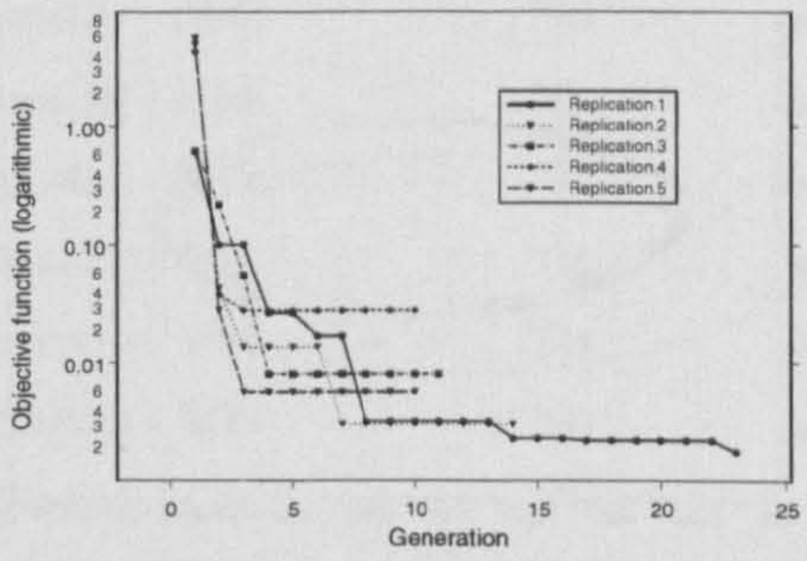

(d)

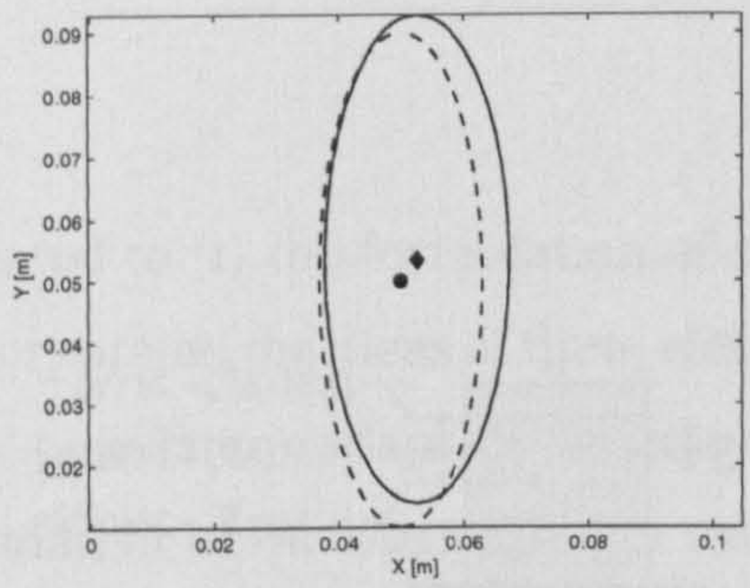

(e)

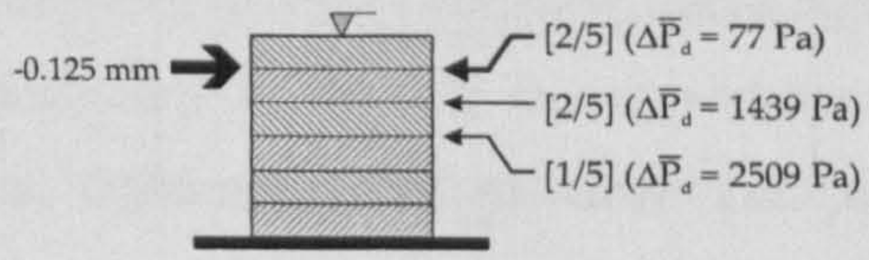

(f)

Figure 5.16. Results of damage characterisation for a sample nine (E4012D90). (a) Zoomed DSPI's out-of-plane displacements; (b) detection of the edge of the bulge using a laplacian filter (black points); (c) initial estimation of delamination parameters using the detected edges (—-) versus original flaw in the sample (−−); (d) convergence history from genetic algorithm (GA) after five replications with random initial population; (e) planar location, size and orientation of delamination predicted from GA (—-) versus original flaw in the sample (−−); (f) predicted depth of the flaw from the GA, thick black arrow on the left indicates the depth of the delamination in the experimental sample. Arrows on the right indicate the predicted depth, and the computed average pressure $\bar{p}_d$ of the air trapped inside of the delamination. Note that numbers in square brackets indicate the relative frequency that the GA predicted a particular depth during five replications.

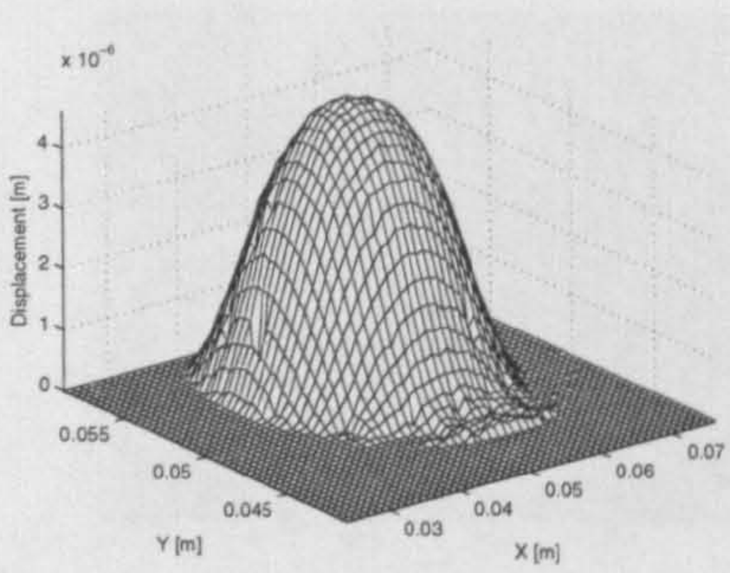

(a)

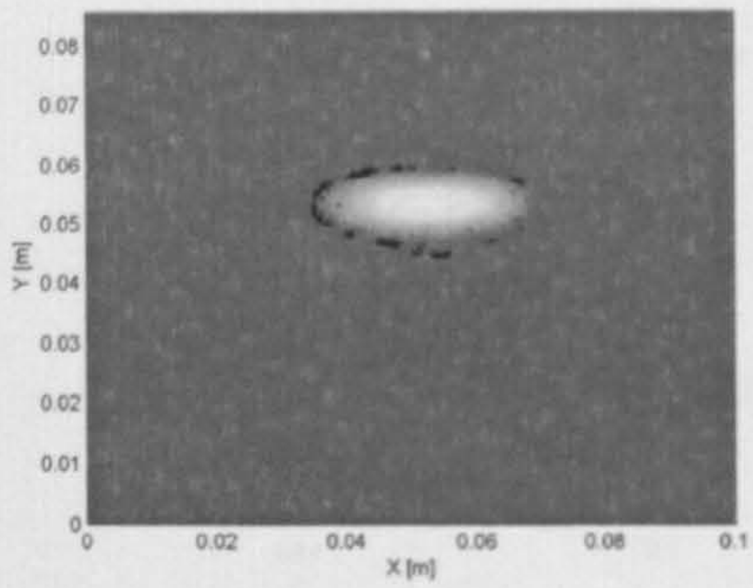

(b)

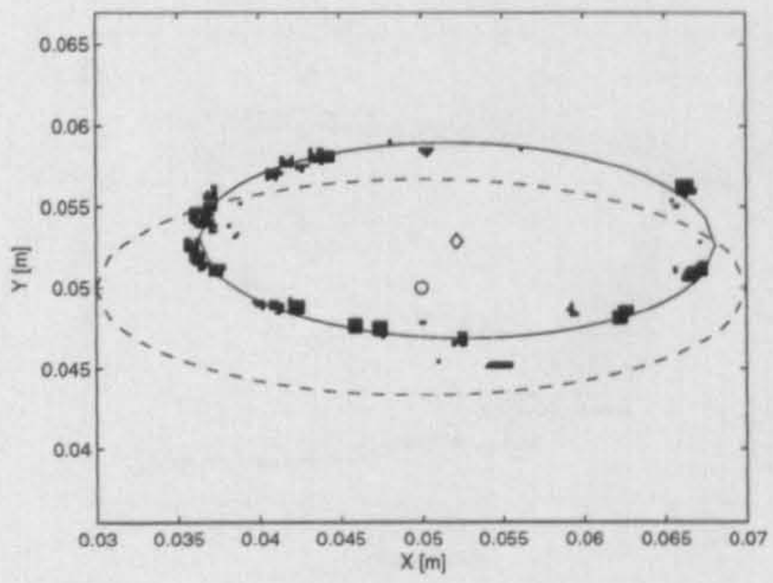

(c)

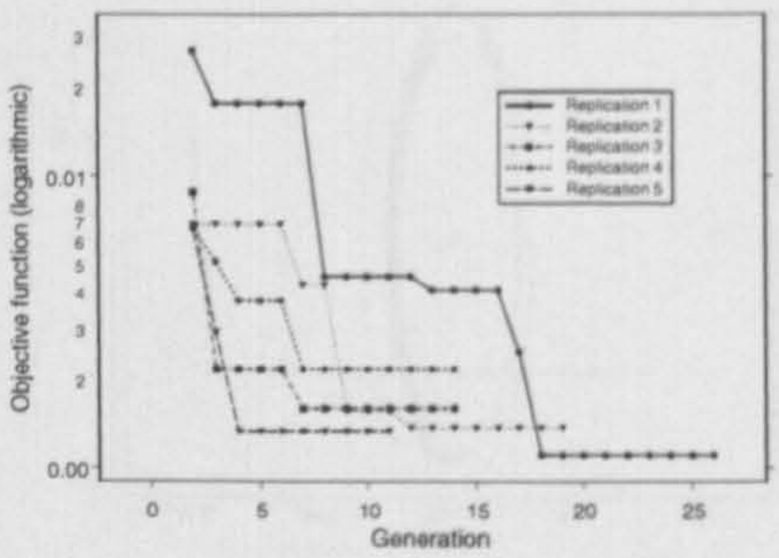

(d)

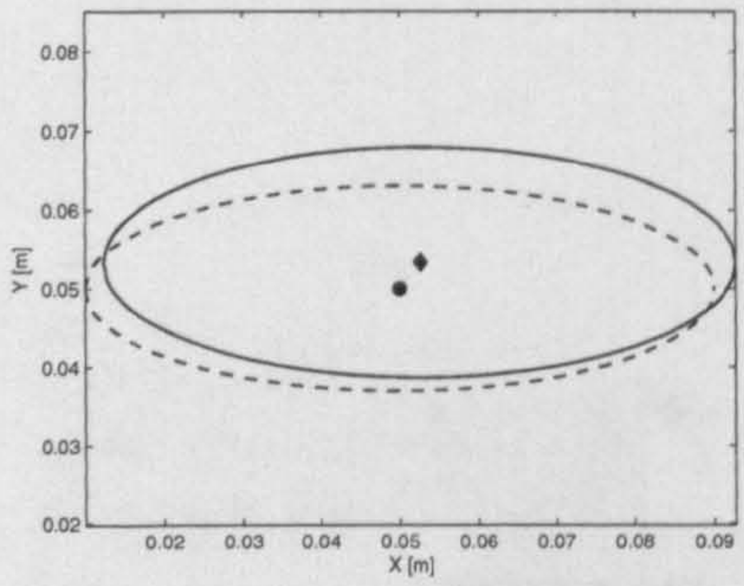

(e)

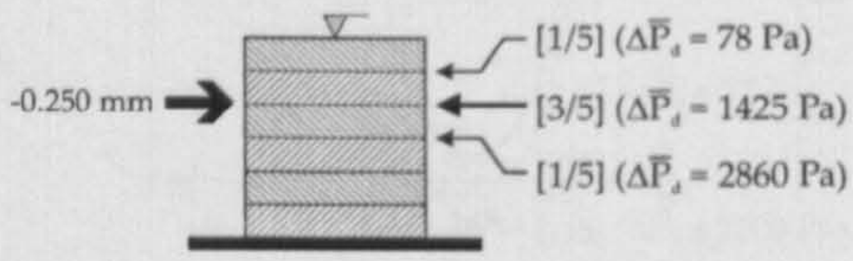

(f)

Figure 5.17. Results of damage characterisation for a sample ten (E4023D0).
(a) Zoomed DSPI's out-of-plane displacements; (b) detection of the edge of the bulge using a laplacian filter (black points); (c) initial estimation of delamination parameters using the detected edges (—) versus original flaw in the sample (– –); (d) convergence history from genetic algorithm (GA) after five replications with random initial population; (e) planar location, size and orientation of delamination predicted from GA (—) versus original flaw in the sample (– –); (f) predicted depth of the flaw from the GA, thick black arrow on the left indicates the depth of the delamination in the experimental sample. Arrows on the right indicate the predicted depth, and the computed average pressure $\bar{p}_d$ of the air trapped inside of the delamination. Note that numbers in square brackets indicate the relative frequency that the GA predicted a particular depth during five replications.

Table 5.3. Initial estimation of size and position of delamination from bulge's edge.

The initial estimation of the size and position of delamination from bulge's edge predicts damages with smaller area than the real delamination inside of the composite laminate. The centre of the damage is not predicted accurately.

Sample	*Name*	*Shape*	*Was the size of the damage predicted accurately?*	*Was the centre predicted accurately*
1	10C12D	Circular	No [smaller - 50%]	No
2	10C23D	Circular	No [smaller - 20%]	No
3	20C12D	Circular	No [smaller - 30%]	No
4	20C23D	Circular	No [smaller - 30%]	No
5	40C12D	Circular	Yes [smaller - 8%]	Yes
6	40C23D	Circular	Yes [smaller - 5%]	Yes
7	E2012D90	Elliptical	No [smaller - 40%]	No
8	E2023D0	Elliptical	Yes [larger - 15%]	No
9	E4012D90	Elliptical	No [smaller - 20%]	Yes
10	E4023D0	Elliptical	No [smaller - 25%]	No

pointed to (1) the formulation of a delamination identification technique that incorporated the ideas of finite element analysis, inverse problems, and a novel low-population adaptive range genetic algorithm; and (2) the experimental validation of the methodology using real DSPI measurements from composite laminates with embedded delaminations.

5.7.1 Formulation of the identification methodology - Sub question A

A novel six-step computational methodology was proposed for the post-processing of experimental DSPI data into meaningful numerical quantification of delamination in composite laminates. The first step in the methodology is the segmentation of the DSPI measurements that aims for the identification of the region where the damage is present. The tool used with this purpose is a laplacian-based edge detection technique that isolates regions of low deformation from regions with high displacements. The second step, is the transfor-

Table 5.4. Delamination Identification Methodology: convergence history for all experimental samples.

The rate of success of LARGA for five repetitions using random initial populations of size five shows encouraging results. The number of generations (iterations) used to search was small, as well as, the time used for the identification. The limited number of successful identifications, in special in samples 7 and 8, can be explained by the limited resolution of the DSPI technique, and the severe discontinuities present in the out-of-plane displacement fields.

Sample	*Name*	*Converged replications to global minimum?*	*How many generations were used to converge?*	*How long did it take? (seconds)*
1	10C12D	2 [R3 and R4]	11	711
2	10C23D	2 [R1 and R4]	12	275
3	20C12D	2 [R3 and R4]	17	1220
4	20C23D	0	18	475
5	40C12D	4 [R2, R3, R4, R5]	16	1128
6	40C23D	4 [R1, R2, R4, R5]	17	1226
7	E2012D90	0	17	1262
8	E2023D0	0	14	2983
9	E4012D90	2 [R1 ,R2]	14	294
10	E4023D0	3 [R1, R2, R5]	16	385

mation of the DSPI's bulge edge into numerical parameters of size and planar location of an idealised ellipse that can be used later as initial values for the search of the correct values of size, orientation and depth of the delamination.

Cost-efficiency, in terms of *speed* and *accuracy* is introduced in the identification methodology in steps three to six. In step three the concept of Central Geometric Moments (CGM) was used to reduce the large amount of data contained in DSPI into a reduced set of moments that were easily manipulated during the iterative process of the identification methodology. An interested aspect of CGM is that they compress the experimental data, maintaining at the same time the physical significance of such data. The fourth step in the methodology was the design of a purpose-based finite element (FE) model that represented a composite laminate with a trial debonding. The FE model was designed in such a way that delaminations were represented in the most accu-

Table 5.5. Delamination Identification Methodology: prediction of size and position of delamination for all experimental samples.

In genaral the sizes of the delamiantion predicted by LARGA were modestly larger than the size of the real delaminations in the composite panel. The planar location of the delamination was predicted with great accuracy.

Sample	*Name*	*Shape*	*Is the size of the damage predicted accurately?*	*Was the centre predicted accurately*
1	10C12D	Circular	Yes [bigger - 2.21%]	Yes [4.72%]
2	10C23D	Circular	No [bigger - 23.0%]	Yes [3.79%]
3	20C12D	Circular	Yes [bigger - 0.06%]	Yes [4.60%]
4	20C23D	Circular	Yes [bigger - 9.80%]	Yes [3.92%]
5	40C12D	Circular	Yes [bigger - 5.35%]	Yes [2.67%]
6	40C23D	Circular	Yes [bigger - 0.42%]	Yes [1.60%]
7	E2012D90	Elliptical	Yes [bigger - 2.82%]	Yes [0.63%]
8	E2023D0	Elliptical	Yes [bigger - 5.66%]	Yes [2.00%]
9	E4012D90	Elliptical	Yes [bigger - 7.90%]	Yes [1.80%]
10	E4023D0	Elliptical	Yes [bigger - 11.0%]	Yes [11.0%]

rate way, and the solution time was maintained low. The fifth step involved again the use of CGM for the representation of the out-of-plane displacements from the FE model with a trial debonding. In the final step of the methodology a novel low-population adaptive range genetic algorithm (LARGA) was introduced for the fast quantitative determination of the geometrical parameters of the delamination embedded in the laminate.

To the knowledge of the author of this thesis, there is not a systematic approach in the literature, like the one reported in this chapter, for the identification of delamination in composite panels. The only related work on this area was performed by Panni [1] in 2002 (see chapter 2, section 2.6 where it was discussed extensively).

Table 5.6. Delamination Identification Methodology: prediction of depth of delamination and pressure of air trapped inside of the crack.

The LARGA-based identification methodology shows that the precise prediction of the depth of the delamination can be obtained almost the 50% of the time. However, it must be noted that erroneous classifications of depth are located just one interlaminar layer above or below of the correct location. Results for the pressure of the air traped inside of the delamination are inconclussive, as there are not experimental measurements of anaylitical calculations to verify their correctness.

Sample	*Name*	*Shape*	*How many replications predicted the depth accurately?*	*Change of pressure inside of delamination*
1	10C12D	Circular	2 out of 5	41 Pa
2	10C23D	Circular	2 out of 5	695 Pa
3	20C12D	Circular	2 out of 5	65 Pa
4	20C23D	Circular	0 out of 5	-
5	40C12D	Circular	4 out of 5	99 Pa
6	40C23D	Circular	4 out of 5	270 Pa
7	E2012D90	Elliptical	0 out of 5	-
8	E2023D0	Elliptical	0 out of 5	-
9	E4012D90	Elliptical	2 out of 5	77 Pa
10	E4023D0	Elliptical	3 out of 5	1425 Pa

5.7.2 Experimental validation of the methodology - Sub question B

The computational identification methodology was validated against ten experimental samples manufactured and tested at Loughborough University. The main findings of the validation program are as follows:

Laplacian-based edge detection. DSPI measurements of a delaminated composite panel display a characteristic *bulge* that can be isolated using the laplacian-based edge detection technique. From the identification methodology, it can be concluded that the edge can be completely determined if DSPI experiments do not present discontinuities. It was observed that this is usually true for circular delaminations with diameter greater than 10 *mm* (samples 3, 4,

5, and 6). For DSPI experiments that present abrupt discontinuities, (samples 1, 2, 7, 8, 9 , and 10), the bulge's edge is usually incomplete, covering angles that oscillates between 180 and 270 degrees.

Initial parameters of delamination. In here, the aim was to give an initial estimation of the size and planar location of the delamination using the edges detected above. It can be concluded that independently of the completeness of the edge, the area of the delamination is under-predicted. Regarding the planar position of the delamination, it is possible to conclude that if the edge of the bulge is fully resolved, then the planar coordinates of the centre of the crack are predicted in a more accurate way.

Convergence of the genetic algorithm. It was found that if random initial populations are used during five repetitions for the same algorithm, an average of the 50% of such repetitions converge the global optimum of the optimisation space. The other 50% converge converges to local minima, or does not converge at all. The validation using a random population for every replication has not been explored in the literature, where researchers usually use the same initial population every time. The author of this thesis believes that this *tradition* can be criticised from several points of view: (1) when an algorithm with a given initial population converges to the global minimum of the objective function, successive runs with the same population *will* also converge the global minimum in an almost different generation. The main reason for this is that if the initial population converged it was because it has in its genes the proper traits that after many random combinations were present in a single individual. Therefore, if the same algorithm is re-started, the analyst only needs to wait long enough to observe again an individual with the proper combination of genes. (2) It is impossible to *engineer* an initial population if the answer of an optimisation problem is not known. Therefore, if a finite initial population is generated randomly, then there is not a prescribed guarantee that it will converge to the global optimum of an objective function. However, if the population is composed of a large number of individuals, then the chance of *catch*

the global minimum increases, but at the same time the computational time increases making such approximation extremely inefficient and not practical.

The proposed LARGA algorithm did achieve the requirements of speed and accuracy needed for its use in real-time in-service analysis. Convergence times ranged from five minutes (sample 2) to fifty minutes in the worst scenario (sample 8), where the algorithm did not converge at all. The number of generations (iterations) was less than 20 in all cases.

Identified parameters of the delamination. Size, planar location and depth of delamination were the primary objectives of the proposed identification methodology. Independently of the completeness of the DSPI measurements, the size of the predicted delamination was bigger than the real delamination embedded in the laminate. Normal over predictions were in the range of five to ten percent, but in one case (sample 2) the over prediction was much bigger. The planar location of delaminations was predicted with accuracy greater than 95% in nine of the ten samples. The predicted depth of the delaminations was predicted correctly 50% of the times, taking into account that always a different initial population was used in the LARGA. In those cases where the delamination was not predicted accurately, the identification methodology reported depths that were close to the real value.

Chapter 6

CONCLUSION AND FUTURE WORK

This chapter is divided in three section. Firstly, conclusions about the research questions are presented. They were drawn at the end of each chapter. Therefore they are presented again here for convenience. Secondly, the main contributions of this thesis are listed, and finally, suggestions for future work are detailed.

6.1 Conclusions about research questions

6.1.1 Research Question 1

Delamination modelling techniques Historically two main approaches have been used to model delamination in composite laminates: the classical laminated plate theory and the theory of elasticity. The former was deprecated during the 80's as a consequence of (a) its inability to predict accurately the shear stresses in the interface of the laminate and (b) the increasing availability of computer power during the early 70's, that opened the possibility to implement complex numerical routines needed to calculate the solutions of the constitutive equations provided by the theory of elasticity.

Solutions to the theory of elasticity have been found through two different approaches: Finite Differences (FD) and the Finite Element Method (FEM). Finite differences have been used to solve problems of stress and strains in laminates, however it lacks the flexibility of FEM to deal with complex laminate shapes. Research on modelling of delamination since 1980 has included, as a general rule, some form of finite element simulation.

To date, finite element models of delamination take advantage of three important conclusions derived from the studies on low-velocity impact during the 70's and 80's: Firstly, delamination represents a major component of damage that evolves accordingly to a definite pattern. Secondly, delamination is present only at interfaces between plies with different fibre orientation. Finally, if delamination is present, the debonded area has an elliptical or peanut shape.

Literature concerning the modelling of delamination through the FEM can be classified in four groups accordingly to the type of interface used between the delaminated and base regions. They are the hybrid element interface, de-equivanlenced crack, degraded inter-laminar layer, and sub-structure.

In the hybrid element interface technique, both sub-laminates are connected through a combination of spring and beam elements. It has been successfully used in studies of low-velocity impact. However, a major drawback in its implementation is the dependency between the size of the delamination and the coarseness of the FE mesh. Another disadvantage is that the solution of the FE model requires large amounts of CPU time. The de-equivalenced crack technique has been used to model buckling in composite laminates where there are not overlapping between the sub-laminates. Researchers using this technique have reported a good agreement between the predictions of the FE model and experimental measurements.

The degraded inter-laminar layer model is the most simple of all the models. However, it is the one with less agreement with experimental data. In this technique, the delamination is simulated through a reduction in the elastic properties of the elements that are just beneath of the delaminated region. The last technique is labelled as delamination as sub-structure where the model include only the delaminated region. This is the most cost-effective technique in terms of CPU solution time; however, there is not research available on the evaluation of the performance of this model against experimental data.

Digital Speckle Pattern Interferometry (DSPI) This is an experimental technique that has been proved to be capable for precise measurements sensitivity of the order of the wavelength of light from diffusely scattering objects.

DSPI produces real-time fringe patterns that typically represent contours of constant displacement component depth. However, fringe patterns provide visual information to the trained eye, but they are generally noisy. Loss of accuracy in the technique is due to systematic and random errors.

Systematic errors appear form the effect of higher harmonics , miscalibration and vibration. Higher harmonics can be produced for non-linearities in the detector array. Miscalibration represented by a poor alignment of the device or motion of the specimen while the experiment is being carried. Vibration and other environmental disturbances such air currents can cause significant errors. Random errors are introduced due to variations of the laser output power or electronic noise in the detector camera.

Researchers using DSPI to detect delamination in laminates have found that small and deep delaminations are difficult to detect if the sensitivity of the system is poor, or there is not strict control on the pressures inside of the vacuum chamber.

Compact representation of DSPI data The theory of two dimensional moments is a paradigm that is widely used by researchers on pattern recognition. By using moments, it is possible to reduce large sets of experimental data into small arrays containing the convolution of the experimental data with a suitable base-function family. Two types of moments are commonly used by researchers: Zernike and Geometric.

Zernike moments appeal researchers by their properties like orthogonally, rotation invariance, robustness to moderate levels of noise, and efficiency in terms of the non-redundancy provided by lower order moments. However, some of these properties make them not useful to characterise damage. Zernike moments contain information about an image hath is independent of the size, planar position and relative angular orientation.

On the other hand, central geometric moments offer attributes that make them attractive to be used in the characterization of delamination. Firstly, they are sensitive to the location of the crack that is given by the equation 2.3. Secondly, this type of moments are sensitive to the size of the image that are representing. Finally, the orientation of the flaw can be discriminated using CGM,

because these moments are function of the angle of orientation of the features of the image.

Characterization of damage Progress has been made to understand and identify the damage of truss structures. Some authors suggested that the static load distribution in the structure affects the damage detection, and indicated that although structural damage is non-linear in behaviour, the use of loads of small magnitudes result in structures behave only in their elastic ranges. It was showed also those standard modal properties such as resonant frequencies and mode shapes are poor indicators of damage, and consequently the methods studied were inconsistent and did not clearly characterise the damage location.

Having developed an understanding for damage identification in truss structures, researchers have turned their attention to characterise flaws in composite materials. It has been found that the damage detection using structural waves is sensitive to manufacturing tolerances, decreasing its applicability in problems where exist input noise from uncertainty in geometrical properties. Also it has been showed that for damage detection based on strain flexibility methods failed to locate damage in some elements.

The findings of studies examining the use of neural networks and genetic algorithms in composite panels have been mixed. It was stated that it was easier to predict damage location than size due to location is a discrete variable and size out put is a continuous variable. However, there were no established procedures for choosing the optimal number of hidden layers in neural network architectures, or for choosing the operators and its values in genetic algorithms. Also it has been mentioned that the performance of both neural networks and genetic algorithms decline gradually in the presence of noisy or incomplete input data and they were not accurate to identify the location and depth of the damage. Moreover, studies using genetic algorithm using experimental data have not provided accurate predictions of damage in terms of shape, size and position. Of the two approaches, genetic algorithms offers some advantages when used it in-service where the exact nature of laminate lay up, and materials properties is not known *a-priori*.

Genetic algorithms have shown to be effective at searching large domains for a global optimal point by sampling a small fraction of the total solution space. This ability has made them attractive for researchers working in the solution of inverse problems and optimisation.

Latest research on characterisation of delamination in composites The latest and closest research linked to this thesis was performed by David Panni at Loughborough University (2002). Panni developed a general method to integrate a FE model with genetic algorithm in order to design and optimise composite structures. As an extension of his research, he showed that at, least theoretically, is possible to characterise delamination in laminates. He showed that if the shape of the delamination could be fully resolved, then the depth of the delamination was found with total accuracy. Panni concluded that problems in his model existed in terms of the *a-priori* knowledge needed to be incorporated, like for example the areas of the laminate that did not contain delaminations, and the on-line calibration of the genetic algorithm in terms of the value of its parameters.

6.1.2 Research Question 2

6.1.2.1 Parametric representation of delamination - Sub question A

Delamination represents a major component of damage that evolves according to a definite pattern. Geometrically, delamination can be approximated an elliptical-shaped crack with with six parameters: (1,2) the planar location, (3) length of the delamination, (4) width, (5) angle of orientation, and (6) depth below the measured surface of the laminate. The findings of laplacian-based techniques for the detection of edges in out-of-plane displacements from the DSPI technique, indicate that is possible to determine the size and orientation of flaw, but in general this approach will provide results that under predict the area of the delamination.

6.1.2.2 Type of FE mesh to represent delamination - Subjection B

Two possible FE meshing paradigms can be applied for the geometric representation of delamination in a FE model. These are mapped and free meshing. The findings from numerical experiments indicate that a mapped mesh is not flexible enough to cope with the geometry of elliptical delaminations. The principal reasons for this are that (1) in order to accurately represent the boundary of the flaw, it is necessary to increase the resolution of the mesh, increasing at the same time the CPU time needed to solve the FE model, and (2) complex, and not always precise, routines are needed to search the mesh in order to determine which nodes must be delaminated.

On the other hand, free meshing is a flexible and cost-efficient paradigm to represent the geometry of damage. This paradigm is parallel to the solution of classical or forward problems in the sense that the FE mesh is generated in a geometric model a laminate after the flaw is merged with laminate model. The findings indicate that using a well designed free mesh it is possible to represent a parametric delamination with high accuracy, and with low computational cost in terms of the number of FE elements needed in the model.

6.1.2.3 Delamination model - Sub question C

Studies in the literature concerning the simulation of the physics in the literature provide two models that can be used to represent the physics of delamination during a DSPI experiment. These are the de-equivalenced crack and the sub-structure model. The former has an element of intuitiveness that could make them attractive to use in the following manner: once the FE mesh of a laminate composite has been implemented, then search and de-equivalence the nodes of the mesh that are inside of the delaminated region. The findings indicate that although this technique could represent the physics of delamination, it is not cost-effective in terms of the computational time required to both de-equivalenced the mesh, and solve the FE model.

On the other hand, the sub-structure approach is not intuitive, but it provides a direct connection between the physics of the delamination and the type of mesh required in the analysis. Findings indicate that this delamination model works best with free meshing, satisfying multiple objectives simultane-

ously: (1) accurate representation of the geometry (boundary) of the flaw, and (2) compact FE models that are cheap to run.

6.1.2.4 Boundary conditions - Sub question D

Boundary conditions refer to the combination of both displacement constraints and external loads on a FE model. If the delamination model to use is sub-structure, then the displacement constraints have defined presented in the literature. They are (1) cantilever-cantilever around the boundary of the delaminated sub laminate. On the other hand, the determination of the external loads that act on the delaminated region during a DPSI experiment is rather complex.

The two main forces on the delaminated region are the pressure in the vacuum chamber and the pressure of the air inside of the delamination. The findings of the interpretation of the integral-differential equation that correlates the out-of-plane displacements and the pressures on the delaminated region, indicate that in order to calculate the pressure of the air inside of the delamination, it is necessary to know the exact volume of air contained inside of the bulge. If this volume is not known, then the problem of characterisation of delamination from DSPI measurements is ill-posed, and in consequence, a unique determination of the parameters of the delamination is not possible.

6.1.3 Research Question 3

6.1.3.1 Formulation of the inverse problem - Sub question A

The problem of characterisation of delamination in composite laminates can be formulated as an inverse problem where the measured response of the surface of the laminate is used to predict the geometric parameters of the flaw. Mathematically, the inverse problem can be formulated using the output error criterion that relates the measured response of the laminate from DSPI and the displacements obtained from a FE model with a trial debonding.

The output error criterion leads naturally to an optimisation problem where the objective function is written as the minimisation of the difference between the measured and computed FE displacements, and the variables to optimise are the geometric parameters of an idealised delamination in a FE model.

6.1.3.2 Reformulation of the inverse problem - Sub question B

The classical formulation of the inverse problem leads to non-efficient solution algorithms as a consequence of the number of measurements that are provided by the DSPI technique. The large amount of data contained in the array of experimental results can be represented by a finite set of central geometric moments.

Central geometric moments are able to represent accurately the physical content of the experimental results because they are sensitive to the size, location, and orientation of the displacement field contained in both the DSPI measurements, and the FE model that encapsulates the delamination to be characterised. These moments are equivalent to geometric moments that are calculated from the centroid of the out-of-plane displacement field.

The computation of geometric moments involves the calculation of a convolution of the out-of-plane displacements with a predefined family of monomial functions. In case of the measurements from DSPI, geometric moments can be computed replacing the integral of area for a double summation. In the case of the FE model, a formula that also uses a double summation was developed in order to take advantage of the design of the FE mesh.

Out-of-plane displacements from both the DSPI technique and a FE model can be compared using a seven-moment similarity measure, which is based in low order central geometric moments. A comparison of this condition is cost-effective because it reduces the time of computation used in such comparison.

The use of central geometric moments involves the reformulation of the delamination characterisation problem, as an inverse problem where the central geometric moments computed form the measured response of the surface of the laminate is used to predict the geometric parameters of the flaw. This new version of the inverse problem can be formulated using the output error criterion that relates the central geometric moments from DSPI and the moments obtained from the displacements of a FE model with a trial crack.

The output error criterion is written as an optimisation problem where the objective function is written as the minimisation of a seven-moment similarity measure.

6.1.3.3 Solution of the inverse problem - Sub question C

The formulation of non-destructive crack identification problems leads naturally to non-differentiable, non-convex optimisation problems. Traditional local minimisation techniques can not be used to solve such optimisation because (1) they usually converge to local minima close to the starting point of search, and (2) they require the information about the derivates of the objective function. Thus, a global optimisation method is required for the numerical solution of the optimisation problem.

In a genetic algorithm, the set of unknown delamination parameters are represented as a chromosome of genes using real number encoding. Furthermore, due to the stochastic nature of genetic algorithms, a initial population of trial delaminations is assumed. For each set of alleles of the genes in the chromosome of an individual, the error function $\Psi_{err}(\vec{z}, p_d^t)$, that is the difference between measured and calculated central geometric moments, is calculated. In accordance to the terminology used in genetic algorithms, the minimisation problem is transformed into a maximisation problem. Therefore, instead of an error (or objective) function, a fitness function is introduced.

The mechanism of work of genetic algorithms is inspired on the concepts of natural selection and genetics. In the selection step, individuals with higher fitness function values are chosen to breed and to inherit their characteristics to the next generation. A cross over operator allows interchanging genetic content between individuals within the reproduction step. Finally, random genes in individuals are randomly mutated during the creation of a new generation.

6.1.4 Research Question 4

6.1.4.1 Formulation of the identification methodology - Sub question A

A novel six-step computational methodology was proposed for the post-processing of experimental DSPI data into meaningful numerical quantification of delamination in composite laminates. The first step in the methodology is the segmentation of the DSPI measurements that aims for the identification of the region where the damage is present. The tool used with this purpose is a laplacian-based edge detection technique that isolates regions of low defor-

mation from regions with high displacements. The second step, is the transformation of the DSPI's bulge edge into numerical parameters of size and planar location of an idealised ellipse that can be used later as initial values for the search of the correct values of size, orientation and depth of the delamination.

Cost-efficiency, in terms of *speed* and *accuracy* is introduced in the identification methodology in steps three to six. In step three the concept of Central Geometric Moments (CGM) was used to reduce the large amount of data contained in DSPI into a reduced set of moments that were easily manipulated during the iterative process of the identification methodology. An interested aspect of CGM is that they compress the experimental data, maintaining at the same time the physical significance of such data. The fourth step in the methodology was the design of a purpose-based finite element (FE) model that represented a composite laminate with a trial debonding. The FE model was designed in such a way that delaminations were represented in the most accurate way, and the solution time was maintained low. The fifth step involved again the use of CGM for the representation of the out-of-plane displacements from the FE model with a trial debonding. In the final step of the methodology a novel low-population adaptive range genetic algorithm (LARGA) was introduced for the fast quantitative determination of the geometrical parameters of the delamination embedded in the laminate.

To the knowledge of the author of this thesis, there is not a systematic approach in the literature, like the one reported in this chapter, for the identification of delamination in composite panels. The only related work on this area was performed by Panni [1] in 2002 (see chapter 2, section 2.6 where it was discussed extensively).

6.1.4.2 Experimental validation of the methodology - Sub question B

The computational identification methodology was validated against ten experimental samples manufactured and tested at Loughborough University. The main findings of the validation program are as follows:

Laplacian-based edge detection. DSPI measurements of a delaminated composite panel display a characteristic *bulge* that can be isolated using the laplacian-based edge detection technique. From the identification methodology, it can be concluded that the edge can be completely determined if DSPI experiments do not present discontinuities. It was observed that this is usually true for circular delaminations with diameter greater than 10 *mm* (samples 3, 4, 5, and 6). For DSPI experiments that present abrupt discontinuities, (samples 1, 2, 7, 8, 9 , and 10), the bulge's edge is usually incomplete, covering angles that oscillates between 180 and 270 degrees.

Initial parameters of delamination. In here, the aim was to give an initial estimation of the size and planar location of the delamination using the edges detected above. It can be concluded that independently of the completeness of the edge, the area of the delamination is under-predicted. Regarding the planar position of the delamination, it is possible to conclude that if the edge of the bulge is fully resolved, then the planar coordinates of the centre of the crack are predicted in a more accurate way.

Convergence of the genetic algorithm. It was found that if random initial populations are used during five repetitions for the same algorithm, an average of the 50% of such repetitions converge the global optimum of the optimisation space. The other 50% converge converges to local minima, or does not converge at all. The validation using a random population for every replication has not been explored in the literature, where researchers usually use the same initial population every time. The author of this thesis believes that this *tradition* can be criticised from several points of view: (1) when an algorithm with a given initial population converges to the global minimum of the objective function, successive runs with the same population *will* also converge the global minimum in an almost different generation. The main reason for this is that if the initial population converged it was because it has in its genes the proper traits that after many random combinations were present in a single individual. Therefore, if the same algorithm is re-started, the analyst only needs to wait long enough to observe again an individual with the proper combina-

tion of genes. (2) It is impossible to *engineer* an initial population if the answer of an optimisation problem is not known. Therefore, if a finite initial population is generated randomly, then there is not a prescribed guarantee that it will converge to the global optimum of an objective function. However, if the population is composed of a large number of individuals, then the chance of *catch* the global minimum increases, but at the same time the computational time increases making such approximation extremely inefficient and not practical.

The proposed LARGA algorithm did achieve the requirements of speed and accuracy needed for its use in real-time in-service analysis. Convergence times ranged from five minutes (sample 2) to fifty minutes in the worst scenario (sample 8), where the algorithm did not converge at all. The number of generations (iterations) was less than 20 in all cases.

Identified parameters of the delamination. Size, planar location and depth of delamination were the primary objectives of the proposed identification methodology. Independently of the completeness of the DSPI measurements, the size of the predicted delamination was bigger than the real delamination embedded in the laminate. Normal over predictions were in the range of five to ten percent, but in one case (sample 2) the over prediction was much bigger. The planar location of delaminations was predicted with accuracy greater than 95% in nine of the ten samples. The predicted depth of the delaminations was predicted correctly 50% of the times, taking into account that always a different initial population was used in the LARGA. In those cases where the delamination was not predicted accurately, the identification methodology reported depths that were close to the real value.

6.2 Main Contributions of this Thesis

The detection of defects in a structure is a ubiquitous problem across many industries, including aerospace, automotive, energy transmission and construction. This study has taken a significant step forward in closing the gap between detection and characterisation of delamination in composite laminates. The original contributions to the advancement of knowledge that have been made in the course of this research project are as follows:

1 A cost-effective finite element model of a delamination in a composite laminate has been developed. The strength of the model lies in the fact that it balances the need for an accurate representation of the damage, and the time taken for its solution.

2 A numerical tool consisting of a laplacian-based edge detection technique and a least-square minimisation technique has been developed for the *automatic detection* of delamination. Given a particular DSPI experimental set, analysts can use this tool to determine the existence of damage.

3 A mathematical model, based on the Euler-Bernoulli Beam equation, has been developed that correlates the out-of-plane displacements with the external forces acting on the delaminated sub laminate when a DSPI experiment is performed. This model demonstrated that the problem of identification of delamination is in general ill-posed.

4 A reformulation of the inverse problem of delamination identification has been suggested that integrates the concept of Central Geometric Moments (CGM). It was demonstrated that CGM are able to represent accurately the physical content of the DSPI experimental results because they are sensitive to the size, location, and orientation of the displacement field contained in both the DSPI measurements, and the FE model that encapsulates the delamination to be characterised.

5 A novel computational methodology for the automatic identification of delamination in composite panels has been both developed, and experimentally validated. This methodology is flexible to allow the changing environment that is common in-service, and efficient in the sense that its results are relevant and they are obtained in short periods of time.

6 An original low-population adaptive-range genetic algorithm (LARGA) has been developed using the ANSYS APDL macro-language. The result is a versatile algorithm that exploits the functionality of commercial available FE software. This genetic algorithm demonstrated that is possible to use a low number of individuals during and optimisation search, without a

penalty in accuracy, but improving significantly the time invested to find the global optimum of an objective function.

6.3 Future Work

The approach outlined in this study can be extended if the following research tasks are performed.

6.3.1 The use of new materials and loading conditions

In order to validate the generality of the identification methodology proposed in this thesis, it is suggested to device an experimental program that includes composite materials with different lay-ups, and isotropic materials. It is also suggested to prepare delaminated composite panels using low-velocity impacts in order to check the accuracy of the identification methodology under a more realistic scenario.

DSPI not only generates out-of-plane displacements but also maps of shear deformation. A complete new research can be implemented in order to use these shear maps in order characterise flaws in composite materials.

6.3.2 The use of other optimisation paradigms

An exciting area of research can be found in the optimisation side of the delamination identification technique. Instead of using genetic algorithms as a main tool for the minimisation of the difference between the experimental data and the results from a finite element model, it would possible to use any of the following optimisation paradigms: ants colony, memetic algorithms, particle swarm, neural networks, and case-based reasoning. The following paragraphs provide a brief description of each one.

6.3.2.1 Ants Colony

Ants Colony Optimisation (ACO) is a class of algorithms, whose main underlying idea, loosely inspired by the behaviour of real ants, is that of a parallel search over several constructive computational threads based on local problem data and on a dynamic memory structure containing information on the quality of previously obtained result. The collective behaviour emerging from the

interaction of the different search threads has proved effective in solving combinatorial optimization (CO) problems.

6.3.2.2 Memetic Algorithms

Memetic Algorithms is a population-based approach for heuristic search in optimisation problems. They have shown that they are orders of magnitude faster than traditional Genetic Algorithms for some problem domains. Basically, they combine local search heuristics with crossover operators.

6.3.2.3 Particle Swarm

Particle Swarm Optimization (PSO) is motivated by social behaviour of organisms such as bird flocking and fish schooling. PSO as an optimization tool, provides a population-based search procedure in which individuals called particles change their position (state) with time. In a PSO system, particles fly around in a multidimensional search space. PSO combines local search methods with global search methods, attempting to balance exploration and exploitation.

6.3.2.4 Neural Networks

Neural networks are computing mechanisms made of a large number of simple, highly interconnected processing elements, which manipulate information by their dynamic state response to external inputs. One of the properties of the neural networks is its ability to learn and generalise from examples and to adapt with changing scenarios. Neural networks are able to map causal models - for estimation and prediction-, and inverse mapping -from effect to possible cause. In their design, neural networks try to mimic some of the learning activities of the human brain.

6.3.2.5 Case-based reasoning

Case-based reasoning (CBR) is an interesting artificial intelligence (AI) paradigm that crosses the line between scientific information and human cognition. The main advantage of the CBR methodology resides in the potential to develop a tool that learns as cases are resolved.

References

[1] D. C. Panni. *Integrating the finite element method and genetic algorithms to solve structural damage detection and design optimisation problems.* Phd thesis, Loughborough University, 2002.

[2] P. K. Rastogi, editor. *Digital Speckle Pattern Interferometry and Related Techniques.* John Wiley & Sons, Inc., Baffins Lane, England, 1st. edition, 2001.

[3] J. D. Achenbach and J. H. Hemann. Tensile failure of interface bonds in a composite body subject to compresive loads. *AIAA Journal*, 6(10):2040–2043, 1968.

[4] N. J. Pagano. Exact solutions for composite laminates in cylindrical bending. *Journal of Composite Materials*, 3:398–411, 1969.

[5] J. M. Whitney. The effect of transverse shear deformation on the bending of laminated plates. *Journal of Composite Materials*, 3:534–547, 1969.

[6] A. H. Puppo and H. A. Evensen. Interlaminar shear in laminated composites under generalized plane stress. *Journal of Composite Materials*, 4:204–220, 1970.

[7] R. B. Pipes and N. J. Pagano. Interlaminar stresses in composite laminates under uniform axial extension. *Journal of Composite Materials*, 4:538–548, 1970.

[8] N. J. Pagano and R. B. Pipes. The influence of stacking sequence on laminate strength. *Journal of Composite Materials*, 5:50–57, 1971.

[9] N. J. Pagano and R. B. Pipes. Some observations on the interlaminar strength of composite laminates. *International Journal of Mechanical Sciences*, 15:679–688, 1973.

[10] N. J. Pagano. On the calculation of interlaminar normal stress in composite laminate. *Journal of Composite Materials*, 8:65–81, 1974.

[11] A. Harris and O. Orringer. Investigation of angle-ply delamination specimen for interlaminar strength test. *Journal of Composite Materials*, 12:285–299, 1978.

[12] R. Garcia and M. D. Rhodes. Effect of low-velocity impact on gr/pi compression laminates. In H. B. Dexter and J. G. Davis, editors, *Graphite/Polyamide Composites*, pages 239–249, Hampton, Virginia, USA, 1979. NASA.

[13] W. J. Cantwell, J. Morton, and P. T. Curtis, editors. *A study of the impact resistance and subsequent O-compression fatigue performance of non-woven and mixed-woven composites*, volume 2 of *Structural Impact and Crashworthiness*. Elsevier Science Publishing Co.,, Oxford, 1984.

[14] H. T. Wu and G. S. Springer. Measurements of matrix cracking and delamination caused by impact on composite plates. *Journal of Composite Materials*, 22:518–532, 1988.

[15] D. Liu. Impact-induced delamination - a view of bending stiffness mismatching. *Journal of Composite Materials*, 22:674–691, 1988.

[16] L. E. Malvern, C. T. Sun, and D. Liu. Delamination damage in central impacts at subperforation speeds on laminated kevlar/epoxy plates. In P. A. Lagace, editor, *Composite Materials: Fatigue and Fracture*, volume Second, pages 387–405. American Society for Testing and Materials, Philadelphia, USA., 1989.

[17] H. Y. Choi and F. Chang. A model for predicting damage in graphite/epoxy laminated composites resulting from low velocity point impact. *Journal of Composite Materials*, 26(14):2134–2169, 1992.

[18] A. D. Reddy, L. W. Rehfield, and R. S. Hagg. Influence of prescribed delaminations on stiffness-controlled behavior of composite laminates. In ASTM, editor, *Effects of defects in composite materials:a symposium*, pages 71–83, San Francisco, Calif., 1984. Philadelphia.

[19] S. Mohammadi, D.R.J. Owen, and D. Peric. A combined finite/discrete element algorithm for delamination analysis of composites. *Finite Elements in Analysis and Design*, 28(4):321–336, 1998.

[20] R. Borg, L. Nilsson, and K. Simonsson. Simulation of delamination in fiber composites with a discrete cohesive failure model. *Composites Science and Technology*, 61(5):667–677, 2001.

[21] K. S. Kim and C. S. Hong. Delamination growth in angle-ply laminated composites. *Journal of Composite Materials*, 20:423–438, 1986.

[22] B. D. Davidson. Delamination buckling: Theory and experiment. *Journal of Composite Materials*, 25:1351–1377, 1991.

[23] M. Zako and T. Tsujikami. Development of simulation program for delamination of laminated composites. *J. Soc. Mat. Sci., Japan*, 43(489):684–689, 1994.

[24] G. A. Davies and X. Zhang. Impact damage prediction in carbon composite structures. *International Journal of Impact Engineering*, 16(1):149–170, 1995.

[25] Z. Zou, S. R. Reid, S. Li, and P. D. Soden. Application of a delamination model to laminated composite structures. *Composte Structures*, 56:375–389, 2002.

[26] K. N. Shivakumar and J. D. Whitcomb. Buckling of a sublaminate in a quasi-isotropic composite laminate. *Journal of Composite Materials*, 19:2–18, 1985.

[27] G. P. Sendeckyj and G. E. Maddux. Comparison of holographic, radiographic, and ultrasonic techniques for damage detection in composite materials. In B. Noton, R. Signorelli, K. Street, and L. Phillips, editors, *ICCM2*, pages 1037–1056. The Metallurgical Society, 1978.

[28] G. E. Maddux and G. P. Sendeckyj. Holographic techniques for defect detection in composite materials. In R. B. Pipes, editor, *Nondestructive Evaluation and Flaw Criticality for Composite Materials*, pages 26–44. ASTM, STP 696, 1979.

[29] D. J. Hillman and R. L. Hillman. Thermographic inspection of carbon epoxy structures. In W. S. Johnson, editor, *Delamination and Debonding of Materials, ASTM STP 876*, pages 481–493. American Society for Testing and Materials, Philadelphia, USA., 1985.

[30] R. D. Adams and P. Cawley. A review of defect types and nondestructive testing techniques for composties and bonded joints. *NDT International*, 21(4):208–222, 1988.

[31] W. J. Cantwell and J. Morton. The significance of damage and defects and their detection in composite materials: A review. *Journal of Strain Analysis for Engineering Design*, 27(1):29–42, 1992.

[32] F. Aymerich and S. Meili. Ultrasonic evaluation of matrix damage in impacted composite laminates. *Compostes: Part B*, 31:1–6, 2000.

[33] J. K. Kim. Recent developments in impact damage assessment of fibre composites. In S. R. Reid and G. Zhou, editors, *Impact Behaviour of Fibre-Reinforced Composite Materials and Structures*, pages 33–74. Woodhead Publishing Limited, Cambridge, England., 2000.

[34] J. Pohl, S. Herold, G. Mook, and F. Michel. Damage detection in smart cfrp composites using impedance spectroscopy. *Smart Materials and Structures*, 10(4):834–841, 2001.

[35] G. Marsh. Finding flaws in composites. *Reinforced Plastics*, December:42 –46, December, 2002 2002.

[36] N. S. Mera, L. Elliot, and D. B. Ingham. Detection of subsurface cavities in ir-cat by areal coded algorithm. *Applied Soft Computing*, 2:129–139, 2002.

[37] J. N. Butters and J. A. Leenertz. Speckle pattern adn holographic techniques in engineering metrology. *Optics and Lasers in Engineering*, 3(1):26–30, 1971.

[38] O. Lokberg. On site inspection by compact tv-holography. In *Int. Conf. on Post Failure Analysis Techniques for Fibre Reinforced Composites*, volume 13, pages 1-9, Air Force Wright Aeronautical Laboratories, 1985.

[39] J. M. Huntley. Automated fringe pattern analysis in experimental mechanics: a review. *Journal of Strain Analysis*, 33(2):105-125, 1998.

[40] M. J. Fago and A. M. Wass. Experimental investigation of the behavior of edge delaminations using holographic interferometry. *Optical Engineering*, 37(5):1420-1428, 1998.

[41] M. Hertwig, T. Flemming, and R. Usinger. Speckle interferometry for detection of subsurface damage in fibre-reinforced composites. *Measurement Science and Technology*, 5(2):100-104, 1994.

[42] Z. Y. Zhang, M. O. W. Richardson, M. Wisheart, J. R. Tyrer, and J. Petzing. Non destructive testing of grp composite materials containing impact damage by espi. In *5th International Conference on Automated Composites*, pages 395-405, Glasgow, UK, 1997.

[43] M. O. W. Richardson, Z. Y. Zhang, M. Wisheart, J. R. Tyrer, and J. Petzing. Espi nondestructive testing of grp composite materials containing impact damage. *Composites Part A*, 29(7):721-729, 1998.

[44] J. R. Tyrer, J. Petzing, D. Robertson, and W. Abdullah Saffey. Automatic defect categorisation using a laser speckle method. pages 235-239, 1999.

[45] J. M. Huntley, C. R. Coggrave, and Y. Shen. Real time speckle interferogram analysis and its application to sub-surface delamination crack detection in carbon fibre composites. In *10th International Conference on Fracture*, Hawaii, 2001.

[46] A. Davila, P. D. Ruiz, G. H. Haufmann, and J. M. Huntley. Measurement of sub-surface delaminations in carbon fibre composites using high-speed phase-shifted speckle interferometry and temporal phase unwrapping. *Optics and Lasers in Engineering*, 40(5-6):447-458, 2003.

[47] J. M. Huntley. Random phase measurement errors in digital speckle pattern interferometry. *Optics and Lasers in Engineering*, 26:131-150, 1997.

[48] R. Höfling and P. Priber. Automatic fringe pattern recognition usin invariant moments. In W. Jptner and Osten W., editors, *Second International workshop on automatic processing of fringe patterns*, pages 374-381, Bremen, 1993. Akademie Verlag.

[49] M. R. Teague. Image analysis via the general theory of moments. *J. Opt. Soc. Am.*, 70(8):920-930, 1980.

[50] S. P. Timoshenko and J. M. Gere. *Mechanics of Materials*. Van Nostrand Reihhold, NewYork, London, 1972.

[51] A. Papoulis. *Probability, random variables, and stochastic processes.* McGraw-Hill, Inc., New York, USA., 3rd. edition, 1991.

[52] M-K. Hu. Visual pattern recognition by moment invariants. *IRE Transactions on Information Theory*, pages 179–187, 1962.

[53] T. H. Reiss. The revised fundamental theorem of moment invariants. *IEEE Transactions on Pattern Analyisis and Machine Intelligence*, 13(8):830–833, 1991.

[54] G. Taubin and D. B. Cooper. Recognition and positioning of rigid objects using algebraic moment invariants. In *Geometric Methods in Computer Vision*, volume 1570, pages 175–186. SPIE, 1991.

[55] S. Dudani, K. Breeding, and R. McGhee. Aircraft identification by moment invariants. *IEEE Trans. on Computers*, C-26(1):39–45, 1977.

[56] I. Balslev. Noise tolerance of moment invariants in pattern recongnition. *Pattern Recognition Letters*, 19:1183–1189, 1998.

[57] F. A. Sadjadi and E. L. Hall. Three-dimensional moment invariants. *IEEE Transactions on Pattern Analyisis and Machine Intelligence*, PAMI-2(2):127–136, 1980.

[58] A. P. Reeves, R. J. Prokop, S. A. Andrews, and F. P. Kuhl. Three-dimensional shape analysis using moments and fourier descriptors. *IEEE Transactions on Pattern Analyisis and Machine Intelligence*, 10(6):937–943, 1988.

[59] Th. M. Hupkens and J. de Clippeleir. Noise and intensity invariant moments. *Pattern Recognition Letters*, 16:371–376, 1995.

[60] C-H. Teh and R. T. Chin. On image analysis by the method of moments. *IEEE Transactions on Pattern Analyisis and Machine Intelligence*, 10(4):496–513, 1988.

[61] A. G. Mamistvalov. n-dimensional moment invariants and conceptual mathematical theory of recognition n-dimensional solids. *IEEE Transactions on Pattern Analyisis and Machine Intelligence*, 20(8):819–831, 1998.

[62] A. Khotanzad and Y. A. Hong. Invariant image recognition by zernike moments. *IEEE Transactions on Pattern Analyisis and Machine Intelligence*, 12(5):489–497, 1990.

[63] Whoi-Yul Kim and Yong-Sung Kim. A region-based shape descriptor using zernike moments. *Signal Processing: Image Communication*, 16(1-2):95–102, 2000.

[64] Chao Kan and Mandyam D. Srinath. Invariant character recognition with zernike and orthogonal fourier-mellin moments. *Pattern Recognition*, 35(1):143–154, 2002.

[65] Chee-Way Chong, P. Raveendran, and R. Mukundan. Translation invariants of zernike moments. *Pattern Recognition*, 36(8):1765–1773, 2003.

[66] K. H. Laerman. Contribution to solving inverse problems in ndt of structures. In *Experimental Mechanics - Advances in Design, Testing and Analysis.*, pages 755-760. Oxford. UK., 1998.

[67] A. M. Maniatty and C. Surace. Finite element analysis of some inverse elasticity problems. *Journal of Engineering Mechanics*, 115:1303-1317, 1989.

[68] S. Kubo. Inverse problems related to the mechanics of and fracture of solids and structures. *JSME International journal*, 31:157-166, 1988.

[69] P. Hajela and J. Soeiro. Structural damage detection based on static and modal analisis. *AIAA Journal*, 28(6):1110-1115, 1990.

[70] P. Hajela and J. Soeiro. Recent developments in damage detection based on system identification methods. *Structural optimization*, 2:1-10, 1990.

[71] A. D. Nurse, J. M. Huntley, D. C. Panni, J. Petzing, J. Sherrat, and J. R. Tyrer. Developments in inverse analysis for in-situ flaw detection in composite material structures. In *13th European Conference on Fracture*, pages 303-310, San Sebastian, 2000.

[72] Y. Narkis. Identification of crack location in vibrating simply supported beams. *Journal of Sound and Vibration*, 172(4):549-558, 1994.

[73] C. P. Ratcliffe. Damage detection using a modified laplacian operator on mode shape data. *Journal of Sound and Vibration*, 204(3):505-517, 1997.

[74] C. R. Farrar and D. A. Jauregui. Comparative study of damage identification algorithms applied to a bridge: I. experiment. *Smart Materials and Structures*, 7(5):704-719, 1998.

[75] C. R. Farrar and D. A. Jauregui. Comparative study of damage identification algorithms applied to a bridge: Ii. numerical study. *Smart Materials and Structures*, 7(5):720-731, 1998.

[76] L. R. Ray and L. Tian. Damage detection in smart structures through sensitivity enhancing feedback control. *Journal of Sound and Vibration*, 227(5):987-1002, 1999.

[77] A. S. Purekar and D.J. Pines. Detecting damage in non-uniform beams using the dereverberated transfer function response. *Smart Materials and Structures*, 4(4):429-444, 2000.

[78] Y Aoki and O. Byon. Application of localized flexibility method to damage identification in cfrp laminated plate. *Key Engineering Materials*, 183-187:1093-1098, 2000.

[79] P. F. Pai and S. Jin. Locating structural damage using operational deflection shapes. *Proceedings of SPIE - The International Society for Optical Engineering*, 3985:271-282, 2000.

[80] R. Thornburgh and A. Chattopadhyay. Unified approach to modeling matrix cracking and delamination in laminated composite structures. *AIAA Journal*, 39(1):153-160, 2001.

[81] A. C. Okafor and A. Dutta. Structural damage detection in beams by wavelet transforms. *Smart Materials and Structures*, 9(6):906–917, 2000.

[82] O. Byon and Y. Nishi. Damage identification of cfrp laminated cantilever beam by using neural network. *Key Engineering Materials*, 141-143(1):55–64, 1998.

[83] Y. J. Wu, K. W. Wong, and T. G. Zhuang. Limited samples wavelet network and its application for damage detection composites. *Optical Engineering*, 39(4):1002–1008, 2000.

[84] Y. Y. Kim and E.H. Kim. New damage detection method based on a wavelet transform. In *Proceedings of the International Modal Analysis Conference - IMAC*, volume 2, pages 1207–1212. SEM, 2000.

[85] M. Sanayei and R. B. Nelson. Identification of structural element stiffnesses from incomplete static test data. In *DataSAE Aerospace Technology Conference and Exposition*, pages 1–12, Long Beach, California, 1986. SAE.

[86] M. Sanayei and O. Onipede. Damage assessment of structures using static test data. *AIAA Journal*, 29(7):1174–1179, 1991.

[87] M. Sanayei and S. F. Scampoli. Structural element stiffness identification from static test data. *Journal of Engineering Mechanics*, 117(5):1021–1036, 1991.

[88] M. R. Banan, M. R. Banan, and K. D. Hjelmstad. Parameter estimation of structures from static response. i. computational aspects. *Journal of Structural Engineering*, 120(11):3243–3258, 1994.

[89] M. R. Banan, M. R. Banan, and K. D. Hjelmstad. Parameter estimation of structures from static response. ii: Numerical simulation studies. *Journal of Structural Engineering*, 120(11):3259–3283, 1994.

[90] P. L. Liu and H. T. Lin. Direct identification of non-uniform beams using static strains. *International Journal of Solids and Structures*, 33(19):2775–2787, 1996.

[91] M. Sanayei and M. J. Saletnik. Parameter estimation of structures from static strain measurements. i: Formulation. *Journal of Structural Engineering*, 122:555–562, 1996.

[92] M. Sanayei and M. J. Saletnik. Parameter estimation of structures from static strain measurements. ii: Error sensitivity analysis. *Journal of Structural Engineering*, 122:563–572, 1996.

[93] M. Sanayei, G. R. Imbaro, J. A. S. McClain, and L. C. Brown. Structural model updating using experimental static measurements. *Journal of Structural Engineering*, 123(6):792–798, 1997.

[94] P. L. Liu and C. C. Chian. Parametric identification of truss structures using static strains. *Journal of Structural Engineering*, 123:927–933, 1997.

[95] H. Fukunaga, H. Sekine, and Y. Tani. Stiffness and damage identification of laminated plates using static deflection. *Journal of Reinforced Plastics and Composites*. 18(13):1173–1185, 1999.

[96] An-Sing Chen and Mark T. Leung. Regression neural network for error correction in foreign exchange forecasting and trading. *Computers & Operations Research*. 31(7):1049–1068, 2004.

[97] A. Kaveh and H. Servati. Design of double layer grids using artificial neural networks. In B. Kumar and B. H. V. Topping, editors, *Artificial Intelligence Applications in Civil and Structural Engineering*, pages 93–101, Edingburgh, 1999. Civil-Comp Press.

[98] A. J. Skinner and J. O. Broughton. Neural networks in computational materials science: training algorithms. *Modelling and Simulation in Materials Science and Engineering*, 3(3):371–390, 1995.

[99] X. Wu, J. Ghaboussi, and J. Garret. Use of neural networks in detection fo structural damage. *Computer and Structures*, 12(4):649–659, 1992.

[100] J. N. Kudva, N. Munir, and P. W. Tan. Damage detection in smart structures using neural networks and finite-element analyses. *Smart Materials and Structures*, 1(2):106–112, 1992.

[101] A. S. Islam and K. C. Craig. Damage detection in composite structures using piezoelectric materials. *Smart Materials and Structures*, 3(3):318–328, 1994.

[102] Z. Szewczyk and P. Hajela. Damage detection in structures based on feature-sensitive neural networks. *Journal of Computing in Civil Engineering*, 8(2):163–178, 1994.

[103] J. Rhim and S. W. Lee. Neural network approach for damage detection and identification of structures. *Computational Mechanics*, 16(6):437–443, 1995.

[104] R. Ceravolo, A. De Stefano, and D. Sabia. Hierarchical use of neural techniques in structural damage recognition. *Smart Materials and Structures*, 4(4):270–280, 1995.

[105] A. C. Okafor, K. Chandrashekhara, and Y. P. Jiang. Delamination prediction in composite beams with built-in piezoelectric devices using modal analysis and neural network. *Smart Materials and Structures*, 5(3):338–347, 1996.

[106] C. H. Tsai and D. S. Hsu. Damage diagnosis of existing reinforced concrete structures. In B. Kumar and B. H. V. Topping, editors, *Artificial Intelligence Applications in Civil and Structural Engineering*, pages 85–92, Edinburgh, 1999. Civil-Comp Press.

[107] Y. Q. Ni, B. S. Wang, and J. M. Ko. Selection of input vectors to neural networks for structural damage identification. *Proceedings of SPIE - The International Society for Optical Engineering*, 3671:270–280, 1999.

[108] C. C. Chang, T. Y. P. Chang, Y. G. Xu, and M. L. Wang. Structural damage detection using an iterative neural network. *Journal of Intelligent Material Systems and Structures*, 11(1):33–42, 2000.

[109] M. T. Valoor and K. Chandrashekhara. Thick composite-beam model for delamination prediction by the use of neural networks. *Composites Science and Technology*, 60(9):1763–1769, 2000.

[110] A. W. Otieno, O. Nyongesa, P. L. Rosin, A. C. Okafor, and V. S. Rao. Fuzzy logic and neural network applications in damage detection and characterization with shearography. In S. Adali, E. V. Morozov, and V. E. Verijenko, editors, *ICCST 3*, pages 335–341, Durban, South Africa, 2000.

[111] S. I Ishak, G. R. Liu, H. M. Shang, and S. P. Lim. Locating and sizing of delamination in composite laminates using computational and experimental methods. *Composites Part B: Engineering*, 32(4):287–298, 2001.

[112] J. L. Zapico, M. P. Gonzalez, and K. Worden. Damage assessment using neural networks. *Mechanical Systems and Signal Processing*, 17(1):119–125, 2003.

[113] J. Holland. *Adaptation in Natural and Artificial Systems*. Univ. of Michigan Press, Michigan, 1975.

[114] L. Davies. *Genetic Algorithms and Simulated Annealing*. Pitman, 1987.

[115] D. E. Goldberg. *Genetic Algorithm in Search, Optimization, and Machine Learning*. Addison-Wesley, Reading, MA., 1989.

[116] G. Roth and M. D. Levine. Geometric primitive extraction using a genetic algorithm. *IEEE Transactions on Pattern Analyisis and Machine Intelligence*, 16(9):901–905, 1994.

[117] J. M. Doyle. A genetic algorithm for determining the location of structural impacts. *Experimental Mechanics*, pages 37–44, 1994.

[118] A. Oyama, S. Obayashi, and T. Nakamura. Real-coded adaptive range genetic algorithm applied to transonic wing optimization. *Applied Soft Computing*, 16:1–9, 2001.

[119] P. Hajela and C. J. Lin. Genetic search strategies in multicriterion optimal design. *Structural optimization*, 4:99–107, 1992.

[120] P. Hajela and E. Lee. Genetic algorithms in truss topological optimization. *International Journal of Solids and Structures*, 32:3341–3357, 1995.

[121] F. Y. Cheng and D. Li. Genetic algorithm development for multiobjective optimisation of structures. *AIAA Journal*, 36:1105–1112, 1998.

[122] Fuat Erbatur, Oguzhan Hasancebi, Ilker Tutuncu, and Hakan Kilic. Optimal design of planar and space structures with genetic algorithms. *Computers & Structures*, 75(2):209–224, 2000.

[123] M. S. Hayalioglu. Optimum design of geometrically non-linear elastic-plastic steel frames via genetic algorithm. *Computers & Structures*, 77(5):527–538, 2000.

[124] M. W. Suh and M. B. Shim. Crack identification using hybrid neuro-genetic technique. *Journal of Sound and Vibration*, 284(4):617–635, 2000.

[125] M. Krawczuk and W. Ostachowicz. Spectral finite element and genetic algorithm for crack detection in cantilever rod. *Key Engineering Materials*, 204-205:241–250, 2001.

[126] Y. He, F. Chu, and D. Guo. Detection and configuration of the shaft crack in a rotor-bearing system by genetic algorithm. *Key Engineering Materials*, 204-205:221–230, 2001.

[127] Y. He, D. Guo, and F. Chu. Using genetic algorithms to detect and configure shaft crack for rotor-bearing system. *Computer Methods in Applied Mechanics and Engineering*, 190:5895–5906, 2001.

[128] G. R. Liu and S. C. Chen. Flaw detection in sandwich plates based on time-harmonic response using genetic algoritms. *Computer Methods in Applied Mechanics and Engineering*, 190:5505–5514, 2001.

[129] Z. L. Yang, G. R. Liu, and K. Y. Lam. An inverse prodedure for crack detection using integral strain measured by optical fibers. *Smart Materials and Structures*, 11(1):72–78, 2002.

[130] P. J. Sherrat, D. C. Panni, and A. D. Nurse. Damage assessment of composite structures using inverse analysis and genetic algorithms. *Key Engineering Materials*, 204-205:409–418, 2001.

[131] Y. Xia and H. Hao. A genetic algorithm for structural damage detection based on vibration data. In *Proceedings of IMAC-XIX: A Conference on Structural Dynamics*, volume 2, pages 1381–1387, Kissimmee, FL, United States, 2001.

[132] D. C. Panni and A. D. Nurse. Integrating genetic algorithms and finite element analyses for structural inverse problems. In M. Mohammadian, R. Sarker, and X. Yao, editors, *Computational Intelligence in Control*, page 348. Idea Group Publishing, Hershey, USA., 2003.

[133] J. S. Lim. *Two Dimensional Signal and Image Processing*. Prentice-Hall signal processing series. Prentice Hall, London, 1990.

[134] B. S. Everitt. *Introduction to optimization methods and their application to statistics.* Chapman and Hall Ltd, London, UK, 2nd edition, 1987.

[135] J. J. McKeown, D. Meegan, and D. Sprevak. *An introduction to unconstrained optimisation.* IOP Publishing, Bristol, UK, 1990.

[136] R. D. Cook. *Finite Element Modeling for Stress Analysis.* John Wiley & Sons. Inc., New York, 1995.

[137] E. Ducheyne. *Multiple objective forest management using GIS and genetic optimisation techniques.* Phd, University of Ghent, 2003.

[138] G. E. Stavroulakis. *Inverse and crack identification in engineering mechanics*, volume 46 of *Applied optimization.* Kluwer Academic Publishers, Dordrecht, The Netherlands, 2001.

[139] R. Mukundan and K. R. Ramakrishnan. *Moment Functions in Image Analysis.* World Scientific Publishing Co Pte Ltd, Singapore, 1998.

[140] S. X Liao. *Image analysis by moments.* Phd, The University of Manitoba, 1993.

[141] G. Rudolph. Convergence analysis of canonical genetic algorithms. *IEEE Trans. on Neural Networks*, 5(1):96–101, 1994.

[142] M. Arakawa and I. Hagiwara. Development of adaptive real range (arrange) genetic algorithms. *JSME International journal. J series*, 41(4):969–977, 1998.

[143] P. Hajela. Genetic search - an approach to the nonconvex optimization problem. *AIAA Journal*, 28:1205–1210, 1990.

[144] J. E. Baker. Adaptive selection methods for genetic algorithms, 1985.

[145] J. J. Grefenstette, editor. *Rank-based selection.* IOP Publishing and Oxford University Press, Oxford, 1997.

[146] J. E. Baker. Reducing bias and inefficiency in the selection algorithm. In J. J. Grefenstette, editor, *Proceedings of the Second International Conference on Genetic Algorithms*, pages 14–21. Lawrence Erlbaum Associates, Publishers, 1987.

[147] J. J. Grefenstette, editor. *Proportional selection and sampling algorithms.* IOP Publishing and Oxford University Press, Oxford, 1997.

[148] M Gorges-Schleuter. Explicit parallelism of genetic algorithms through population structures. In *"Parallel Problem Solving from Nature 1 (PPSN1)*, pages 150–159, Dormunt, Germany, 1990.

[149] H. M. Voigt, I. Santibanez, and J. Born. Hierarchically structured distributed genetic algorithm. In *Parallel Problem Solving from Nature 2 (IPPSN2)*, pages 145–154, Brussels, Belgium, 1992.

[150] H. Muhlenbein and D. Schlierkamp. Analysis of selection, mutation and recombination in genetic algorithms. Technical report, GMD Technical Report 93-24, 1993.

[151] T. Blickle and L. Thiele. A comparison of selection schemes used in genetic algorithms. Technical report, TIK Report 11, December 1995.